ELECTRON TRANSFER DISSOCIATION AND COLLISION-INDUCED DISSOCIATION MASS SPECTROMETRY OF METALLATED OLIGOSACCHARIDES

by

RANELLE MARIE SCHALLER-DUKE

CAROLYN J. CASSADY, COMMITTEE CHAIR
JOHN B. VINCENT
SHANE C. STREET
ŁUKASZ CIEŚLA
SHANLIN PAN

A DISSERTATION

Submitted in partial fulfillment of the requirements
for the degree of Doctor of Philosophy
in the Department of Chemistry and Biochemistry
in the Graduate School of
The University of Alabama

TUSCALOOSA, ALABAMA

2019

ABSTRACT

Investigations of metallated glycans through tandem mass spectrometry (MS/MS) can further the field of glycomics, the sequencing of the human glycome. The field is hindered by the lack of an analytical technique that can determine all the stereo-diverse features of carbohydrates. In this dissertation, electron transfer dissociation (ETD) and collision-induced dissociation (CID) are utilized with metal-adducted oligosaccharides to explore the potential of these techniques to sequence glycans. The resulting mass spectra provide significant insight and information about the structure of oligosaccharides and how to distinguish between these complicated isomeric species.

Using univalent, divalent, and trivalent transition metal adducts is valuable to glycan analysis. The ETD process requires multiply charged ions, which do not form via protonation for neutral glycans, and CID of protonated glycans produces uninformative glycosidic bond cleavage. The univalent and trivalent metals investigated did not produce ions sufficient for ETD studies, but CID of the trivalent metal adducts showed significant fragmentation. Dissociation of $[M + Met]^{2+}$ from the divalent metals formed various fragment ions with ETD producing more cross-ring and internal cleavages, which are necessary for structural analysis. The two dissociation techniques are complementary. For both ETD and CID of all glycans studied, $[M + Co]^{2+}$ provided the most uniform structurally informative dissociation.

Permethylation is a common derivatization technique used in the study of glycans. Permethylation reduces the hydrophilicity of oligosaccharides by replacing all hydrogen atoms on oxygen and nitrogen atoms with methyl groups. Permethylation increases ion intensity in

electrospray ionization (ESI) and prevents rearrangements of certain monosaccharides. In this study, permethylation reduced the fragmentation by both ETD and CID for the metallated glycans. The spectra for non-derivatized metallated oligosaccharides was more structurally informative, especially with ETD. For some exact mass ions, permethylation reduced the ambiguity in the spectra.

The trivalent lanthanide metal series was investigated as metal adducts. ESI on mixtures of trivalent metals and tetrasaccharides produced $[M + Met - H]^{2+}$, $[M + Met + NO_3]^{2+}$, and $[M + Met - 2H]^{+}$. For the larger heptasaccharide, both $[M + Met - H]^{2+}$ and $[M + Met]^{3+}$ formed. Dissociation of these ions by both ETD and CID yields extensive sequence information. All trivalent lanthanide cations are suitable for sequencing glycans, and the fragmentation did not vary by metal identity.

LIST OF ABBREVIATIONS AND SYMBOLS

AI	absolute intensity
AI-ECD	activated ion electron capture dissociation
Asn	asparagine
bar	unit of pressure
CAD	collisionally activated dissociation
CID	collision-induced dissociation
Da	Dalton
DCM	dichloromethane
DMSO	dimethyl sulfoxide
e-*	low energy electron
ECD	electron capture dissociation
EDD	electron detachment dissociation
EI	electron ionization
EID	electron induced dissociation
EM	electron multiplier
ESI	electrospray ionization
ET	electron transfer
ETD	electron transfer dissociation
ETnoD	electron transfer no dissociation
ExD	electron-based dissociation

eV	electron volt
FAB	fast atom bombardment
Fru	fructose
g	grams
Gal	galactose
GAGs	glycosaminoglycans
GlcA	glycuronic acid
Glu	glucose
HCl	hydrochloric acid
HCT	high capacity trap
ICC	ion charge control
ICR	ion cyclotron resonance
IdoA	iduronic acid
IE	ionization energy
IE2	second ionization energy
IE3	third ionization energy
IR	infrared
IRMPD	infrared radiation multiphoton dissociation
ISD	in-source decay
J	joule
K	kilo (prefix)
L	Liters
LC	liquid chromatography

µ	micro (prefix)
m	milli (prefix)
m	meter
M	moles/liter (concentration)
MALDI	matrix-assisted laser desorption ionization
MeOH	methanol
Met	metal
mol	mole(s)
MS	mass spectrometry
MS/MS	tandem mass spectrometry
MS^n	tandem mass spectrometry
MQ H_2O	Milli-Q ultra pure water
m/z	mass-to-charge ratio
n	nano (prefix)
NaOH	sodium hydroxide
nCI	negative chemical ionization
p	pico (prefix)
Pro	proline
PSD	post-source decay
psi	pounds per square inch (pressure)
PTM	post-translational modification
QIT	quadrupole ion trap
Q/R^3	Charge/ionic radius^3

RE	recombination energy
rf	radio frequency
s	second
Ser	serine
S/N	signal-to-noise ratio
SNFG	symbolic nomenclature for glycans
t	time
TOF	time-of-flight
Torr	unit of pressure
UVPD	ultraviolet photon dissociation
V	volt
v/v	volume to volume

ACKNOWLEDGMENTS

I believe that the successful achievement of an individual is backed by the contributions of many and that the contributions of many are required for great success. I am thankful for the opportunity to acknowledge all the people that have contributed to my success in this program.

The work presented in the dissertation was directed under the guidance of my advisor Dr. Carolyn J. Cassady. I would like to express my deepest gratitude to her. Dr. Cassady has continually provided guidance and support to help me achieve my goals. Her knowledge, advice, and patience are unparalleled and have forged my success at The University of Alabama. She is thoughtful through science and approaches research with an enthusiasm, dedication, and intelligence that is inspirational to all her students.

I would like to thank all the members of my graduate committee, including Dr. Łukasz Cieśla, Dr. Shanlin Pan, Dr. Shane Street, Dr. John Vincent, and former committee member Dr. Margaret Johnson. Their valuable advice and suggestions throughout my time in the program were greatly appreciated.

I appreciate Dr. Street and Dr. Vincent for providing me with many of the metal salts that were used in my research. I am grateful to Dr. Qiaoli Liang for training and assistance with the HCTultra QIT MS. Dr. Michael Jennings and Lisa Fealy were extremely helpful with discussions and assistance on organic synthesis and derivatizations of the oligosaccharides in this project.

Financial support from the National Institutes of Health, The University of Alabama Department of Chemistry and Biochemistry, The University of Alabama National Alumni

Association's License Tag Fellowship, and The University of Alabama Graduate Council Writing Fellowship is gratefully acknowledged.

Many thanks also go out to all the Cassady group members that I have had the opportunity to work with during my time in the program. I have loved watching the growth of this lab. Dr. Changgeng Feng, Dr. Chelsea Plummer, Dr. Juliette Commodore, Chelsea McMillen, Xinyao Jing, Can Cui, Matt Mireles, Nnenna Dieke, Surakshya Thapa, and Ramesh Karki, it has been our conversations both scientific and otherwise that have made the Cassady group great. I truly appreciate all the support and friendships. Juliette, your patience while training me and assistance and discussion on metal cations whenever I needed it will never be forgotten. I would also like to thank Mallikharjuna R. Bogala for beginning the oligosaccharide project in the Cassady group.

I have had the pleasure of working with several undergraduate students during my graduate school tenure, Randy Persaud, Sarah Puckett, and Taylor Perkins. They all performed many experiments related to enhanced protonation using MALDI and were great company in the lab. I am indebted to them for their contributions and commitment.

Finally, I would like to thank my family and friends for their never-ending love and support. My mom has always encouraged me and was instrumental in raising me to be a person that never gives up even when challenged. My sister Sarah was always just a phone call away whenever I needed to talk and had immense faith in me when I was not sure I could finish. Her entire families support carried me through. Lisa Fealy was by my side in the program and could understand the frustrations that come with getting a Ph.D. and was always supportive and able to "bring me back down to earth". My best friend Hannah Padilla and I met as chemistry majors in undergrad, and she has always believed in me and never allowed me to doubt myself. My

husband Christopher had unmeasurable patience and motivation for me, even when we were apart either due to deployments or career moves. He was always willing to listen to my practice talks, read and edit manuscripts and chapters, and help make figures. This has been a test of endurance, and I am so excited to see what comes next.

CONTENTS

LIST OF TABLES

LIST OF FIGURES

CHAPTER 1: INTRODUCTION AND OVERVIEW OF THE DISSERTATION

Every living organism produces biomolecules that provide the means for all biological functions. To better understand biological processes, the structure of these molecules must be elucidated. Carbohydrates are one of the four major classes of biomolecules and are the most abundant organic material found in nature.[1] Carbohydrates have a variety of functions. In most living organisms, they provide a significant source of energy and participate in many cellular processes including intercellular communication.[2-4] The terms glycan, polysaccharide, and carbohydrate are interchangeable and defined as "compounds consisting of a large number of monosaccharides linked glycosidically".[5] Glycans also serve as a structural component to many different organisms; they form the cell walls of bacteria, exoskeleton of insects, and cellulose in plants.[2-4] Perhaps most relevant to humans is their functions as post-translational modifications on proteins.

The recent sequencing of the human genome in 2003 was a revealing and catalytic landmark event.[6] Surprisingly, the human genome only appears to encode for about 30,000 proteins, which emphasizes the importance of understanding how these proteins function in the human body and how these proteins are affected by post-translational modifications.[3,7,8] Glycosylation is well established to be one of the most common post-translational modifications found in eukaryotic proteins and occurs on more than half of the proteins in the human body.[9,10] The glycosylation of proteins has many roles including modifying solubility, controlling protein folding, and stabilizing proteins. Carbohydrates attached to proteins also can present or conceal

cellular antigens to or from other proteins, cells, viruses, or bacteria and modulate hormone and enzyme activities.[1-4,8,9]

Three key types of protein-linked glycans are involved in cellular processes in eukaryotes.[11,12] 1) *N*-linked glycans are bonded to the nitrogen atom on the side chain of the amino acid asparagine (Asn) in the sequence Asn-X-Ser or Asn-X-Thr, where Ser is serine and Thr is threonine. *N*-linked glycans facilitate protein folding and are able to change protein structure to turn on and off different protein functions. 2) *O*-linked glycans play a key role in cell adhesion and are found bonded to the oxygen atom on a Ser or Thr residue.
3) Glycosaminoglycans (GAGs) are attached to a Ser residue in the sequence Ser-Gly-X-Gly (Gly is glycine) to form proteoglycans. (The X on N-linked glycans and GAGs can be any amino acid residue other than proline, Pro.) Proteoglycans consist of a core protein bonded with one or more highly anionic GAGs; they are found on cell surfaces and abundant in extracellular spaces such as connective tissues. Carbohydrates can even be useful in detecting and fighting cancer. Human mucin-1 (MUC1) is a glycoprotein that when found with lesser glycosylation is associated with increased rates of cancer.[13-15] Sialyl Lewis^X and Sialyl Lewis^A are trisaccharides and tetrasaccharides, respectively, that participate in cell recognition, including how a human egg attracts a sperm.[16] Cancer cells over produce these saccharides, and they may be useful in cancer biomarker studies.[17,18]

The oligosaccharides on the cell surface vary from species to species, among individuals of the same species, and even between different cell types in the same individual.[4] The profiling of glycans between disease and normal states and during different stages of growth and development provides insight for future research and drug development. Glycomics or glycobiology is a developing field that focuses on a thorough knowledge of glycan structures to

better understand glycan biological functions. A lack of analytical and scientific tools that can thoroughly analyze glycan structures has hindered the study of glycan structure-function relationships, despite their importance in vital biological processes. Consequently, developing fast, sensitive, and accurate analytical methods is crucial to decipher the structures of oligosaccharides.

With the rising interest in glycomics, methods for the characterization of carbohydrates have come into focus. Unlike proteins and nucleic acids, carbohydrate structures have multiple levels of complexity. The number of naturally occurring residues or "monosaccharide building blocks" is much larger for glycans than any other biomolecule, and the residues can be linked in multiple ways, including possibly branched to several other residues. Three sequential DNA nucleotides can be combined to give 64 three-unit structures based on the four possible nucleotides, while the 20 amino acids can yield 8,000 different three amino acid peptides; however, glycans can assemble into more than 9,000,000 unsubstituted trisaccharides.[19,20] Due to isomeric heterogeneities, absence of scientific methods for glycan amplification, and multiple levels of structural complexity, glycan structural determination is extremely challenging. The main objective of oligosaccharide structural analysis is to elucidate monosaccharide composition, topology, linkage patterns, and stereochemical configuration, and to locate sites of phosphorylation or sulfonation.

Scientists have developed various enzymatic, chemical, and physical chemical techniques to study the different levels of glycan structure. The purity and quality of the oligosaccharide sample being studied greatly affects the chosen method. Nuclear magnetic resonance (NMR) spectroscopy is capable in theory of offering complete structural characterization of a glycan, but large amounts of pure sample (> 1 mg) are required, which is not always available for clinical

and biological samples. Recent advancements in mass spectrometry (MS) and tandem mass spectrometry (MS/MS or MS^n) techniques have expanded the characterization and structural analysis of glycans. First, the accurate mass of a glycan can easily give the composition of said glycan. Further necessary structural information such as glycosidic bond linkage, topology and stereochemistry is partially obtainable with the use of MS/MS. The mechanisms of glycan fragmentation must be thoroughly understood to achieve complete structural characterization.

Vibrational activation based techniques such as collision-induced dissociation (CID), (which is also known as collisionally activated dissociation (CAD)), and infrared multiphoton dissociation (IRMPD) are the most commonly used methods for glycan MS/MS studies.[21-30] Both CID and IRMPD are "slow heating" techniques that result in cleavage of glycosidic bonds (B, Y, C, and Z type fragments according to the Domon and Costello nomenclature). Glycosidic bond cleavages do not allow for the elucidation of detailed structural information. (The nomenclature for dissociation of glycans will be discussed thoroughly in Chapter 2.) It is well established that CID, which involves an energetic collision of precursor ion and inert neutral species, is an energy-based process that typically breaks the weakest bonds in the molecule or facilitates low energy rearrangement of the molecule. Although IRMPD produces the same types of fragment ions as CID, it has higher fragmentation efficiency, and does not require a collision gas, but instead uses the absorption of large number of infrared (IR) photons for dissociation.

Electron-based fragmentation techniques, such as electron capture dissociation (ECD), electron detachment dissociation (EDD), electron-induced dissociation (EID), and electron transfer dissociation (ETD), are relatively recently developed ion activation techniques and rely on ion-electron interactions to induce fragmentation. These techniques are generally referred to

as ExD. These ion-electron interactions produce different fragmentation patterns for biomolecules than vibrational excitation-based dissociation. Electron capture, transfer, and detachment triggers gas-phase radical ion chemistry, but the precise mechanisms of these reactions have yet to be fully determined and are still widely debated.[31-35]

Budnik et al.[36] performed the first ExD experiment on glycans in 2003. In their study, singly protonated, doubly protonated, and sodiated glycans were investigated using ECD, EID and CAD. The doubly charged glycans with ECD produced mainly B and C ions with hydrogen transfers and neutral loss. EID using 8-13 eV electrons as bombarding agents was shown to produce fragmentation similar to that produced by ECD (capture of low energy ~1eV electrons) on both the singly and doubly protonated ions. Ions were also observed in the EID and CID spectra that indicate vibrational activation may be occurring. The authors found that the ExD experiments produced more complicated spectra with no additional structural information when compared to the CAD spectra that provided full sequence coverage.

In 2005, IRMPD, ECD, and EDD were compared for characterization of a ganglioside monosialotetrahexosylganglioside (GM1) by McFarland and co-workers.[37] IRMPD produced fewer fragmentation types, even with the use of long irradiation time and different levels of laser power. EDD produced complementary fragments to IRMPD but showed low fragmentation efficiency and an extensive amount of hydrogen loss, which complicated the spectral interpretation. ECD produced extensive fragmentation of the glycan, allowing complete sequence elucidation. The success of this experiment suggested that ECD shows promise as a glycan analytical technique.

Electron detachment dissociation was successfully applied to the analysis of GAGs by Wolff et al. in 2007.[38,39] EDD is the negative ion complement of ECD, where a multiply charged

negative ion is irradiated with 15-20 eV electrons causing electron detachment and dissociation of the ion of interest. The results indicated that EDD produced complete glycosidic and cross-ring cleavage across the molecule without significant SO_3 loss, unlike IRMPD. The identification of sulfate positions is important due to varying biological functions. EDD also distinguished epimers of heparin sulfate containing either glucuronic acid (GlcA) or iduronic acid (IdoA). Significant problems in the study were low fragmentation efficiency and hydrogen transfers, complicating spectral interpretation.

In 2007, Adamson and Håkansson[40] systematically studied the effects of metal cation adduction on the ECD fragmentation of model oligosaccharides. The authors investigated ECD with linear and branched glycans adducted with alkali, alkaline earth, and transition metal cations. Cross-ring cleavages on both ends of the glycan dominated the ECD spectra when compared to IRMPD. The authors found producing small fragment ions with less than three monosaccharide residues difficult. The study showed that low fragmentation efficiency could be overcome by using activated ion ECD (AI-ECD). In AI-ECD, the precursor ion is "activated" by collisions with background gas, IR irradiation, or increasing the temperature of the ion cyclotron resonance (ICR) cell prior to the electron capture process. The fragmentation patterns observed varied by metal cation, and the metal cation coordination to the glycan was proposed to determine the ECD fragmentation pattern. The metal cation coordinating with multiple oxygens on the glycans may promote cross-ring cleavage.

In 2008, Zhao et al.[41] reported that using hot-ECD (electrons with 5-14 eV electron energy) to investigate sodiated permethylated maltoheptaose produced full sets of linkage determining cross-ring cleavage ions. This technique also produced full structural information on a variety of branched N-glycans, which was not seen with CAD. When the hot-ECD

spectrum was compared to the ECD spectrum of sodiated native maltoheptaose,[35] the fragmentation observed was completely different. This variance could have been caused by the change in electron energy, or by the lack of permethylation of the glycans.

Permethylated metallated oligosaccharides were investigated using ETD by Han and Costello in 2011.[35] Isotopic labeling was utilized prior to permethylation to study the exact mass ions and assist in determining a mechanism of fragmentation. The study found that compared to CID, ETD of magnesium (Mg) adducted glycans produced mainly C and Z ions accompanied by extensive cross-ring fragment ions. The authors also utilized ETD-CID and were able to elucidate the linkage patterns and structures for multiple milk oligosaccharides. This study further demonstrated the utility of electron-based techniques with metal adducts.

Metal ions can be adducted to glycans to assist in the formation of positive ions for MS analysis. Carbohydrate molecules generally possess several functional groups, typically, hydroxyls, amines, and/or carboxylic acids. These functional groups are suitable for metal ion coordination, and metal coordination chemistry of carbohydrates has been studied extensively in the solid state,[42-44] in solution,[45-48] and in the gas phase.[49,50] Several review articles on carbohydrate coordination chemistry also exist.[48,51,52] Most relevant to this dissertation is that stereoisomeric glycans have been found to form diastereomeric coordination complexes in the presence of metal cations.[48,49,51] This means that stereochemical differences in the glycans are translated into differences in the complexes that are formed with metal adduction. These metal complexes may then differ in physical properties such as retention times or ionization efficiencies and even affect the presence or absence of various product ions during MS/MS fragmentation. Metal-glycan adduction has been found to produce abundant sequence

information with MS/MS. Metal cations can also be utilized as charge carriers to form the multiply charged cations necessary for ECD and ETD, which is further discussed in Chapter 2.

Studies using a variety of metal ions have shown that metallated oligosaccharides can provide structurally informative fragmentation in both positive and negative ion modes.[40,53-61] Adamson and Håkansson[40] complexed alkali, alkaline earth, and transition metal ions to several underivatized oligosaccharides and found that metallation greatly improved the structurally informative fragmentation by ECD and IRMPD, although no single metal ion stood out as optimal. Costello and co-workers[35] studied five permethylated metallated oligosaccharides, finding that magnesium provided the most fragmentation by ETD and that complementary fragmentation occurs by CID and ETD. In mass spectrometry studies of oligosaccharides sodiated precursor ions are commonly studied due to the difficulty of achieving protonation and the relative ease that glycans adduct sodium or other metal cations from the environment.[21,25,55]

The research in this dissertation focuses on metal adduction of model oligosaccharides, which are difficult to protonate and to study with electron-based techniques. Emphasis is placed on structural analysis and the utility of fragmentation with ETD. Goals of this research are to explore the ability of ETD and CID to provide structurally informative fragmentation on several oligosaccharides with and without derivatization using a variety of metal adducts as cationizing agents. Another goal of this research is to further elucidate and understand the mechanism of electron-based techniques when utilizing metal cations.

Chapter 2 discusses all necessary theoretical and experimental techniques for the research contained in this dissertation. The theory and components of mass spectrometry are discussed, along with the procedure for conducting mass spectrometry experiments in the Bruker HCTultra PTM Discovery System quadrupole ion trap (QIT). The mathematical equations that describe

the physics and relationships for *m/z*, and ion trapping are presented. Experimental procedures and instrument conditions related to ionization, mass analysis, and tandem mass spectrometry are described. The nomenclature for MS/MS of oligosaccharides, the structures of the oligosaccharides studied in this dissertation, and procedures for derivatization and isotopic labeling of the oligosaccharides are given.

Chapters 3-5 focus on ETD and CID studies of metallated oligosaccharides. Chapter 3 studies adduction of the oligosaccharides with univalent, divalent, and trivalent metals including alkaline earth, alkali, and transition metals. Chapter 4 utilizes the same metal cations as discussed in Chapter 3 but investigates the effects of derivatization, specifically permethylation, on the ionization and dissociation of the metal-adducted oligosaccharides. Chapter 5 expands upon the work in Chapters 3 and 4 by examining the effects of trivalent lanthanide metal cationization on dissociation of both derivatized and non-derivatized oligosaccharides.

Chapter 3 specifically discusses the ability of metal cationization to provide structural characterization of oligosaccharides by ETD and CID. The experiments investigated the ions that are formed by electrospray ionization (ESI) and the product ions after dissociation. The study included nitrates salts of sodium (Na^+), potassium (K^+), magnesium (Mg^{2+}), calcium (Ca^{2+}), chromium (Cr^{3+}), iron (Fe^{3+}), cobalt (Co^{2+}), nickel (Ni^{2+}), copper (Cu^{2+}), zinc (Zn^{2+}), and aluminum (Al^{3+}). Addition of a metal cation can facilitate the formation of positively charged ions, which is useful for oligosaccharide analysis where the biomolecules tend to deprotonate. The oligosaccharides preferentially adducted with univalent metal cations to form $[M + Met]^+$, and occasionally $[M + 2Met]^{2+}$, divalent metal cations would form $[M + Met]^{2+}$, and a small amount of proton loss was observed with divalent and trivalent metal cations generating $[M + Met - H]^+$, and $[M + Met - 2H]^+$. Electron transfer dissociation and CID of the singly metallated

doubly charged ions provided useful sequence information with Co^{2+} providing the most structurally informative fragmentation. These studies focused on the type and abundance of product ions formed and how this varied with different oligosaccharides and metal cations.

Chapter 4 investigates derivatization of the oligosaccharides and how it affects ETD and CID of metal-adducted glycans. The metals and sugars included in the study were the same as used in Chapter 3. Permethylation converts all the hydroxyl groups of an oligosaccharide to methoxy groups and is a common derivatization technique for the study of glycans. Permethylation increases ionization efficiency of metallated oligosaccharides but is not necessary for good ionization efficiency. The trivalent metal cations did not adduct to the permethylated glycans probably due to charge density and the inability to lose protons. The divalent metals were used for MS/MS studies on the $[M + Met]^{2+}$ formed and, again, Co^{2+} yielded the most useful and efficient fragmentation. Significantly less cross-ring fragmentation was observed with CID of the derivatized glycans. Permethylation occasionally decreased ambiguity found with exact mass ions by both ETD and CID but did not improve the structural information found by MS/MS studies. To date, this is the only study directly comparing MS/MS of permethylated and non-permethylated oligosaccharides.

Chapter 5 expands the studies in Chapters 3 and 4 to the trivalent lanthanide series. The ability of lanthanide metals to adduct to native and permethylated oligosaccharides and form cations useful for structural analysis is discussed. Both ETD and CID were used on the metal-adducted ions formed by ESI. All lanthanide metal ions except radioactive promethium (Pm) were studied. ESI formed $[M + Met - H]^{2+}$ for the tetrasaccharides studied and $[M + Met]^{3+}$ for the heptasaccharide. For each glycan, all of the trivalent lanthanides included in the study produced the same fragmentation patterns by both ETD and CID, only varying with isotopic

patterns and occasionally product ion intensity. As expected, CID with trivalent metal cationization produced more fragmentation than with the univalent and divalent metals discussed in Chapter 3.

Chapter 6 revisits and gives a summary to the most important findings in this dissertation and reviews the impact of this work on the fields of MS and glycomics. Experiments to expand these studies are proposed.

REFERENCE

1. Voet, D.; Voet, J. G. *Biochemistry;* John Wiley & Sons: New York, 1995.

2. Varki, A. Biological roles of oligosaccharides: All of the theories are correct. *Glycobiology* **1993**, *3*, 97-130.

3. Parodi, A. J. Protein glucosylation and its role in protein folding. *Annu. Rev. Biochem.* **2000**, *69*, 69-93.

4. Varki, A.; Cummings, R. D.; Esko, J. D.; Stanley, P.;Hart, G. W.; Aebi, M.; Darvill, A. G.; Kinoshita, T.; Packer, N. H.; Prestegard, J. H.; Schnaar, R. L.; Seeberger, P. H.,Eds. *Essentials of Glycobiology;* Cold Spring Harbor Laboratory Press: New York, 2015.

5. Moss, G. P.; Smith, P. A. S.; Tavernier, D. Glossary of class names of organic compounds and reactive intermediates based on structure. *Pure Appl. Chem.* **1995**, *67*, 1307-1375.

6. Venter, J. C.; Adams, M. D.; Myers, E. W.; Li, P. W.; Mural, R. J.; Sutton, G. G.; Smith, H. O.; Yandell, M.; Evans, C. A.; Holt, R. A. The sequence of the human genome. *Science* **2001**, *291*, 1304-1351.

7. Claverie, J-M. What if there are only 30,000 human genes? *Science* **2001**, *291*, 1255-1257.

8. Krištić, J.; Lauc, G. Ubiquitous importance of protein glycosylation. *Methods Mol. Biol.* **2017**, *1503*, 1-12.

9. Spiro, R. G. Glycoproteins. *Adv. Protein Chem.* **1973**, *27*, 349-467.

10. Apweiler, R.; Hermjakob, H.; Sharon, N. On the frequency of protein glycosylation, as deduced from analysis of the SWISS-PROT database. *Biochim. Biophys. Acta. Gen. Subj.* **1999**, *1473*, 4-8.

11. Corfield, A. P.; Berry, M. Glycan variation and evolution in the eukaryotes. *Trends Biochem. Sci.* **2015**, *40*, 351-359.

12. Reuter, G.; Gabius, H. J. Eukaryotic glycosylation: Whim of nature or multipurpose tool? *Cell Mol. Life Sci.* **1999**, *55*, 368-422.

13. Goletz, S.; Thiede, B.; Hanisch, F-G; Schultz, M.; Perter-Katalinic, J.; Muller, S.; Seitz, O.; Karsten, U. A sequencing strategy for the localization of O-glycosylation sites of MUC1 tandem repeats by PSD-MALDI mass spectrometry. *Glycobiology* **1997**, *7506*, 881-896.

14. Vlad, A. M.; Kettel, J. C.; Alajez, N. M.; Carlos, C. A.; Finn, O. J. MUC1 immunobiology: From discovery to clinical applications. *Adv. Immunol.* **2004**, *82*, 249-293.

15. Nath, S.; Mukherjee, P. MUC1: A multifaceted oncoprotein with a key role in cancer progression. *Trends Mol. Med.* **2014**, *20*, 332-342.

16. Clark, G. F. The role of carbohydrate recognition during human sperm–egg binding. *Hum. Reprod.* **2013**, *28*, 566-577.

17. Nishihara, S.; Hiraga, T.; Ikehara, Y.; Kudo, T.; Iwasaki, H.; Morozumi, K.; Akamatsu, S.; Tachikawa, T.; Hisashi, N. Molecular mechanisms of expression of Lewis b antigen and other Type I Lewis antigens in human colorectal cancer. *Glycobiology* **1999**, *9*, 607-616.

18. Yuriev, E.; Farrugia, W.; Scott, A. M.; Ramsland, P. A. Three-dimensional structures of carbohydrate determinants of Lewis system antigens: Implications for effective antibody targeting of cancer. *Immunol. Cell Biol.* **2005**, *83*, 709.

19. Laine, R. A. A calculation of all possible oligosaccharide isomers both branched and linear yields 1.05 x 10(12) structures for a reducing hexasaccharide - the isomer-barrier to development of single-method saccharide sequencing or synthesis systems. *Glycobiology* **1994**, *4*, 759-767.

20. Laine, R. A. Information capacity of the carbohydrate code. *Pure Appl. Chem.* **1997**, *69*, 1867.

21. Zaia, J. Mass spectrometry of oligosaccharides. *Mass Spectrom. Rev.* **2004**, *23*, 161-227.

22. Park, Y.; Lebrilla, C. B. Application of Fourier transform ion cyclotron resonance mass spectrometry to oligosaccharides. *Mass Spectrom. Rev.* **2005**, *24*, 232-264.

23. Penn, S. G.; Cancilla, M. T.; Lebrilla, C. B. Collision-induced dissociation of branched oligosaccharide ions with analysis and calculation of relative dissociation thresholds. *Anal. Chem.* **1996**, *68*, 2331-2339.

24. Harvey, D. J. Collision-induced fragmentation of underivatized N-linked carbohydrates ionized by electrospray. *J. Mass Spectrom.* **2000**, *35*, 1178-1190.

25. Lemoine, J.; Strecker, G.; Leroy, Y.; Fournet, B.; Ricart, G. Collisional-activation tandem mass spectrometry of sodium adduct ions of methylated oligosaccharides: Sequence analysis and discrimination between α-NeuAc-(2→3) and α-NeuAc-(2→6) linkages. *Carbohydr. Res.* **1991**, *221*, 209-217.

26. Zaia, J.; Miller, M. J. C.; Seymour, J. L.; Costello, C. E. The role of mobile protons in negative ion CID of oligosaccharides. *J. Am. Soc. Mass Spectrom.* **2007**, *18*, 952-960.

27. Ashline, D. J.; Lapadula, A. J.; Liu, Y. H.; Lin, M.; Grace, M.; Pramanik, B.; Reinhold, V. N. Carbohydrate structural isomers analyzed by sequential mass spectrometry. *Anal. Chem.* **2007**, *79*, 3830-3842.

28. Ashline, D.; Singh, S.; Hanneman, A.; Reinhold, V. Congruent strategies for carbohydrate sequencing. 1. mining structural details by MS^n. *Anal. Chem.* **2005**, *77*, 6250-6262.

29. Zhang, J. H.; Schubothe, K.; Li, B. S.; Russell, S.; Lebrilla, C. B. Infrared multiphoton dissociation of O-linked mucin-type oligosaccharides. *Anal. Chem.* **2005**, *77*, 208-214.

30. Xie, Y. M.; Lebrilla, C. B. Infrared multiphoton dissociation of alkali metal-coordinated oligosaccharides. *Anal. Chem.* **2003**, *75*, 1590-1598.

31. Liu, H.; Håkansson, K. Divalent metal ion-peptide interactions probed by electron capture dissociation of trications. *J. Am. Soc. Mass Spectrom.* **2006**, *17*, 1731-1741.

32. Chen, X.; Fung, Y. M. E.; Chan, W. Y. K.; Wong, P. S.; Yeung, H. S.; Chan, T. W. D. Transition metal ions: Charge carriers that mediate the electron capture dissociation pathways of peptides. *J. Am. Soc. Mass Spectrom.* **2011**, *22*, 2232-2245.

33. Kleinnijenhuis, A. J.; Mihalca, R.; Heeren, R. M. A.; Heck, A. J. R. Atypical behavior in the electron capture induced dissociation of biologically relevant transition metal ion complexes of the peptide hormone oxytocin. *Int. J. Mass Spectrom.* **2006**, *253*, 217-224.

34. Huang, Y.; Pu, Y.; Yu, X.; Costello, C. E.; Lin, C. Mechanistic study on electron capture dissociation of the oligosaccharide-Mg^{2+} complex. *J. Am. Soc. Mass Spectrom.* **2014**, *25*, 1451-1460.

35. Han, L.; Costello, C. E. Electron transfer dissociation of milk oligosaccharides. *J. Am. Soc. Mass Spectrom.* **2011**, *22*, 997-1013.

36. Budnik, B. A.; Haselmann, K. F.; Elkin, Y. N.; Gorbach, V. I.; Zubarev, R. A. Applications of electron-ion dissociation reactions for analysis of polycationic chitooligosaccharides in Fourier transform mass spectrometry. *Anal. Chem.* **2003**, *75*, 5994-6001.

37. McFarland, M. A.; Marshall, A. G.; Hendrickson, C. L.; Nilsson, C. L.; Fredman, P.; Månsson, J. Structural characterization of the GM1 ganglioside by infrared multiphoton dissociation, electron capture dissociation, and electron detachment dissociation electrospray ionization FT-ICR MS/MS. *J. Am. Soc. Mass Spectrom.* **2005**, *16*, 752-762.

38. Wolff, J. J.; Amster, I. J.; Chi, L.; Linhardt, R. J. Electron detachment dissociation of glycosaminoglycan tetrasaccharides. *J. Am. Soc. Mass Spectrom.* **2007**, *18*, 234-244.

39. Wolff, J. J.; Chi, L.; Linhardt, R. J.; Amster, I. J. Distinguishing glucuronic from iduronic acid in glycosaminoglycan tetrasaccharides by using electron detachment dissociation. *Anal. Chem.* **2007**, *79*, 2015-2022.

40. Adamson, J. T.; Håkansson, K. Electron capture dissociation of oligosaccharides ionized with alkali, alkaline earth, and transition metals. *Anal. Chem.* **2007**, *79*, 2901-2910.

41. Zhao, C.; Xie, B.; Chan, S.; Costello, C. E.; O'Connor, P. B. Collisionally activated dissociation and electron capture dissociation provide complementary structural information for branched permethylated oligosaccharides. *J. Am. Soc. Mass Spectrom.* **2008**, *19*, 138-150.

42. Tajmir-Riahi, H. D-glucose adducts with zinc-group metal ions. synthesis, and spectroscopic and structural characterization of Zn(II), Cd(II), and Hg(II) complexes with d-glucose, and the effects of metal-ion binding on the sugar anomeric structures. *Carbohydr. Res.* **1989**, *190*, 29-37.

43. Weis, W. I.; Drickamer, K.; Hendrickson, W. A. Structure of a C-type mannose-binding protein complexed with an oligosaccharide. *Nature* **1992**, *360*, 127-134.

44. Harrowfield, J. M.; Mocerino, M.; Skelton, B. W.; Wei, W.; White, A. H. Metal complexes of carbohydrates: Isolation and characterisation of cobalt(III) complexes containing N-substituted glycosylamine ligands derived from ethane-1,2-diamine and glucosamine. *J. Chem. Soc., Dalton Trans.* **1995**, 783-797.

45. Angyal, S. J. Complexes of metal-cations with carbohydrates in solution. *Adv. Carbohydr. Chem. Biochem.* **1989**, *47*, 1-43.

46. Angyal, S. J. Complexes of carbohydrates with metal cations.1. determination of extent of complexing by NMR-spectroscopy. *Aust. J. Chem.* **1972**, *25*, 1957-1966.

47. Angyal, S. J. Complexing of carbohydrates with copper ions: A reappraisal. *Carbohydr. Res.* **1990**, *200*, 181-188.

48. Allscher, T.; Klüfers, P.; Mayer, P. Carbohydrate–metal complexes : Structural Chemistry of Stable Solution Species. In *Glycoscience: Chemistry and Chemical Biology*; Fraser-Reid, B. O., Tatsuta, K. and Thiem, J., Eds.; Springer Berlin Heidelberg: Berlin, Heidelberg, 2008; 1077-1139.

49. Zheng, Y. J.; Ornstein, R. L.; Leary, J. A. A density functional theory investigation of metal ion binding sites in monosaccharides. *J. Mol. Struct. Theochem* **1997**, *389*, 233-240.

50. Ngoka, L. C.; Gal, J. F.; Lebrilla, C. B. Effects of cations and charge types on the metastable decay-rates of oligosaccharides. *Anal. Chem.* **1994**, *66*, 692-698.

51. Whitfield, D. M.; Stojkovski, S.; Sarkar, B. Metal coordination to carbohydrates. structures and function. *Coord. Chem. Rev.* **1993**, *122*, 171-225.

52. Bandwar, R. P.; Rao, C. P. Transition metal–saccharide chemistry and biology: An emerging field of multidisciplinary interest. *Curr. Sci.* **1997**, *72*, 788-796.

53. Bythell, B. J.; Abutokaikah, M. T.; Wagoner, A. R.; Guan, S.; Rabus, J. M. Cationized carbohydrate gas-phase fragmentation chemistry. *J. Am. Soc. Mass Spectrom.* **2017**, *28*, 688-703.

54. Cancilla, M. T.; Penn, S. G.; Carroll, J. A.; Lebrilla, C. B. Coordination of alkali metals to oligosaccharides dictates fragmentation behavior in matrix assisted laser desorption ionization/Fourier transform mass spectrometry. *J. Am. Chem. Soc.* **1996**, *118*, 6736-6745.

55. Lemoine, J.; Fournet, B.; Despeyroux, D.; Jennings, K. R.; Rosenberg, R.; De Hoffman, E. Collision-induced dissociation of alkali metal cationized and permethylated oligosaccharides: Influence of the collision energy and of the collision gas for the assignment of linkage position. *J. Am. Soc. Mass Spectrom.* **1993**, *4*, 197-203.

56. Harvey, D. J. Ionization and collision-induced fragmentation of N-linked and related carbohydrates using divalent cations. *J. Am. Soc. Mass Spectrom.* **2001**, *12*, 926-937.

57. Zhou, W.; Håkansson, K. Electron capture dissociation of divalent metal-adducted sulfated N-glycans released from bovine thyroid stimulating hormone. *J. Am. Soc. Mass Spectrom.* **2013**, *24*, 1798-1806.

58. Liu, H.; Håkansson, K. Electron capture dissociation of divalent metal-adducted sulfated oligosaccharides. *Int. J. Mass Spectrom.* **2011**, *305*, 170-177.

59. Asam, M. R.; Glish, G. L. Tandem mass spectrometry of alkali cationized polysaccharides in a quadrupole ion trap. *J. Am. Soc. Mass Spectrom.* **1997**, *8*, 987-995.

60. El Firdoussi, A.; Lafitte, M.; Tortajada, J.; Kone, O.; Salpin, J. Characterization of the glycosidic linkage of underivatized disaccharides by interaction with Pb^{2+} ions. *J. Mass Spectrom.* **2007**, *42*, 999-1011.

61. Sible, E. M.; Brimmer, S. P.; Leary, J. A. Interaction of first row transition metals with alpha 1-3, alpha 1-6 mannotriose and conserved trimannosyl core oligosaccharides: A comparative electrospray ionization study of doubly and singly charged complexes. *J. Am. Soc. Mass Spectrom.* **1997**, *8*, 32-42.

CHAPTER 2: EXPERIMENTAL METHODS, INSTRUMENTATION AND THEORY

2.1 Overview

This chapter includes a discussion of all theory and experimental procedures utilized in this dissertation. All research was performed on a Bruker (Billerica, MA, USA) HCTultra PTM Discovery System high capacity quadrupole ion trap (QIT) mass spectrometer with electrospray ionization (ESI). Following the introduction of ESI, the theory of the QIT will be discussed. The multi-stage tandem mass spectrometry (MS/MS or MS^n) techniques of collision-induced dissociation (CID) and electron transfer dissociation (ETD) were used to investigate oligosaccharide structure and will be described after instrumentation theory. Procedures for isotopic labeling and permethylation of the oligosaccharides, along with structure and fragmentation nomenclature, will conclude this chapter.

2.2 Electrospray Ionization

Beginning in the 1980s, ESI was developed for use in mass spectrometry by J.B. Fenn and co-workers[1-3] based on earlier work by Dole.[4] Nonvolatile, polar compounds such as proteins, nucleic acids, and carbohydrates can be ionized with ESI.[5-7] The development of this technique revolutionized mass spectrometry, and Fenn was recognized as a 2002 Nobel laureate in Chemistry for developing ESI. The ability to be coupled with separation techniques such as liquid chromatography (LC) has greatly expanded the utilization of ESI. An additional advantage of ESI is that high molecular weight species often appear as multiply charged ions, effectively extending the mass range of the mass spectrometer. This is also important as some

MS/MS techniques, such as ETD and electron capture dissociation (ECD), require multiply charged ions. ESI is a soft ionization technique that forms quasi-molecular ions with little to no fragmentation during the ionization process. Ions are transferred into the gas phase directly from solution. In the work presented in this dissertation, the sample oligosaccharide concentration in the solution undergoing ESI was ~10 µM with metal ion concentrations of 50-100 µM. The oligosaccharides were dissolved in 50:50 v/v methanol-water. The solution was pushed through a syringe and transfer line into the ESI needle using a KD Scientific (Hollistion, MA, USA) syringe pump with a flow rate of 180 µL/hr. All samples were analyzed in the positive ion mode.

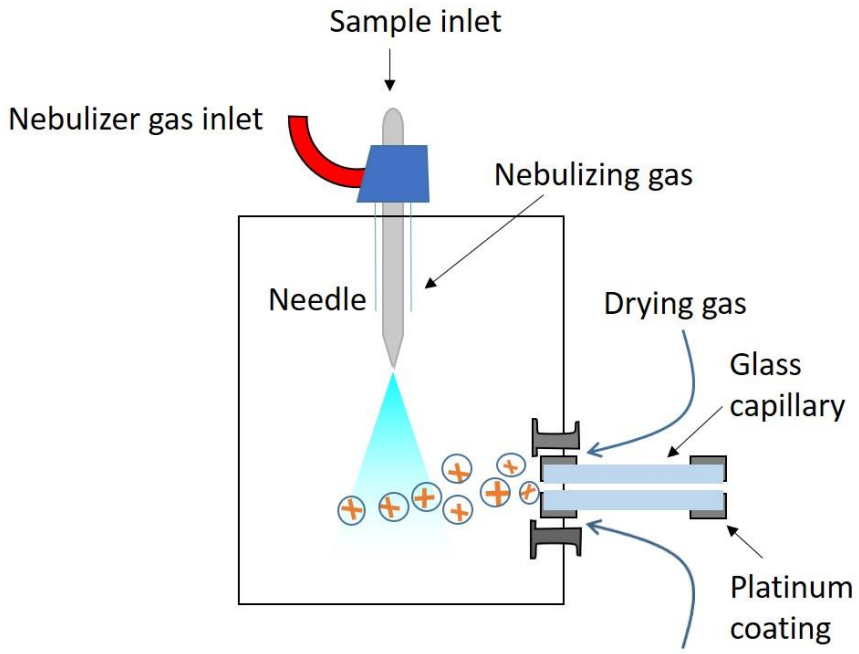

Figure 2.1 Schematic of electrospray ionization.

During the ESI process the sample solution travels through a thin metal needle and is introduced into a strong electric field, as shown in Figure 2.1. The perpendicular arrangement of the needle to the capillary minimizes the entry of neutrals into the mass analyzer. On the Bruker

HCTultra, the electric field is formed by keeping the needle at ground and placing a high voltage of negative 3-4 kV on the capillary entrance and end cap electrode when producing positive ions. The potential difference between the capillary and needle creates an electric field that assists in charging the droplets. The surface of the solution acquires a net positive charge (when in positive ion mode), and the liquid at the tip of the needle forms a Taylor cone. A nebulizing gas at 5-10 psi flows parallel to the needle to assist in formation of the Taylor cone. These droplets undergo desolvation to form quasi-molecular ions. Desolvation is assisted by a drying gas set at a constant temperature and pressure. The drying gas temperature is typically 200-250°C with a flow rate of ~5 L/min. The drying and nebulizing gas are both nitrogen in the Bruker HCTultra. Some debate exists as to the mechanism by which quasi-molecular ions are formed in ESI.[2,4,8-16] In the charge density or single ion droplet theory, these droplets break apart due to Coulombic explosions as the reach the Rayleigh limit. The Rayleigh limit is the point at which the surface tensions are overcome by the charge density. As the drying gas evaporates the solvent, the droplets shrink and repeatedly undergo the Coulombic explosion process until each remaining droplet only contains one single ion. According to the ion evaporation theory, ions are ejected directly from the droplet as they emerge from the tip of the Taylor cone. Schematics of both mechanisms can be seen in Figure 2.2. Regardless of the mechanism, highly (positively) charged droplets emerge from the tip of the cone, are desolvated, and travel through a potential gradient to the capillary entrance. The capillary is glass, where both sides are coated with platinum to allow different voltages to be applied to the exit and entrance. Ions leave the capillary and are held in a storage octupole until they are pulsed through the partition to a region of decreased pressure, then into the QIT through an octupole guide and electrostatic lenses as seen in Figure 2.3.

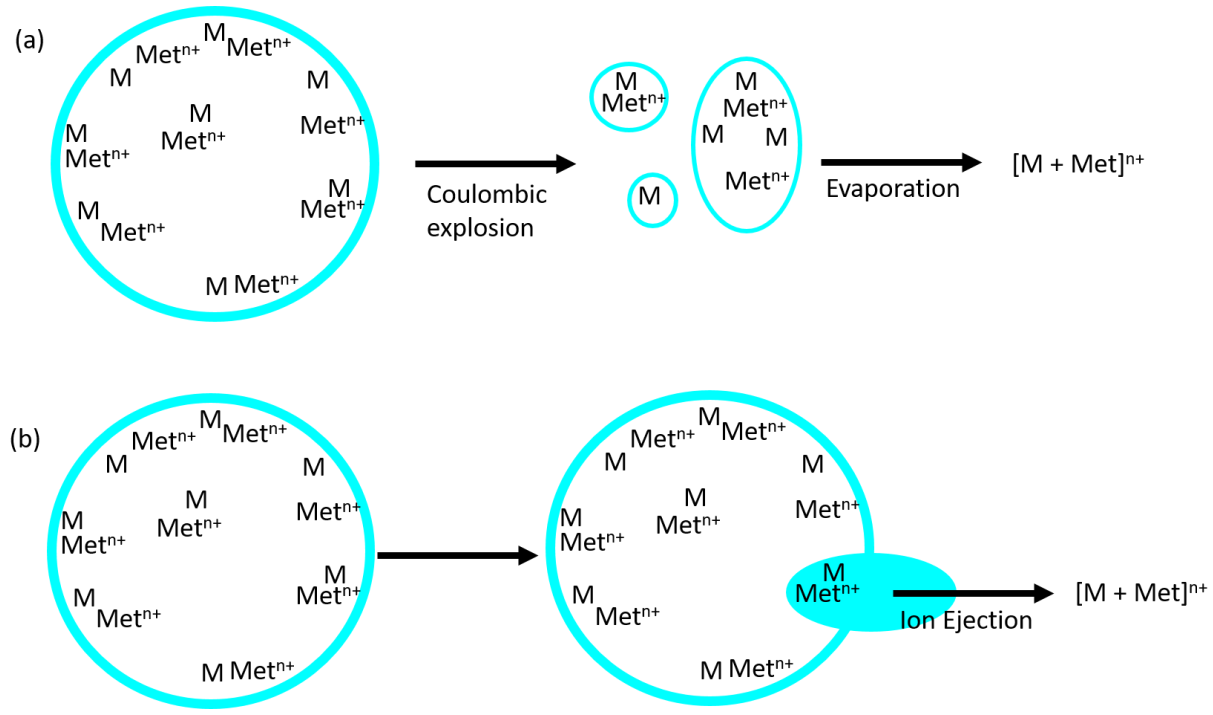

Figure 2.2 Comparison of electrospray ion formation mechanisms: (a) charge density theory and (b) single ion droplet theory, where M represents the organic molecule and Met^{n+} represents the metal cation.

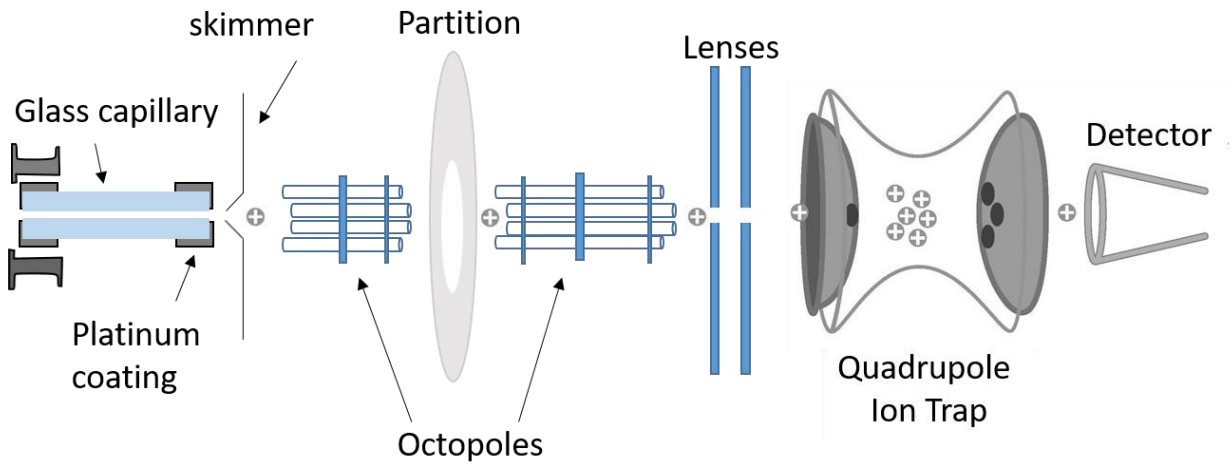

Figure 2.3 Schematic showing transfer of ions from the ESI source to the QIT in the Bruker HCTultra.

2.3 Quadrupole Ion Trap

The QIT was developed by Wolfgang Paul as the radiofrequency (RF) ion trap in 1955 and was originally called the Paul trap.[17] Paul shared the 1989 Nobel prize in Physics for this work.[18] A QIT is formed with three stainless steel electrodes: one ring electrode and two endcap electrodes. The ions enter the ion trap through a hole in one of the endcap electrodes, and their kinetic energy is cooled by collisions with helium (He) atoms in the bath gas. Upon entering the trap, ions are guided to the center of the trap by the quadrupolar field that is established by an alternating current on the ring electrode. The field in a QIT is uncoupled, meaning the forces along the x, y, and z axes are independent of one another, and may be determined separately. Various voltages applied to these electrodes form a "potential well" and can trap both positive and negative ions. If an ion drifts away from the center of the trap, the electric field will guide it back, working as a restoring force. The QIT on the Bruker HCTultra is a high capacity spherical ion trap (HCT).[19] The HCT has an optimum geometry and applies RF voltages to all three electrodes, which results in a spherical cloud of ions in the center of the trap. He is contained in the trap as a bath gas at pressures of ~10^{-5} Torr to cool the ions and assist in trapping. The ions being close together in the center of the trap increases trap storage capacity and also facilitates the overlap of ions for MS/MS reactions. In a trap of ideal geometry,

$$r_0^2 = 2z_0^2 \qquad (2.1)$$

where r_0 is the distance from the center of the trap to the ring electrode and z_0 is the distance from the center to one endcap electrode.[20-22]

The general expression, written in cylindrical polar coordinates for a quadrupole potential takes the form:

$$\Phi_{(r,z)} = A(r^2 - 2z^2) + C \qquad (2.2).$$

The constants A and C are determined by the boundary conditions on the electrodes and have the following values defined in equations 2.3 and 2.4 for a set of electrodes with shapes that can be seen in Figure 2.4.

$$A = \frac{\Phi_0}{r_0^2 + 2z_0^2} \qquad (2.3)$$

$$C = \frac{2\Phi_0 z_0^2}{r_0^2 + 2z_0^2} \qquad (2.4)$$

Where,

$$\Phi_0 = \Phi_0^R - \Phi_0^E \qquad (2.5)$$

and Φ_0^R and Φ_0^E are the potentials applied to the ring and endcap electrodes, respectively. It is important to note that in typical QIT operating conditions, the endcaps are grounded so, $\Phi_0^E = 0$.

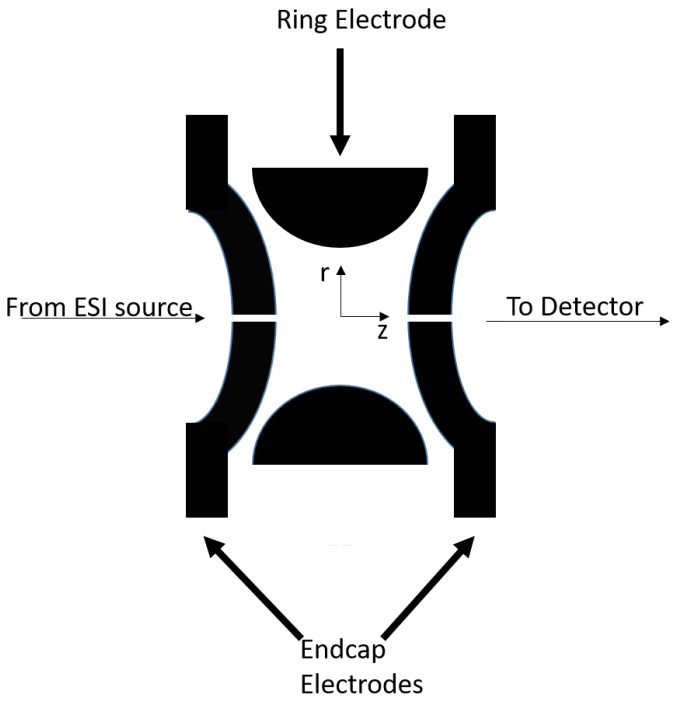

Figure 2.4 "Cut away" view of the quadrupole ion trap.

With the knowledge that the endcap electrode is at 0 V (ground), and combining equations 2.1, 2.2, 2.3, and 2.4, the potential felt by an ion at location r, z within the trap can be expressed as

$$\Phi_{(r,z)} = \frac{\Phi_0^R\ (r^2-2z^2)}{2r_0^2} + \frac{\Phi_0^R}{2} \qquad (2.6).$$

Typically, Φ_0^R is chosen to be some combination of RF and DC voltages such that

$$\Phi_0^R = U + V\ cos\omega t \quad (2.7).$$

U is the amplitude of the direct current (DC) voltage, V is the amplitude of the RF voltage, ω is the RF frequency, and t is time.

The potential that is felt by an ion will affect the ions motion in the QIT. In general, the force exerted in the u direction (where u represents either the r or z directions) on a charged particle in a field is expressed by

$$F_u = ma = m\frac{d^2u}{dt^2} = -e\frac{\delta\Phi}{\delta u} \qquad (2.8)$$

Therefore,

$$F_r = m\frac{d^2r}{dt^2} = -\frac{er(Vcos\omega t+U)}{r_0^2} \qquad (2.9)$$

$$F_z = m\frac{d^2z}{dt^2} = \frac{2ez(Vcos\omega t+U)}{r_0^2} \qquad (2.10)$$

Ion motion is best described by Mathieu's second-order linear differential equation shown in equation 2.11.[20-22] In this equation u represents both r and z polar coordinates, ξ is a dimensionless parameter (ξ = ωt/2), ω is frequency, t is time, and a_u and q_u are known as dimensionless trapping parameters. The "a" parameter is directly proportional to the applied DC voltage and inversely proportional to mass, while "q" is directly proportional to the applied RF amplitude and inversely proportional to the mass.

$$\frac{d^2u}{d\xi^2} + (a_u - 2q_u cos2\xi) = 0 \qquad (2.11)$$

Substitution of ωt/2 for ξ in equation 2.11 gives

$$\frac{d^2u}{dt^2} = \frac{\omega^2}{4}\frac{d^2u}{d\xi^2} \qquad (2.12).$$

Substitution of equation 2.11back into equation 2.12, followed by multiplication by mass of the ion m and rearrangement gives

$$m\frac{d^2u}{dt^2} = -m\frac{\omega^2}{4}(a_u - 2q_u cos2\omega t)u \qquad (2.13).$$

The left-hand side of equation 2.13 has previously been represented in equation 2.8 and can be considered the force on an ion in all directions u. The right-hand sides of equations 2.13 and 2.9 and 2.10 can be compared. Recalling that u represents polar motion in both the r and z directions allows the force to be expressed in terms of the dimensionless trapping parameters a and q as shown in equations 2.14, 2.15, 2.16, and 2.17, where z is an ion's nominal charge and e is the charge of an electron.

$$a_r = \frac{4zeU}{mr_0^2\omega^2} \quad (2.14) \quad \text{and} \quad a_z = -\frac{8zeU}{mr_0^2\omega^2} \quad (2.15)$$

$$q_r = -\frac{2zeV}{mr_0^2\omega^2} \quad (2.16) \quad \text{and} \quad q_z = \frac{4zeV}{mr_0^2\omega^2} \quad (2.17)$$

The solutions to these derivations represent solutions to the Mathieu equation, expressed as regions of "stability" or "instability" of ions and can be used to determine whether ions possessing a particular *m/z* will remain confined in the trap under a given set of conditions. The solutions to the Mathieu equation, in terms of a and q can be represented graphically as shown in Figure 2.5.

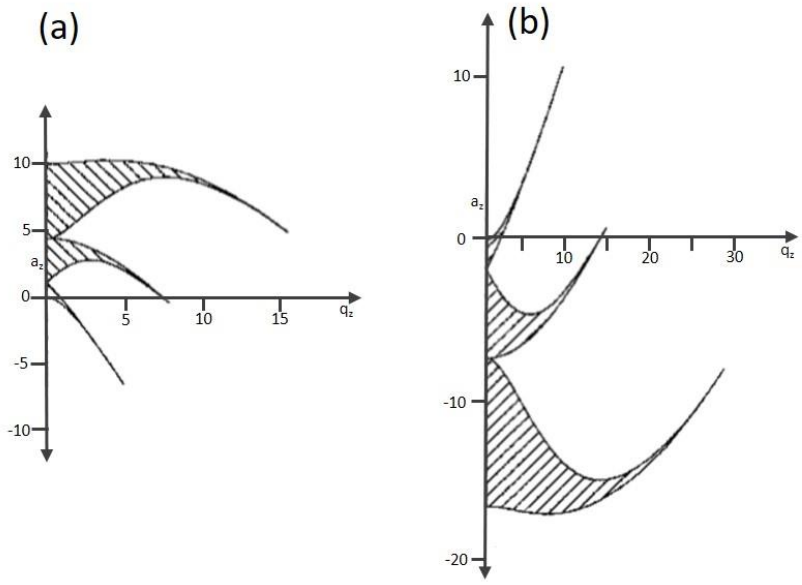

Figure 2.5 Solutions to the Matthieu equation, showing three stability regions in (a_z, q_z) space: (a) the z-direction and (b) the r-direction of the ion trap. Reproduced and modified from reference 21, with permission of John Wiley & Sons, Ltd.

Figure 2.5 presents two plots of a_z versus q_z and a_r versus q_r, where the shaded regions represent where the trajectory of an ion will be "stable" in either the z(a) or r(b) direction and remain within the bounds of the trap. However, conditions under which the ion will be stable in both the r and z directions are required. Therefore, the two aforementioned graphs must be plotted on the same axes (a_z, q_z) and the regions of overlap must be noted, as shown in Figure 2.6 and Figure 2.7. At a particular V, all ions above a specific mass-to-charge-ratio (*m/z*) remain trapped according to q_{max} for a certain instrument. q_{max} is the intersection of q_z with the stability boundary, and for most QITs is 0.908.[20-22] The relationship between ionic *m/z* and q_{max} can be seen in equation 2.18.

$$\frac{m}{z} = \frac{4eV}{q_{max}\omega^2 r_0^2} \qquad (2.18)$$

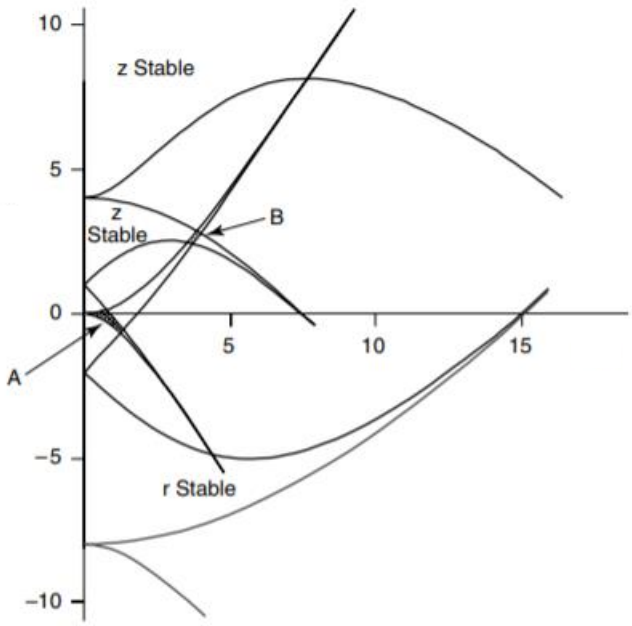

Figure 2.6 Mathieu stability diagram in (a_z, q_z) space, denoting regions of overlap. Reproduced from reference 21 with permission of John Wiley & Sons, Ltd.

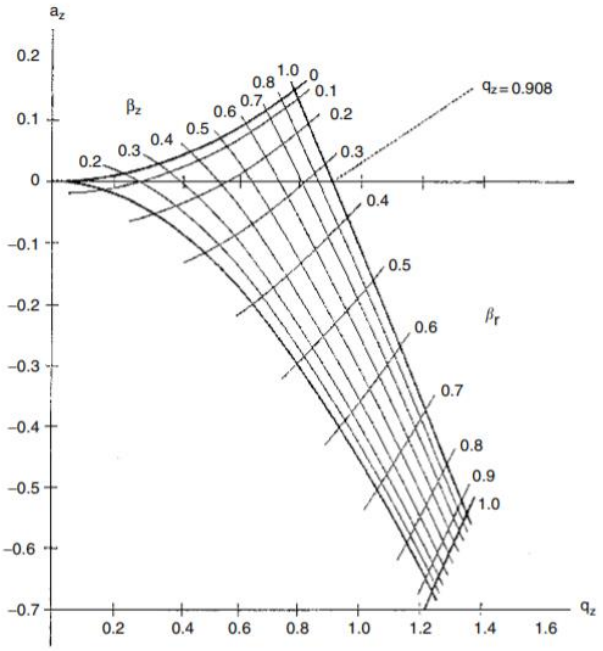

Figure 2.7 Mathieu stability diagram in (a_z, q_z) space for the region of simultaneous stability A in both the r- and z-directions. Reproduced from reference 21, with permission of John Wiley & Sons, Ltd.

Detection occurs as the ions cross the stability boundary in the z direction and can therefore be ejected through small holes in the endcaps of the trap. To detect all ions in the trap, the ions will be pushed to the right of the stability diagram, over the z-stability boundary by a linear ramp of the RF amplitude. The ions exit the trap and enter a region of higher vacuum, where they are detected by a Daly detector. Since RF amplitude and *m/z* map linearly to each other for a given q_z value, the raw signal versus time data is easily translated into signal vs *m/z*. The Daly detector consists of a metal conversion dynode "door knob," a phosphor screen, a glass or quartz window, and a photomultiplier as can be seen in Figure 2.8.

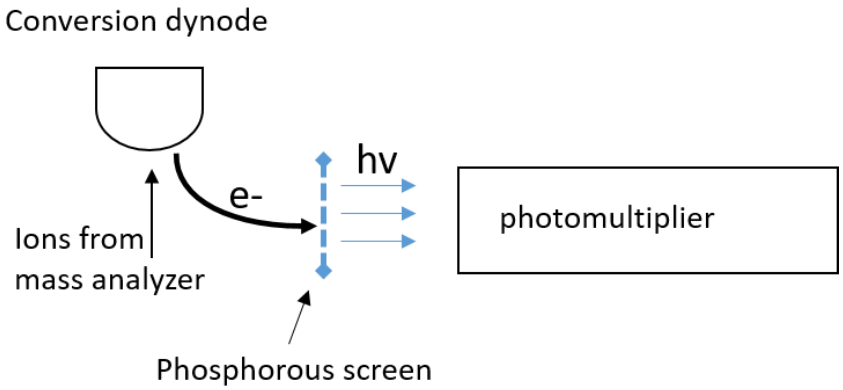

Figure 2.8 Schematic of Daly detector.

The phosphor screen prevents the ions and neutrals from coming into contact with the photomultiplier and greatly increases the lifetime of the detector. Ions hit the metal conversion dynode and release secondary electrons that pass through the phosphor screen and are converted into photons. The photons then pass through a quartz window and strike a photomultiplier tube (PMT), which operates as an electron multiplier following the photo-emissive surface. Several dynodes are separated from each other, where each sequential dynode is 100-200 V more

positive potential than the previous. At each dynode every electron hitting the dynode induces emission of multiple electrons, which will accelerate to the next metal plate and induce emission of more electrons. A gain of as much as 10^7 electrons is possible. These emitted electrons strike the surface opposite the dynode funnel, and an electrical current is measured, which relates to the intensity of the ion at the *m/z* being detected.

2.4 Tandem Mass Spectrometry (MS/MS)

Combining more than one stage of mass analysis can be very useful for identifying compounds in complex mixtures, for determining the structures of unknown species, and even for differentiating isomeric species. This technique utilizing multiple stages of mass analysis is known as tandem mass spectrometry (MS/MS or MS^n). From a mixture of ions collected in the QIT, ions of a particular *m/z* value are selected and isolated. Isolation of an ion of a particular *m/z* is completed in two different steps because ions with a lower *m/z* are ejected in a different manner from the trap than those with higher *m/z*. As discussed previously, the ring electrode restricts ions to the center of the ion trap at low voltages, but at higher voltages exists a point where the ion is ejected out of the trap in the z direction (Figure 2.4). This was described by equation 2.17, where q_z is a unitless value that determines at which point ions in the quadrupolar field become unstable (usually $q_z > 0.908$). This method of ejection ions from the trap as they become unstable is called "mass selective instability." The voltage (V) necessary on the ring electrode to eject a given ion can be calculated because the radius of the ion trap is constant, as is the alternating current (AC) frequency on the ring electrode.

$$V = \frac{r^2 \omega^2 q_z m}{4ze} \quad (2.19)$$

Based on this fundamental stability equation, why ions with masses higher than the ion of interest cannot be ejected using mass selectivity instability is easily understood. The voltage

required to eject an ion increases as the *m/z* increases; therefore, ejecting any ion with a higher *m/z* than the ion of interest would also eject the ion being isolated. Thus, higher mass ions must be ejected in a different way. Higher mass ions are ejected by taking advantage of the fact that an ion trapped in a quadrupolar field will be moving in a somewhat undefined path at any given frequency. This frequency is called the "axial secular frequency", and the motion is comparable to each ion traversing back and forth in the QIT in a path along a surface of a p-orbital that may be as wide as the trap itself. The frequency of any given ion is related to its q value, so ions of higher mass (lower q value at given ring voltage) have a lower frequency than ions with a lower mass. Every ion with a unique *m/z* has a unique axial secular frequency. Ions can be selectively ejected by applying a frequency on the end-cap electrodes that exactly matches the ions axial secular frequency. This "resonant" excitation accelerates the specific ions trajectory in the z direction, and thus ejects the ion out of the QIT.[20-22]

A visual representation of these two ejection processes can be seen in Figure 2.9. The three graphs are on the same time scale but represent different processes. In graph (a), the voltage on the ring electrode is increased over time, which corresponds to the ions below *m/z* 600 being ejected as their q_z value exceeds 0.908, which is shown on graph (b). After ejection of the lower mass ions, the voltage on the ring electrode is dropped to maintain a q_z value of 0.25 for the ions remaining in the QIT. Graph (c) then depicts the scanning down of axial secular frequencies of the remaining ions that are higher than 604 *m/z* in order to eject them from the trap via resonant excitation. Once the ion of interest is isolated, different types of ion fragmentation can take place.

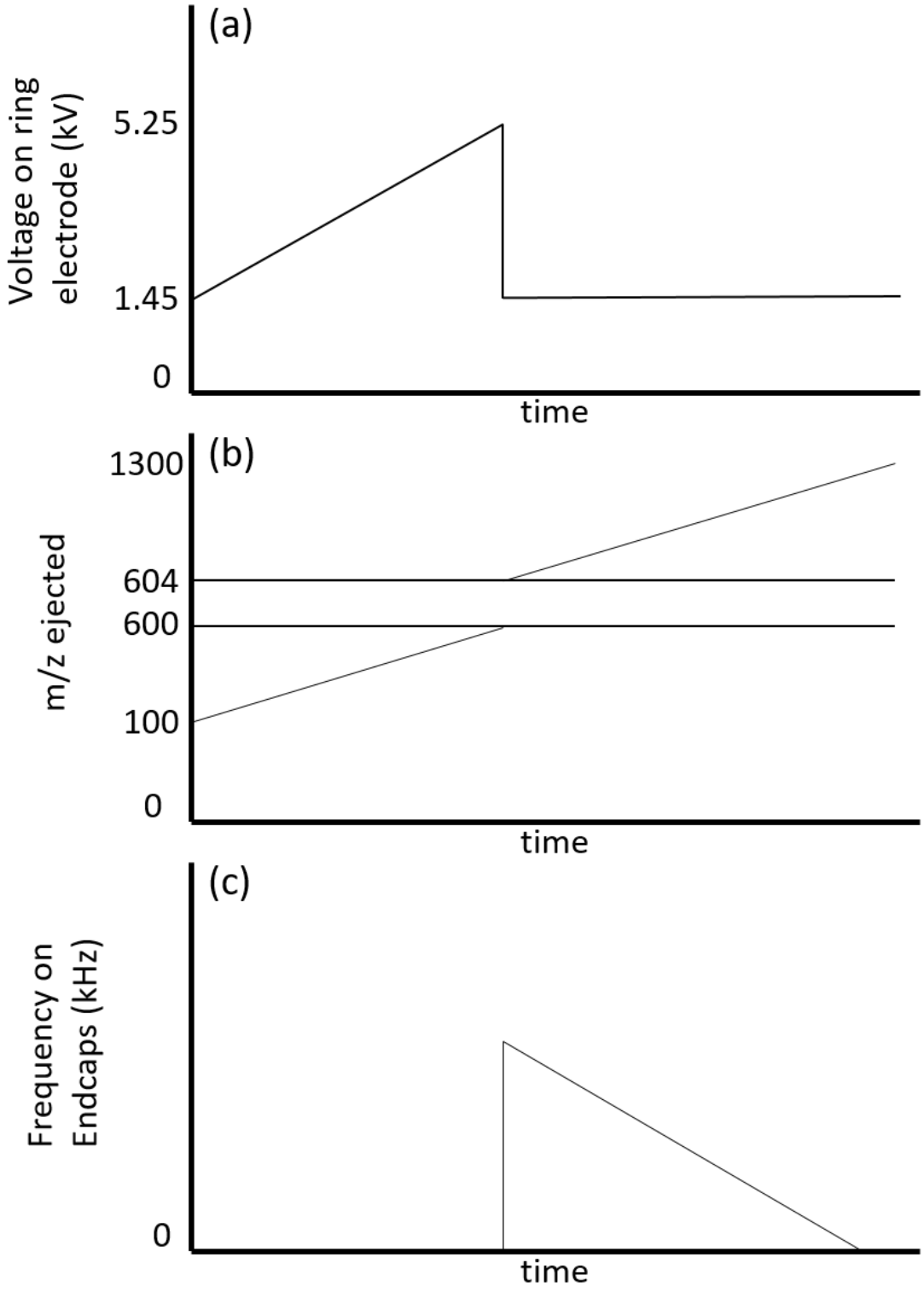

Figure 2.9 A graphical depiction of ion isolation (a) ejecting ions below *m/z* 600 by increasing the voltage on the ring electrode, (b) *m/z* of ions ejected over time, and (c) ejection of ions above *m/z* 604 by resonant excitation using axial secular frequencies on the endcaps.

2.4.1 Collision-Induced Dissociation

Electrospray ionization generally produces low energy quasi-molecular ions with little to no fragmentation in the ion source. These ions can be dissociated in the QIT via collision-induced dissociation (CID) or collisionally activated dissociation (CAD) to produce sequence informative fragmentation.[21] Collision-induced dissociation is the most common method of MS/MS and occurs in three steps in time in the QIT: isolation, dissociation, and analysis. After the ion of interest is isolated, as discussed in Section 2.4, it must be "activated." The activation process is similar to the process used to eject high *m/z* ions. The ion is held at a low q_z value and then excited for a short amount of time using an AC voltage applied to the endcap electrodes at the axial secular frequency of the ion. The voltage must be high enough that the ion can gain kinetic energy, but not so high that the ion is ejected from the QIT. The kinetic energy will accelerate the ion in the z direction where it will collide with the He gas that is present in the trap. The He gas in a QIT serves as both a bath gas to collisionally cool the ions and also as the CID collision gas. As the ions experience multiple collisions with the He bath gas, the kinetic energy of the ions can be transferred to internal vibrational energy, which is distributed along the ion inducing unimolecular dissociation. The process of CID can be expressed as two separate events, collisional activation and then unimolecular dissociation, which are shown in the following equations 2.19 and 2.20 where m_1 is the precursor ion, He is the helium collision gas, He′ is the helium atom after collision, and m_2^+ and m_3 are the products of the collision.

Collisional activation: $m_1^+ + He \rightarrow m_1^{+*} + He'$ (2.20)

Unimolecular dissociation: $m_1^{+*} \rightarrow m_2^+ + m_3$ (2.21)

The product ions are detected through ion ejection, or one product ion can be isolated for another CID experiment.

Typically, two types of CID: high energy (3-10 keV collision energies) and low energy (1-100 eV collision energies) are utilized. The experiments described in this dissertation are low energy CID, which is the only CID experiment possible on the Bruker HCTultra PTM Discovery system. For carbohydrates, low energy CID typically breaks the glycosidic bonds in the molecule, which leads to limited linkage information.[23-25]

2.4.2 Electron Transfer Dissociation

The more recent MS/MS electron-based dissociation (ExD) techniques have been very promising to biomolecule sequencing since the emergence of electron capture dissociation (ECD) in 1998.[26] Electron transfer dissociation (ETD) was invented by Hunt and co-workers in 2004.[27] Unlike CID, ETD is a non-ergodic process that produces more complete biomolecule sequence coverage due to randomized cleavages and preservation of post translational modifications (PTMs) in peptides, as well as sites of glycosylation in carbohydrates. Multiply charged precursor ions are necessary for ETD to prevent the transfer of an electron from neutralizing the ion of interest. In ETD, radical anions are produced in the negative chemical ionization (nCI) source and then transferred into the QIT where the multiply charged precursor ions have been trapped. The location of the nCI source and the transfer optics can be seen in Figure 2.10. The ETD reagents such as anthracene or fluoranthene have low electron affinities. These reagents first capture electrons that are produced in a two-step process, where an electron ionization (EI) filament at 75 eV emits high energy electrons that interact with methane in the nCI source to produce low energy electrons. After the ETD reagent captures the low energy electron, the resulting radical anion is transferred to the QIT via electrostatic focusing. The reagent ion (fluoranthene) and the

multiply charged precursor ion undergo an ion/ion reaction. The now charge reduced precursor ion undergoes recombinative dissociation producing fragment ions. This process is shown in Figure 2.11.

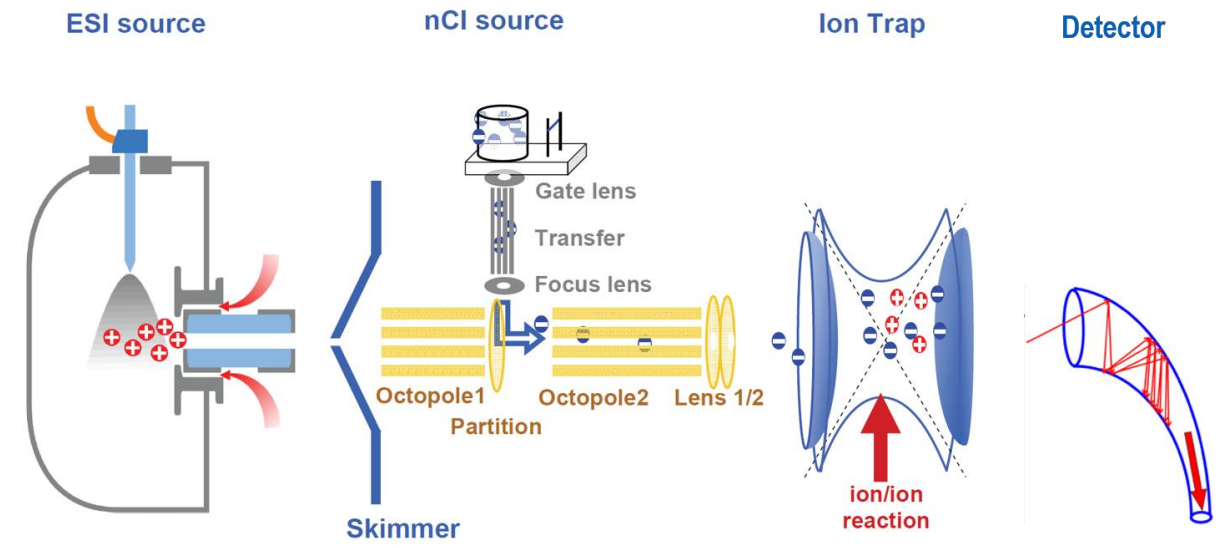

Figure 2.10 Schematic of Bruker HCTultra PTM Discovery System showing the nCI source and the process of ETD with positive and negative ions in the QIT. (used with permission from reference 5)

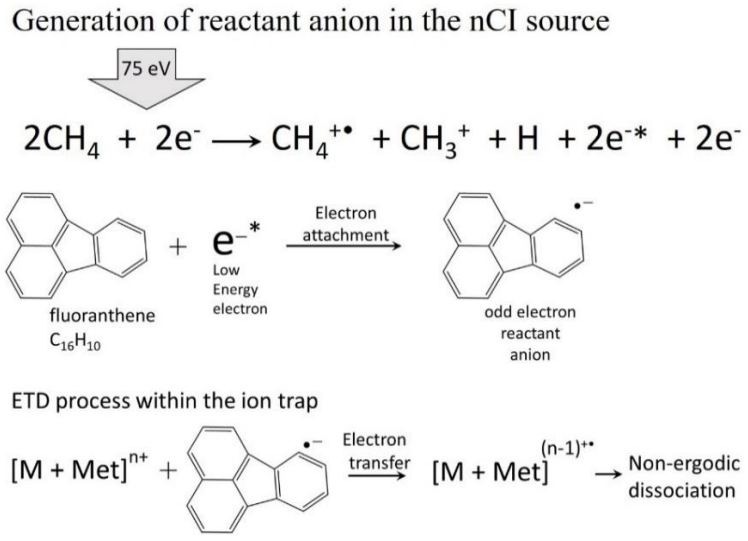

Figure 2.11 ETD process in the nCI source and QIT.

The non-ergodic nature of ETD produces different product ions than CID and the resulting spectra are complementary. Occasionally an electron is transferred, and no dissociation occurs in a process known as electron transfer no dissociation (ETnoD). "Smart decomposition" is a process in which ETD occurs followed by resonant excitation at very low energy; this minimizes ETnoD and enhances ETD product ion formation by removing hydrogen bonds that may hold the fragment ions together. The mechanism of ETD for metallated carbohydrate ions as examined in this dissertation is uncertain, but Costello and co-workers[28] proposed that the electron is captured at the metal ion, reducing the metal ion. The reduced metal ion then abstracts a hydroxyl group from the sugar, forming a carbon radical that induces fragmentation. This is discussed in more detail in Chapters 3 and 5.

2.5 Oligosaccharide Structures

Carbohydrates are one of the four major classes of biomolecules. Unlike proteins and nucleic acids, oligosaccharide biosynthesis is not template driven. The building blocks of oligosaccharides are monosaccharides. Figure 2.12 shows common monosaccharides found in mammalian biological systems. Monosaccharides can be aldehydes or ketones, known as aldoses or ketoses, respectively, with multiple hydroxyl groups. Many of the monosaccharides shown in Figure 2.12 have multiple diastereomeric forms that can evolve from any of the carbons on the ring and form many different epimers. For example, glucose, galactose, and mannose in Figure 2.12 are epimers that vary at one diastereomeric position. In addition, these monosaccharides may be modified by enzymes to form amino or acidic monosaccharides with amines, acetylated amines, or carboxylic acids replacing the hydroxyl groups. The amines and hydroxyl groups on the monosaccharides can also be phosphorylated or sulfated. These

modifications create a vast amount of structural complexity in the monosaccharide building blocks.

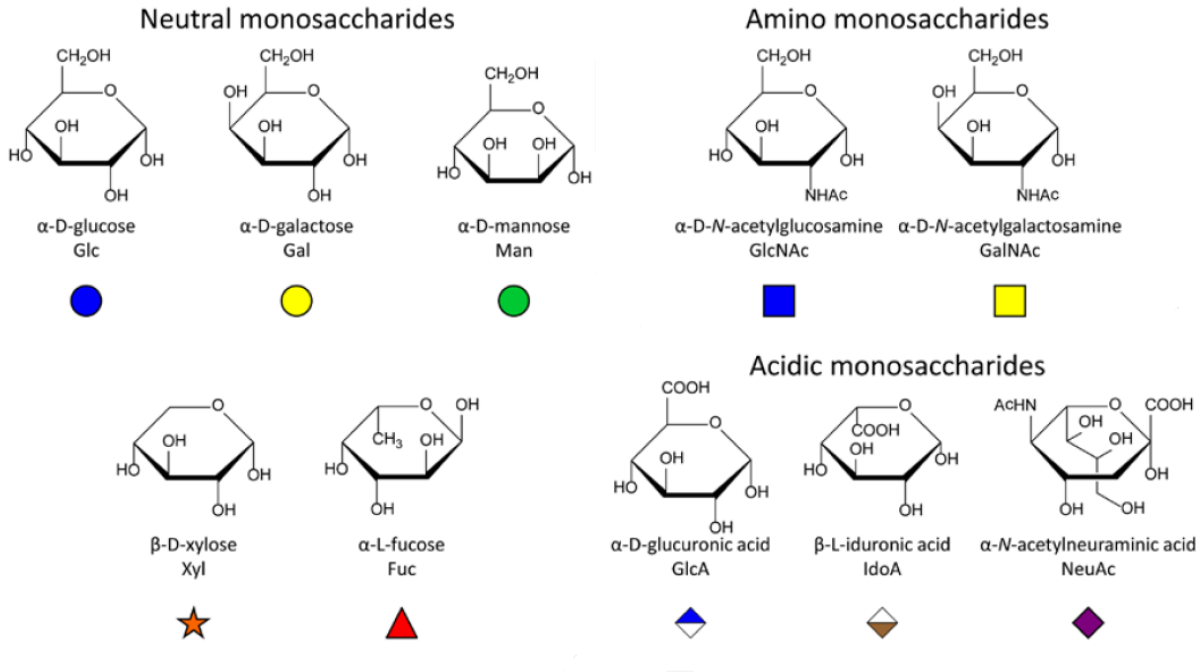

Figure 2.12 The structure, names, and symbols of some common monosaccharides found in biological systems.

Chains of carbohydrates are formed by glycosidic bonds between the hemiacetal group on one monosaccharide to a hydroxyl group on a second monosaccharide. The anomeric configuration of the C-1 carbon determines if the glycosidic bond is an α-glycosidic bond or β-glycosidic bond. Large linear and branched oligomers are found when one or more of the monosaccharide units has multiple glycosidic bonds connected to other monosaccharide residues. In order to assist in visualizing this structural complexity, a symbolic nomenclature for glycans (SNFG) was created.[29] The SNFG nomenclature can be seen in Table 2.1 and consists of many rules, including use of the same shading/color for all monosaccharides with the same

stereochemistry. Also, symbols should be logical and easy to remember, and modifications of monosaccharides will be indicated with small attached letters, using numbers to indicate linkage positions. This symbolic nomenclature makes visually representing oligosaccharides much easier, especially as they become larger or contain branching. The carbon contained in the glycosidic bond is represented by the position of the line coming off the shape or labeled, α-glycosidic bonds are shown as dashed lines, and β-glycosidic bonds are shown as solid lines. An example of using the symbols to represent a larger glycan and the way glycosidic bond position is represented can be seen in Figure 2.13.

The oligosaccharides studied in this dissertation were reducing tetrasaccharides maltotetraose (α-D-Glc-(1→4)-α-D-Glc-(1→4)-α-D-Glc-(1→4)-Glc), which was purchased from MP Biomedicals (Santa Ana, CA, USA); 3α,4β,3α-galactotetraose (α-D-Gal-(1→3)-β-D-Gal-(1→4)-α-D-Gal-(1→3)-D-Gal), from Santa Cruz Biotechnology (Dallas, TX, USA); reducing heptasaccharide maltoheptaose (α-D-glc-(1→4)-α-D-Glc-(1→4)-α-D-Glc-(1→4)-α-D-Glc-(1→4)-α-D-Glc-(1→4)-α-D-Glc-(1→4)-Glc), from Sigma-Aldrich (St. Louis, MO, USA); non-reducing tetrasaccharides nystose (β-D-Fru-(2→1)-β-D-Fru-(2→1)-β-D-Fru-(2↔1)-α-D-Glc), from Sigma-Aldrich (St. Louis, MO, USA); and stachyose (α-D-Gal-(1→6)-α-D-Gal-(1→6)-α-D-Glc(1↔2)-β-D-Fru), from Acros Organics (Morris Plains, NJ, USA). The symbolic structure of these oligosaccharides can be seen in Figure 2.14 and the expanded structure can be seen in Figure 2.15.

Table 2.1 Symbolic nomenclature for glycans.

SHAPE	White (Generic)	Blue	Green	Yellow	Orange	Pink	Purple	Light Blue	Brown	Red
Filled Circle	Hexose	Glc	Man	Gal	Gul	Alt	All	Tal	Ido	
Filled Square	HexNAc	GlcNAc	ManNAc	GalNAc	GulNAc	AltNAc	AllNAc	TalNAc	IdoNAc	
Crossed Square	Hexosamine	GlcN	ManN	GalN	GulN	AltN	AllN	TalN	IdoN	
Divided Diamond	Hexuronate	GlcA	ManA	GalA	GulA	AltA	AllA	TalA	IdoA	
Filled Triangle	Deoxyhexose	Qui	Rha		6dGul	6dAlt		6dTal		Fuc
Divided Triangle	DeoxyhexNAc	QuiNAc	RhaNAc			6dAltNAc		6dTalNAc		FucNAc
Flat Rectangle	Di-deoxyhexose	Oli	Tyv		Abe	Par	Dig	Col		
Filled Star	Pentose		Ara	Lyx	Xyl	Rib				
Filled Diamond	Deoxynonulosonate		Kdn				Neu5Ac	Neu5Gc	Neu	Sia
Flat Diamond	Di-deoxynonulosonate		Pse	Leg		Aci		4eLeg		
Flat Hexagon	Unknown	Bac	LDmanHep	Kdo	Dha	DDmanHep	MurNAc	MurNGc	Mur	
Pentagon	Assigned	Api	Fru	Tag	Sor	Psi				

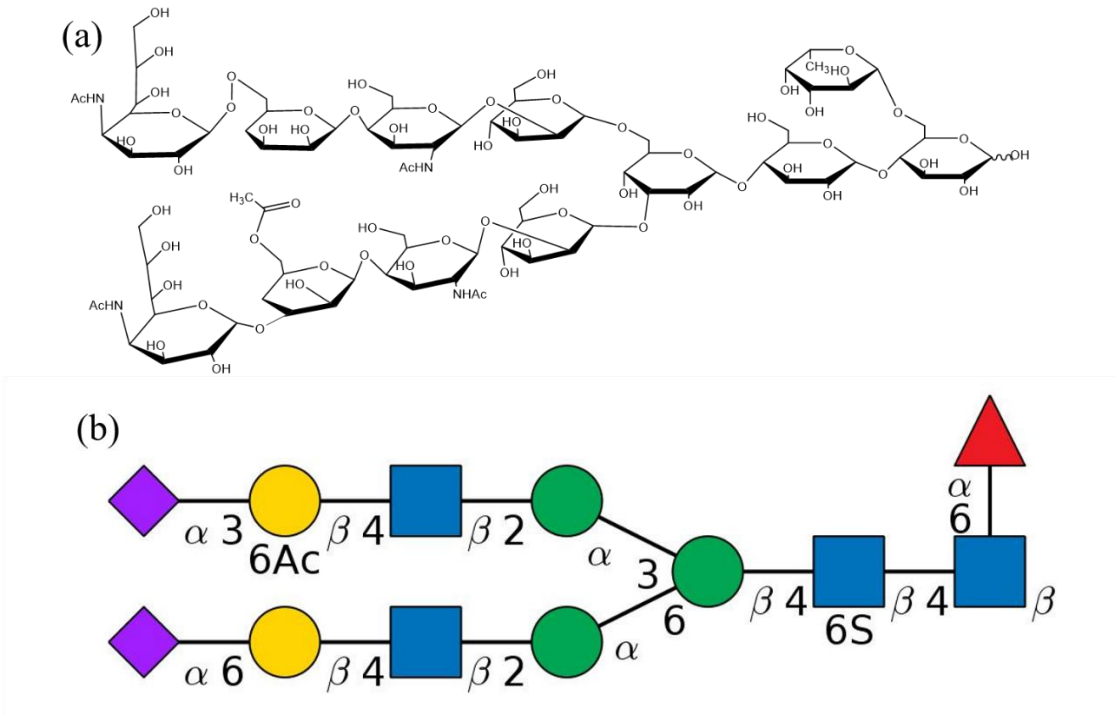

Figure 2.13 An example of symbolic representation of a branched glycan. (a) The structure of a branched glycan that includes 12 monosaccharides with three branches and (b) the SNFG symbolic representation of the same 12 monosaccharides.

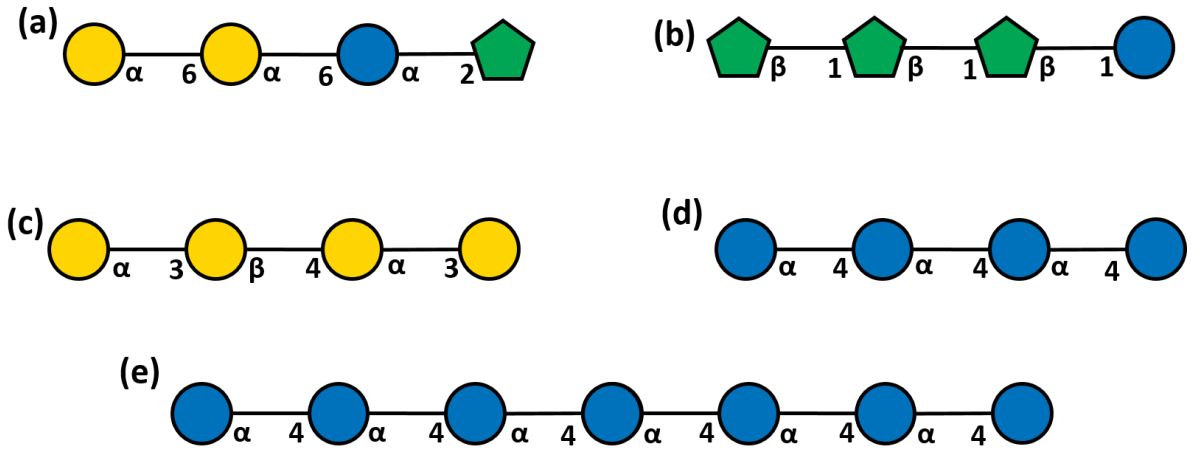

Figure 2.14 Symbolic representation of oligosaccharides included in this study: (a) stachyose, (b) nystose, (c) 3α,4β,3α-galactotetraose, (d) maltotetraose, and (e) maltoheptaose.

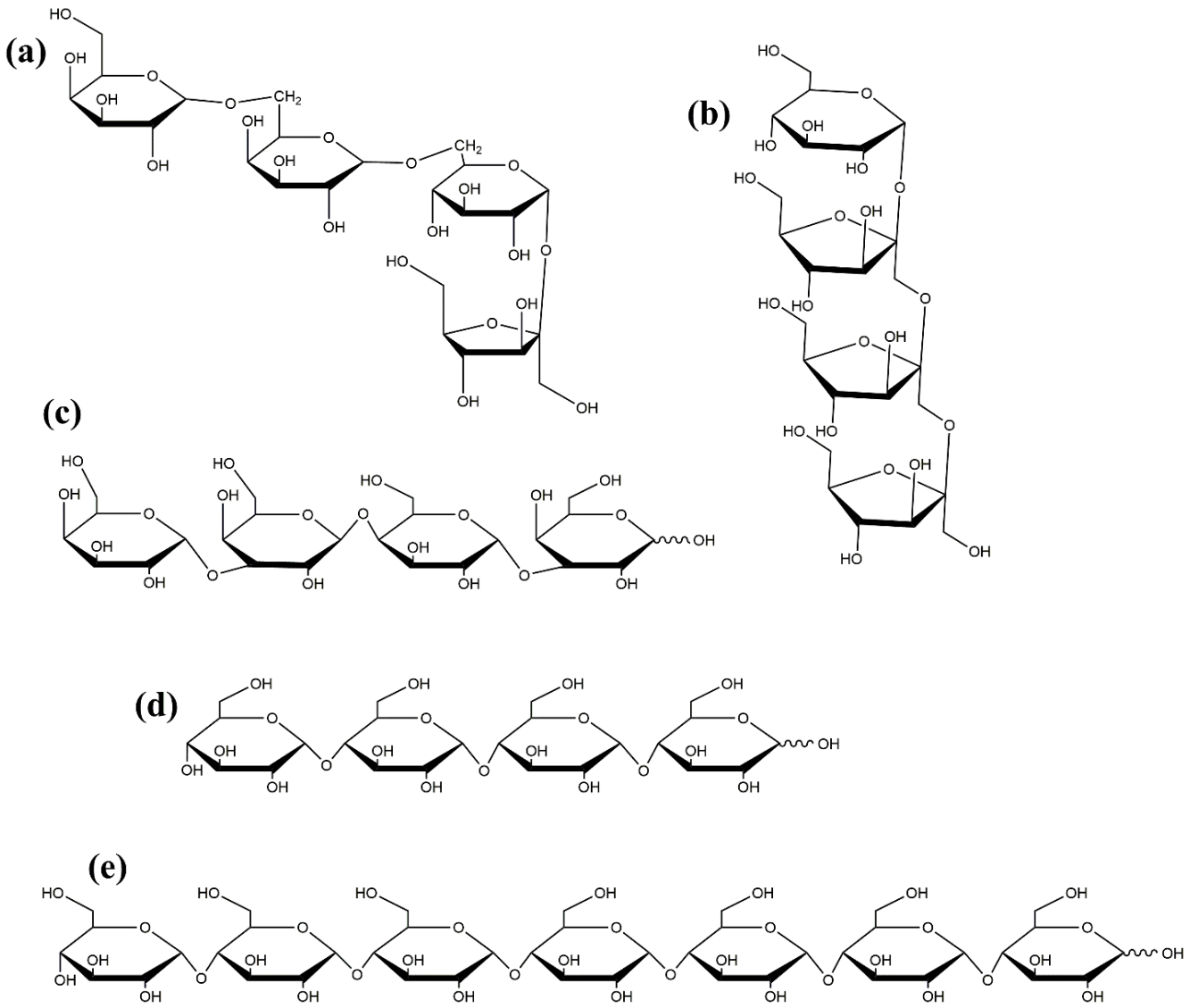

Figure 2.15 Expanded structures of oligosaccharides included in this study: (a) stachyose, (b) nystose, (c) 3α,4β,3α-galactotetraose, (d) maltotetraose, and (e) maltoheptaose.

2.6 Derivatization of the Oligosaccharides

2.6.1 Isotopic Labeling of the Oligosaccharides

Isotopic ^{18}O labeling of reducing sugars was performed to allow for differentiation of product ions that result from the reducing end versus the non-reducing end of the oligosaccharides. In this dissertation, isotopic ^{18}O labeling of the reducing end oxygen in the reducing sugars maltotetraose, galactotetraose, and maltoheptaose was completed by dissolving enough oligosaccharide sample in 100 µL of $H_2{}^{18}O$ to create a 0.1 M sample solution. The samples were stored in sealed vials in a desiccator at room temperature for three weeks. During this time, the exchange of the reducing end ^{16}O in the oligosaccharides with ^{18}O occurred. Before MS analysis, the samples were diluted to 10 µM of oligosaccharide and prepared following the procedure previously discussed in Section 2.2.

2.6.2 Permethylation of the Oligosaccharides

Permethylation is a derivatization process in which all hydroxyl groups (-OH) in a carbohydrate are converted into methoxy groups ($-OCH_3$). In the research discussed in this dissertation, permethylation was completed using the procedure of Ciucanu and Kerek, as improved by Ciucanu and Costello.[30,31] Approximately 8 mg of oligosaccharide was dissolved in 1.0 ml of dimethyl sulfoxide (DMSO), after the sample is fully dissolved, 10 µL of Milli-Q ultra pure water (MQ H_2O) was added along with 70 mg of finely powdered sodium hydroxide (NaOH) (at least three equivalents per mol of replaceable hydrogen (H).) The sample was vortexed for two minutes to create a suspension. Finally, 122.5 µL (four equivalents per mol of replaceable H) methyl iodide (CH_3I) was added, and the sample was vortexed for five minutes and stirred vigorously with a stir bar for five minutes. The reaction was quenched with 2 ml of MQ H_2O and neutralized by adding 0.1 M hydrochloric acid (HCl) dropwise. The permethylated

products were extracted by washing the sample with 2 ml of dichloromethane (DCM), vortexing and centrifuging for two minutes. This was repeated five times on the aqueous layer, while combining the organic layers. The combined organic layers were then washed five times by adding 2 ml of MQ H_2O, vortexing, and centrifuging. The washed organic layers were transferred to a round bottom flask and rotovapped at 40°C. The sample was redissolved in 50:50 MeOH:H_2O to a final concentration of 2 mM. After derivatization, permethylated oligosaccharide samples were purified using Spectrum Labs (Waltham, MA, USA) Spectra/Por dialysis tubing to remove salts and derivatization byproducts.

2.7 Oligosaccharide Fragmentation Nomenclature

The widely used and accepted glycan fragmentation nomenclature was introduced by B. Domon and C.E. Costello in 1988 in order to describe the dissociation observed in high energy fast atom bombardment (FAB) MS/MS spectra.[32] As can be seen in Figure 2.16, charge retention on the non-reducing end of the oligosaccharide denotes the corresponding fragment ions as A_i, B_i, and C_i ions, where the subscript i represents the position of the monosaccharide as counted from the non-reducing end. When the reducing end of the glycan retains the charge the fragment ions are assigned as X_j, Y_j, and Z_j, where j represents the position of the monosaccharide as counted from the reducing end. A_i and X_j ions, shown in red represent cleavages across a glycan ring and are called cross-ring cleavages. These fragment ions require two bonds to be broken during dissociation to be observed in the spectrum. Glycan rings are numbered 0-5 starting from the oxygen in the ring. The two bonds broken in the cross-ring cleavage are indicated by numeric superscripts such as $^{0,2}A_1$ and $^{1,5}X_1$, as seen in Figure 2.16. B_i, C_i, Y_j, and Z_j ions shown in blue represent glycosidic bond cleavages. B_i and Z_j ions do not contain the glycosidic oxygen, whereas C_i and Y_j ions do. When a glycan contains branches, they

are represented using Greek letters as subscripts, α, β, γ, starting with the largest branch. Secondary branches are represented by superscript primes also in decreasing order of size such that α′ and α″ would indicate there are two secondary branches coming off of the α branch and that α′ is larger than α″.

The Domon-Costello nomenclature does not consider non-reducing sugars. For the non-reducing sugars used in this dissertation research, the parent monosaccharide is considered to be the reducing end. For stachyose, this is the fructose; and for nystose, the glucose unit. In Figure 2.15, all oligosaccharides studied in this dissertation are drawn with the reducing end (or parent monosaccharide) on the right except for nystose where the parent monosaccharide is on top of the molecule. All product ions contain metals ions and any loss or addition of hydrogen or any other neutrals from the product ions will be specifically noted; for example, $[Y_2 + Co - H_2O]^{2+}$, represents a Co metallated glycosidic fragment ion containing the glycosidic oxygen formed after cleavage of the first glycan ring with a neutral loss of water.

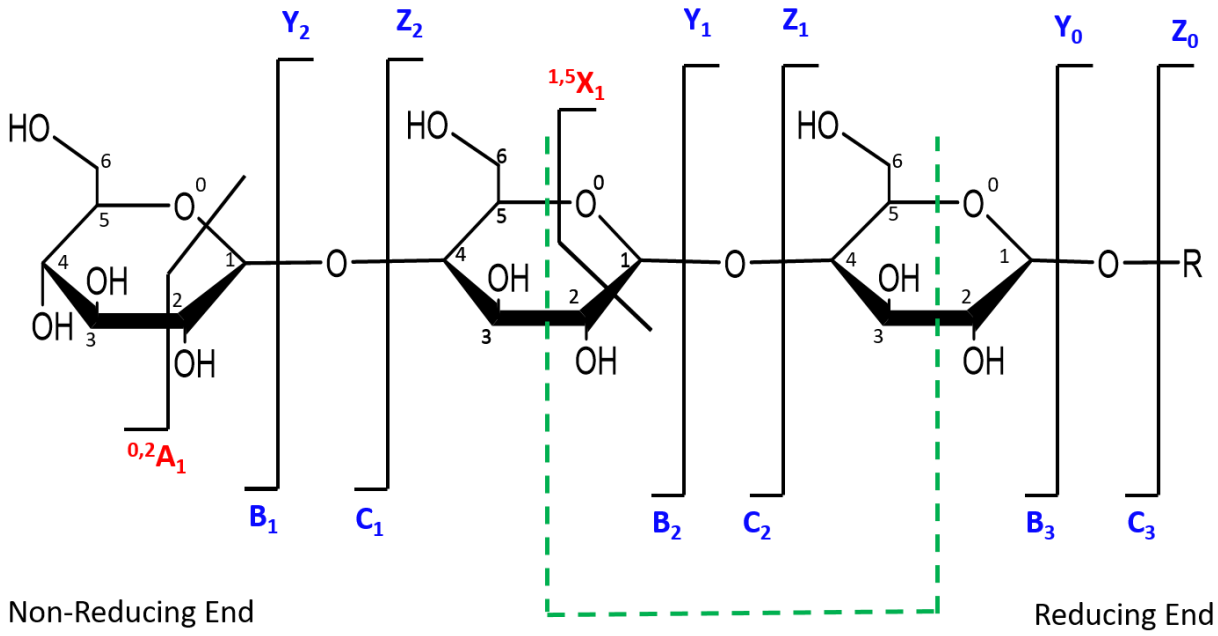

Figure 2.16 Glycan fragmentation nomenclature of Domon and Costello.

REFERENCES

1. Yamashita, M.; Fenn, J. B. Electrospray ion-source - another variation on the free-jet theme. *J. Phys. Chem.* **1984**, *88*, 4451-4459.

2. Fenn, J. B.; Mann, M.; Meng, C. K.; Wong, S. F. Electrospray ionization--principles and practice. *Mass Spectrom. Rev.* **1990**, *9*, 37-70.

3. Fenn, J. B.; Mann, M.; Meng, C. K.; Wong, S. F.; Whitehouse, C. M. Electrospray ionization for mass spectrometry of large biomolecules. *Science* **1989**, *246*, 64-71.

4. Dole, M.; Mack, L. L.; Hines, R. L. Molecular beams of macroions. *J. Chem. Phys.* **1968**, *49*, 2240.

5. Whitehouse, C. M.; Dreyer, R. N.; Yamashita, M.; Fenn, J. B. Electrospray ionization for liquid chromatographs and mass spectrometers. *Anal. Chem.* **1985**, *57*, 675-679.

6. Stacey, C. C.; Kruppa, G. H.; Watson, C. H.; Wronka, J.; Laukien, F. H.; Banks, J. F.; Whitehouse, C. M. Reverse-phase liquid chromatography/electrospray-ionization Fourier-transform mass spectrometer in the analysis of peptides. *Rapid Commun. Mass Spectrom.* **1994**, *8*, 513-516.

7. Ikonomou, M. G.; Blades, A. T.; Kebarle, P. Investigations of the electrospray interface for liquid-chromatography mass-spectrometry. *Anal. Chem.* **1990**, *62*, 957-967.

8. Gaskell, S. J. Electrospray: principles and practice. *J. Mass Spectrom.* **1997**, *32*, 677-688.

9. Smith, R. D.; Loo, J. A.; Loo, R. R. O.; Busman, M.; Udseth, H. R. Principles and practice of electrospray ionization - mass-spectrometry for large polypeptides and proteins. *Mass Spectrom. Rev.* **1991**, *10*, 359-451.

10. Kebarle, P. A brief overview of the present status of the mechanisms involved in electrospray mass spectrometry. *J. Mass Spectrom.* **2000**, *35*, 804-817.

11. Kebarle, P.; Peschke, M. On the mechanisms by which the charged droplets produced by electrospray lead to gas phase ions. *Anal. Chim. Acta* **2000**, *406*, 11-35.

12. Kebarle, P.; Heunghaw, H. On the mechanism of electrospray mass spectrometry. In *Electrospray Ionization Mass Spectrometry*; Cole, R. B., Ed.; Wiley: New York, 1997; pp 3-63.

13. Ikonomou, M. G.; Blades, A. T.; Kebarle, P. Electrospray-ion spray: A comparison of mechanisms and performance. *Anal. Chem.* **1991**, *63*, 1989-1998.

14. Wilm, M. S.; Mann, M. Electrospray and Taylor-cone theory, Doles beam of macromolecules at last. *Int. J. Mass Spectrom.* **1994**, *136*, 167-180.

15. Gomez, A.; Tang, K. Q. Charge and fission of droplets in electrostatic sprays. *Phys. Fluids* **1994**, *6*, 404-414.

16. Tang, K.; Gomez, A. On the structure of an electrostatic spray of monodisperse droplets. *Phys. Fluids* **1994**, *6*, 2317-2332.

17. Paul, W.; Raether, M. Das elektrische massenfilter. *Physik* **1955**, *140*, 262-273.

18. Paul, W. Electromagnetic traps for charged and neutral particles. *Rev. Mod. Phys.* **1990**, *62*, 531-540.

19. Bruker Daltonics *HCTultra PTM Discovery System User Manual;* Billerica, MA, 2006.

20. March, R. E. An introduction to quadrupole ion trap mass spectrometry. *J. Mass Spectrom.* **1997**, *32*, 351-369.

21. March, R. E.; Todd, J. F. J. *Quadrupole Ion Trap Mass Spectrometry;* John Wiley & Sons: Hoboken, New Jersey, 2005.

22. March, R. E. Quadrupole ion traps. *Mass Spectrom. Rev.* **2009**, *28*, 961-989.

23. Zaia, J. Mass spectrometry of oligosaccharides. *Mass Spectrom. Rev.* **2004**, *23*, 161-227.

24. Penn, S. G.; Cancilla, M. T.; Lebrilla, C. B. Collision-induced dissociation of branched oligosaccharide ions with analysis and calculation of relative dissociation thresholds. *Anal. Chem.* **1996**, *68*, 2331-2339.

25. Park, Y.; Lebrilla, C. B. Application of Fourier transform ion cyclotron resonance mass spectrometry to oligosaccharides. *Mass Spectrom. Rev.* **2005**, *24*, 232-264.

26. Zubarev, R. A.; Kelleher, N. L.; McLafferty, F. W. Electron capture dissociation of multiply charged protein cations. A nonergodic process. *J. Am. Chem. Soc.* **1998**, *120*, 3265-3266.

27. Syka, J. E. P.; Coon, J. J.; Schroeder, M. J.; Shabanowitz, J.; Hunt, D. F. Peptide and protein sequence analysis by electron transfer dissociation mass spectrometry. *Proc. Natl. Acad. Sci. USA* **2004**, *101*, 9528-9533.

28. Huang, Y.; Pu, Y.; Yu, X.; Costello, C. E.; Lin, C. Mechanistic study on electron capture dissociation of the oligosaccharide-Mg^{2+} Complex. *J. Am. Soc. Mass Spectrom.* **2014**, *25*, 1451-1460.

29. Varki, A.; Cummings, R. D.; Aebi, M., et al. Symbol nomenclature for graphical representations of glycans. Glycobiology 2015, 25, 1323-1324.

30. Ciucanu, I.; Costello, C. E. Elimination of oxidative degradation during the per-O-methylation of carbohydrates. *J. Am. Chem. Soc.* **2003**, *125*, 16213-16219.

31. Ciucanu, I.; Kerek, F. A simple and rapid method for the permethylation of carbohydrates. *Carbohydr. Res.* **1984**, *131*, 209-217.

32. Domon, B.; Costello, C. E. A systematic nomenclature for carbohydrate fragmentations in FAB-MS/MS spectra of glycoconjugates. *Glycoconj. J.* **1988**, *5*, 397-409.

CHAPTER 3: ELECTRON TRANSFER DISSOCIATION AND COLLISION-INDUCED DISSOCIATION OF UNDERIVATIZED METALLATED OLIGOSACCHARIDES

3.1 Overview

Electron transfer dissociation (ETD) and collision-induced dissociation (CID) were used to investigate underivatized, metal-cationized oligosaccharides formed via electrospray ionization (ESI). Reducing and non-reducing sugars were studied including the tetrasaccharides maltotetraose, 3α,4β,3α-galactotetraose, stachyose, and nystose and a heptasaccharide, maltoheptaose. Univalent alkali, divalent alkaline earth, divalent and trivalent transition metal ions, and a group 13/boron group trivalent metal ion were adducted to the non-permethylated oligosaccharides. ESI generated $[M + Met]^+$, $[M + 2Met]^{2+}$, $[M + Met]^{2+}$, $[M + Met - H]^+$, and $[M + Met - 2H]^+$ most intensely along with low intensity nitrate adducts depending on the metal and sugar ionized. The ability of these metal ions to produce oligosaccharide adduct ions by ESI had the general trend: $Ca^{2+} > Mg^{2+} > Ni^{2+} > Co^{2+} > Zn^{2+} > Cu^{2+} > Na^+ > K^+ > Al^{3+} \approx Fe^{3+} \approx Cr^{3+}$. Although trivalent metals were utilized, no triply charged ions were formed. Metal cations allowed for high ESI signal intensity without permethylation. ETD and CID on $[M + Met]^{2+}$ produced various glycosidic and cross-ring cleavages, with ETD producing more cross-ring and internal ions, which are useful for structural analysis. Product ion intensities varied based on glycosidic-bond linkage and identity of monosaccharide sub-unit, and metal-adducts. ETD and CID showed high fragmentation efficiency, often with complete precursor dissociation, depending on the identity of the adducted metal ion. Loss of water was occasionally observed,

but elimination of small neutral molecules was not prevalent. For both ETD and CID, [M + Co]$^{2+}$ produced the most uniform structurally informative dissociation with all oligosaccharides studied. The ETD and CID spectra were complementary.

3.2 Introduction

Oligosaccharides are an important sub-class of carbohydrates containing a small number of monosaccharides including hexoses, pentoses, hexosamines, uronic acids, dexoyhexoses, and sialic acids. Each unit is bonded to the next at different positions of the pyranose or furanose ring through an α or β glycosidic bond. The variability in the bonding positions for the monosaccharide units allows a variety of highly branched, linear, or stacked structures. Oligosaccharides are found naturally with O-linked or N-linked oligomers, sulfated as glycosaminoglycans (GAGs), or as sialylated glycoconjugates.[1] These modifications are also common for glycopeptides and glycolipids. This configurational diversity allows oligosaccharides to participate in many cellular and biological processes in the body, including protein folding and stabilization, molecular recognition within cells, energy storage and extraction, protein-ligand targeting, and protein function modulation.[1,2] The biological function of oligosaccharides can depend greatly on structure. Characterization of oligosaccharide structure requires knowledge of linkage, position, branching, sequence, anomeric configuration, and covalent modifications.[3]

Mass spectrometry (MS) is an important technique for structural analysis of oligosaccharides, offering advantages such as high speed, sensitivity, and minimal sample requirements. Both ESI and matrix-assisted laser desorption/ionization (MALDI) have been used to produce quasi-molecular ions for high mass species in the gas phase in both positive and negative ion modes.[4-6] Many monosaccharides and polymers of monosaccharide units have the

same chemical formula and mass-to-charge ratios (*m/z*), which limits the utility of high resolution MS. Fragmentation of the molecule via tandem mass spectrometry (MS/MS or MS^n) is key to distinguishing between various oligosaccharides. Glycans can undergo two major types of fragmentation in MS/MS: glycosidic cleavage and cross-ring cleavage.[7] Glycosidic cleavages are able to provide information on composition, branching, and sequence within the molecule, while cross-ring cleavages can provide information on linkage types.

Several MS/MS techniques have been utilized for carbohydrate studies, including CID,[8-14] post-source decay (PSD) and in-source decay (ISD),[15,16] infrared multiphoton dissociation (IRMPD),[17-21] ultraviolet photodissociation (UVPD),[22-25] and electron-based ion activation methods (ExD).[8,17,18,21,26-38] However, neutral underivatized oligosaccharides are difficult to protonate.[7,9,39-43] Duffin et al.[39] reported that protonated ions of 11 oligosaccharides were only produced via ESI after CID of ammoniated or sodiated precursor ions. Bahr et al.[44] discussed that underivatized oligosaccharides are unable to be ionized at the same sensitivity as peptides and proteins due to hydrophility and found that derivatization and nano-ESI increases surface activity and enhances protonation. When protonation is successful, fragmentation varies based on the MS/MS technique employed and often involves gas-phase rearrangements of the ions. Several studies revealed that low-energy CID of protonated oligosaccharides produces mainly glycosidic cleavages.[9,42,45] Use of high-energy CID[45,46] or metallated precursor ions with low-energy CID[9,10,47] enhances cross-ring cleavages. Electron-based ion activation methods have been utilized to reduce the loss of labile modifications that is observed in CID and IRMPD, and to improve sequence coverage of oligosaccharides.[21,28,29,32,34,48,49]

Studies using a variety of metal ions have shown that metallated oligosaccharides can provide structurally informative fragmentation in both positive and negative ion

modes.[13,16,38,46,47,50-60] Adamson and Håkansson[38] complexed alkali, alkaline earth, and transition metal ions to several underivatized oligosaccharides and found that with electron capture dissociation (ECD) and IRMPD metallation greatly improved the structurally informative fragmentation, although no one metal ion stood out as optimal. Costello and co-workers[28] studied five permethylated metallated oligosaccharides, finding that magnesium provided the most fragmentation by ETD and that complementary fragmentation occurs by CID and ETD. Permethylation involves conversion of the free hydroxyl groups on the sugar into methoxy groups; this can simplify MS analysis by improving ionization, and facilitating characterization of glycosidic bond positions and branching.[40,61-66] However, even with permethylation sodiated precursor ions are commonly studied due to the difficulty of achieving protonation.[7,10,45]

The goal of this project is to explore the ability of ETD and CID to provide structural information on several underivatized oligosaccharides with a variety of metal adducts. Alkali, alkaline earth, first row transition metals, and a group 13/boron group metal were used to investigate the effects of charge, ionic radius, ionization/recombination energy, and valency of the metal adduct on oligosaccharide dissociation.

3.3 Experimental

All experiments were performed using a Bruker HCTultra PTM Discovery System high capacity quadrupole ion trap mass spectrometer (Bruker Daltonics, Billerica, MA, USA) as described in Chapter 2. Sample solutions were made with a 10:1 metal ion-oligosaccharide molar ratio and infused into an ESI source at a flow rate of 180 µL/h using a KD Scientific (Holliston, MA, USA) syringe pump. Final oligosaccharide concentrations were 10 µM in methanol-water at a 50:50 volume ratio. Source conditions for positive ion mode were capillary voltage: -3500 V; end plate offset: -500 V; capillary exit voltage: 120 V; nebulizer: 10 psi;

drying gas: 10 L/min; and drying gas temperature: 250°C. The amplitude of the voltage for CID experiments was 0.8 to 1.2 V and the collision gas was helium (He) with a 30% to 200% collision energy sweep.

Isotopic ^{18}O-labeling of the reducing end oxygen in the reducing sugars maltotetraose, galactotetraose, and maltoheptaose involved dissolving enough oligosaccharide in 100 µL of $H_2{}^{18}O$ to create a 0.1 M sample. A second identical sample was prepared with a 10:1 ratio of $Co(NO_3)_2$ to oligosaccharide. Both samples were stored in sealed vials in a desiccator at room temperature for three weeks. The extent of isotopic labeling was periodically monitored by MS. The solution with the Co^{2+} exchanged most quickly. Before MS analysis, the samples were diluted to 10 µM of oligosaccharide.

The ETD experiments used fluoranthene, generated in a negative chemical ionization (nCI) source, as the reagent anion and methane as the nCI reagent gas. Further discussion of ETD can be found in Chapter 2. Reagent ions were accumulated for 20.0 ms, the reaction time was optimized at 400 ms, and the low *m/z* cutoff was 120 *m/z*. The ETD ion charge control (ICC) target was 250,000 to 400,000. The "smart decomposition" function was employed to further dissociate any charge reduced product ions by using resonant excitation to overcome attractive forces that may hold oligosaccharide fragments together following ETD. Precursor ion isolation widths for CID and ETD were varied from 2.0 *m/z* to 4.0 *m/z* to achieve maximum product ion intensity. Standard enhanced resolution mode was employed for MS and MS/MS experiments with a scan speed of 8,100 *m/z* per second. Spectra shown are averages of 200 scans. Compass DataAnalysis was used for data processing.

The oligosaccharides studied are listed in Section 2.2. The metal salts were nitrates of sodium (Na^+), potassium (K^+), magnesium (Mg^{2+}), calcium (Ca^{2+}), chromium (Cr^{3+}), iron (Fe^{3+}),

cobalt (Co^{2+}), nickel (Ni^{2+}), copper (Cu^{2+}), zinc (Zn^{2+}), and aluminum (Al^{3+}). $H_2{}^{18}O$ was purchased from Sigma-Aldrich (St. Louis, MO, USA). Ultrapure Milli-Q 18 MΩ water was produced with a Barnstead (Dubuque, IA, USA) E-pure system.

3.4 Results and Discussion

Relevant metal properties can be seen in Table 3.1, while structures of the oligosaccharides in this study are in Figure 2.15. Maltotetraose consists of four glucose units with identical linkages between the rings, whereas 3α,4β,3α-galactotetraose has galactose units with α and β linkages on different ring positions. These are both linear, reducing sugars. Stachyose and nystose are stacking, non-reducing sugars with a variety of monosaccharide units and glycosidic bond linkages. Maltoheptaose was included to examine size effects as it contains seven glucose units.

3.4.1 Metallated Oligosaccharide Ion Formation by ESI

The predominant ion in the ESI spectra for all oligosaccharide solutions with no added metal salt is $[M + Na]^+$, where M is the oligosaccharide. Na^+ is a common MS contaminant, most likely from the glassware or solvent system. As previously mentioned, sodiated oligosaccharide ions are much more common than protonated ions.[7] Singly-protonated oligosaccharide ions, $[M + H]^+$, were generated by the addition of a small amount of acid, such as 1% acetic acid (by volume); however, degradation of the sugar occurred. In the absence of metal salt, no multiply charged ions formed, even upon the addition of up to 5% acid.

To generate metal-adducted oligosaccharide ions, each of the five oligosaccharides were complexed with all surveyed metals individually. Table 3.2 indicates the ions observed after additions of the various nitrate salts to the oligosaccharides. To achieve the highest intensity of metallated ions, the molar ratio of metal ion (Met) to oligosaccharide (M) was optimized at 10:1.

Table 3.1 Comparison of physical properties of metal ions included in study.

Metal	Charge (Q)[a]	Ionic Radius (R)[b]	Charge Density (Q/R^3)[c]	First Ionization Energy (kJ/Mol)	Second Ionization Energy (kJ/Mol)	Third Ionization Energy (kJ/Mol)	Electron Configuration
Na	1	0.116	640	495.8	4562	6910.3	[Ne]
Mg	2	0.086	3140	737.7	1450.7	7732.7	[Ne]
Al	3	0.0675	9750	577.5	1816.7	2744.8	[Ne]
K	1	0.152	284	418.8	3052	4420	[Ar]
Ca	2	0.114	1350	589.8	1145.4	4912.4	[Ar]
Cr	3	0.0755	6970	652.9	1590.6	2987	$[Ar]3d^3$
Fe	3	0.0785	6200	762.5	1561.9	2957	$[Ar]3d^5$
Co	2	0.0885	2890	760.4	1648	3232	$[Ar]3d^7$
Ni	2	0.083	3500	737.1	1753	3395	$[Ar]3d^8$
Cu	2	0.087	3040	745.5	1957.9	3555	$[Ar]3d^9$
Zn	2	0.088	2940	906.4	1733.3	3833	$[Ar]3d^{10}$

[a] Q in 1.6×10^{-19} C.

[b] R in nm.[67]

[c] Q/R^3 in 1.6×10^{-19} C/nm^3.

Table 3.2 ESI ion formation for all sugars upon addition of metal nitrates

	Tetrasaccharides				Heptasaccharide
Metal Adducted	Maltotetraose	3α,4β,3α-galactotetraose	Nystose	Stachyose	Maltoheptaose
Na^{+}, K^{+}	B[a] $[M + Met]^{+}$[b] M $[2M + Met]^{+}$ W $[M + 2Met]^{2+}$	B $[M + Met]^{+}$ M $[2M + Met]^{+}$ W $[M + 2Met]^{2+}$	B $[M + Met]^{+}$ M $[2M + Met]^{+}$ W $[M + 2Met]^{2+}$	B $[M + Met]^{+}$ M $[2M + Met]^{+}$ W $[M + 2Met]^{2+}$	S $[M + Met]^{+}$ W $[2M + Met]^{+}$ B $[M + 2Met]^{2+}$ M $[M + 2Met + NO_3]^{2+}$
Mg^{2+}, Ca^{2+}	B $[M + Met]^{2+}$ W $[2M + Met]^{2+}$ M $[M + Met + NO_3]^{+}$ M $[M + Met – H]^{+}$ W $[M + Met – H – H_2O]^{+}$	B $[M + Met]^{2+}$ W $[2M + Met]^{2+}$ M $[M + Met + NO_3]^{+}$ M $[M + Met – H]^{+}$ W $[M + Met – H – H_2O]^{+}$	B $[M + Met]^{2+}$ W $[2M + Met]^{2+}$ M $[M + Met + NO_3]^{+}$ M $[M + Met – H]^{+}$ W $[M + Met – H – H_2O]^{+}$	B $[M + Met]^{2+}$ W $[2M + Met]^{2+}$ M $[M + Met + NO_3]^{+}$ M $[M + Met – H]^{+}$ W $[M + Met – H – H_2O]^{+}$	B $[M + Met]^{2+}$ W $[2M + Met]^{2+}$ W $[M + Met – H]^{+}$ W $[M + Met + NO_3]^{+}$ M $[M + 2Met + NO_3]^{3+}$ M $[M + 2Met + NO_3 – H]^{2+}$
Co^{2+}, Ni^{2+}, Zn^{2+}, Cu^{2+}	B $[M + Met]^{2+}$ W $[2M + Met]^{2+}$ M $[M + Met – H]^{+}$ W $[M + Met + NO_3]^{+}$ W $[M + Met – H_2O]^{2+}$	B $[M + Met]^{2+}$ W $[2M + Met]^{2+}$ M $[M + Met – H]^{+}$ W $[M + Met + NO_3]^{+}$ W $[M + Met – H_2O]^{2+}$	B $[M + Met]^{2+}$ W $[2M + Met]^{2+}$ M $[M + Met – H]^{+}$ W $[M + Met + NO_3]^{+}$ W $[M + Met – H_2O]^{2+}$	B $[M + Met]^{2+}$ W $[2M + Met]^{2+}$ M $[M + Met – H]^{+}$ W $[M + Met + NO_3]^{+}$ W $[M + Met – H_2O]^{2+}$	B $[M + Met]^{2+}$ W $[2M + Met]^{2+}$ W $[M + Met – H]^{+}$ M $[M + 2Met – 2H]^{2+}$ W $[M + Met + NO_3]^{+}$ W $[M + 2Met + NO_3]^{3+}$ W $[M + 2Met + NO_3 – H]^{2+}$ W $[M + Met – H_2O]^{+}$
Al^{3+}	M $[M + Al – 2H]^{+}$	M $[M + Al – 2H]^{+}$	M $[M + Al – 2H]^{+}$	M $[M + Al – 2H]^{+}$	W $[M + Al – H]^{2+}$ W $[M + Al + NO_3 – H]^{+}$
Cr^{3+}	W $[M + Cr – 2H]^{+}$	W $[M + Cr – 2H]^{+}$	W $[M + Cr – 2H]^{+}$	W $[M + Cr – 2H]^{+}$	W $[M + Cr – H]^{2+}$ W $[M + Cr + NO_3 – H]^{+}$
Fe^{3+}	M $[M + Fe – 2H]^{+}$ M $[M + Fe – H]^{+}$	M $[M + Fe – 2H]^{+}$ M $[M + Fe – H]^{+}$	M $[M + Fe – 2H]^{+}$ M $[M + Fe – H]^{+}$	M $[M + Fe – 2H]^{+}$ M $[M + Fe – H]^{+}$	M $[M + Fe]^{2+}$ W $[M + Fe + NO_3 – H]^{+}$ S $[M + Fe – H_2O]^{2+}$

[a] B represents the base peak in the spectrum (100% intensity), S represents a strong ion intensity 70-100% of base peak, M represents a medium ion intensity 30-70% of base peak, and W represents a weak ion less than 30% of base peak ion intensity.

[b] Met denotes the metal adducted to the oligosaccharide.

Ratios of 1:1, 5:1, 20:1 and 50:1 were also studied. Our finding that one molar ratio worked well for all metal ions contrasts with the results of Leary and co-workers,[54] who found that both ionic radii and counter ions affect metal ion coordination to oligosaccharides and concluded that concentration optimization of each metal and sugar may be necessary. Figure 3.1 shows proposed interactions between the metal cations and both linear and stacked glycans.

The monovalent group I ions Na^+ and K^+ yielded intense $[M + Met]^+$ for all tetrasaccharides, as well as $[M + 2Met]^{2+}$ for the larger maltoheptaose. Divalent metal ions from group II or the transition series (Mg^{2+}, Ca^{2+}, Co^{2+}, Ni^{2+}, Cu^{2+}, and Zn^{2+}) formed predominately $[M + Met]^{2+}$ with all sugars.

Electrospray on solutions of the oligosaccharides with the trivalent metal ions Al^{3+}, Cr^{3+}, and Fe^{3+} did not consistently produce multiply charged ions or adduct ions; many times, adducts were not observed or occurred at low intensity. No $[M + Met]^{3+}$ was seen with $[M + Met - 2H]^+$ forming instead. (The exception is maltoheptaose, as shown in Table 3.2.) This lack of $[M + Met]^{3+}$ is surprising because analogous ions often form with peptides.[68-72] Fe^{3+}, Cr^{3+}, and Al^{3+} have not been included in other oligosaccharide studies. As seen in Table 3.1, the ionic radii of the trivalent metal ions are similar to the radii of the other metal ions that coordinate well to the oligosaccharides. In addition, Angyal[73] reported that metals with ionic radii between 0.100 nm and 0.110 nm bind most strongly to monosaccharides in solution. None of the metal ions studied have ionic radii in this specific range, although most are within ±0.02 nm. Any ionic radii effect may be offset by charge density; higher charge with near equivalent ionic radii causes the trivalent metal ions to have a higher charge density than the mono- and divalent metal ions studied. Charge density is the charge on the ion divided by the volume it takes up.

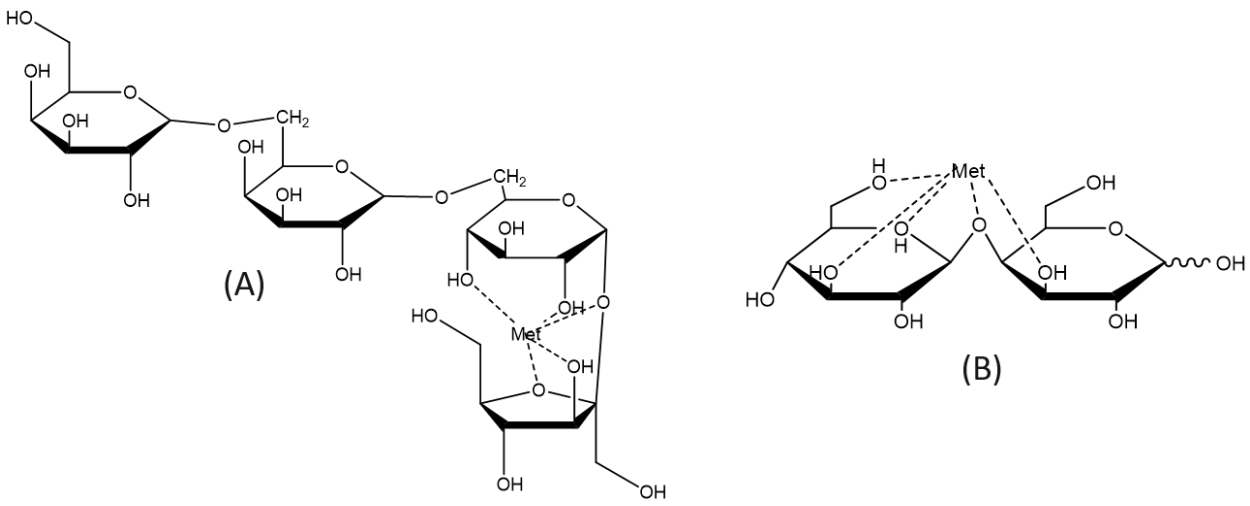

Figure 3.1 Proposed structures for metal ion coordination to both (a) stacked and (b) linear glycans.

The charge densities range from 284 Q/R^3 for K^+ to 9750 Q/R^3 for Al^{3+}. Metal cations accept electrons from weakly coordinated oxygen atoms on monosaccharides; however, water molecules can displace the coordinated cation, allowing only the strongest metal coordination to remain.[73] Due to their high charge density, trivalent metals should more strongly coordinate to an oxyanion than to a hydroxyl group, thereby favoring the loss of protons during ESI to produce $[M + Met - 2H]^+$.

The arrangement of the hydroxyl groups on a monosaccharide affects its ability to complex to metal ions.[74-76] A series of experiments were conducted to compare the ability of the metal ions to adduct and ionize the oligosaccharides. Working with each oligosaccharide separately, a solution was first prepared that contained 1 μM of oligosaccharide and all 11 metal ions at 10 μM each; the intensities of the ions produced by ESI were examined. Then, the metal that produced the base peak in the spectrum was removed and the experiment was repeated with the remaining metals. This process was continued until only two metal ions remained. The trend in the ability of the metal ions to produce adduct ions was the same for all five oligosaccharides: $Ca^{2+} > Mg^{2+} > Ni^{2+} > Co^{2+} > Zn^{2+} > Cu^{2+} > Na^+ > K^+ > Al^{3+} \approx Fe^{3+} \approx Cr^{3+}$. Similar results have been seen in the literature where Harvey[47] found that $Ca^{2+} > Mn^{2+} > Mg^{2+} > Co^{2+} > Cu^{2+}$ for adduction to maltoheptaose and Leary and co-workers[54] reported that Ca^{2+} produced the most intense ions in their study of two sugars with Ca^{2+}, Mn^{2+}, Co^{2+}, Zn^{2+}, and Cu^{2+}. Considering $[M + Ca]^{2+}$ as the most easily produced ion, the greatest ion intensity was found for stachyose and maltotetraose (absolute intensities in the low 10^5 range), with ions from galactotetraose of intermediate abundance (high 10^4), and nystose and maltoheptaose providing the lowest ion yields (low 10^4). This result has no obvious correlation to whether the oligosaccharides are linear or stacked.

3.4.2 Effect of Metal Ion on Dissociation

Domon and Costello nomenclature[77] as described in Chapter 2 will be used to label the ionic oligosaccharide fragments. Many of the product ions are exact mass ions with the same chemical formula, making them indistinguishable in the spectrum. These exact mass/isobaric ions are noted in the spectrum with a comma between two possible ion labels. Colors used to illustrate the product ions in this dissertation are red for cross-ring cleavages, blue for glycosidic bond cleavages, and green for internal cleavages. The labels for internal ions indicate the glycosidic bond cleavage involved and additional mass lost from cross-ring cleavage. For example, [C_4, Y_4 + Co – 60] indicates the cleavage is either C_4 or Y_4 with loss of 60 Da through a cross-ring cleavage and retention of Co^{2+}. The various possible exact mass/isobaric cross-ring cleavages, sorted by mass lost, are shown in Table 3.3. All product ions in Table 3.3 are observed with both CID and ETD, except for the loss of 120 Da, which was only observed with CID. Undissociated precursor ion is labeled in light blue with a large diamond arrow head and ions involving neutral losses are labeled in black. Han and Costello[28] found that fragmentation of the oligosaccharide is more likely on the non-reducing end than the reducing end of reducing sugars, with which the ^{18}O isotopic labeling of the reducing sugars in this current study agreed.

The identity of the metal ion affects fragmentation patterns with both ETD and CID. This can be seen in Figures 3.2 and 3.3, respectively, for maltotetraose. Maltotetraose will be discussed as representative for all oligosaccharides in this study. All ETD and CID product ions from maltotetraose with every metal studied were metallated except for products containing only one glucose unit. Protonated glucose product ions were observed with loss of one, two, three, and four water molecules in all CID spectra. These singly charged protonated monosaccharide ions occur in the CID spectra and are common in other CID studies;[47] however, they are not

Table 3.3 Possible isobaric cross-ring cleavage assignments based on mass lost.

Mass Loss	Maltotetraose	3α,4β,3α-galactotetraose	Nystose	Stachyose	Maltoheptaose
60 Da ($C_2H_4O_2$)	$^{1,3}X_n$ $^{0,4}X_n$ $^{2,4}X_{n*}$ $^{0,2}A_{n*}$ [a]	$^{1,3}X_1$ $^{1,3}X_3$ $^{0,4}X_n$ $^{2,4}X_{n*}$ $^{0,2}A_{n*}$	$^{0,4}X_n$ $^{2,4}X_n$ $^{1,3}X_0$	$^{1,3}X_n$ $^{2,4}X_n$ (not on fructose)	$^{1,3}X_n$ $^{0,4}X_n$ $^{2,4}X_{n*}$ $^{0,2}A_{n*}$
90 Da ($C_3H_6O_3$)	$^{1,4}X_{n*}$ $^{0,3}X_{n*}$ $^{1,4}A_{n*}$ $^{0,3}A_{n*}$	$^{0,3}X_0$ $^{0,3}X_2$ $^{1,4}X_0$	$^{1,4}X_0$ $^{0,3}X_n$	$^{0,3}X_{n*}$ $^{1,4}X_n$ (not on fructose)	$^{1,4}X_{n*}$ $^{0,3}X_{n*}$ $^{1,4}A_{n*}$ $^{0,3}A_{n*}$
120 Da ($C_4H_8O_4$)	$^{2,4}A_{n*}$ $^{0,2}X_{n*}$	Not observed	Not observed	Not observed	$^{2,4}A_{n*}$ $^{0,2}X_{n*}$

[a] n represents the position of the monosaccharide ring that is undergoing cross-ring cleavage and can be any monosaccharide unit remaining in the sugar after the glycosidic bond cleavage, while n* must be the same subscript as on the corresponding glycosidic bond cleavage.

[b] Loss of 60 Da and 90 Da were observed with both CID and ETD, whereas loss of 120 Da was only observed with CID.

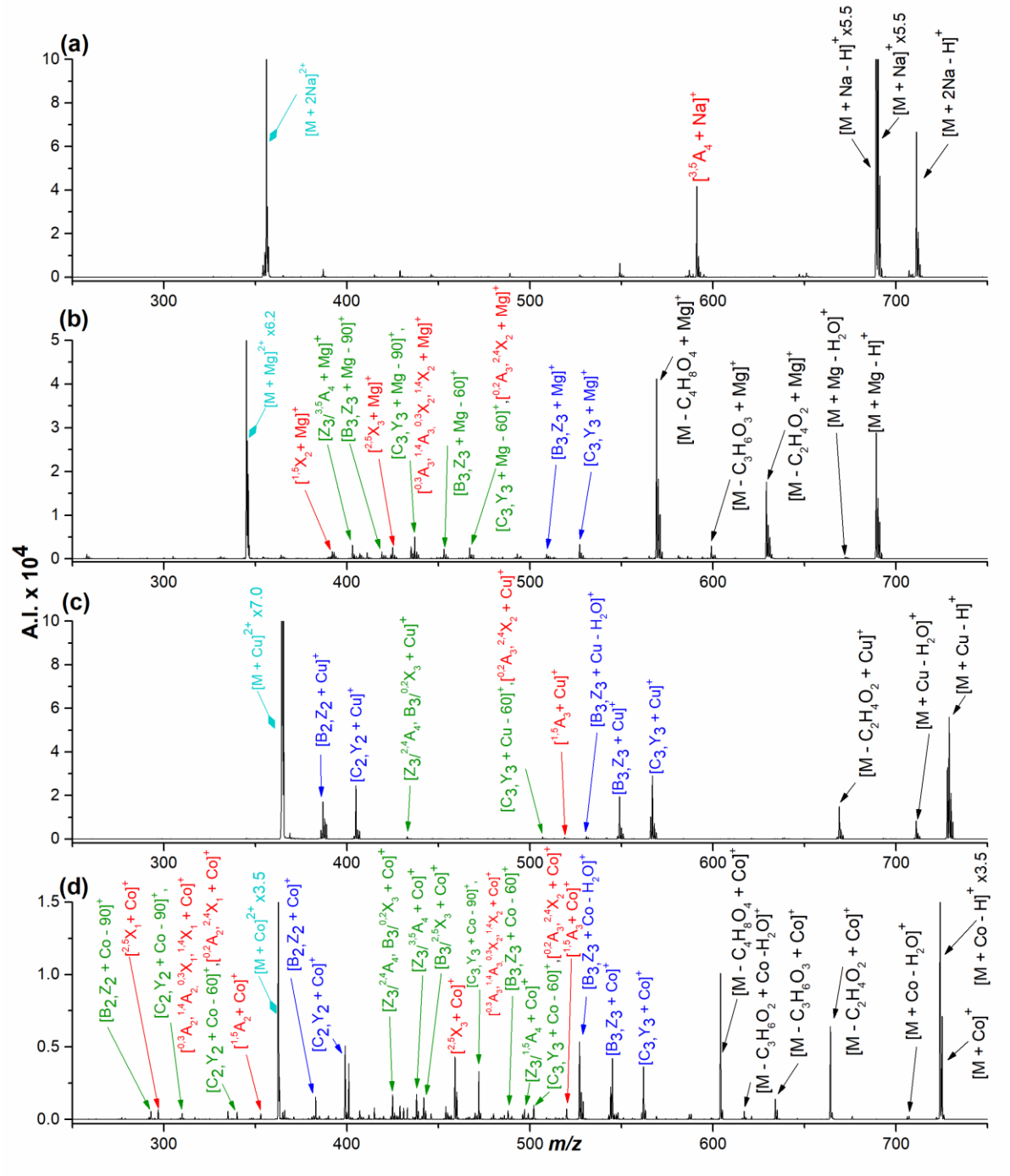

Figure 3.2 ETD mass spectra of maltotetraose for (a) $[M + 2Na]^{2+}$, (b) $[M + Mg]^{2+}$, (c) $[M + Cu]^{2+}$, and (d) $[M + Co]^{2+}$. Colors used to illustrate the product ions are red for cross-ring cleavages, blue for glycosidic bond cleavages, and green for internal cleavages. Refer to Table 3.3 for identities of internal cleavages indicated by mass lost. Undissociated precursor ion is labeled in light blue with a large light blue diamond arrow head. Product ions involving solely neutral losses are labeled in black.

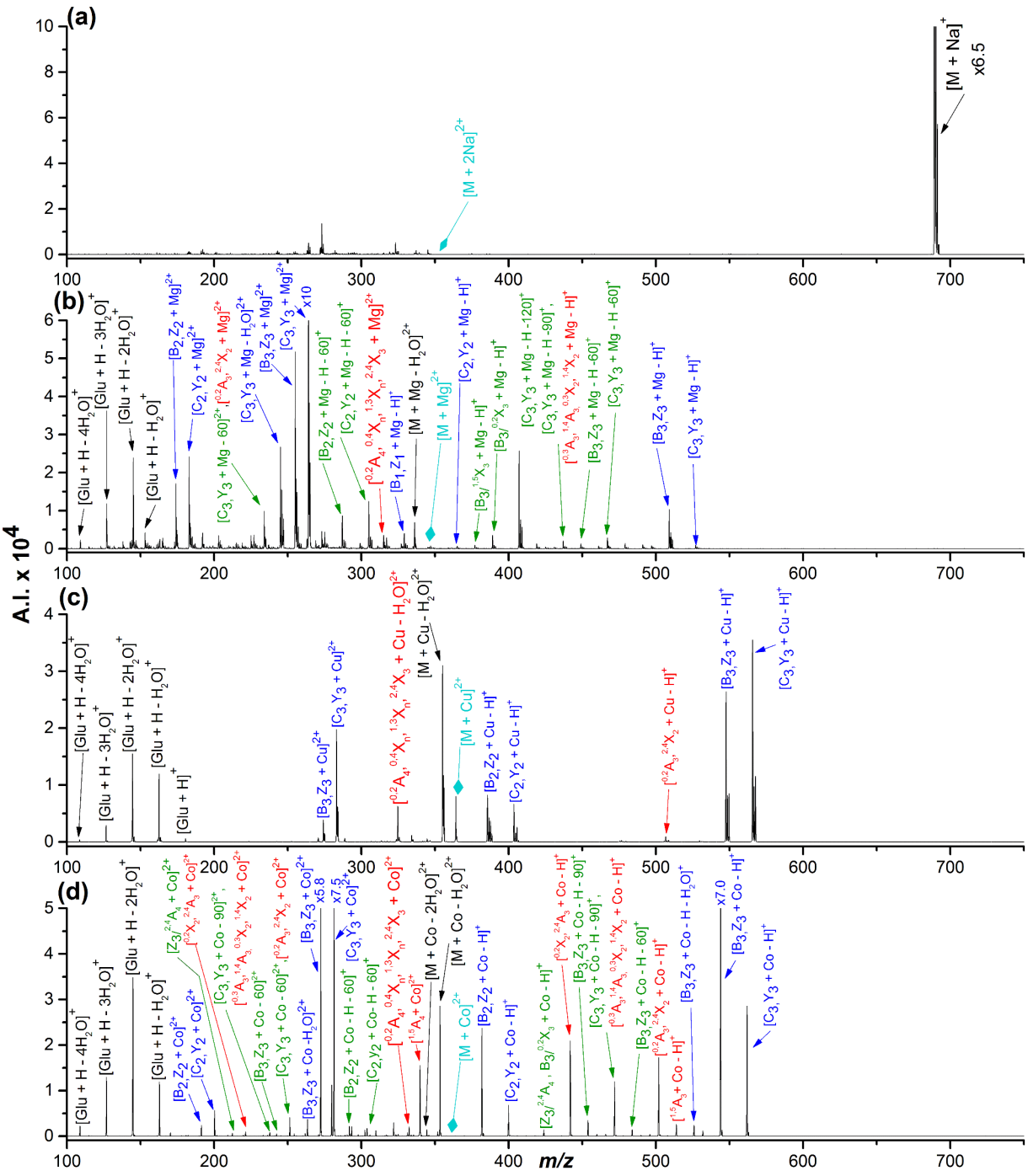

Figure 3.3. CID mass spectra of maltotetraose for (a) $[M + 2Na]^{2+}$, (b) $[M + Mg]^{2+}$, (c) $[M + Cu]^{2+}$, and (d) $[M + Co]^{2+}$. Refer to the Figure 3.1 caption for an explanation of the color codes.

found by ETD. With the singly charged cations Na^+ and K^+, little to no dissociation occurred during ETD or CID. This is illustrated by the CID spectrum of $[M + K]^+$ from maltotetraose in Figure 3.4. In Figure 3.2(a) ETD on $[M + 2Na]^{2+}$ results in loss of an adducted sodium ion, as well as formation of the charge reduced species $[M + 2Na]^+$ and very few cleavage ions. In Figure 3.3(a), CID on $[M + 2Na]^{2+}$ results in loss of one adducted metal ion and few product ions. These spectra are not structurally informative. This is also true for the MS/MS spectra of sodiated and potassiated ions from the other sugars studied. This predominant pathway of metal ion loss for doubly sodiated or potassiated ions was also noted in an ECD study by Adamson and Håkansson.[38]

For the alkaline earth metals, ETD and CID with Mg^{2+} showed significantly more product ions than with Ca^{2+}. The spectra of $[M + Ca]^{2+}$ from maltotetraose can be seen in Figures 3.5 and 3.6, while the ETD spectrum of $[M + Mg]^{2+}$ from maltotetraose is in Figure 3.2(b). The majority of the product ions are related to the terminal glucose units; the middle of the molecule undergoes limited fragmentation. The only glycosidic bond cleavage is loss of one terminal glucose unit with product ions having both loss and retention of the oxygen in the glycosidic bond. All internal ions also contain these glycosidic bond cleavages, along with either another glycosidic bond cleavage or a cross-ring cleavage. Product ions that correspond to cross ring cleavage loss of 30 Da ($C_2H_4O_2$), 60 Da ($C_3H_6O_3$), and 120 Da ($C_4H_8O_4$) are very intense and there are multiple isobaric possibilities. $^{1,5}X_2$ is the only product that solely corresponds to cleavage of one of the middle glucose rings. CID of $[M + Mg]^{2+}$ from maltotetraose results in both doubly and singly charged product ions, as can be seen in Figure 3.3(b). Glycosidic bond cleavage occurred between every monosaccharide sub-unit. Due to the symmetry of the

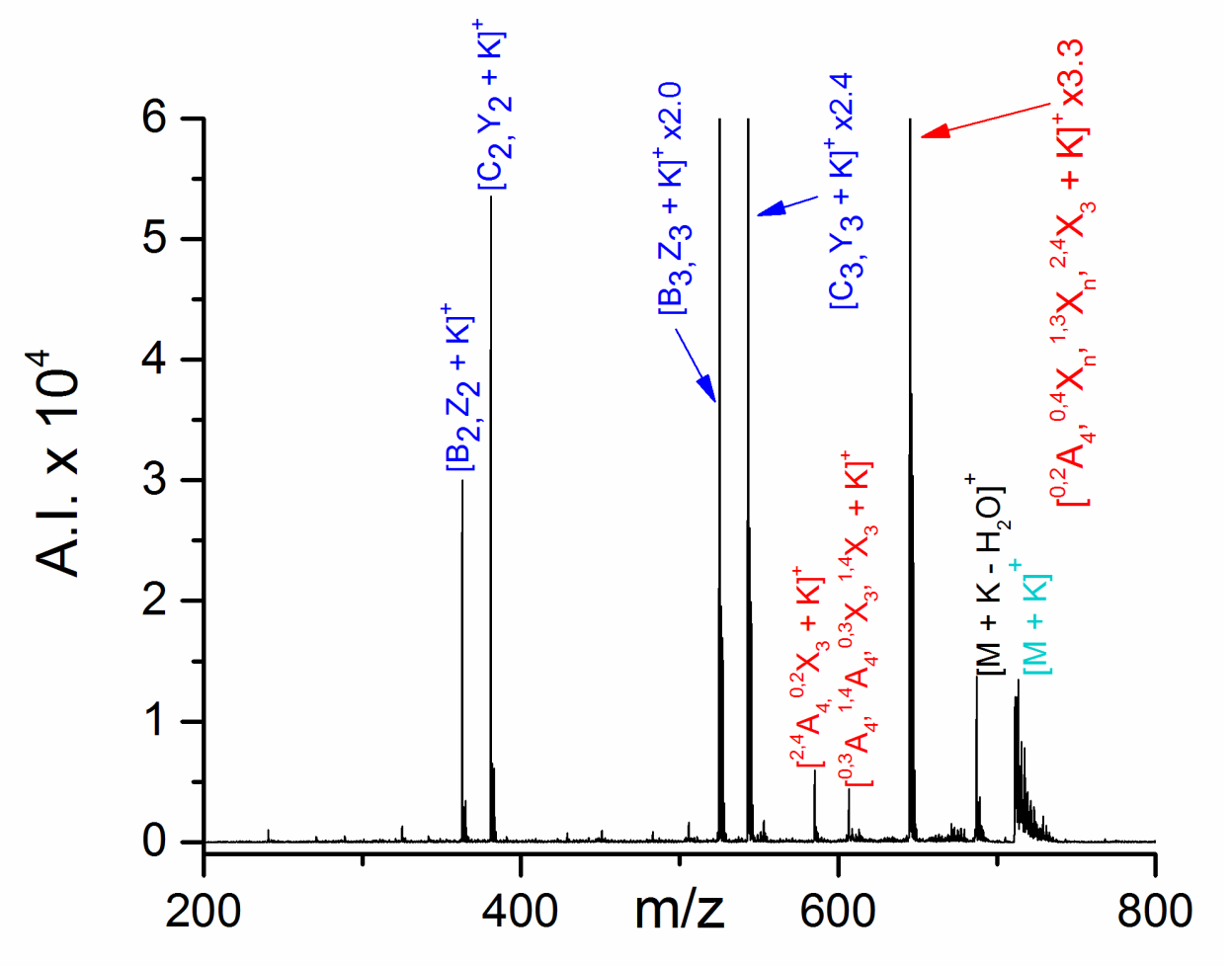

Figure 3.4 Collision-induced dissociation mass spectrum of maltotetraose for $[M + K]^+$. Refer to the Figure 3.1 caption for an explanation of the color codes.

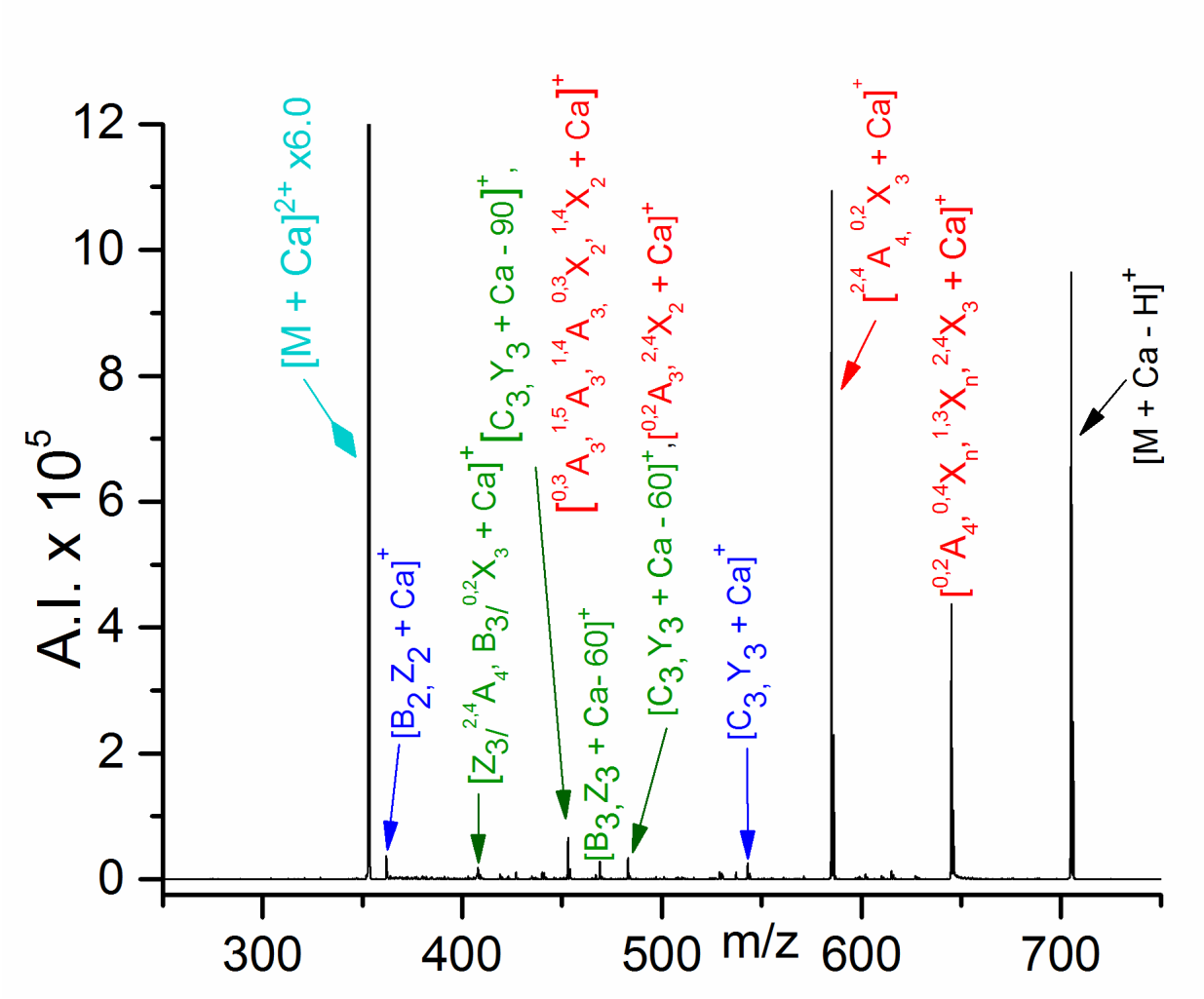

Figure 3.5 Electron transfer dissociation mass spectrum of maltotetraose for $[M + Ca]^{2+}$. Refer to the Figure 3.1 caption for an explanation of the color codes.

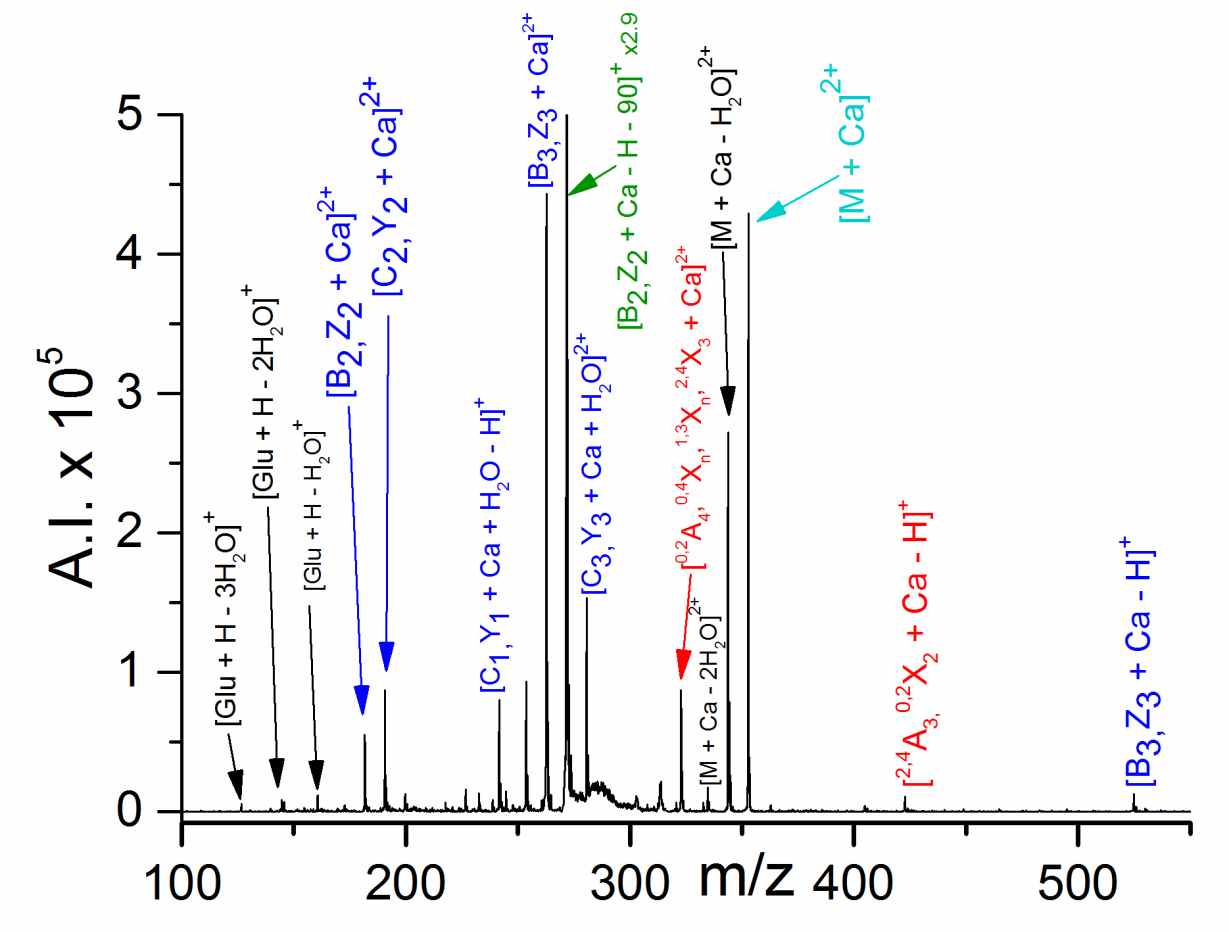

Figure 3.6 Collision-induced dissociation mass spectrum of maltotetraose for $[M + Ca]^{2+}$. Refer to the Figure 3.1 caption for an explanation of the color codes.

oligosaccharides, there are many indistinguishable exact mass product ions. The ion at *m/z* 315 is the only product ion that corresponds to cross-ring cleavage alone and could be $^{0,2}A_4$, $^{0,4}X_n$, $^{1,3}X_n$, or $^{2,4}X_3$. Isotopic labeling with ^{18}O on the reducing end of the reducing sugars showed that most exact mass cross-ring cleavages are A-ions, so this product ion is most likely $^{0,2}A_4$. All other cross-ring cleavage products are a part of an internal ion and are accompanied by a glycosidic bond cleavage. The intensities of the cross-ring cleavage product ions and internal cleavages are low.

The divalent transition metals Cu^{2+}, Ni^{2+}, and Zn^{2+} produce few product ions from ETD on $[M + Met]^{2+}$, while Co^{2+} produces abundant structurally informative product ions (as discussed below). CID on $[M + Met]^{2+}$ with Ni^{2+}, Co^{2+}, and Zn^{2+} show very similar fragmentation; however, with Cu^{2+} there is very little product ion formation. ETD and CID spectra of $[M + Cu]^{2+}$ from maltotetraose can be seen in Figures 3.2(c) and 3.2(c), respectively. Although both ETD and CID on $[M + Cu]^{2+}$ from maltotetraose produce glycosidic bond cleavage between every monosaccharide residue, these spectra have few product ions. The ETD spectrum contains a few cross-ring and internal product ions at low intensity, while CID yields only two cross-ring product ions and no internal cleavages. The relative lack of dissociation with Cu^{2+} is consistent with CID studies by Leary and co-workers,[14,54,78] Zhu et al.,[57] and Harvey.[47] ETD and CID spectra of $[M + Met]^{2+}$ from maltotetraose with Ni^{2+} and Zn^{2+} can be seen in Figures 3.7, 3.8, 3.9, and 3.10.

From the present data, Co^{2+} appears to be the most promising metal for obtaining informative oligosaccharide fragmentation. This is consistent with work by Leary and co-workers,[53,54] where Co^{2+} coordinated easily to oligosaccharides and CID provided extensive structural information, including linkage positions. The results in the current study suggest that

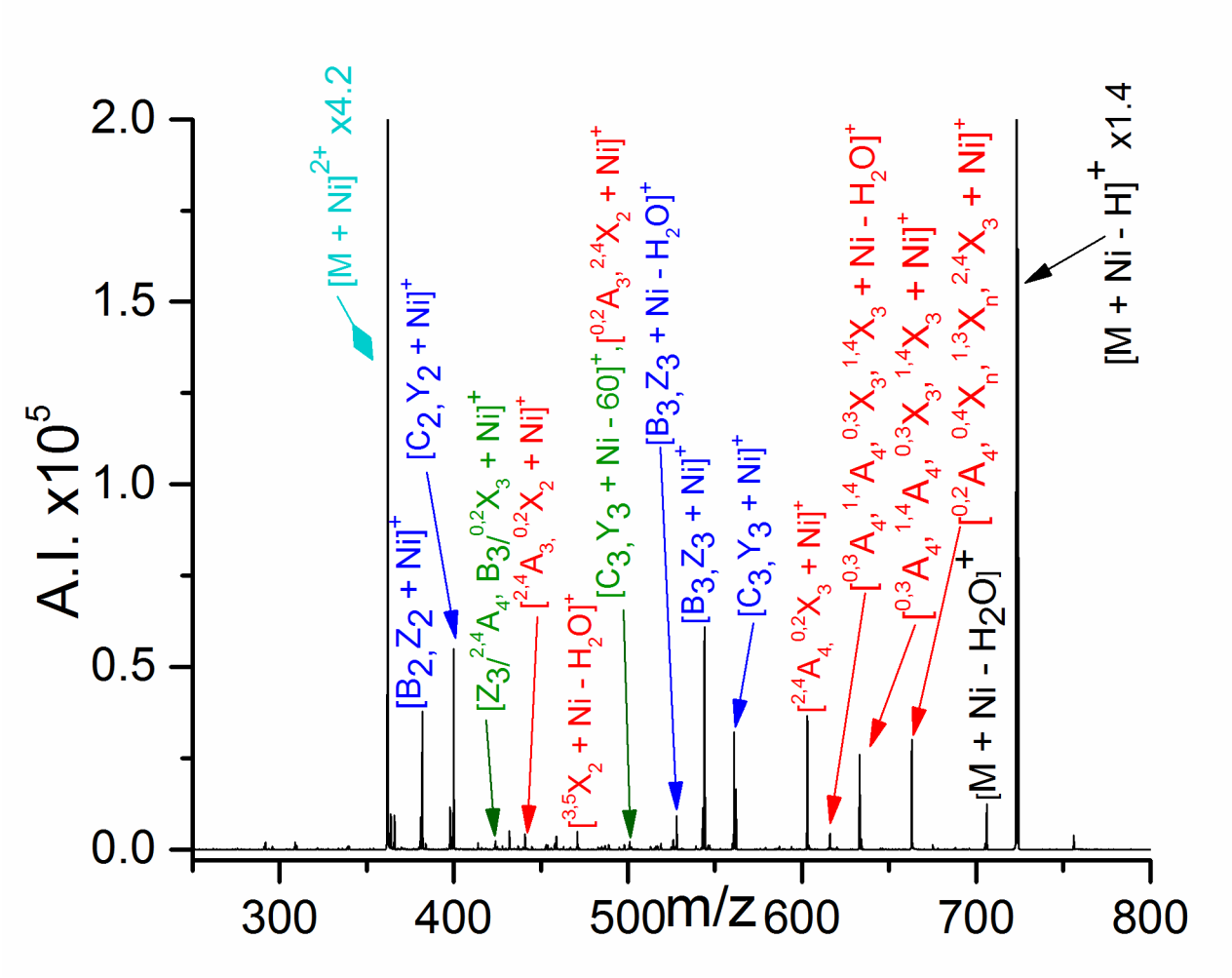

Figure 3.7 Electron transfer dissociation mass spectrum of maltotetraose for $[M + Ni]^{2+}$. Refer to the Figure 3.1 caption for an explanation of the color codes.

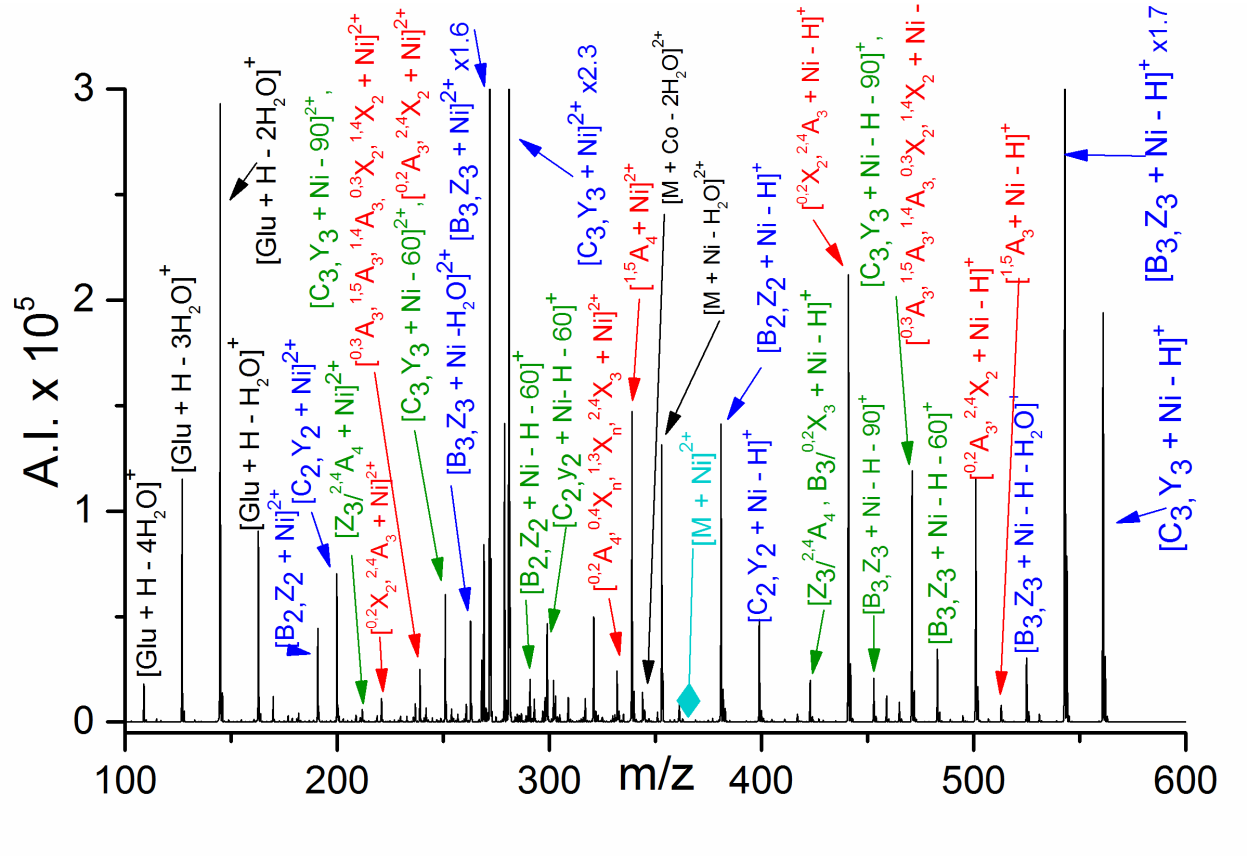

Figure 3.8 Collision-induced dissociation mass spectrum of maltotetraose for $[M + Ni]^{2+}$. Refer to the Figure 3.1 caption for an explanation of the color codes.

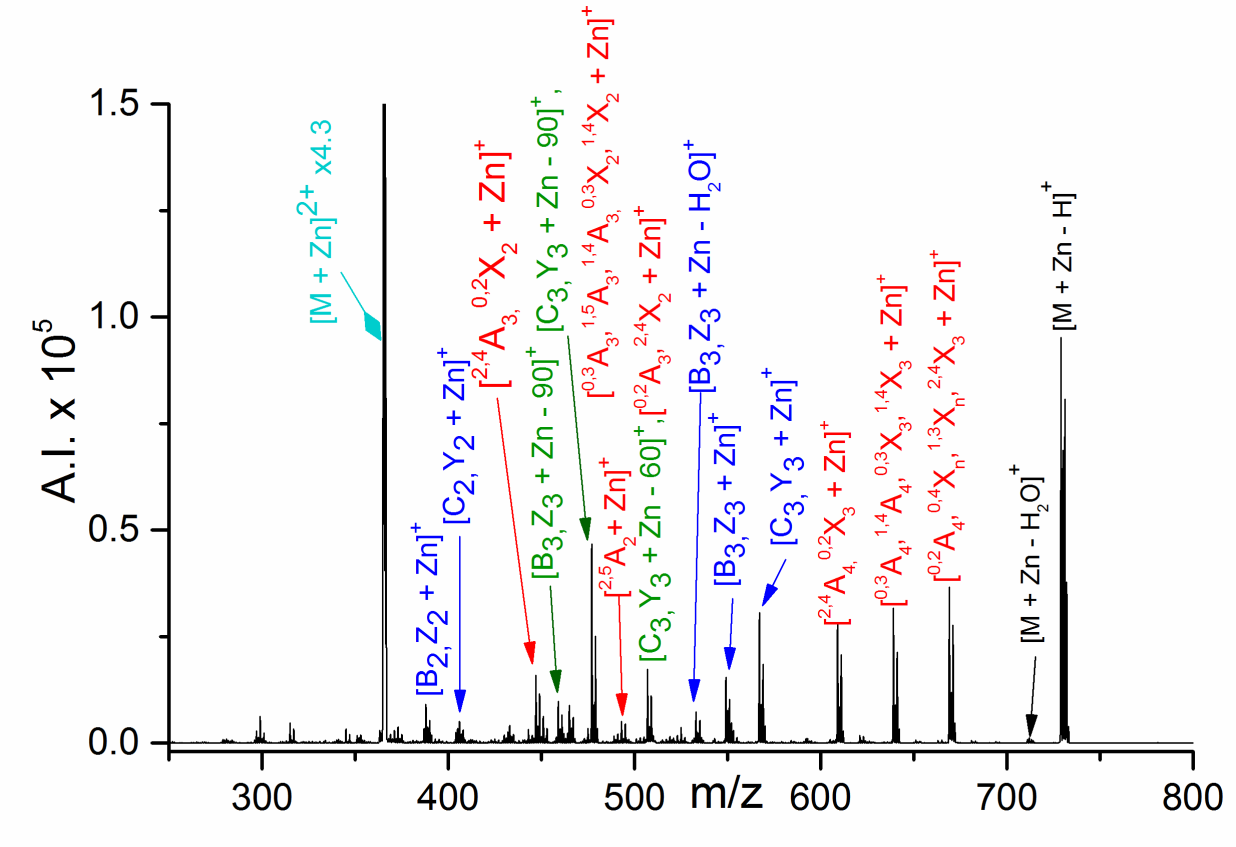

Figure 3.9 Electron transfer dissociation mass spectrum of maltotetraose for $[M + Zn]^{2+}$. Refer to the Figure 3.1 caption for an explanation of the color codes.

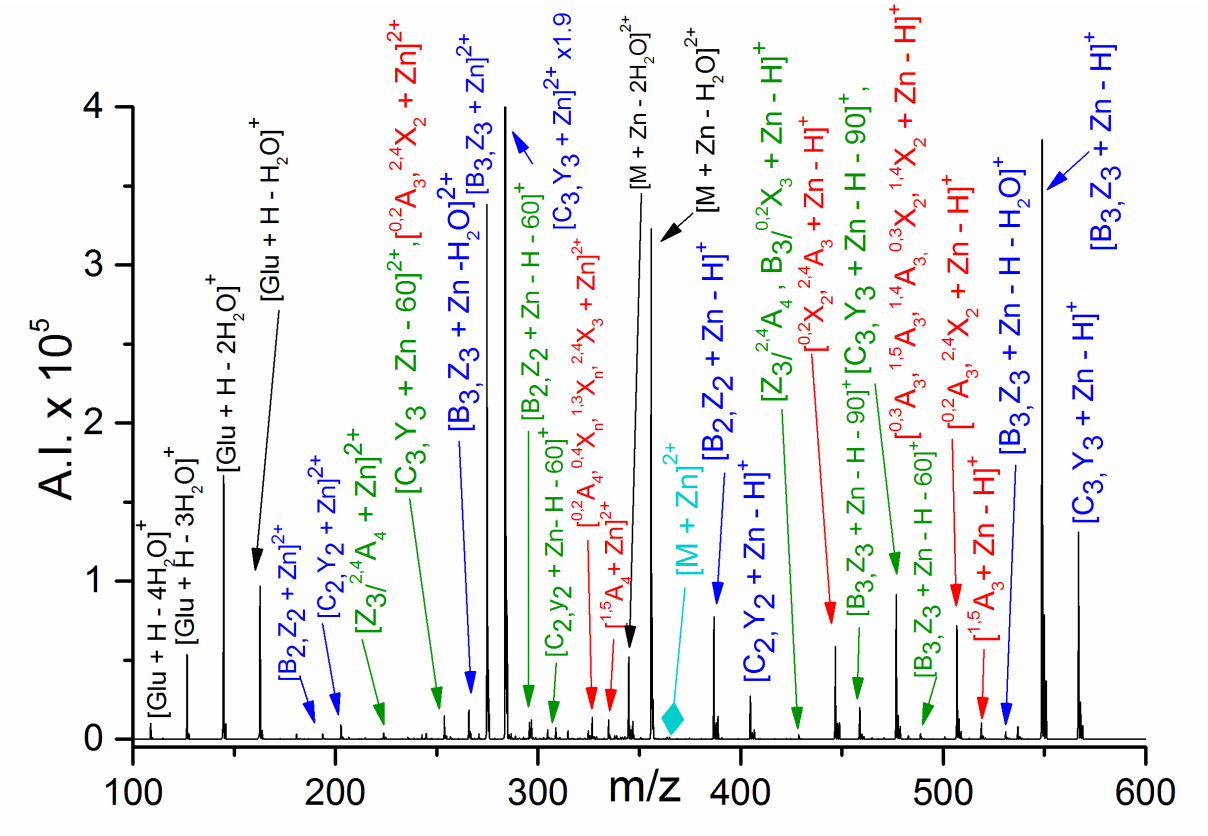

Figure 3.10 Collision-induced dissociation mass spectrum of maltotetraose for $[M + Zn]^{2+}$. Refer to the Figure 3.1 caption for an explanation of the color codes.

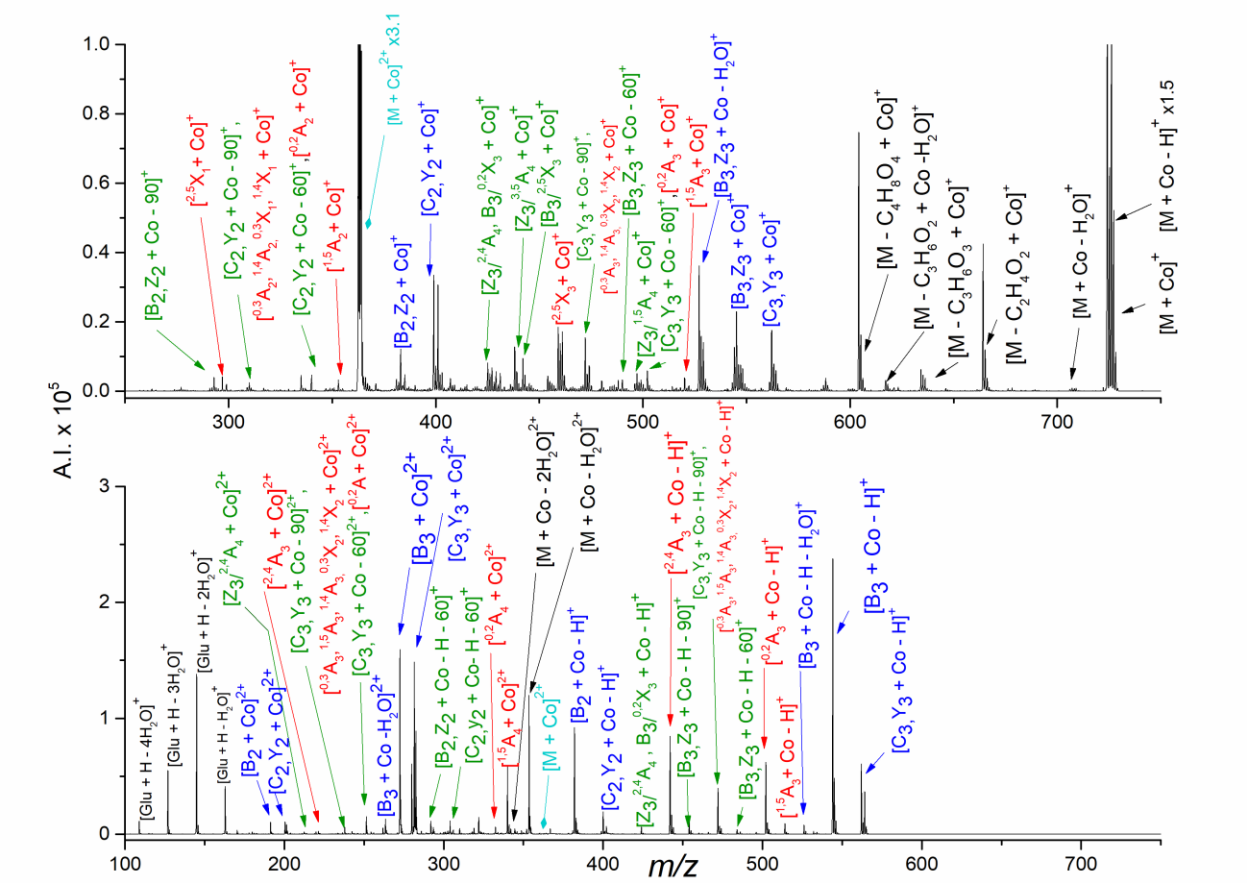

Figure 3.11 Mass spectra from (a) ETD and (b) CID of $[M + Co]^{2+}$ from maltotetraose with ^{18}O isotopic labeling at the reducing end. Refer to the Figure 3.1 caption for an explanation of the color codes.

this is also true with electron-based techniques such as ETD. Figures 3.2(d) and 3.3(d) show ETD and CID spectra for $[M + Co]^{2+}$ from maltotetraose. In addition, Figure 3.11 shows ETD and CID spectra from $[M + Co]^{2+}$ from isotopically labeled maltotetraose. Both dissociation methods yield complete glycosidic bond fragmentation and many other product ions. ETD produced many cross-ring cleavages on the terminal glucose units and $^{2,5}X$ cross-ring product ions that were not present in the spectra of other metal adducts. CID on $[M + Co]^{2+}$ displayed 100% fragmentation efficiency with no precursor ion remaining. Fragmentation efficiency describes the amount of precursor ion that is dissociated into product ions and is calculated as Σ I(fragment ion)/I(precursor before dissociation), where I is ion intensity. The CID spectrum in Figure 3.11 has more water loss products than the maltotetraose spectra of other metals; for example, many of the glycosidic bond product ions are accompanied by water loss. The product ions of the cobalt-adducted maltotetraose from both dissociation methods are of higher intensity than for the other metal adducts. Isotopic labeling of the oxygen on the reducing end of maltotetraose allows differentiation of the fragment ions from the reducing and non-reducing ends of the oligosaccharide. Although glycosidic bond cleavage occurs between every glucose unit, all ETD and CID product ions from maltotetraose are comprised of at least two glucose units. The only product ions that do not contain at least two glucose units are internal cleavages, probably due to the fact that bond cleavage is occurring twice. Another key difference in the ETD and CID spectra is that with CID the only ions that contain the reducing end are Y ions from the non-reducing side of the glycosidic oxygen; however, in ETD, both Y and Z ions from both sides of the glycosidic oxygen are observed. The majority of the cross-ring cleavages include the non-reducing side of the molecule.

The trivalent metal cations induced more cross-ring cleavage and internal cleavage than the divalent cations with CID. However, they did not produce multiply charged precursor ions, making ETD with these metals impossible. CID of $[M + Al - 2H]^+$ and $[M + Cr - 2H]^+$ from maltotetraose produced extensive fragmentation throughout the molecule, as seen in Figures 3.12 and 3.13. The fragmentation, with extensive cross-ring and internal cleavages, more closely resembled ETD than CID from the divalent metal adducts of Co^{2+}, Ni^{2+}, and Zn^{2+}. The product ions corresponding to cross-ring cleavage of the terminal rings or cross-ring cleavages with loss of mass less than 120 Da are only observed with ETD of the divalent metal cations, although they occur with CID for the trivalent metal ions. CID of $[M + Cr - 2H]^+$ from maltotetraose produced $[B_1, Z_1 + Cr - 2H + H_2O]^+$, which was not found in any other spectra. Also, CID of these ions did not form the protonated glucose product ions with loss of water that occur in all other CID spectra. CID of $[M + Fe - H]^+$ can be seen in Figure 3.14 and showed similar fragmentation to that with the other two trivalent metal cations, although not as extensive. This could be due to the fact that some Fe^{3+} can be reduced to Fe^{2+} during ionization when using the ESI source design on the Bruker HCTultra.[79,80]

The number of structurally informative product ions generated with each metal ion varied for the other tetrasaccharides included in the study. For maltotetraose and maltoheptaose (that have linear chains of glucose residues with 1-4 glycosidic bonds), the metals that produce the most fragmentation are Co^{2+} and Zn^{2+}. For galactotetraose, a linear sugar with varying monomers and linkages, adduction with Co^{2+}, Zn^{2+}, and Ni^{2+} produced similar structural information. ETD and CID spectra of $[M + Co]^{2+}$ from isotopically labeled galactotetraose are shown in Figures 3.15(a) and 3.15(b), respectively. The non-isotopically labeled spectra are in Figure 3.16. Co^{2+}, Zn^{2+}, and Ni^{2+} produced the most fragmentation for stachyose, a non-

reducing stacked oligosaccharide. CID and ETD on $[M + Co]^{2+}$ from stachyose can be seen in Figures 3.17(a) and 3.17(b), respectively. Minimal structural information was obtained for nystose, a non-reducing stacked sugar, but similar patterns of fragmentation occur with Co^{2+}, Ni^{2+}, Cu^{2+}, and Zn^{2+}. Figures 3.18(a) and 3.18(b) show CID and ETD spectra for $[M + Co]^{2+}$ from nystose. Although many fragment ions are seen in the spectra, they mainly consist of indistinguishable exact mass/isobaric internal cleavages.

Multiple metal ion properties can influence coordination to and dissociation of the oligosaccharides. The size of the metal affects both methods of fragmentation.[14,16,38,54] In the present study, the metals that produced the most consistent and informative fragmentation had ionic radii between 0.083 and 0.089 nm. Metal ions tend to coordinate to multiple oxygens on an oligosaccharide simultaneously.[13,14,16,55,56,81] Therefore, these smaller ionic radii may allow the metals to have a choice of numerous locations, possibly behaving as a mobile cation and increasing fragmentation. The larger ions, such as Na^{+}, K^{+}, and Ca^{2+}, with an ionic radius of greater than 0.1 nm may be restricted in where they bind or they may hold together dissociated product ions through simultaneous coordination at multiple sites. Several studies have shown that larger metal cations yield decreased fragmentation by PSD and CID.[13,14,16]

Electron-based dissociation mechanisms have been studied more thoroughly for peptides than for glycans. Liu and Håkansson[82] proposed that the electron is first captured at the metal ion and then transferred to the peptide backbone; for divalent metal ions, a lower second ionization energy (IE) may facilitate electron movement and enhance fragmentation. Chen et al.,[83] however, suggested that electronic configuration of the metal dictates ECD fragmentation to a greater degree than the second IE. This is based on their observation that metal ions with

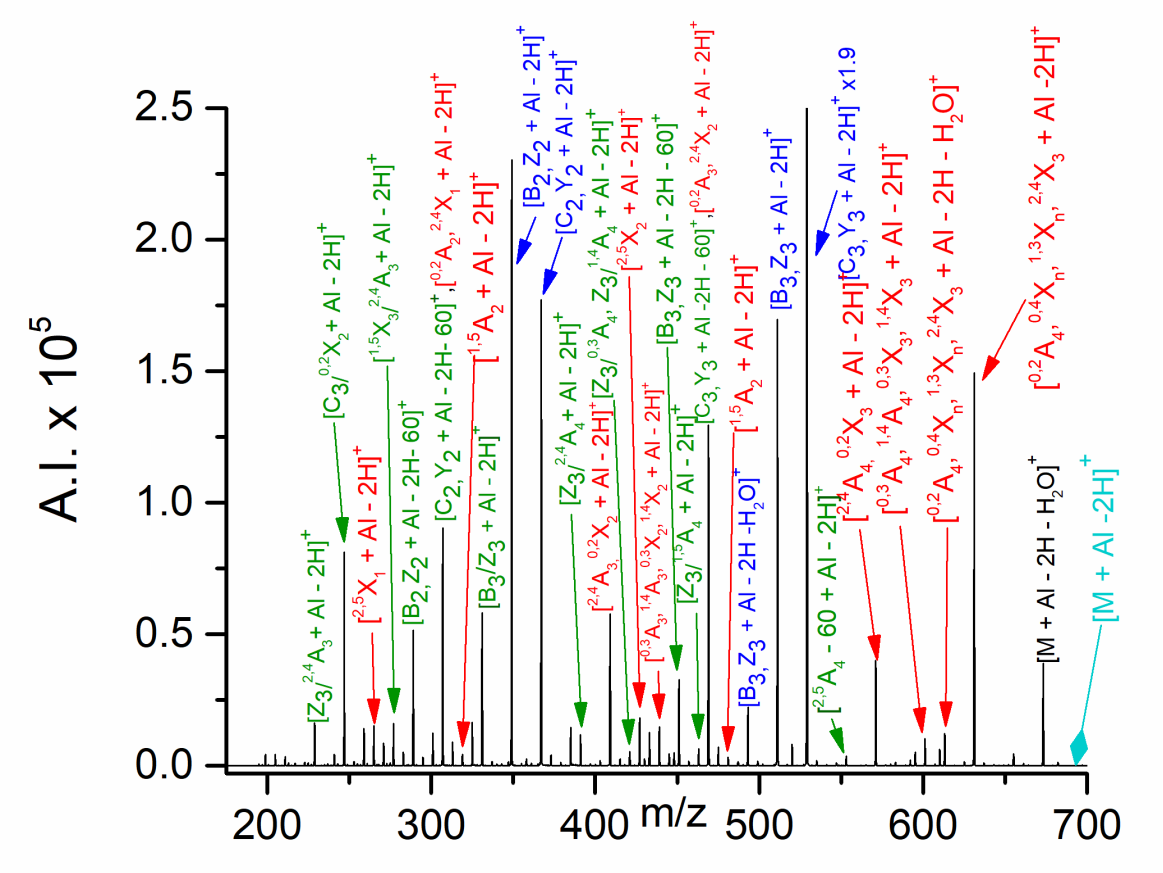

Figure 3.12 Collision-induced dissociation mass spectrum of maltotetraose for $[M + Al - 2H]^+$. Refer to the Figure 3.1 caption for an explanation of the color codes

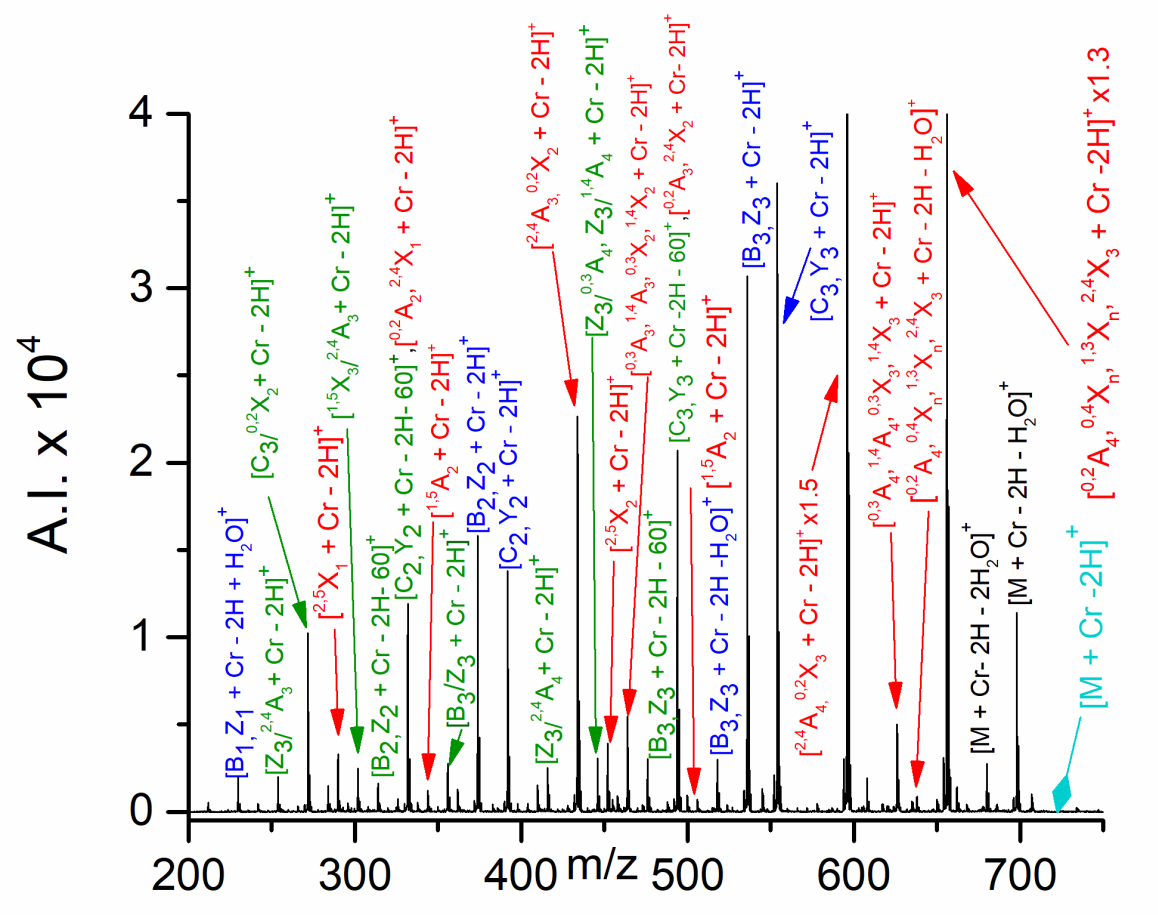

Figure 3.13 Collision-induced dissociation mass spectrum of maltotetraose for $[M + Cr - 2H]^+$. Refer to the Figure 3.1 caption for an explanation of the color codes.

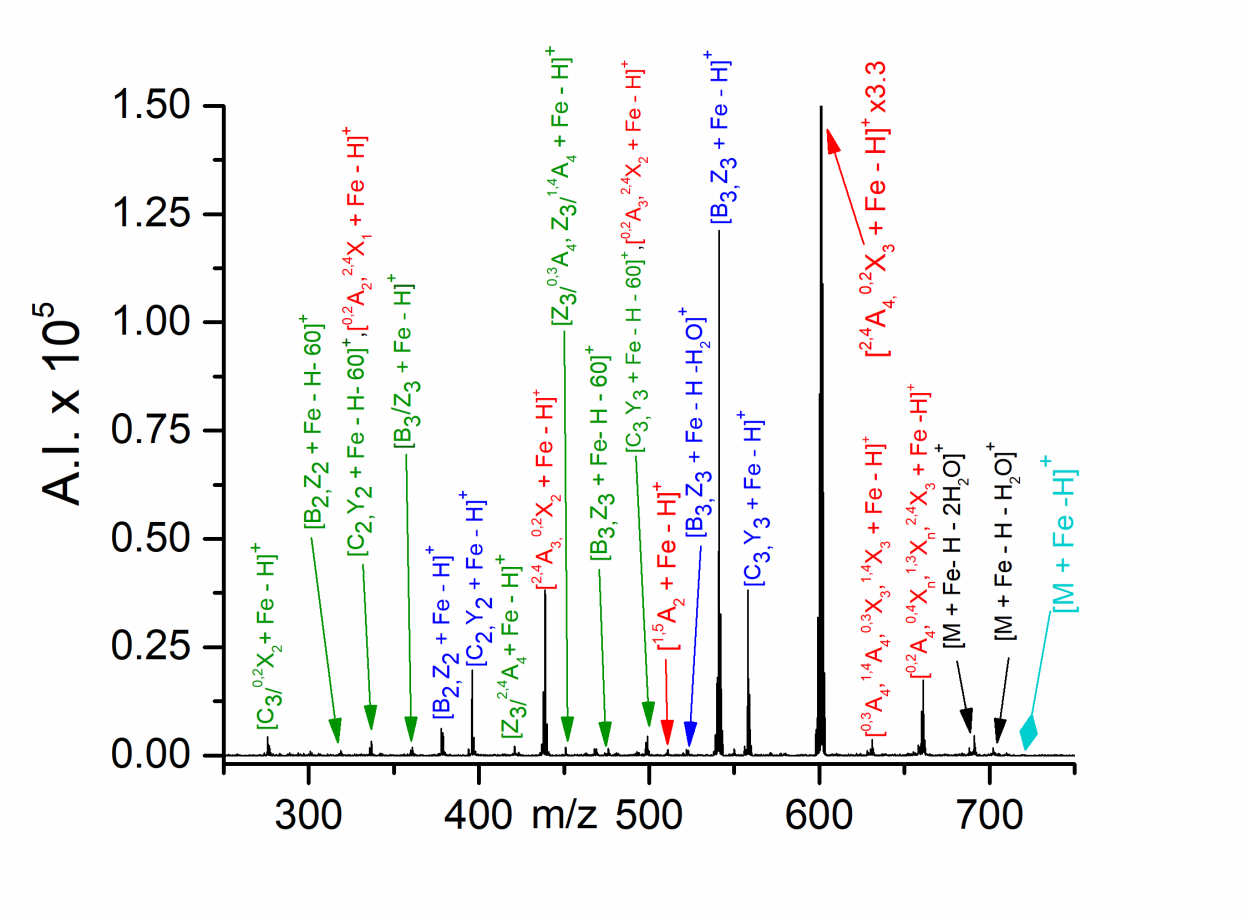

Figure 3.14 Collision-induced dissociation mass spectrum of maltotetraose for $[M + Fe - H]^+$. Refer to the Figure 3.1 caption for an explanation of the color codes.

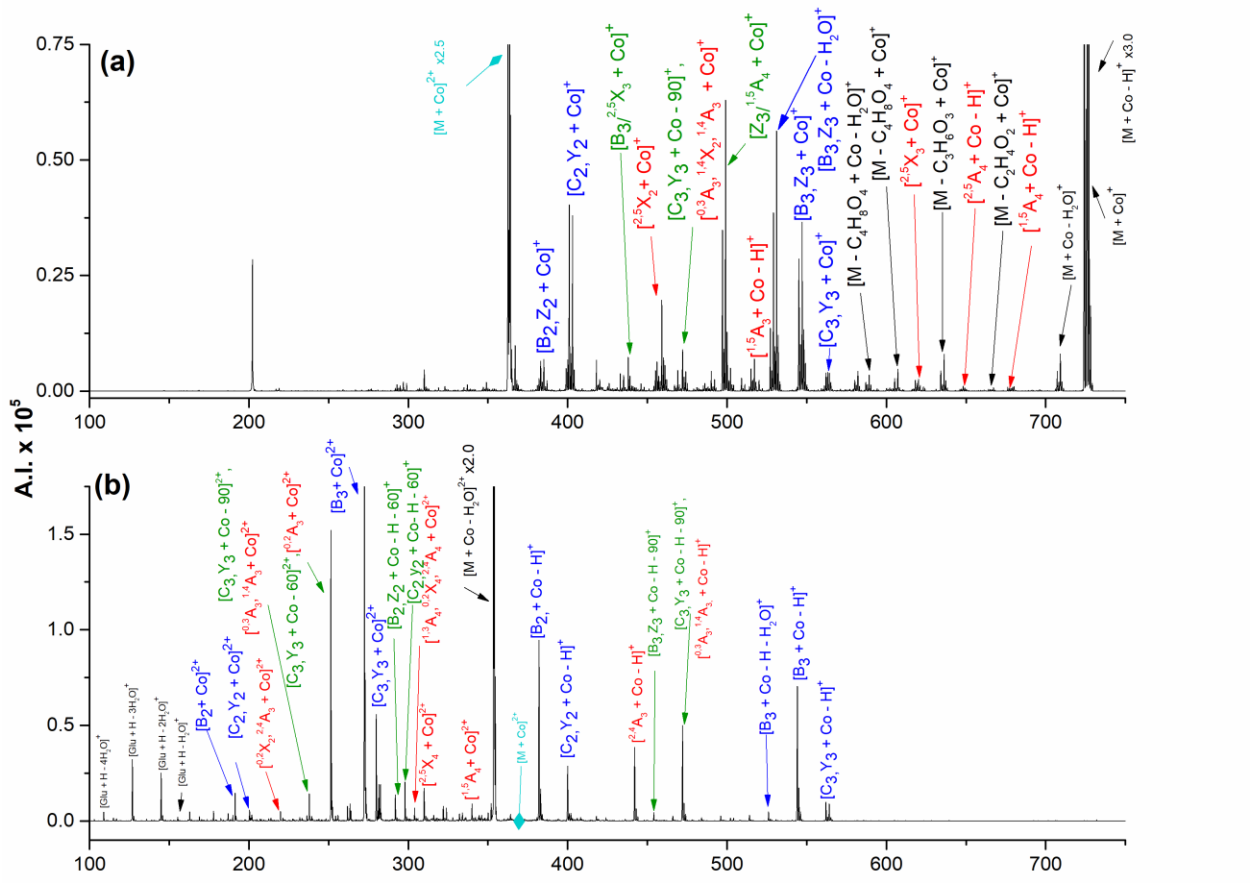

Figure 3.15 Mass spectra from (a) ETD and (b) CID of $[M + Co]^{2+}$ from galactotetraose with ^{18}O isotopic labeling at the reducing end. Refer to the Figure 3.1 caption for an explanation of the color codes.

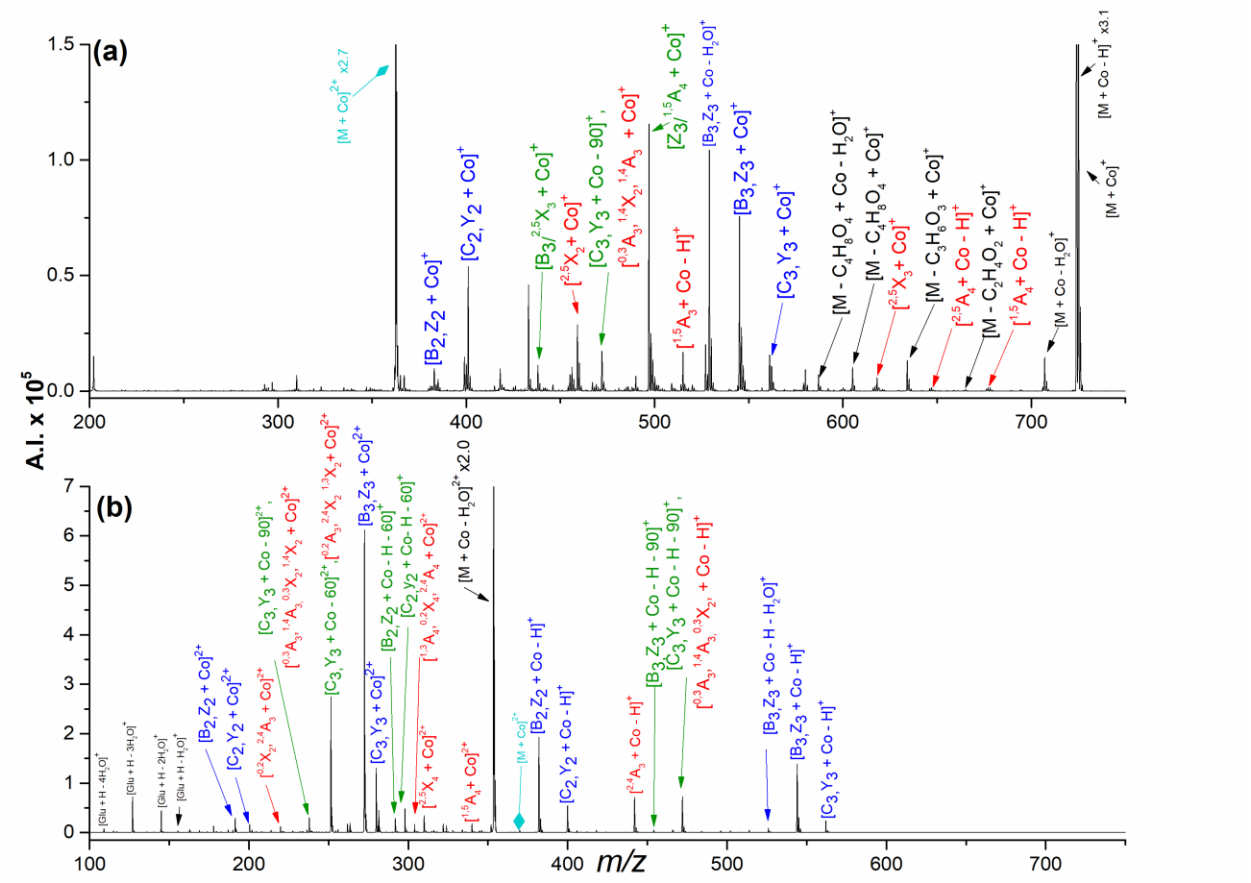

Figure 3.16 Mass spectra from (a) ETD and (b) CID of $[M + Co]^{2+}$ from non-isotopically labeled galactotetraose. Refer to the Figure 3.1 caption for an explanation of the color codes.

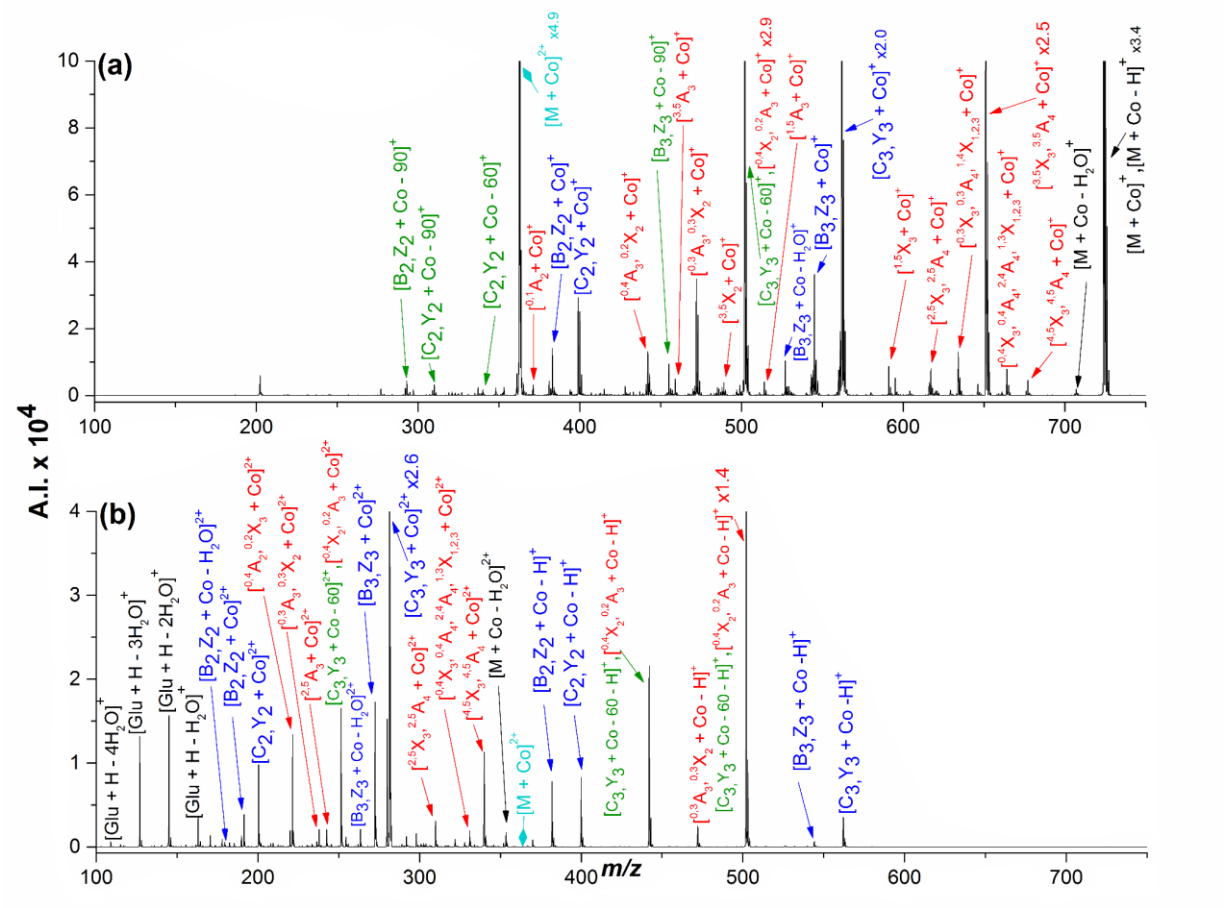

Figure 3.17 Mass spectra from (a) ETD and (b) CID of $[M + Co]^{2+}$ from stachyose. Refer to the Figure 3.1 caption for an explanation of the color codes.

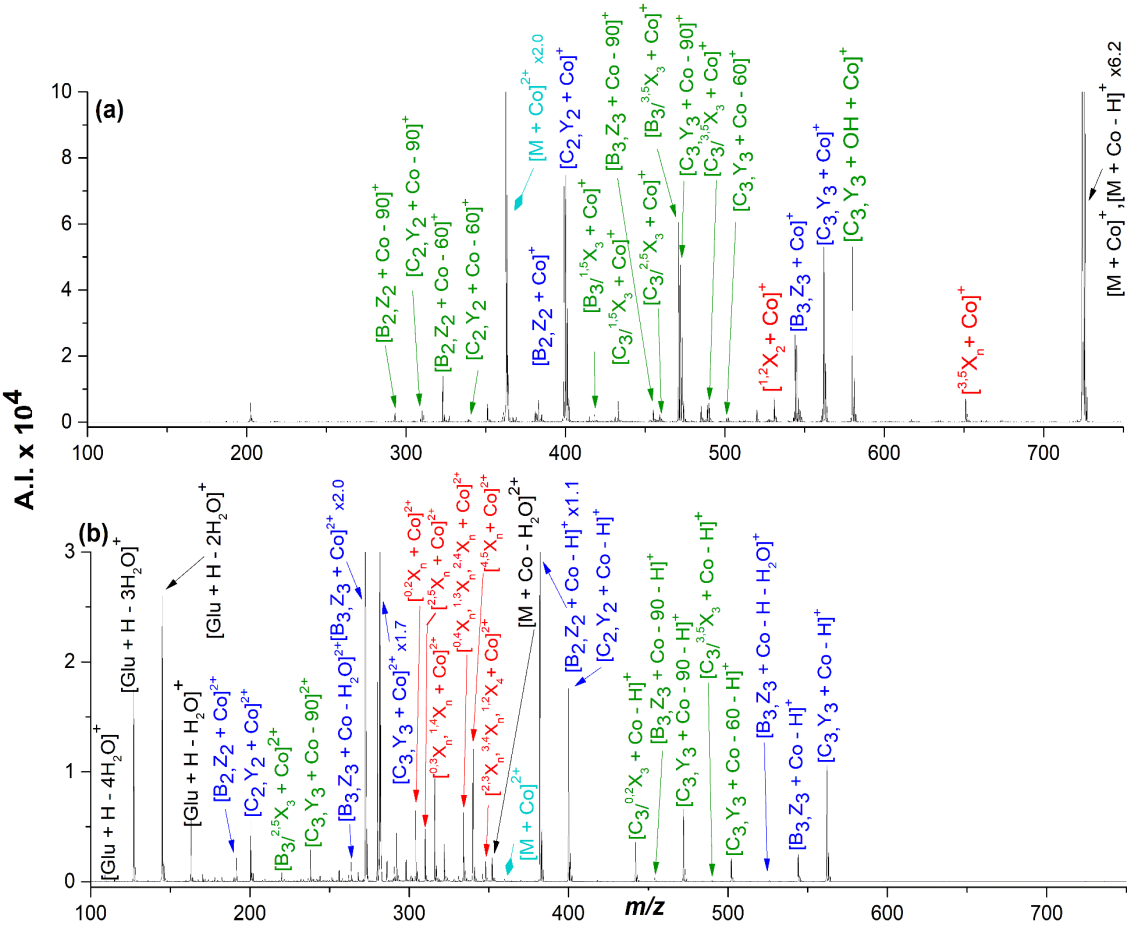

Figure 3.18 Mass spectra from (a) ETD and (b) CID of $[M + Co]^{2+}$ from nystose. Refer to the Figure 3.1 caption for an explanation of the color codes.

half or fully filled d orbitals show different fragmentation patterns than metals with partially filled d shells. Supporting this theory, Kleinnijenhuis et al.[84] proposed that Cu^{2+} captures an electron during ECD, reducing Cu^{2+} to the more stable d^{10} Cu^{1+}, which explains the limited fragmentation they observed from $[Peptide + Cu]^{2+}$. These concepts should hold true for ETD and either could explain why Cu^{2+} adducts show less extensive dissociation for the oligosaccharides in the current study. Cu^{2+} has the highest second IE of the divalent metals included in the study at 1957.9 kJ/mol, as well as a $3d^9$ electronic configuration that favors metal ion reduction. This contrasts with Co^{2+}, which has a much lower second IE of 1648.0 kJ/mol and an electron configuration of $3d^7$, where extensive fragmentation is observed for $[M + Co]^{2+}$ with oligosaccharides. The enhanced dissociation seen with Co^{2+} versus Ni^{2+} (where both metals have similar solution-phase characteristics and are part of the iron triad) may be explained by the fact that Co^{2+} has a slightly larger ionic radius, significantly reducing the charge density on the metal ion (2890 Q/R^3 for Co^{2+} versus 3500 Q/R^3 for Ni^{2+}).

In a study of glycans, Adamson and Håkansson[38] reported that coordination number of a metal ion and the second IE of the metal can affect ECD fragmentation. Metal second IE may be important but cannot be the overriding factor because in our work Co^{2+}, Ni^{2+}, and Zn^{2+} produce more fragmentation for oligosaccharides than the lower second IE metals Mg^{2+} and Ca^{2+}. This may relate to the fact that Mg^{2+} and Ca^{2+} already have stable electron configurations of [Ne] and [Ar], respectively. Another factor that could explain the current results was proposed by Costello and co-workers,[26] who used theoretical calculations to suggest that the electron is captured at Mg^{2+} to form Mg^{+}. This reduced Mg^{1+} then abstracts a hydroxyl group (•OH) from the sugar, forming a carbon radical that induces fragmentation. In this mechanism, an electron does not need to be transferred to the sugar to induce fragmentation.

3.4.3 Effect of Oligosaccharide Structure on Dissociation

The identity of the oligosaccharide affects fragmentation, as can be seen in Figures 3.2, 3.3, 3.11, 3.15, 3.17, 3.18, and 3.19 which all show dissociation using Co^{2+}. ETD fragmentation efficiency of the tetrasaccharides decreased in the order maltotetraose > stachyose > 3α,4β,3α-galactotetraose > nystose with most of the metal ions. ETD on metallated maltotetraose and 3α,4β,3α-galactotetraose generally produce a greater variety of product ions, while maltotetraose and stachyose generate more cross-ring cleavage ions. This could be caused by the types of glycosidic bonds or the identity of the monosaccharide units in the molecule. The reducing sugars show more extensive cross-ring and internal fragmentation near the reducing end than the non-reducing end. ^{18}O isotopic labeling of the reducing sugars indicates that majority of the cross-ring product ions contain the non-reducing end. Linkage determination is possible by examination of cross-ring cleavage product ions and secondary fragment ions. One example is in comparing ETD on galactotetraose and maltotetraose. Maltotetraose contains $[B_2, Z_2 + Co - 90]$, $[C_2, Y_2 + Co - 60]$ and $[C_2, Y_2 + Co - 90]$, which can be indicative of a 1,4 glycosidic bond. These internal ions along with $[B_3, Z_3 + Co - 60]$ are not observed in the galactotetraose spectra. The ETD spectrum of nystose as seen in Figure 3.18 lacks the neutral loss product ions seen above *m/z* 600 with the other tetrasaccharides. In order to accurately assign structural information, it is important that a variety of structurally informative product ions accompany high ETD efficiency.

The low product ion formation for stachyose and nystose may lie in the fact that they are non-reducing sugars that cannot be hydrolyzed into the aldehyde structure which exists in the "open" form in solution.[85] Stachyose and nystose are also stacked sugars, where some or all the monosaccharide units in the chain are flexible due to their glycosidic bond linkage and can stack

above each other. Nystose has three flexible furanose rings,[86,87] while stachyose has rotational flexibility in the terminal monosaccharides and flexibility between the two middle monosaccharides.[88] Nystose produced more electron transfer no dissociation (ETnoD) ions than the other oligosaccharides. With supplemental collisional activation on the charge reduced ETnoD ion, the fragmentation efficiency of nystose was improved and resulted in products that are a mixture of ions formed by ETD and CID. This suggests that metal cations likely coordinate more strongly to multiple oxygens between stacked monosaccharides than between linear chains. The metal ions may be able to bind at different sites on the oligosaccharide depending on these structural differences, which can influence fragmentation pathways.[28] If the metal ion is coordinated to oxygens on multiple rings along with a glycosidic oxygen, the dissociation yield may be decreased. However, as previously mentioned, the ability of metals to ionize the oligosaccharide is independent of the oligosaccharide's structural characteristics.

The effects of structural differences can be seen by comparing the spectra from maltotetraose (Figures 3.2 and 3.3) to those from the non-reducing sugar nystose (Figure 3.18 for $[M + Co]^{2+}$). The ETD spectrum of nystose is dominated by product ions from internal cleavages with one glycosidic bond cleavage and one cross-ring cleavage, while CID on $[M+ Co]^{2+}$ yields cross-ring cleavage between every carbon on the monosaccharide unit (the exact monosaccharide unit can not be distinguished). This is indicative of each monosaccharide unit being linked together via only one carbon that is a part of the ring such as the 2-1 glycosidic bonds present in nystose. Very little cross-ring cleavage is seen by ETD of nystose; however, a product ion unique to this sugar is $^{1,2}X_2$, which corresponds to loss of a terminal monosaccharide unit and CH_2OH. Even with little dissociation, ETD and CID still yield complementary fragmentation.

3.4.4 Effect of Chain Length on Dissociation

Maltoheptaose was compared to maltotetraose to study the effects of chain length on fragmentation of metal-adducted oligosaccharides. ETD and CID spectra of $[M + Co]^{2+}$ from ^{18}O labelled maltoheptaose can be seen in Figure 3.19, while the maltotetraose spectra are in Figure 3.11. (Spectra from non-labeled maltoheptaose are in Figure 3.20.) ETD on maltoheptaose produced the same type of fragment ions as on maltotetraose, and all 7 glucose units underwent dissociation. Glycosidic bond cleavage occurred between every glucose unit with both dissociation techniques. Maltoheptaose generally produced larger product ions; ETD products from maltoheptaose contain at least four glucose units, while CID products have at least three glucose units from doubly charged precursor ions and at least two units from singly charged precursor ions. In contrast, maltotetraose yields products with a minimum of two glucose units by both ETD and CID. As with maltotetraose, for CID on maltoheptaose the only ions that contain the reducing end are Y ions that occurred on the non-reducing side of the glycosidic oxygen; however, in the ETD spectra, both Y and Z ions are present, on both sides of the glycosidic oxygen. The types of product ions and efficiency of dissociation did not vary between maltotetraose and maltoheptaose. This implies that when the monosaccharide unit remains the same a longer chain does not significantly affect fragmentation, but more studies are necessary to confirm this phenomenon.

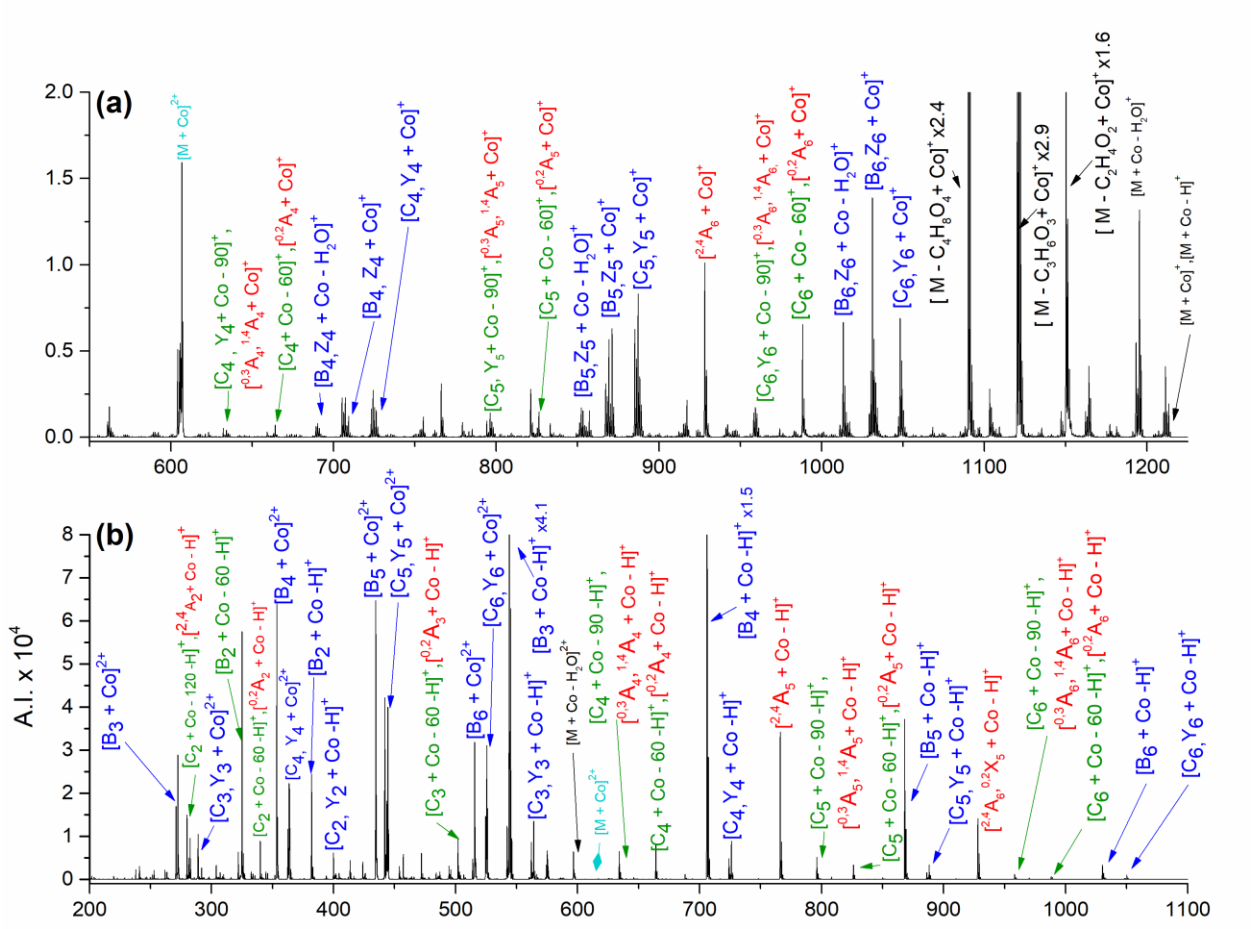

Figure 3.19 Mass spectra from (a) ETD and (b) CID of $[M + Co]^{2+}$ from maltoheptaose with ^{18}O isotopic labeling at the reducing end. Refer to the Figure 3.1 caption for an explanation of the color codes.

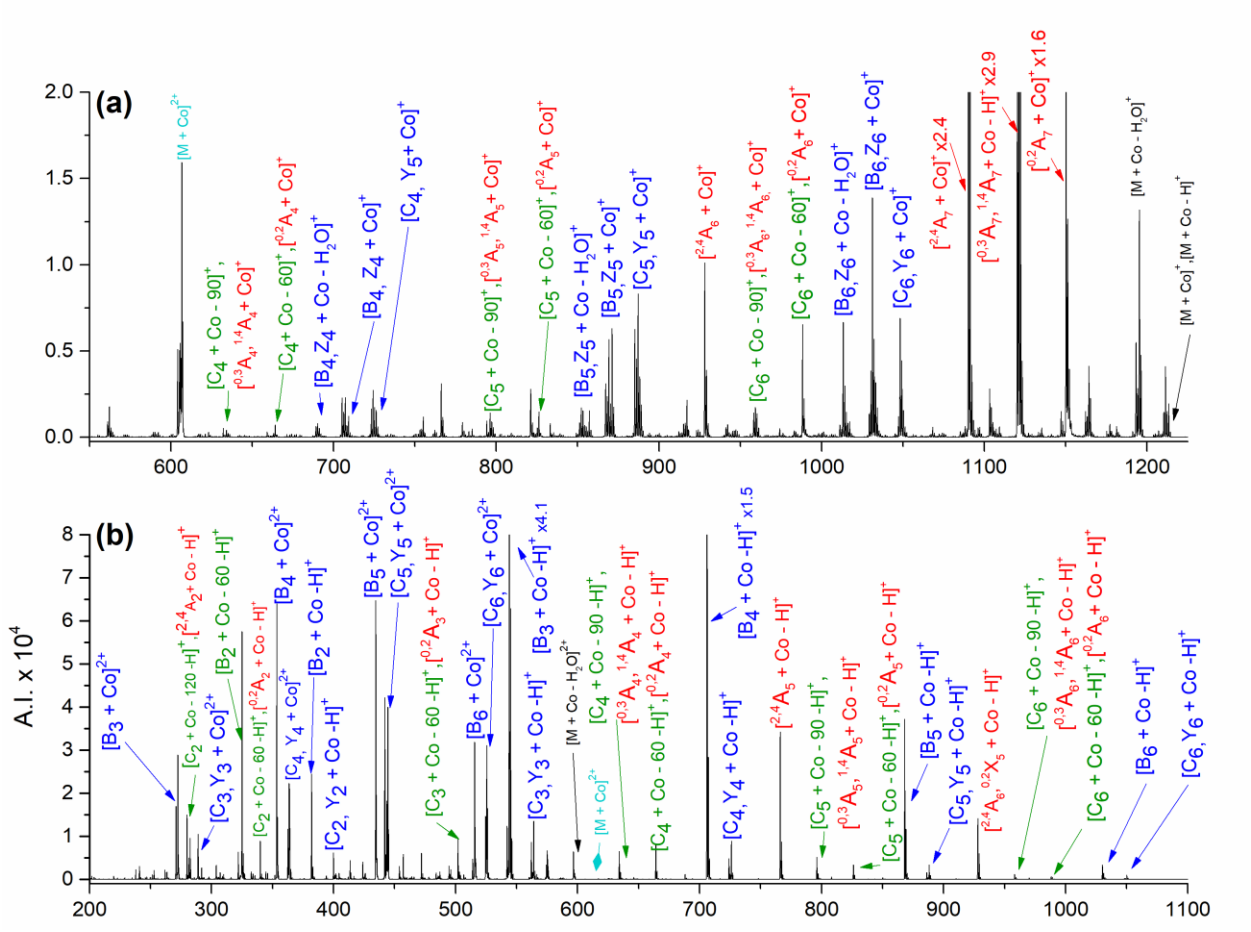

Figure 3.20 Mass spectra from (a) ETD and (b) CID of $[M + Co]^{2+}$ from non-isotopically labeled maltoheptaose. Refer to the Figure 3.1 caption for an explanation of the color codes.

3.5 Conclusions

The current study illustrates the effects of metal-adduction on dissociation of underivatized oligosaccharides. ESI produced intense metallated precursor ions and easily interpretable spectra. Both ETD and CID methods showed high fragmentation efficiency. Cross-ring cleavages and internal cleavages were more prevalent with ETD, while CID yields more glycosidic bond cleavage. The extent and efficiency of dissociation with both ETD and CID is dependent on the metal cation. The differences in fragmentation are likely due to ionic radius, metal coordination, and IE of the metal ions. The trivalent metals used in the study did not readily adduct to the oligosaccharides and produced inconsistent dissociation patterns, possibly due to their high charge density. The most structurally informative fragmentation by both ETD and CID is obtained from $[M + Co]^{2+}$ for all oligosaccharides in the study. Increasing the chain length while monosaccharide and glycosidic bond linkage stay the same did not affect fragmentation for the glycans studied.

REFERENCES

1. Varki, A. Biological roles of oligosaccharides: All of the theories are correct. *Glycobiology* **1993**, *3*, 97-130.

2. Parodi, A. J. Protein glucosylation and its role in protein folding. *Annu. Rev. Biochem.* **2000**, *69*, 69-93.

3. Ashline, D.; Singh, S.; Hanneman, A.; Reinhold, V. Congruent strategies for carbohydrate sequencing. 1. mining structural details by MS^n. *Anal. Chem.* **2005**, *77*, 6250-6262.

4. Fenn, J. B.; Mann, M.; Meng, C. K.; Wong, S. F. Electrospray ionization--principles and practice. *Mass Spectrom. Rev.* **1990**, *9*, 37-70.

5. Fenn, J. B.; Mann, M.; Meng, C. K.; Wong, S. F.; Whitehouse, C. M. Electrospray ionization for mass spectrometry of large biomolecules. *Science* **1989**, *246*, 64-71.

6. Hop, C. E. C. A.; Bakhtiar, R. An introduction to electrospray ionization and matrix-assisted laser desorption/ionization mass spectrometry: Essential tools in a modern biotechnology environment. *Biospectroscopy* **1997**, *3530*, 259-280.

7. Zaia, J. Mass spectrometry of oligosaccharides. *Mass Spectrom. Rev.* **2004**, *23*, 161-227.

8. Zhao, C.; Xie, B.; Chan, S.; Costello, C. E.; O'Connor, P. B. Collisionally activated dissociation and electron capture dissociation provide complementary structural information for branched permethylated oligosaccharides. *J. Am. Soc. Mass Spectrom.* **2008**, *19*, 138-150.

9. Harvey, D. J. Collision-induced fragmentation of underivatized N-linked carbohydrates ionized by electrospray. *J. Mass Spectrom.* **2000**, *35*, 1178-1190.

10. Lemoine, J.; Strecker, G.; Leroy, Y.; Fournet, B.; Ricart, G. Collisional-activation tandem mass spectrometry of sodium adduct ions of methylated oligosaccharides: Sequence analysis and discrimination between α-NeuAc-(2→3) and α-NeuAc-(2 →6) linkages. *Carbohydr. Res.* **1991**, *221*, 209-217.

11. Zaia, J.; Miller, M. J. C.; Seymour, J. L.; Costello, C. E. The role of mobile protons in negative ion CID of oligosaccharides. *J. Am. Soc. Mass Spectrom.* **2007**, *18*, 952-960.

12. Dallinga, J. W.; Heerma, W. Positive ion fast atom bombardment mass spectrometry of some small oligosaccharides. *Biol. Mass Spectrom.* **1991**, *20*, 99-108.

13. Bythell, B. J.; Abutokaikah, M. T.; Wagoner, A. R.; Guan, S.; Rabus, J. M. Cationized carbohydrate gas-phase fragmentation chemistry. *J. Am. Soc. Mass Spectrom.* **2017**, *28*, 688-703.

14. Fura, A.; Leary, J. A. Differentiation of Ca^{2+}-coordinated and Mg^{2+}-coordinated branched trisaccharide isomers: An electrospray ionization and tandem mass spectrometry study. *Anal. Chem.* **1993**, *65*, 2805-2811.

15. Harvey, D. J.; Naven, T. J. P.; Küster, B.; Bateman, R. H.; Green, M. R.; Critchley, G. Comparison of fragmentation modes for the structural determination of complex oligosaccharides ionized by matrix-assisted laser desorption/ionization mass spectrometry. *Rapid Commun. Mass Spectrom.* **1995**, *9*, 1556-1561.

16. Cancilla, M. T.; Penn, S. G.; Carroll, J. A.; Lebrilla, C. B. Coordination of alkali metals to oligosaccharides dictates fragmentation behavior in matrix assisted laser desorption ionization/Fourier transform mass spectrometry. *J. Am. Chem. Soc.* **1996**, *118*, 6736-6745.

17. Wolff, J. J.; Laremore, T. N.; Leach, F. E., III; Linhardt, R. J.; Amster, I. J. Electron capture dissociation, electron detachment dissociation and infrared multiphoton dissociation of sucrose octasulfate. *Eur. J. Mass Spectrom.* **2009**, *15*, 275-281.

18. Leach, F. E.,III; Xiao, Z.; Laremore, T. N.; Linhardt, R. J.; Amster, I. J. Electron detachment dissociation and infrared multiphoton dissociation of heparin tetrasaccharides. *Int. J. Mass Spectrom.* **2011**, *308*, 253-259.

19. Xie, Y. M.; Lebrilla, C. B. Infrared multiphoton dissociation of alkali metal-coordinated oligosaccharides. *Anal. Chem.* **2003**, *75*, 1590-1598.

20. Zhang, J. H.; Schubothe, K.; Li, B. S.; Russell, S.; Lebrilla, C. B. Infrared multiphoton dissociation of O-linked mucin-type oligosaccharides. *Anal. Chem.* **2005**, *77*, 208-214.

21. Adamson, J. T.; Håkansson, K. Infrared multiphoton dissociation and electron capture dissociation of high-mannose type glycopeptides. *J. Proteome Res.* **2006**, *5*, 493-501.

22. Ko, B. J.; Brodbelt, J. S. 193 nm ultraviolet photodissociation of deprotonated sialylated oligosaccharides. *Anal. Chem.* **2011**, *83*, 8192-8200.

23. O'Brien, J. P.; Brodbelt, J. S. Structural characterization of gangliosides and glycolipids via ultraviolet photodissociation mass spectrometry. *Anal. Chem.* **2013**, *85*, 10399-10407.

24. Klein, D. R.; Holden, D. D.; Brodbelt, J. S. Shotgun analysis of rough-type lipopolysaccharides using ultraviolet photodissociation mass spectrometry. *Anal. Chem.* **2016**, *88*, 1044-1051.

25. Ko, B. J.; Brodbelt, J. S. Ultraviolet photodissociation of chromophore-labeled oligosaccharides via reductive amination and hydrazide conjugation. *J. Mass Spectrom.* **2011**, *46*, 359-366.

26. Huang, Y.; Pu, Y.; Yu, X.; Costello, C. E.; Lin, C. Mechanistic study on electron capture dissociation of the oligosaccharide-Mg^{2+} complex. *J. Am. Soc. Mass Spectrom.* **2014**, *25*, 1451-1460.

27. Yu, X.; Jiang, Y.; Chen, Y.; Huang, Y.; Costello, C. E.; Lin, C. Detailed glycan structural characterization by electronic excitation dissociation. *Anal. Chem.* **2013**, *85*, 10017-10021.

28. Han, L.; Costello, C. E. Electron transfer dissociation of milk oligosaccharides. *J. Am. Soc. Mass Spectrom.* **2011**, *22*, 997-1013.

29. Yu, X.; Huang, Y.; Lin, C.; Costello, C. E. Energy-dependent electron activated dissociation of metal-adducted permethylated oligosaccharides. *Anal. Chem.* **2012**, *84*, 7487-7494.

30. Darula, Z.; Medzihradszky, K. F. Glycan side reaction may compromise ETD-based glycopeptide identification. *J. Am. Soc. Mass Spectrom.* **2014**, *25*, 977-987.

31. Yang, J.; Mo, J. J.; Adamson, J. T.; Håkansson, K. Characterization of oligodeoxynucleotides by electron detachment dissociation Fourier transform ion cyclotron resonance mass spectrometry. *Anal. Chem.* **2005**, *77*, 1876-1882.

32. Budnik, B. A.; Haselmann, K. F.; Elkin, Y. N.; Gorbach, V. I.; Zubarev, R. A. Applications of electron-ion dissociation reactions for analysis of polycationic chitooligosaccharides in Fourier transform mass spectrometry. *Anal. Chem.* **2003**, *75*, 5994-6001.

33. Hersberger, K. E.; Håkansson, K. Characterization of *O*-sulfopeptides by negative ion mode tandem mass spectrometry: Superior performance of negative ion electron capture dissociation. *Anal. Chem.* **2012**, *84*, 6370-6377.

34. Wolff, J. J.; Laremore, T. N.; Busch, A. M.; Linhardt, R. J.; Amster, I. J. Electron detachment dissociation of dermatan sulfate oligosaccharides. *J. Am. Soc. Mass Spectrom.* **2008**, *19*, 294-304.

35. Wolff, J. J.; Laremore, T. N.; Aslam, H.; Linhardt, R. J.; Amster, I. J. Electron-induced dissociation of glycosaminoglycan tetrasaccharides. *J. Am. Soc. Mass Spectrom.* **2008**, *19*, 1449-1458.

36. Wolff, J. J.; Laremore, T. N.; Busch, A. M.; Linhardt, R. J.; Amster, I. J. Influence of charge state and sodium cationization on the electron detachment dissociation and infrared multiphoton dissociation of glycosaminoglycan oligosaccharides. *J. Am. Soc. Mass Spectrom.* **2008**, *19*, 790-798.

37. Leach, F. E.,III; Wolff, J. J.; Xiao, Z.; Ly, M.; Laremore, T. N.; Arungundram, S.; Al-Mafraji, K.; Venot, A.; Boons, G.; Linhardt, R. J.; Amster, I. J. Negative electron transfer dissociation Fourier transform mass spectrometry of glycosaminoglycan carbohydrates. *Eur. J. Mass Spectrom.* **2011**, *17*, 167-176.

38. Adamson, J. T.; Håkansson, K. Electron capture dissociation of oligosaccharides ionized with alkali, alkaline earth, and transition metals. *Anal. Chem.* **2007**, *79*, 2901-2910.

39. Duffin, K. L.; Welply, J. K.; Huang, E.; Henion, J. D. Characterization of N-linked oligosaccharides by electrospray and tandem mass spectrometry. *Anal. Chem.* **1992**, *64*, 1440-1448.

40. Kailemia, M. J.; Ruhaak, L. R.; Lebrilla, C. B.; Amster, I. J. Oligosaccharide analysis by mass spectrometry: A review of recent developments. *Anal. Chem.* **2014**, *86*, 196-212.

41. Park, Y.; Lebrilla, C. B. Application of Fourier transform ion cyclotron resonance mass spectrometry to oligosaccharides. *Mass Spectrom. Rev.* **2005**, *24*, 232-264.

42. Reinhold, V. N.; Reinhold, B. B.; Costello, C. E. Carbohydrate molecular weight profiling, sequence, linkage, and branching data: ES-MS and CID. *Anal. Chem.* **1995**, *67*, 1772-1784.

43. Burlingame, A. L.; Boyd, R. K.; Gaskell, S. J. Mass spectrometry. *Anal. Chem.* **1994**, *66*, R-634-R683.

44. Bahr, U.; Pfenninger, A.; Karas, M.; Stahl, B. High sensitivity analysis of neutral underivatized oligosaccharides by nanoelectrospray mass spectrometry. *Anal. Chem.* **1997**, *69*, 4530-4535.

45. Lemoine, J.; Fournet, B.; Despeyroux, D.; Jennings, K. R.; Rosenberg, R.; De Hoffman, E. Collision-induced dissociation of alkali metal cationized and permethylated oligosaccharides: Influence of the collision energy and of the collision gas for the assignment of linkage position. *J. Am. Soc. Mass Spectrom.* **1993**, *4*, 197-203.

46. Harvey, D. J.; Bateman, R. H.; Green, M. R. High-energy collision-induced fragmentation of complex oligosaccharides ionized by matrix-assisted laser desorption/ionization mass spectrometry. *J. Mass Spectrom.* **1997**, *32*, 167-187.

47. Harvey, D. J. Ionization and collision-induced fragmentation of N-linked and related carbohydrates using divalent cations. *J. Am. Soc. Mass Spectrom.* **2001**, *12*, 926-937.

48. Adamson, J. T.; Håkansson, K. Electron detachment dissociation of neutral and sialylated oligosaccharides. *J. Am. Soc. Mass Spectrom.* **2007**, *18*, 2162-2172.

49. Liu, H.; Håkansson, K. Electron capture dissociation of divalent metal-adducted sulfated oligosaccharides. *Int. J. Mass Spectrom.* **2011**, *305*, 170-177.

50. Domann, P.; Spencer, D. I. R.; Harvey, D. J. Production and fragmentation of negative ions from neutral N-linked carbohydrates ionized by matrix-assisted laser desorption/ionization. *Rapid Commun. Mass Spectrom.* **2012**, *26*, 469-479.

51. Asam, M. R.; Glish, G. L. Tandem mass spectrometry of alkali cationized polysaccharides in a quadrupole ion trap. *J. Am. Soc. Mass Spectrom.* **1997**, *8*, 987-995.

52. El Firdoussi, A.; Lafitte, M.; Tortajada, J.; Kone, O.; Salpin, J. Characterization of the glycosidic linkage of underivatized disaccharides by interaction with Pb^{2+} ions. *J. Mass Spectrom.* **2007**, *42*, 999-1011.

53. Konig, S.; Leary, J. A. Evidence for linkage position determination in cobalt coordinated pentasaccharides using ion trap mass spectrometry. *J. Am. Soc. Mass Spectrom.* **1998**, *9*, 1125-1134.

54. Sible, E. M.; Brimmer, S. P.; Leary, J. A. Interaction of first row transition metals with alpha 1-3, alpha 1-6 mannotriose and conserved trimannosyl core oligosaccharides: A comparative electrospray ionization study of doubly and singly charged complexes. *J. Am. Soc. Mass Spectrom.* **1997**, *8*, 32-42.

55. Hofmeister, G. E.; Zhou, Z.; Leary, J. A. Linkage position determination in lithium-cationized disaccharides: Tandem mass spectrometry and semiempirical calculations. *J. Am. Chem. Soc.* **1991**, *113*, 5964-5970.

56. Zhou, Z. R.; Ogden, S.; Leary, J. A. Linkage position determination in oligosaccharides: MS/MS study of lithium-cationized carbohydrates. *J. Org. Chem.* **1990**, *55*, 5444-5446.

57. Zhu, F.; Glover, M. S.; Shi, H.; Trinidad, J. C.; Clemmer, D. E. Populations of metal-glycan structures influence MS fragmentation patterns. *J. Am. Soc. Mass Spectrom.* **2015**, *26*, 25-35.

58. Penn, S. G.; Cancilla, M. T.; Lebrilla, C. B. Fragmentation behavior of multiple-metal-coordinated acidic oligosaccharides studied by matrix-assisted laser desorption ionization Fourier transform mass spectrometry. *Int. J. Mass Spectrom.* **2000**, *195*, 259-269.

59. Huang, Y.; Dodds, E. D. Discrimination of isomeric carbohydrates as the electron transfer products of group II cation adducts by ion mobility spectrometry and tandem mass spectrometry. *Anal. Chem.* **2015**, *87*, 5664-5668.

60. Kornacki, J. R.; Adamson, J. T.; Håkansson, K. Electron detachment dissociation of underivatized chloride-adducted oligosaccharides. *J. Am. Soc. Mass Spectrom.* **2012**, *23*, 2031-2042.

61. Reinhold, V. N.; Sheeley, D. M. Detailed characterization of carbohydrate linkage and sequence in an ion trap mass spectrometer: Glycosphingolipids. *Anal. Biochem.* **1998**, *259*, 28-33.

62. Viseux, N.; de Hoffmann, E.; Domon, B. Structural analysis of permethylated oligosaccharides by electrospray tandem mass spectrometry. *Anal. Chem.* **1997**, *69*, 3193-3198.

63. Ciucanu, I. Per-O-methylation reaction for structural analysis of carbohydrates by mass spectrometry. *Anal. Chim. Acta* **2006**, *576*, 147-155.

64. Heiss, C.; Wang, Z.; Azadi, P. Sodium hydroxide permethylation of heparin disaccharides. *Rapid Commun. Mass Spectrom.* **2011**, *25*, 774-778.

65. Price, N. P. J. Permethylation linkage analysis techniques for residual carbohydrates. *Appl. Biochem. Biotechnol.* **2008**, *148*, 271-276.

66. Viseux, N.; de Hoffmann, E.; Domon, B. Structural assignment of permethylated oligosaccharide subunits using sequential tandem mass spectrometry. *Anal. Chem.* **1998**, *70*, 4951-4959.

67. Shannon, R. D. Revised effective ionic radii and systematic studies of interatomic distances in halides and chalcogenides. *Acta Crystallogr. Sect. A* **1976**, *A32*, 751-767.

68. Chen, X.; Liu, G.; Wong, Y. L. E.; Deng, L.; Wang, Z.; Li, W.; Chan, T. W. D. Dissociation of trivalent metal ion (Al^{3+}, Ga^{3+}, In^{3+} and Rh^{3+})–peptide complexes under electron capture dissociation conditions. *Rapid Commun. Mass Spectrom.* **2016**, *30*, 705-710.

69. Prell, J. S.; Flick, T. G.; Oomens, J.; Berden, G.; Williams, E. R. Coordination of trivalent metal cations to peptides: Results from IRMPD spectroscopy and theory. *J. Phys. Chem. A* **2009**, *114*, 854-860.

70. Commodore, J. J.; Cassady, C. J. Effects of acidic peptide size and sequence on trivalent praseodymium adduction and electron transfer dissociation mass spectrometry. *J. Mass Spectrom.* **2017**, *52*, 218-229.

71. Flick, T. G.; Donald, W. A.; Williams, E. R. Electron capture dissociation of trivalent metal ion-peptide complexes. *J. Am. Soc. Mass Spectrom.* **2013**, *24*, 193-201.

72. Commodore, J. J.; Cassady, C. J. The effects of trivalent lanthanide cationization on the electron transfer dissociation of acidic fibrinopeptide B and its analogs. *J. Am. Soc. Mass Spectrom.* **2016**, *27*, 1499-1509.

73. Angyal, S. J. Complexes of metal-cations with carbohydrates in solution. *Adv. Carbohydr. Chem. Biochem.* **1989**, *47*, 1-43.

74. Angyal, S. J. Complexes of carbohydrates with metal cations.1. Determination of extent of complexing by NMR-spectroscopy. *Aust. J. Chem.* **1972**, *25*, 1957-1966.

75. Franks, F.; Hall, J. R.; Irish, D. E.; Norris, K. The effect of cations on the anomeric equilibrium of D-glucose in aqueous-solutions - a Raman-spectral study. *Carbohydr. Res.* **1986**, *157*, 53-64.

76. Petruŝ, L.; Bílik, V.; Kuniak, Ľ; Stankoviĉ, Ľ Chromatographic-separation of alditols on a cation-exchange resin in the lanthanum form. *Chemicke Zvesti* **1980**, *34*, 530-536.

77. Domon, B.; Costello, C. E. A systematic nomenclature for carbohydrate fragmentations in FAB-MS/MS spectra of glycoconjugates. *Glycoconj. J.* **1988**, *5*, 397-409.

78. Kohler, M.; Leary, J. A. LC/MS/MS of carbohydrates with postcolumn addition of metal chlorides using a triaxial electrospray probe. *Anal. Chem.* **1995**, *67*, 3501-3508.

79. Feng, C.; Commodore, J. J.; Cassady, C. J. The use of chromium(III) to supercharge peptides by protonation at low basicity sites. *J. Am. Soc. Mass Spectrom.* **2015**, *26*, 347-358.

80. Lavanant, H.; Virelizier, H.; Hoppilliard, Y. Reduction of copper(II) complexes by electron capture in an electrospray ionization source. *J. Am. Soc. Mass Spectrom.* **1998**, *9*, 1217-1221.

81. Zheng, Y. J.; Ornstein, R. L.; Leary, J. A. A density functional theory investigation of metal ion binding sites in monosaccharides. *J. Mol. Struct. Theochem* **1997**, *389*, 233-240.

82. Liu, H.; Håkansson, K. Divalent metal ion-peptide interactions probed by electron capture dissociation of trications. *J. Am. Soc. Mass Spectrom.* **2006**, *17*, 1731-1741.

83. Chen, X.; Fung, Y. M. E.; Chan, W. Y. K.; Wong, P. S.; Yeung, H. S.; Chan, T. W. D. Transition metal ions: Charge carriers that mediate the electron capture dissociation pathways of peptides. *J. Am. Soc. Mass Spectrom.* **2011**, *22*, 2232-2245.

84. Kleinnijenhuis, A. J.; Mihalca, R.; Heeren, R. M. A.; Heck, A. J. R. Atypical behavior in the electron capture induced dissociation of biologically relevant transition metal ion complexes of the peptide hormone oxytocin. *Int. J. Mass Spectrom.* **2006**, *253*, 217-224.

85. Voet, D.; Voet, J. G.; Pratt, C. W. *Fundamentals of Biochemistry: Life at the Molecular Level;* John Wiley & Sons: 2013.

86. French, A. D.; Mouhous-Riou, N.; Pérez, S. Computer modeling of the tetrasaccharide nystose. *Carbohydr. Res.* **1993**, *247*, 51-62.

87. Jeffrey, G. A.; Huang, D. B. The tetrasaccharide nystose trihydrate: Crystal structure analysis and hydrogen bonding. *Carbohydr. Res.* **1993**, *247*, 37-50.

88. Jeffrey, G. A.; Huang, D. B. Hydrogen bonding in the crystal structure of the tetrasaccharide stachyose hydrate: A 1:1 complex of two conformers. *Carbohydr. Res.* **1991**, *210*, 89-104.

CHAPTER 4: THE EFFECTS OF PERMETHYLATION ON THE DISSOCIATION OF METALLATED OLIGOSACCHARIDES

4.1 Overview

The effects of permethylation on the electron transfer dissociation (ETD) and collision-induced dissociation (CID) were investigated for five oligosaccharides coordinated with metal cations and ionized using electrospray ionization (ESI). The reducing tetrasaccharides maltotetraose, 3α,4β,3α-galactotetraose; reducing heptasaccharide, maltoheptaose; and non-reducing tetrasaccharides, stachyose and nystose, have been included in the study to try to better understand the structural features that influence the dissociation of metallated sugars.

The overall ion intensity in the ESI spectra of the permethylated metal-adducted oligosaccharides was about ten times higher than non-permethylated oligosaccharides. Permethylation reduced the production of fragment ions from metallated oligosaccharides upon dissociation with both ETD and CID. In general, the spectra for non-derivatized metallated oligosaccharides were more structurally informative, especially when fragmentation was induced by ETD. For many of the metal coordinated species, CID did not produce structurally informative fragmentation. For both ETD and CID, $[M + Co]^{2+}$ produced the most uniform structurally informative dissociation with all oligosaccharides studied. The ETD and CID spectra were complementary.

The majority of the permethylated glycosidic bond fragments produced by CID are C and Y ions, with only stachyose and nystose having B and Z ions, whereas product ions from both sides of the glycosidic bond form with no derivatization. ETD did not change the glycosidic

bond fragmentation when the tetrasaccharides were permethylated. ETD of permethylated oligosaccharides reduced the ambiguity of exact mass ions in some non-permethylated spectra. For both dissociation methods, the product ions in the permethylated and non-permethylated spectra for each oligosaccharide were different. In particular, the cross-ring product ions varied in in both location and type with both dissociation methods, which implies the mechanism of dissociation is affected by permethylation.

4.2 Introduction

Carbohydrates and oligosaccharides have significant and diverse roles in chemistry and biology.[1,2] Oligosaccharides in biological systems can exist as free sugars, glycoproteins, glycolipids, or with other covalent modifications.[3] At the simplest level, oligosaccharides are built from monosaccharides (e.g., hexose and pentose sugars); however, through variation in linkage position, stereochemistry, and ring structure, an enormous number of forms emerge.[4] This diversity explains the vast array of roles carbohydrates can play in immune response, energy storage and extraction, intracellular signaling, and protein folding, among many other cellular and biological processes in the body.[1,2]

Advances in mass spectrometry and soft ionization techniques have furthered the study of glycomics.[5-7] Nevertheless, the wide range of structural isomers make single-stage mass spectrometry (MS) experiments for identification of an unknown carbohydrate nearly impossible. Consequently, tandem mass spectrometry (MS/MS) is commonly utilized in oligosaccharide sequencing.[8,9] Glycans undergo two major types of fragmentation in MS/MS: cleavage of the glycosidic bonds and cleavage across the monosaccharide rings. Cross-ring cleavages are desirable as they provide structural information unavailable with solely glycosidic bond cleavage, potentially distinguishing between oligosaccharide isomers. Enhancement of

cross-ring cleavages has been explored through multiple dissociation techniques including high energy collision-induced dissociation (CID), post-source decay (PSD) and in-source decay (ISD)[10] using matrix-assisted laser desorption ionization (MALDI), infrared multiphoton dissociation (IRMPD),[11-15] ultraviolet photon dissociation (UVPD),[16-19] and electron-based ion activation methods (ExD).[11,12,20-29]

Native oligosaccharides are difficult to ionize, especially compared to peptides. Derivatization of oligosaccharides through permethylation, hydrolysis, reduction, and acetylation has commonly been coupled with mass spectrometry to improve ionization and enhance structural analysis. The first O-methylated sugar was prepared over 100 years ago.[30] Permethylation replaces all hydrogen atoms on oxygen and nitrogen atoms with methyl groups, which greatly reduces the hydrophilicity of the oligosaccharides. Permethylation increases ion intensity in electrospray ionization (ESI) by increasing sample volatility, stability, and the ability to protonate without undergoing water loss. Permethylation is not applicable to oligosaccharides containing sulfate or phosphate groups. Generally, permethylated oligosaccharides preferentially form sodiated quasi-molecular ions, even in the absence of added metal ions.[31-33] Depending on the structural characteristics of the glycans being studied, protonation may or may not occur with ESI. However, the production of protonated quasi-molecular ions can be improved by desalting the samples using on-line reversed-phase liquid chromatography or by dissolving samples in an ammonium acetate buffer.[34,35] Regardless of whether the sodiated or protonated species are formed, these ions are generally singly charged. In addition, permethylation can enhance predictable fragmentation patterns.[34-38] MS/MS can provide characteristic structural information on glycosidic bond positions and branching of permethylated oligosaccharides.[39-41] However, permethylation requires additional wet chemistry steps in the analysis, which is a drawback,

especially with biological samples. Sample loss during the permethylation process is common.[39] Although permethylation has been widely adopted when studying carbohydrates, many studies have attempted to improve the permethylation process and reduce degradation of the sugars [42,43] and significant interest exists in the development of methods to improve the analysis of native glycans.[8,9,44]

Metallation of oligosaccharides by the analysis of mixtures of glycans and metal salts is another technique that is used to improve ionization and structural analysis of oligosaccharides. Metal ion adduction has been combined with MS/MS to provide structurally informative fragmentation in both the positive and negative ion modes.[13,24,28,29,45-59] These studies, which have involved permethylated and native oligosaccharide samples, show that metallation allows for unambiguous location of glycosidic bonds and linkage positions in the oligosaccharides studied. Metallation using higher charge state metal cations allows for utilization of electron-based dissociation techniques (e.g., the work of Chapter 3), which can provide more structurally informative information than other types of MS/MS.[24,28,29,60]

A goal of this work is to investigate the effects of metallation on ionization and dissociation of permethylated oligosaccharides by ESI and electron transfer dissociation (ETD) and CID. This will involve comparison of the ETD and CID spectra for permethylated oligosaccharides to the spectra of the underivatized molecules, which were reported in Chapter 3.

4.3 Experimental

All experiments were performed using a Bruker HCTultra PTM Discovery System high capacity quadrupole ion trap (QIT) mass spectrometer (Bruker Daltonics, Billerica, MA, USA). Ions were produced via ESI on mixtures of metal salts and oligosaccharides in at 10:1 metal salt:oligosaccharide molar ratio. A KD Scientific (Holliston, MA, USA) syringe pump was used

to infuse sample solutions that had a final concentration of 10 µM in methanol:water at a 50:50 volume ratio with a flow rate of 180 µL/hour. The needle at the ESI source was held at ground and a high voltage of -3.5 kV was placed on the capillary, with an end plate offset of -500 V, and a capillary exit voltage of 120 V. Nitrogen was used as the drying gas at 250°C at a flow rate of 10 L/min and also as the nebulizer gas, with the pressure optimized at 10 psi. The amplitude of the activating voltage for CID experiments was 0.8 to 1.2 V, and the collision gas was helium with a 30% to 200% collision energy sweep. All spectra shown are the result of signal averaging of 200 scans.

Fluoranthene served as the reagent ion for ETD experiments and was generated in a negative chemical ionization (nCI) source with methane utilized as the nCI reagent gas. The accumulation time for the reagent anion was 20 ms. The ion charge control (ICC) target was 300,000 to 400,000 to maximize electron transfer. The lower end *m/z* was set at 120 *m/z*, and anion/cation reaction times were optimized at 400 ms. The "smart decomposition" function was employed to further dissociate any charge reduced (ETnoD) product ions by using resonant excitation to overcome attractive forces that may hold oligosaccharide fragments together following ETD.

The oligosaccharides were purchased from various vendors as listed in Section 2.2. The metal salts were nitrates of sodium (Na^+), potassium (K^+), magnesium (Mg^{2+}), calcium (Ca^{2+}), chromium (Cr^{3+}), iron (Fe^{3+}), cobalt (Co^{2+}), nickel (Ni^{2+}), copper (Cu^{2+}), zinc (Zn^{2+}), and aluminum (Al^{3+}). Important metal properties are listed in Table 3.1. $H_2{}^{18}O$ was purchased from Sigma-Aldrich (St. Louis, MO, USA). Ultrapure Milli-Q 18 MΩ water was produced with a Barnstead (Dubuque, IA, USA) E-pure system.

Isotopic labeling of the oxygen on the hydroxyl group of the hemiacetal of the reducing

sugars allows differentiation of the fragment ions from the reducing and non-reducing ends of the oligosaccharide. Isotopic ^{18}O-labeling of the reducing end oxygen in maltoheptaose, maltotetraose, and galactotetraose was completed by dissolving enough oligosaccharide in 100 uL of $H_2{}^{18}O$ to create a 0.1 M sample. The samples were stored in sealed vials in a desiccator at room temperature for about three weeks. The extent of isotopic labeling was periodically monitored by MS. Permethylation was completed using the procedure of Ciucanu and Kerek, as improved by Ciucanu and Costello, and is described in detail in Section 2.6.2.[42,61] After derivatization, permethylated oligosaccharide samples were purified using Spectrum Labs (Waltham, MA, USA) Spectra/Por dialysis tubing to remove salts and derivatization byproducts.

4.4 Results and Discussion

The Domon and Costello nomenclature of labeling MS/MS product ions is used for all spectra and is described in Section 2.7.[62] Colors and notation used to identify the product ions in the spectra are described in Section 3.4.2, and isobaric mass assignments can be found in Table 3.3. The symbolic structure of these oligosaccharides can be seen in Figure 2.14 and the expanded structures are in Figure 2.15.

4.4.1 Ion Formation by ESI

The permethylated oligosaccharides were ionized with all the metal cations included in the study. The trend in the ability for metal ions to produce metal adducts with the permethylated oligosaccharides was: $Ca^{2+} > Mg^{2+} > Ni^{2+} > Co^{2+} > Zn^{2+} > Cu^{2+} > Na^{+} > K^{+} > Al^{3+} \approx Fe^{3+} \approx Cr^{3+}$. This is identical to the trend seen in Chapter 3 with the non-permethylated oligosaccharides.[60] In the work of Chapter 3, the trends of ESI for non-permethylated oligosaccharides were discussed in detail. In the current work, the ion predominately formed with permethylated oligosaccharides with no metal added is $[M + Ca]^{2+}$, compared to $[M + Na]^{+}$

for the non-permethylated oligosaccharides. With the addition of up to 5% acetic acid (by volume), no change in the spectra is present, and no protonated ions are formed.

Addition of the monovalent group I ion Na^{1+} to solutions of the permethylated oligosaccharides resulted in the intense formation of $[M + 2Na]^{2+}$. When the glycans are underivatized as in Chapter 3, this ion forms weakly with the tetrasaccharides, and is the base peak for maltoheptaose.[60] This difference is probably related to the size of oligosaccharide, or the folding that can occur around the metal cation; this folding may be reduced as hydrogen bonding is reduced upon permethylation of the oligosaccharide. Addition of monovalent group I ion K^+ to solutions of the permethylated oligosaccharides resulted in the intense formation of $[M + K]^+$; there were no doubly charged ions produced. The lack of doubly potassiated ions is surprising, since K^+ and Na^+ have the same trends with the underivatized oligosaccharides, as seen in Table 3.2. Addition of the divalent metals to permethylated species produced $[M + Met]^{2+}$ as the base peak in the spectra formed by ESI, which is identical to the non-permethylated study in Chapter 3.[60] (Note that M denotes the oligosaccharide molecule and Met is the metal ion.) ESI using the trivalent metal cations (Al^{3+}, Fe^{3+}, or Cr^{3+}) did not produce any adducts with the permethylated samples despite adduction to underivatized oligosaccharides discussed in Section 3.4.1, where the tetrasaccharides form $[M + Met - 2H]^+$ and maltoheptaose forms $[M + Met]^{3+}$. For all metal cations studied, the ion intensity in the spectra for permethylated metal-adducted oligosaccharides is generally about ten times higher than for non-permethylated oligosaccharides. This is consistent with the permethylated species having less hydrogen bonding, leading to more open structures with a greater ability to coordinate a metal ion. However, the non-permethylated ESI spectra of Chapter 3 still have an average base peak intensity of about 10^7, which is high abundance and more than sufficient for MS/MS studies.[60]

4.4.2 Tandem Mass Spectrometry

As demonstrated in Chapter 3, Co^{2+} allowed consistent, sequence informative fragmentation of the oligosaccharides in the study, and this metal ion will be discussed as representative of the trends seen with the varied oligosaccharides.[60] Figures 4.1 - 4.5 compare ETD and CID spectra of $[M + Co]^{2+}$ permethylated and non-permethylated maltotetraose, galactotetraose, stachyose, nystose and maltoheptaose, respectively. To demonstrate the MS/MS results for the other metals included in the study, ETD and CID spectra of permethylated maltotetraose with Na^{1+}, Mg^{2+}, Ca^{2+}, Ni^{2+}, Cu^{2+}, and Zn^{2+} are in Figures 4.6 - 4.11, respectively. These figures are shown at the end of this chapter. In all spectra examined, there were significantly fewer fragment ions with the permethylated oligosaccharides than the non-permethylated species. The fragmentation trends due to various metal properties and physical glycan properties noted in Chapter 3 for non-permethylated oligosaccharides held for permethylation.[60] The metal cations with smaller ionic radii, and lower charge density (Co^{2+} and Mg^{2+}) produced the most consistent and informative fragmentation with both dissociation methods, presumably with the metal ion behaving as a mobile cation. Stachyose and nystose, stacked, non-reducing sugars had less product ion formation than the other glycans. The reducing sugars show more extensive cross-ring and internal fragmentation near the reducing end than the non-reducing end.

Dissociation using ETD on permethylated metal-adducted oligosaccharides produced only singly charged product ions. Both $[M + Met]^{+}$. and $[M + Met - H]^{+}$ were found as ETD product ions with all metal cations, and neutral losses of methyl (CH_3) and methoxy (CH_3O)

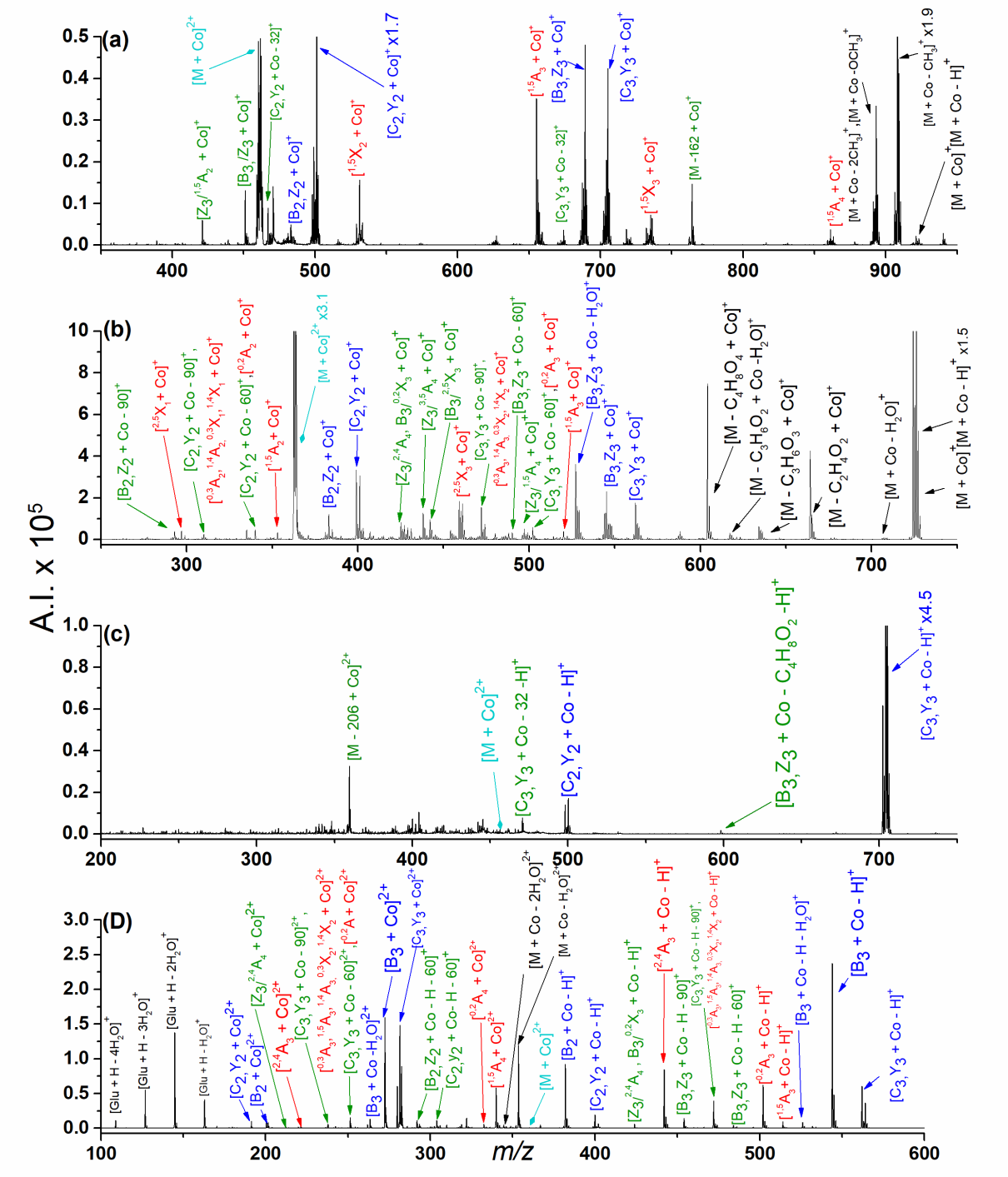

Figure 4.1 Mass spectra from (a) ETD and (c) CID of $[M + Co]^{2+}$ from permethylated maltotetraose as well as (b) ETD and (d) CID of $[M + Co]^{2+}$ from non-permethylated maltotetraose. Colors used to illustrate the product ions are red for cross-ring cleavages, blue for glycosidic bond cleavages, and green for internal cleavages. Undissociated precursor ion is labeled in light blue with a large light blue diamond arrow head. Product ions involving solely neutral losses are labeled in black.

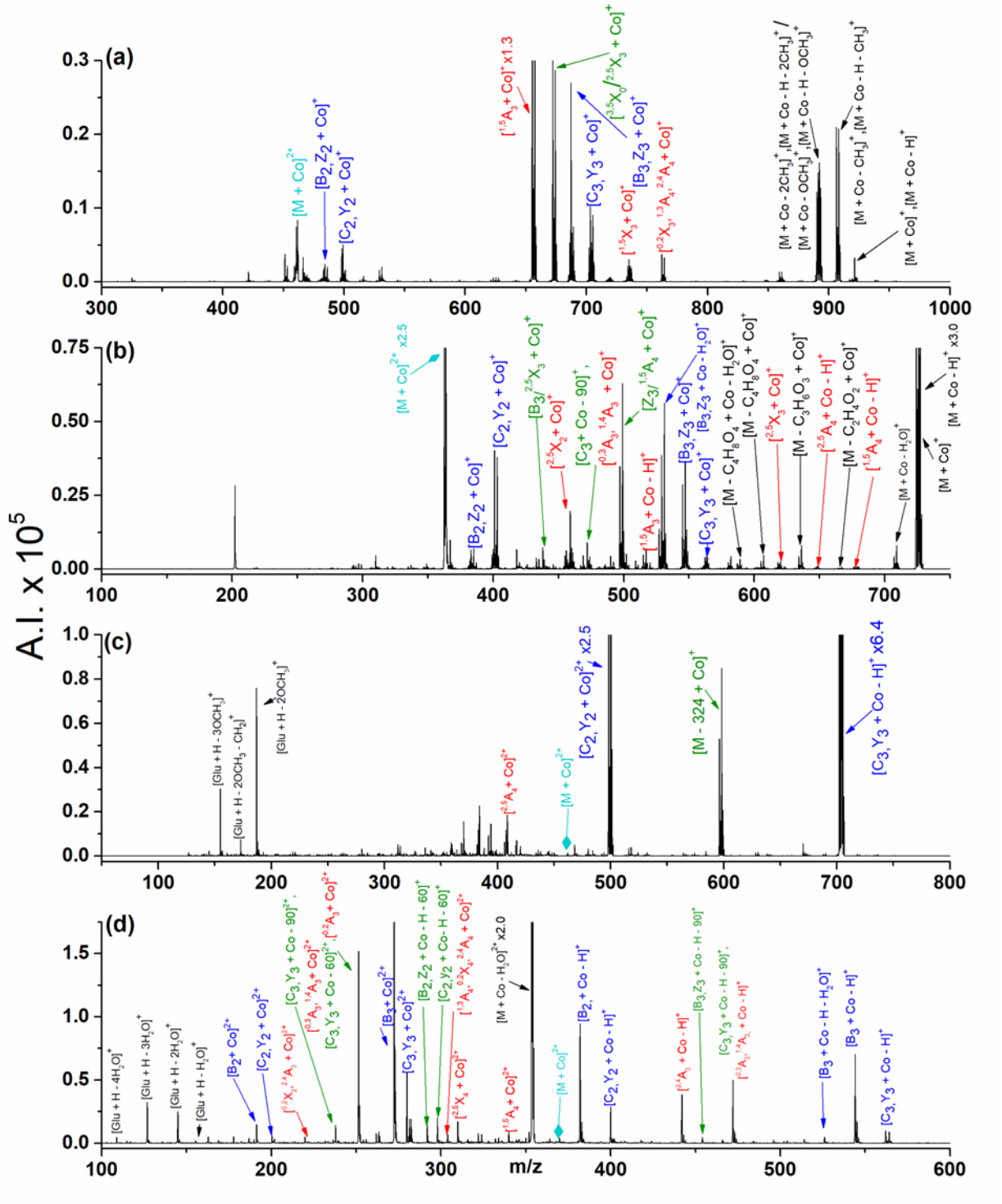

Figure 4.2 Mass spectra from (a) ETD and (c) CID of $[M + Co]^{2+}$ from permethylated galactotetraose as well as (b) ETD and (d) CID of $[M + Co]^{2+}$ from non-permethylated galactotetraose. Refer to the Figure 4.1 caption for an explanation of the color codes.

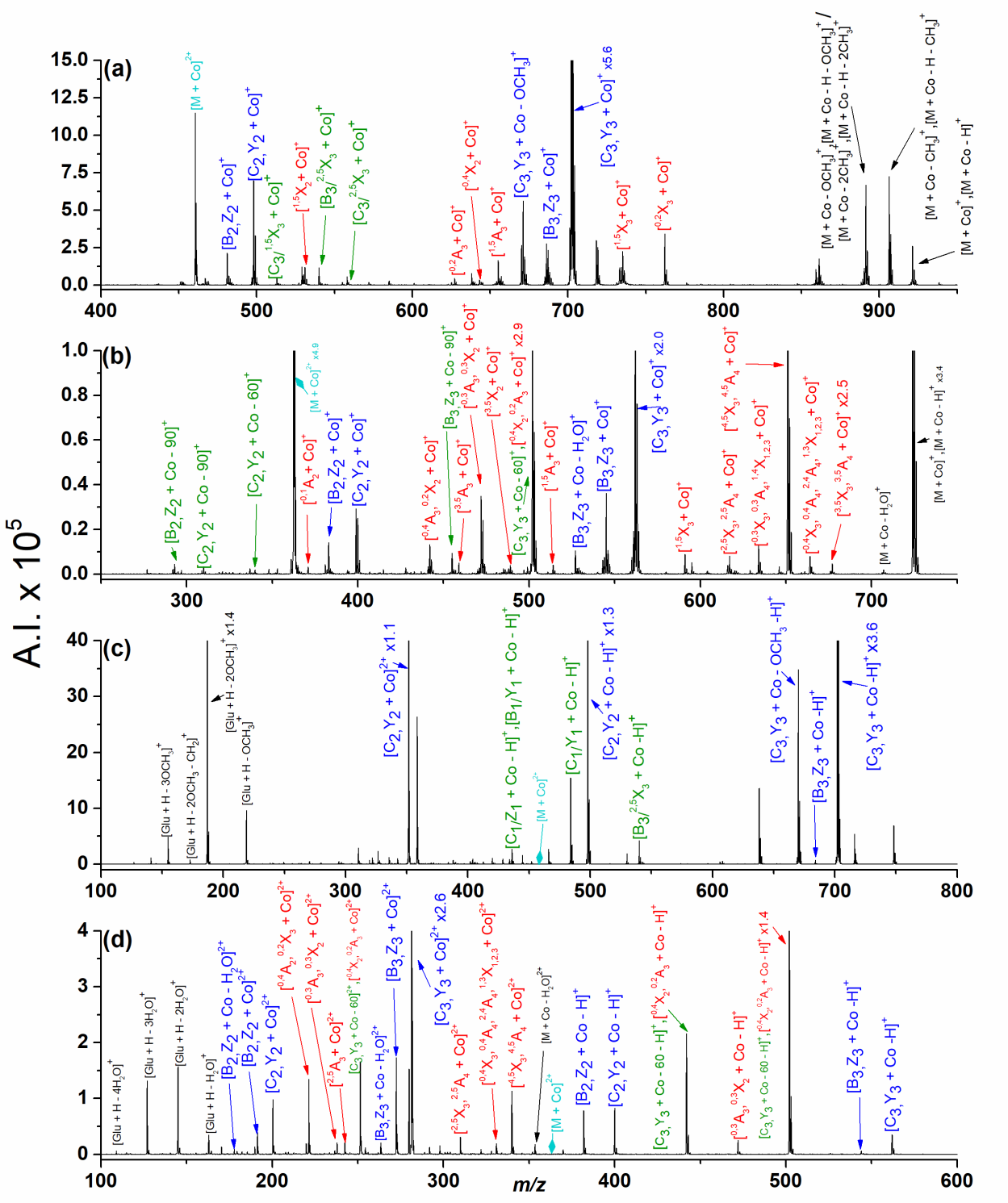

Figure 4.3 Mass spectra from (a) ETD and (c) CID of $[M + Co]^{2+}$ from permethylated stachyose as well as (b) ETD and (d) CID of $[M + Co]^{2+}$ from non-permethylated nystose. Refer to the Figure 4.1 caption for an explanation of the color codes.

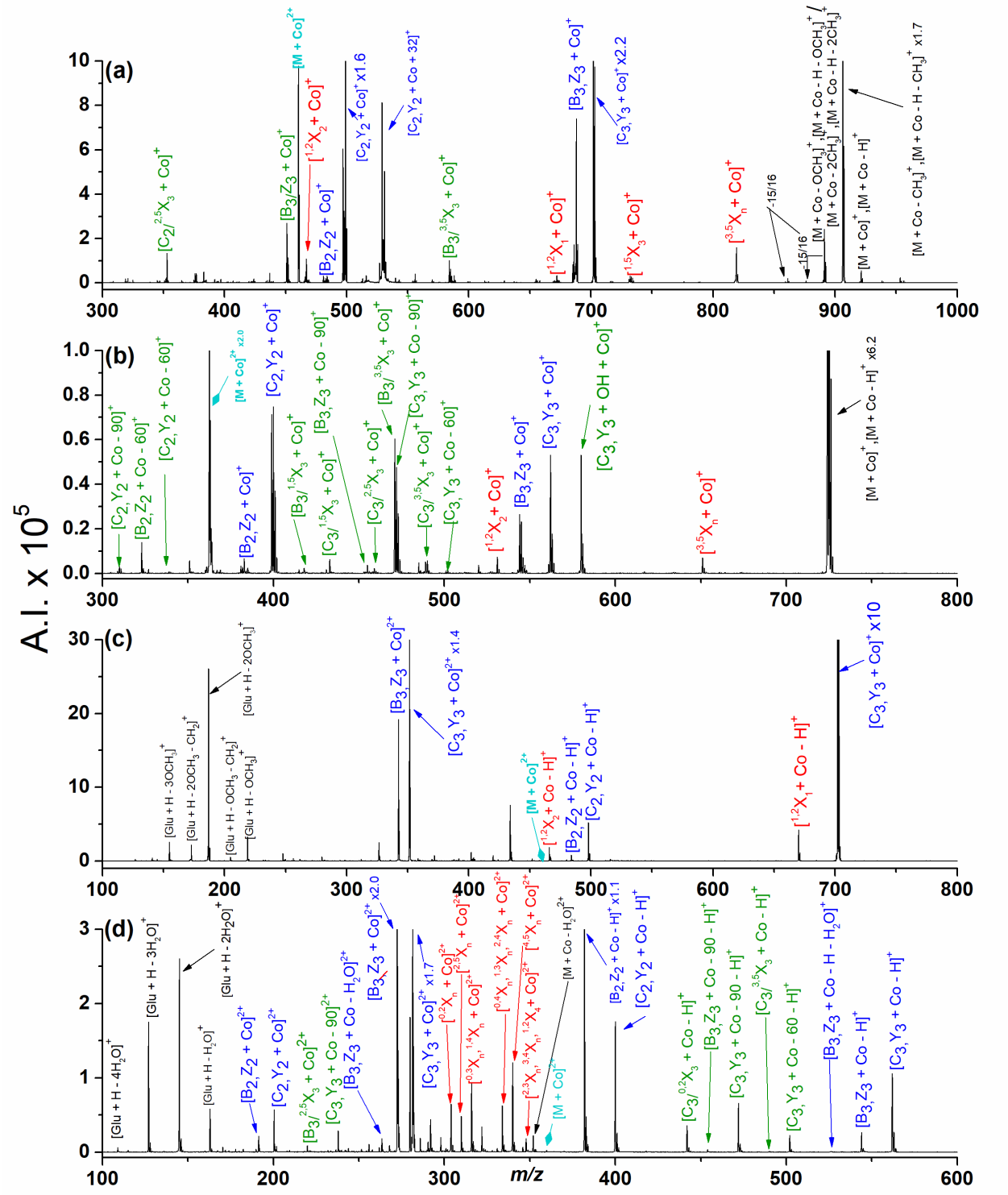

Figure 4.4 Mass spectra from (a) ETD and (c) CID of $[M + Co]^{2+}$ from permethylated nystose as well as (b) ETD and (d) CID of $[M + Co]^{2+}$ from non-permethylated nystose. Refer to the Figure 4.1 caption for an explanation of the color codes.

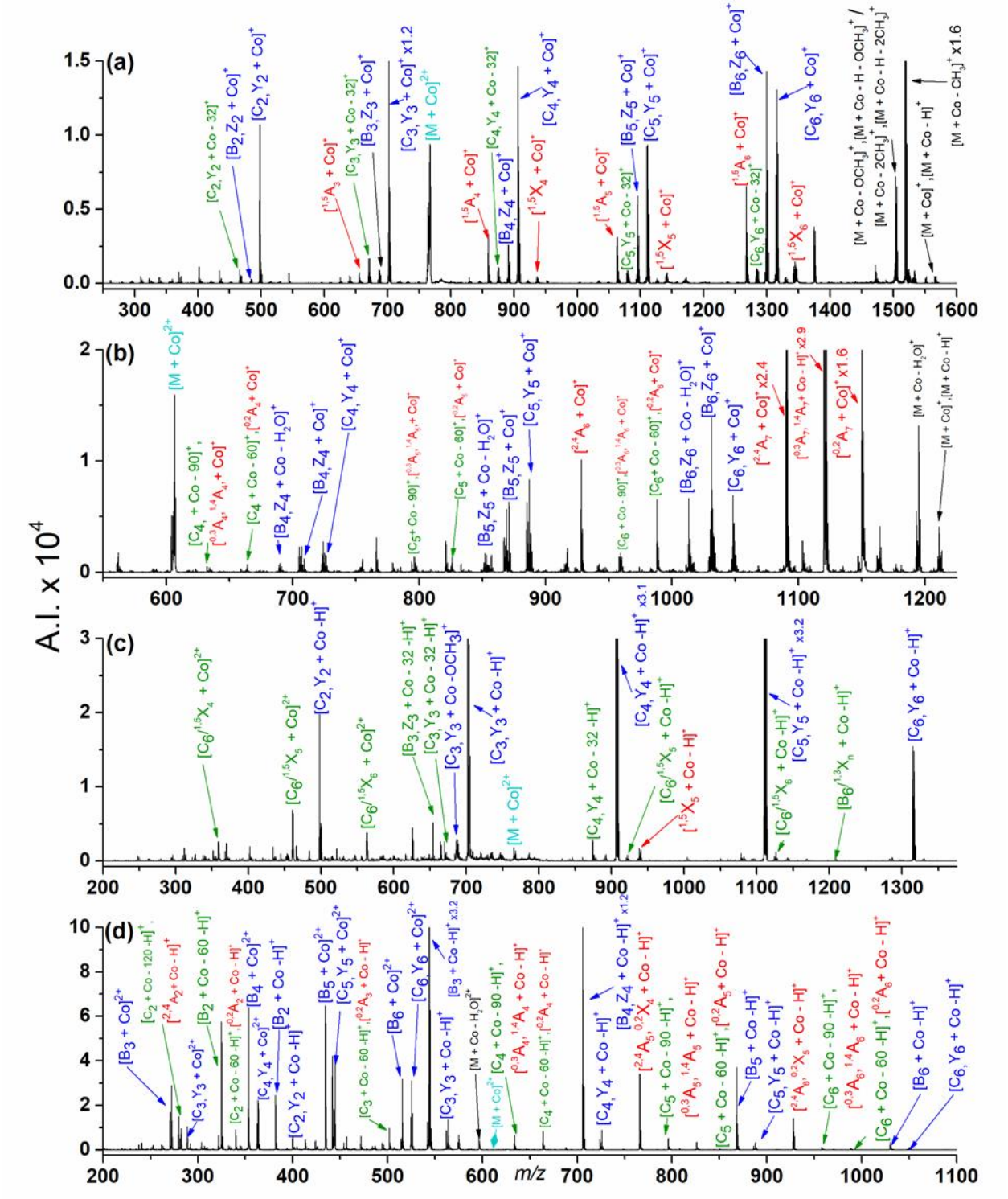

Figure 4.5 Mass spectra from (a) ETD and (c) CID of $[M + Co]^{2+}$ from permethylated maltoheptaose as well as (b) ETD and (d) CID of $[M + Co]^{2+}$ from non-permethylated maltoheptaose. Refer to the Figure 4.1 caption for an explanation of the color codes.

groups from the charge reduced radical, and from various cross-ring and glycosidic fragment ions were observed. Alternatively, loss of water and formaldehyde (CH_2O) occurred with non-permethylated oligosaccharides.[60] The intensity of the neutral loss product ions varied, but in Figures 4.1(a), 4.5(a), and 4.7, loss of CH_3 is the base peak in the spectra. Addition of water to $[M + Met]^{+\cdot}$ and $[M + Met - H]^+$ to form $[M + Met + H_2O]^+$ and $[M + Met - H + H_2O]^+$ in the permethylated spectra does not occur in the non-permethylated spectra. Such water adduct ions were previously noted by Han and Costello.[28]

In general, the number of "unassignable" ions (structural isomers with the same exact mass) is reduced with permethylation, due to the change in oligosaccharide mass upon permethylation. Unfortunately, the overall number of product ions in the spectrum is reduced as well. ETD fragmentation efficiency of the permethylated tetrasaccharides did not change from the non-derivatized analytes and decreased in the order maltotetraose > stachyose > 3α,4β,3α-galactotetraose > nystose with most of the metal ions. Fragmentation efficiency describes the amount of precursor ion that is dissociated into product ions and is calculated as Σ I(fragment ion)/I(precursor before dissociation), where I is ion intensity. ^{18}O isotopic labeling of the reducing sugars indicates that majority of the cross-ring product ions contain the non-reducing end. The isotopic labeling also demonstrated that with CID the only ions that contain the reducing end are Y ions from the non-reducing side of the glycosidic oxygen; however, in ETD, both Y and Z ions from both sides of the glycosidic oxygen are observed. These trends are consistent with and without derivatization.

Dissociation of $[M + Co]^{2+}$ from the four tetrasaccharides by ETD produces the same glycosidic bond cleavages with and without permethylation: $[B_2, Z_2 + Co]^{2+}$, $[C_2, Y_2 + Co]^{2+}$, $[B_3, Z_3 + Co]^{2+}$, and $[C_3, Y_3 + Co]^{2+}$. The greatest differences in the spectra of the permethylated

and non-permethylated glycans involve the cross-ring and internal cleavages, including the location and type of fragment ion. Examining the ETD spectra of non-permethylated maltotetraose, in Figure 4.1(b), there are multiple cross-ring and internal fragment ions that are not produced when the oligosaccharide is permethylated (Figure 4.1(a)), and there are few cross-ring fragments in Figure 4.1(a) overall. There are four cross-ring product ions: $^{1,5}X_2$, $^{1,5}X_3$, $^{1,5}A_3$, and $^{1,5}A_4$, which are four distinct ions with four different cleavage positions and not two complementary cross-ring cleavage ions occurring with both the reducing and non-reducing side of the glycan carrying the charge. The only of these product ions in the non-permethylated spectrum is $^{1,5}A_3$. The same type of pattern emerges for galactotetraose. In the permethylated galactotetraose spectrum of Figure 4.2, two unique cross-ring fragment ions occur, $^{1,5}X_3$, and $^{1,5}A_3$, and there is one ion that is isobaric for three cross-ring fragments not found in the non-permethylated spectrum of Figure 4.2(b). The non-permethylated spectrum contains numerous cross-ring and internal cleavages, many of which are isobaric/exact mass ions. It should be noted, as discussed in Chapter 3, that with native oligosaccharides, exact mass ions have the exact same chemical formula, and not just the same nominal mass. The only product ion in both the permethylated and non-permethylated galactotetraose spectra is $^{1,5}A_3$, which is also found in the maltotetraose spectra.

The ETD spectra of $[M + Co]^{2+}$ from the permethylated reducing tetrasaccharides are more similar to each other than are the previously reported non-permethylated spectra of Chapter 3.[60] This contrasts with the spectra of the non-reducing tetrasaccharides, which exhibit more uniqueness. Figures 4.3(a) and (b) show ETD spectra from permethylated and non-permethylated stachyose. In the non-permethylated spectrum, there is an ion ~2.9 times off scale that can be either $^{0,2}A_3$, $^{0,4}X_2$ or a number of other internal cleavages, all with the same exact

mass and chemical formula. In the permethylated spectrum, both of these cross-ring cleavages have a unique mass, and there are no indistinguishable internal cleavages. ETD of permethylated nystose can be seen in Figure 4.4(a) and shows two additional cross-ring fragment ions, as well as three internal ions that are not in the non-permethylated spectrum of Figure 4.4(b). The ETD fragment ions from maltoheptaose are the same as with maltotetraose (both permethylated and non-permethylated), and can be seen in Figures 4.5(a) and (b). Surprisingly, ETD on permethylated metallated maltoheptaose produces two more glycosidic bond cleavage positions, corresponding to production of $[B_2, Z_2 + Co]^{2+}$, $[C_2, Y_2 + Co]^{2+}$, $[B_3, Z_3 + Co]^{2+}$, and $[C_3, Y_3 + Co]^{2+}$, as well as the associated cross-ring cleavages around these two glycosidic bonds.

In the CID spectra of $[M + Co]^{2+}$ from the non-permethylated metallated oligosaccharides discussed in Chapter 3, ions corresponding to protonated glucose residues with loss of one, two, three, and four water molecules are generated below 180 Da.[60] With permethylation, protonated glucose residues with loss of both methyl and methoxy groups occur for all glycans studied. Overall, the CID spectra of the permethylated oligosaccharides have significantly fewer fragment ions than the spectra for non-derivatized analytes. In Figure 4.1(c) of permethylated maltotetraose and 4.3(c) of permethylated stachyose, there are no cross-ring cleavage product ions. The only metal cation that produced cross-ring fragment ions with permethylated maltotetraose is Ca^{2+}, as can be seen in Figure 4.8. In the permethylated maltotetraose spectra of $[M + Co]^{2+}$, there are no sequence informative fragment ions. In Figure 4.2(c) and (d) of $[M + Co]^{2+}$ from permethylated galactotetraose, CID produces one cross-ring product ion, which is not in the non-permethylated spectra. There are some unique internal cleavages in the CID spectra of permethylated nystose and permethylated maltoheptaose, but regardless of metal ion or

oligosaccharide, the CID spectra are not generally sequence informative. The lack of linkage informative cross-ring fragmentation by CID of permethylated glycans was previously noted by Han and Costello.[28]

Unlike the cross-ring cleavage ions, which have varied positions with and without derivatization, the glycosidic bond cleavages occur between the same rings on the sugar with and without permethylation. However, unlike the underivatized glycans, the permethylated glycans mainly produce C and Y ions that contain the glycosidic bond oxygen, with no B ions present. (A depiction of ion types can be seen in Figure 2.16.) The formation of C and Y ions can be attributed to the fact that the metal cation prefers to bond to the glycosidic oxygen, as opposed to the radical carbon, when the glycosidic bond is broken. The production of C and Y ions is enhanced with permethylation, where the oxygens on the glycans are part of methoxy groups instead of hydroxyl groups, and less likely to bind to a metal cation. The trend of CID only producing C and Y ions holds for $[M + Co]^{2+}$ from permethylated maltotetraose (Figure 4.1(c)), whereas $[M + Co]^{2+}$ from permethylated stachyose in Figure 4.3(c), permethylated nystose in Figure 4.4(c), and permethylated maltoheptaose in Figure 4.5(c) have mostly C and Y ions with a few low intensity B and Z ions. The ability to form B and Z ions for maltoheptaose may be due to the size of the molecule, and this molecule having more "pockets" with available oxygens for the metal cation to interact with, thus resulting in less attraction to oxygen in the glycosidic bond. A similar theory would hold for stachyose and nystose, but instead of size, would relate to the flexibility in the glycosidic bonds for these two "stacking" tetrasaccharides, so there is less rigidity holding the metal cation in one place on the molecule.

4.5 Conclusions

Permethylation of oligosaccharides is a useful technique in mass spectrometry, especially

when utilizing separation techniques; however, derivatization does not appear to significantly improve structural information provided by MS/MS spectra of metallated oligosaccharides. As with the non-permethylated glycans in Chapter 3, the dissociation behavior is dependent on the metal cation, and Co^{2+} yielded the most useful and efficient fragmentation.[60] Permethylation occasionally decreases the ambiguity observed with exact mass ions, and internal fragment ions, but does not consistently lessen spectra ambiguity with every analyte. In the current study, permethylation reduced the information obtained from CID, and further dissociation with CID/CID or CID/ETD is seemingly necessary for sequence analysis. The metal cations used improve ionization via ESI; however, coupling of permethylation with metallation is not necessary for good ionization efficiency by ESI. The fragment ions observed with and without permethylation are not the same; different cross-ring cleavages occur on the same saccharide ring and the same saccharide ring may or may not fragment with derivatization. The bonds that are broken across a glycan ring are key to saccharide identification and, thus, researchers need to be diligent about interpreting unknown spectra using cross-ring fragment assignments. Permethylation is not necessary to obtain sequence informative fragmentation of metallated oligosaccharides, but could be a useful tool to obtain complementary information from MS/MS or to reduce spectral ambiguity with some analytes.

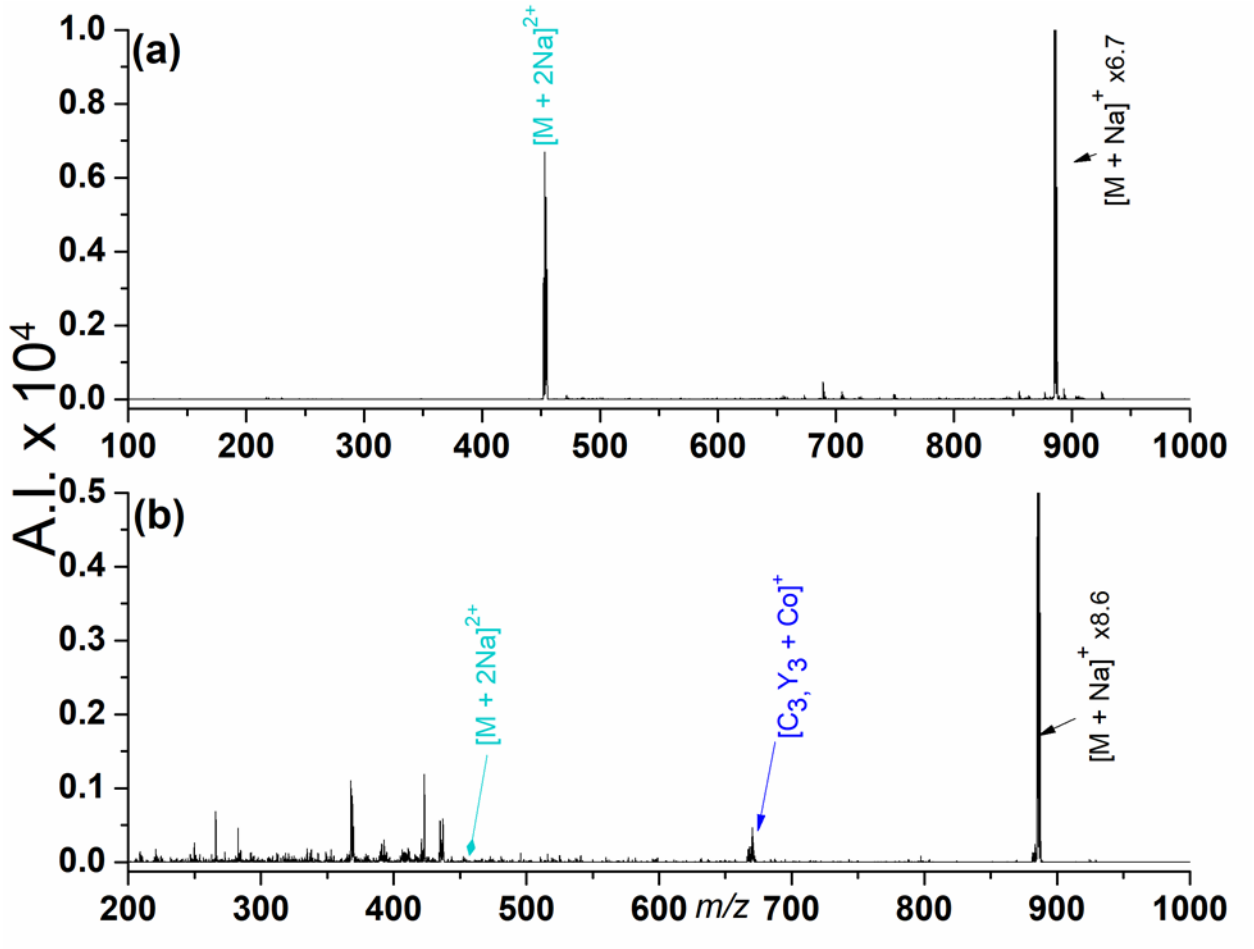

Figure 4.6 Mass spectra from (a) ETD and (b) CID of $[M + Na]^{2+}$ from permethylated maltotetraose. Refer to the Figure 4.1 caption for an explanation of the color codes.

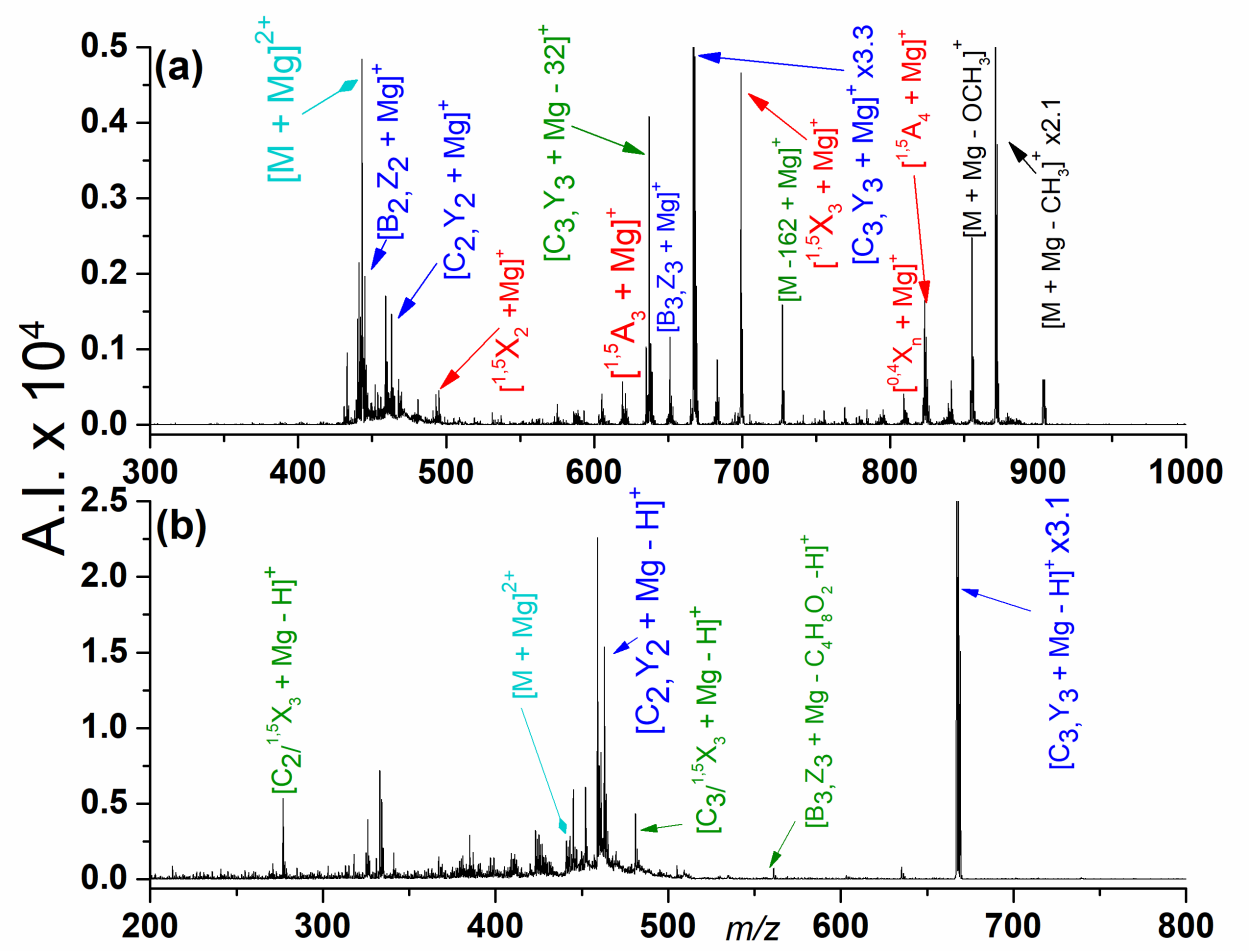

Figure 4.7 Mass spectra from (a) ETD and (b) CID of $[M + Mg]^{2+}$ from permethylated maltotetraose. Refer to the Figure 4.1 caption for an explanation of the color codes.

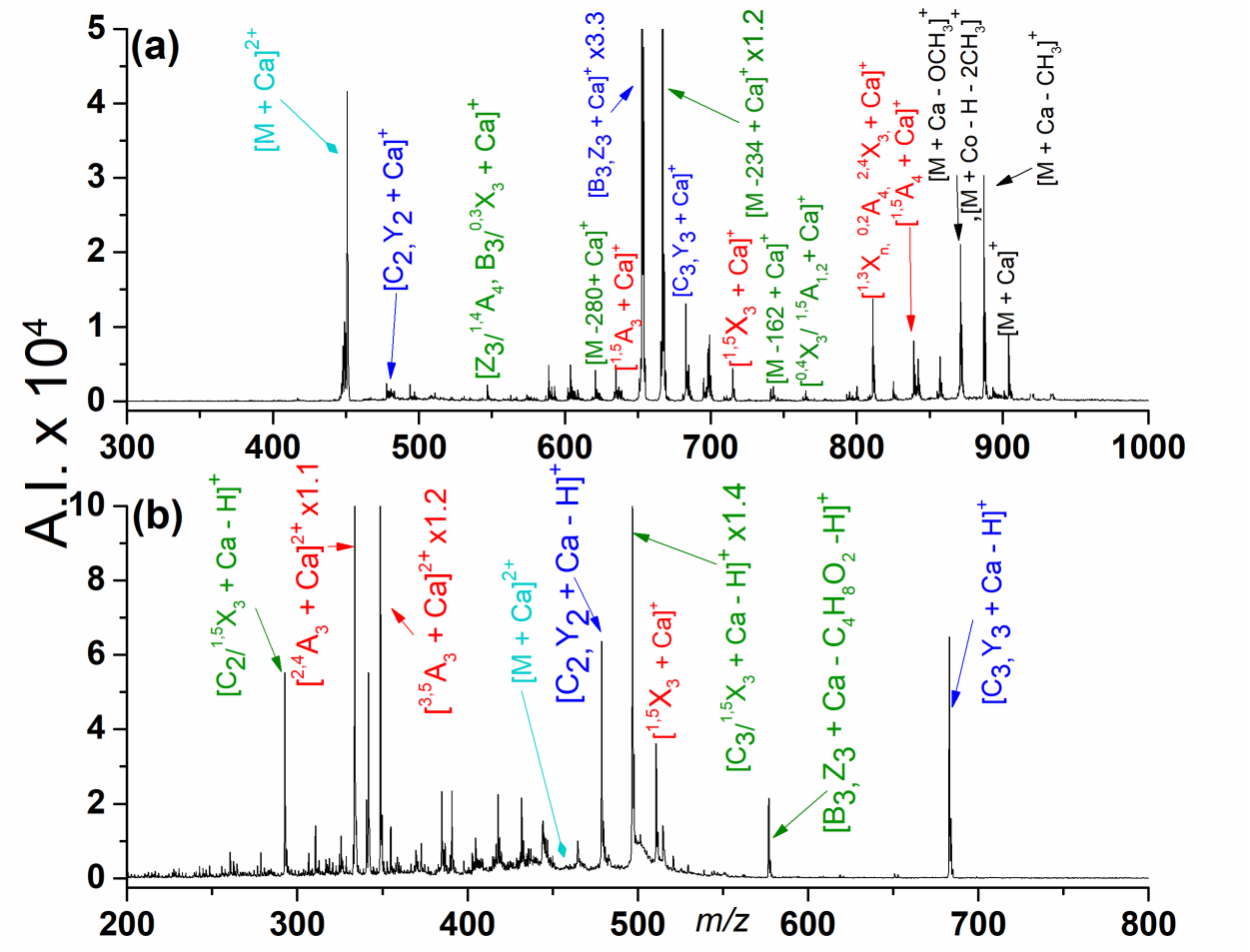

Figure 4.8 Mass spectra from (a) ETD and (b) CID of $[M + Ca]^{2+}$ from permethylated maltotetraose. Refer to the Figure 4.1 caption for an explanation of the color codes.

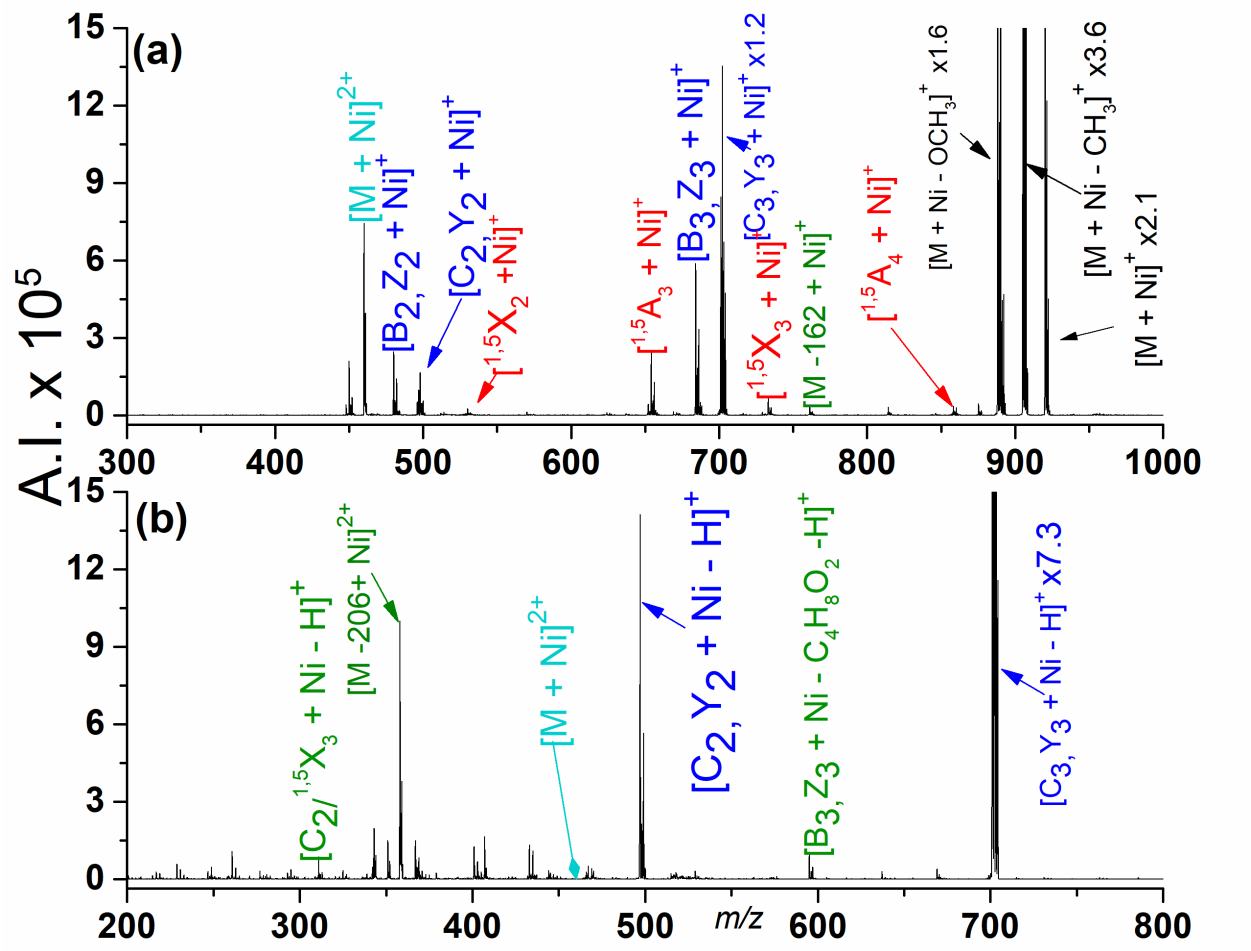

Figure 4.9 Mass spectra from (a) ETD and (b) CID of $[M + Ni]^{2+}$ from permethylated maltotetraose. Refer to the Figure 4.1 caption for an explanation of the color codes.

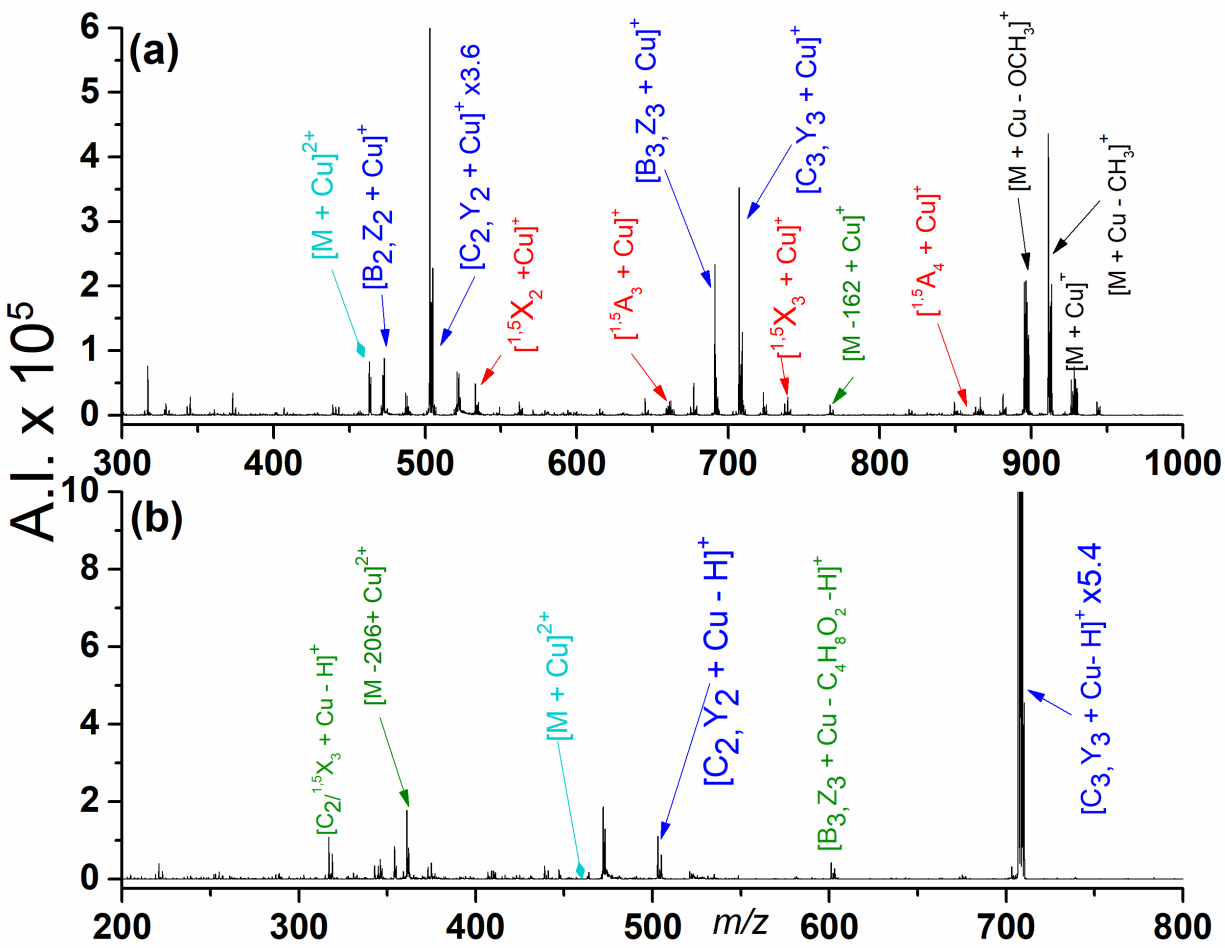

Figure 4.10 Mass spectra from (a) ETD and (b) CID of $[M + Cu]^{2+}$ from permethylated maltotetraose. Refer to the Figure 4.1 caption for an explanation of the color codes.

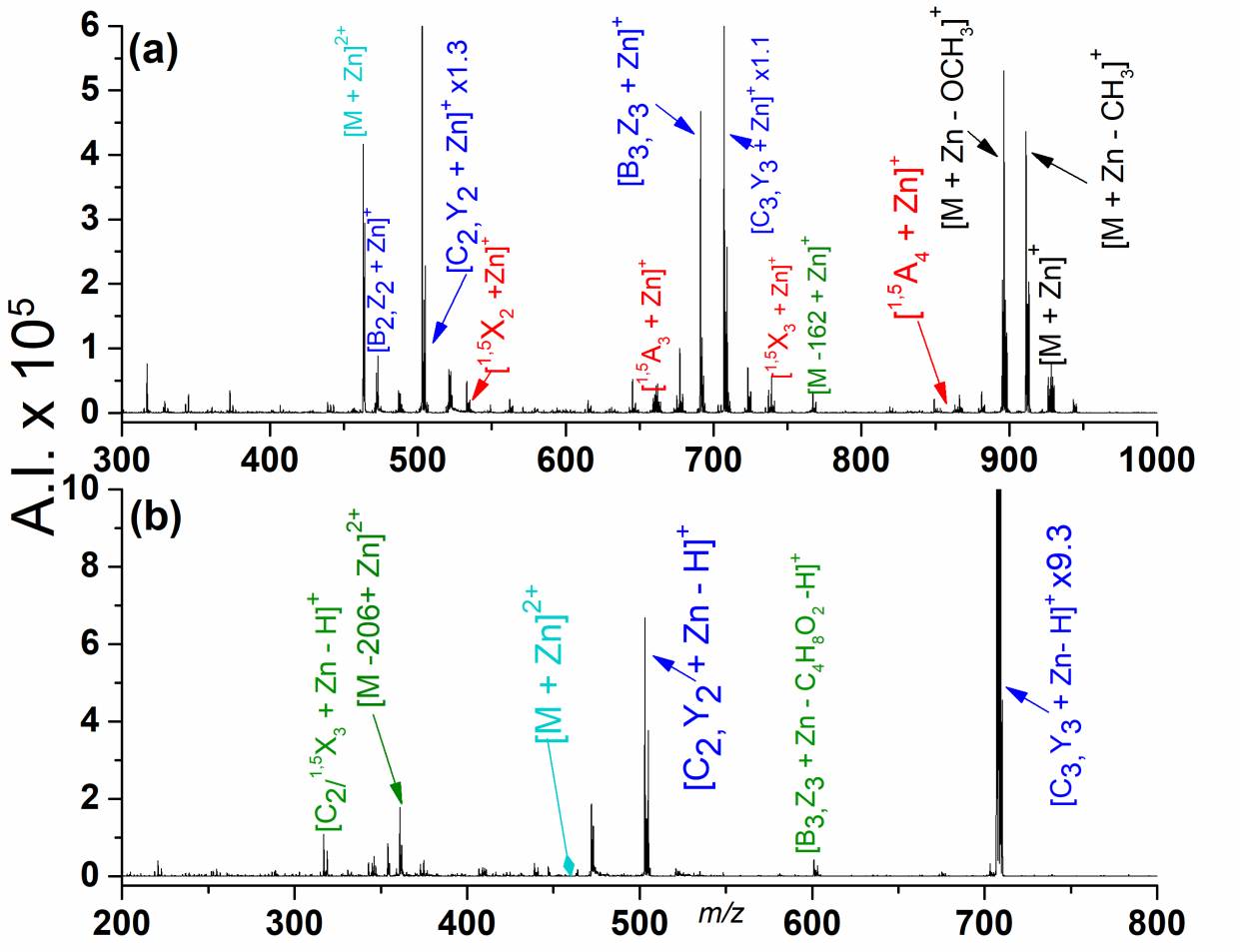

Figure 4.11 Mass spectra from (a) ETD and (b) CID of $[M + Zn]^{2+}$ from permethylated maltotetraose. Refer to the Figure 4.1 caption for an explanation of the color codes.

REFERENCES

1. Varki, A. Biological roles of glycans. *Glycobiology* **2017**, *27*, 3-49.

2. Hart, G. W.; Copeland, R. J. Glycomics hits the big time. *Cell* **2010**, *143*, 672-676.

3. Parodi, A. J. Protein glucosylation and its role in protein folding. *Annu. Rev. Biochem.* **2000**, *69*, 69-93.

4. Laine, R. A. A calculation of all possible oligosaccharide isomers both branched and linear yields 1.05 x 10(12) structures for a reducing hexasaccharide - the isomer-barrier to development of single-method saccharide sequencing or synthesis systems. *Glycobiology* **1994**, *4*, 759-767.

5. Fenn, J. B.; Mann, M.; Meng, C. K.; Wong, S. F. Electrospray ionization--principles and practice. *Mass Spectrom. Rev.* **1990**, *9*, 37-70.

6. Fenn, J. B.; Mann, M.; Meng, C. K.; Wong, S. F.; Whitehouse, C. M. Electrospray ionization for mass spectrometry of large biomolecules. *Science* **1989**, *246*, 64-71.

7. Hop, C E C A; Bakhtiar, R. An introduction to electrospray ionization and matrix-assisted laser desorption/ionization mass spectrometry: Essential tools in a modern biotechnology environment. *Biospectroscopy* **1997**, *3530*, 259-280.

8. Zaia, J. Mass spectrometry of oligosaccharides. *Mass Spectrom. Rev.* **2004**, *23*, 161-227.

9. Kailemia, M. J.; Ruhaak, L. R.; Lebrilla, C. B.; Amster, I. J. Oligosaccharide analysis by mass spectrometry: A review of recent developments. *Anal. Chem.* **2014**, *86*, 196-212.

10. Harvey, D. J.; Naven, T. J. P.; Küster, B.; Bateman, R. H.; Green, M. R.; Critchley, G. Comparison of fragmentation modes for the structural determination of complex oligosaccharides ionized by matrix-assisted laser desorption/ionization mass spectrometry. *Rapid Commun. Mass Spectrom.* **1995**, *9*, 1556-1561.

11. Wolff, J. J.; Laremore, T. N.; Leach, F. E.,III; Linhardt, R. J.; Amster, I. J. Electron capture dissociation, electron detachment dissociation and infrared multiphoton dissociation of sucrose octasulfate. *Eur. J. Mass Spectrom.* **2009**, *15*, 275-281.

12. Leach, F. E.,III; Xiao, Z.; Laremore, T. N.; Linhardt, R. J.; Amster, I. J. Electron detachment dissociation and infrared multiphoton dissociation of heparin tetrasaccharides. *Int. J. Mass Spectrom.* **2011**, *308*, 253-259.

13. Xie, Y. M.; Lebrilla, C. B. Infrared multiphoton dissociation of alkali metal-coordinated oligosaccharides. *Anal. Chem.* **2003**, *75*, 1590-1598.

14. Zhang, J. H.; Schubothe, K.; Li, B. S.; Russell, S.; Lebrilla, C. B. Infrared multiphoton dissociation of O-linked mucin-type oligosaccharides. *Anal. Chem.* **2005**, *77*, 208-214.

15. Adamson, J. T.; Håkansson, K. Infrared multiphoton dissociation and electron capture dissociation of high-mannose type glycopeptides. *J. Proteome Res.* **2006**, *5*, 493-501.

16. Ko, B. J.; Brodbelt, J. S. 193 nm ultraviolet photodissociation of deprotonated sialylated oligosaccharides. *Anal. Chem.* **2011**, *83*, 8192-8200.

17. O'Brien, J. P.; Brodbelt, J. S. Structural characterization of gangliosides and glycolipids via ultraviolet photodissociation mass spectrometry. *Anal. Chem.* **2013**, *85*, 10399-10407.

18. Ko, B. J.; Brodbelt, J. S. Ultraviolet photodissociation of chromophore-labeled oligosaccharides via reductive amination and hydrazide conjugation. *J. Mass Spectrom.* **2011**, *46*, 359-366.

19. Klein, D. R.; Holden, D. D.; Brodbelt, J. S. Shotgun analysis of rough-type lipopolysaccharides using ultraviolet photodissociation mass spectrometry. *Anal. Chem.* **2016**, *88*, 1044-1051.

20. Yu, X.; Jiang, Y.; Chen, Y.; Huang, Y.; Costello, C. E.; Lin, C. Detailed glycan structural characterization by electronic excitation dissociation. *Anal. Chem.* **2013**, *85*, 10017-10021.

21. Zhu, F.; Glover, M. S.; Shi, H.; Trinidad, J. C.; Clemmer, D. E. Populations of metal-glycan structures influence MS fragmentation patterns. *J. Am. Soc. Mass Spectrom.* **2015**, *26*, 25-35.

22. Zhou, W.; Håkansson, K. Electron capture dissociation of divalent metal-adducted sulfated N-glycans released from bovine thyroid stimulating hormone. *J. Am. Soc. Mass Spectrom.* **2013**, *24*, 1798-1806.

23. Liu, H.; Håkansson, K. Electron capture dissociation of divalent metal-adducted sulfated oligosaccharides. *Int. J. Mass Spectrom.* **2011**, *305*, 170-177.

24. Yu, X.; Huang, Y.; Lin, C.; Costello, C. E. Energy-dependent electron activated dissociation of metal-adducted permethylated oligosaccharides. *Anal. Chem.* **2012**, *84*, 7487-7494.

25. Darula, Z.; Medzihradszky, K. F. Glycan side reaction may compromise ETD-based glycopeptide identification. *J. Am. Soc. Mass Spectrom.* **2014**, *25*, 977-987.

26. Zhao, C.; Xie, B.; Chan, S.; Costello, C. E.; O'Connor, P. B. Collisionally activated dissociation and electron capture dissociation provide complementary structural information for branched permethylated oligosaccharides. *J. Am. Soc. Mass Spectrom.* **2008**, *19*, 138-150.

27. Håkansson, K.; Cooper, H. J.; Emmett, M. R.; Costello, C. E.; Marshall, A. G.; Nilsson, C. L. Electron capture dissociation and infrared multiphoton dissociation MS/MS of an N-glycosylated tryptic peptide to yield complementary sequence information. *Anal. Chem.* **2001**, *73*, 4530-4536.

28. Han, L.; Costello, C. E. Electron transfer dissociation of milk oligosaccharides. *J. Am. Soc. Mass Spectrom.* **2011**, *22*, 997-1013.

29. Adamson, J. T.; Håkansson, K. Electron capture dissociation of oligosaccharides ionized with alkali, alkaline earth, and transition metals. *Anal. Chem.* **2007**, *79*, 2901-2910.

30. Purdie, T.; Irvine, J. C. C.-The alkylation of sugars. *J. Chem. Soc., Trans.* **1903**, *83*, 1021-1037.

31. Morelle, W.; Faid, V.; Michalski, J. Structural analysis of permethylated oligosaccharides using electrospray ionization quadrupole time-of-flight tandem mass spectrometry and deutero-reduction. *Rapid Commun. Mass Spectrom.* **2004**, *18*, 2451-2464.

32. Morelle, W.; Slomianny, M. C.; Diemer, H.; Schaeffer, C.; van Dorsselaer, A.; Michalski, J. C. Fragmentation characteristics of permethylated oligosaccharides using a matrix-assisted laser desorption/ionization two-stage time-of-flight (TOF/TOF) tandem mass spectrometer. *Rapid Commun. Mass Spectrom.* **2004**, *18*, 2637-2649.

33. Weiskopf, A. S.; Vouros, P.; Harvey, D. J. Characterization of oligosaccharide composition and structure by quadrupole ion trap mass spectrometry. *Rapid Commun. Mass Spectrom.* **1997**, *11*, 1493-1504.

34. Viseux, N.; de Hoffmann, E.; Domon, B. Structural analysis of permethylated oligosaccharides by electrospray tandem mass spectrometry. *Anal. Chem.* **1997**, *69*, 3193-3198.

35. Viseux, N.; de Hoffmann, E.; Domon, B. Structural assignment of permethylated oligosaccharide subunits using sequential tandem mass spectrometry. *Anal. Chem.* **1998**, *70*, 4951-4959.

36. Harvey, D. J.; Bateman, R. H.; Green, M. R. High-energy collision-induced fragmentation of complex oligosaccharides ionized by matrix-assisted laser desorption/ionization mass spectrometry. *J. Mass Spectrom.* **1997**, *32*, 167-187.

37. Reinhold, V. N.; Sheeley, D. M. Detailed characterization of carbohydrate linkage and sequence in an ion trap mass spectrometer: Glycosphingolipids. *Anal. Biochem.* **1998**, *259*, 28-33.

38. Sheeley, D. M.; Reinhold, V. N. Structural characterization of carbohydrate sequence, linkage, and branching in a quadrupole ion trap mass spectrometer: Neutral oligosaccharides and N-linked glycans. *Anal. Chem.* **1998**, *70*, 3053-3059.

39. Zaia, J. Mass spectrometry and the emerging field of glycomics. *Chem. Biol.* **2008**, *15*, 881-892.

40. Ashline, D.; Singh, S.; Hanneman, A.; Reinhold, V. Congruent strategies for carbohydrate sequencing. 1. mining structural details by MS^n. *Anal. Chem.* **2005**, *77*, 6250-6262.

41. Zaia, J. Mass spectrometry and glycomics. *OMICS* **2010**, *14*, 401-418.

42. Ciucanu, I.; Costello, C. E. Elimination of oxidative degradation during the per-O-methylation of carbohydrates. *J. Am. Chem. Soc.* **2003**, *125*, 16213-16219.

43. Ciucanu, I. Per-O-methylation reaction for structural analysis of carbohydrates by mass spectrometry. *Anal. Chim. Acta* **2006**, *576*, 147-155.

44. Mirgorodskaya, E.; Karlsson, N. G.; Sihlbom, C.; Larson, G.; Nilsson, C. L. Cracking the sugar code by mass spectrometry: An invited perspective in honor of Dr. Catherine E. Costello, recipient of the 2017 ASMS distinguished contribution award. *J. Am. Soc. Mass Spectrom.* **2018**, *29*, 1065-1074.

45. Bythell, B. J.; Abutokaikah, M. T.; Wagoner, A. R.; Guan, S.; Rabus, J. M. Cationized carbohydrate gas-phase fragmentation chemistry. *J. Am. Soc. Mass Spectrom.* **2017**, *28*, 688-703.

46. Rabus, J. M.; Abutokaikah, M. T.; Ross, R. T.; Bythell, B. J. Sodium-cationized carbohydrate gas-phase fragmentation chemistry: Influence of glycosidic linkage position. *Phys. Chem. Chem. Phys.* **2017**, *19*, 25643-25652.

47. Fura, A.; Leary, J. A. Differentiation of Ca^{2+}-coordinated and Mg^{2+}-coordinated branched trisaccharide isomers: An electrospray ionization and tandem mass spectrometry study. *Anal. Chem.* **1993**, *65*, 2805-2811.

48. Cancilla, M. T.; Penn, S. G.; Carroll, J. A.; Lebrilla, C. B. Coordination of alkali metals to oligosaccharides dictates fragmentation behavior in matrix assisted laser desorption ionization/Fourier transform mass spectrometry. *J. Am. Chem. Soc.* **1996**, *118*, 6736-6745.

49. Huang, Y.; Pu, Y.; Yu, X.; Costello, C. E.; Lin, C. Mechanistic study on electron capture dissociation of the oligosaccharide-Mg^{2+} complex. *J. Am. Soc. Mass Spectrom.* **2014**, *25*, 1451-1460.

50. Lemoine, J.; Fournet, B.; Despeyroux, D.; Jennings, K. R.; Rosenberg, R.; De Hoffman, E. Collision-induced dissociation of alkali metal cationized and permethylated oligosaccharides: Influence of the collision energy and of the collision gas for the assignment of linkage position. *J. Am. Soc. Mass Spectrom.* **1993**, *4*, 197-203.

51. Harvey, D. J. Ionization and collision-induced fragmentation of N-linked and related carbohydrates using divalent cations. *J. Am. Soc. Mass Spectrom.* **2001**, *12*, 926-937.

52. Asam, M. R.; Glish, G. L. Tandem mass spectrometry of alkali cationized polysaccharides in a quadrupole ion trap. *J. Am. Soc. Mass Spectrom.* **1997**, *8*, 987-995.

53. El Firdoussi, A.; Lafitte, M.; Tortajada, J.; Kone, O.; Salpin, J. Characterization of the glycosidic linkage of underivatized disaccharides by interaction with Pb^{2+} ions. *J. Mass Spectrom.* **2007**, *42*, 999-1011.

54. Konig, S.; Leary, J. A. Evidence for linkage position determination in cobalt coordinated pentasaccharides using ion trap mass spectrometry. *J. Am. Soc. Mass Spectrom.* **1998**, *9*, 1125-1134.

55. Sible, E. M.; Brimmer, S. P.; Leary, J. A. Interaction of first row transition metals with alpha 1-3, alpha 1-6 mannotriose and conserved trimannosyl core oligosaccharides: A comparative electrospray ionization study of doubly and singly charged complexes. *J. Am. Soc. Mass Spectrom.* **1997**, *8*, 32-42.

56. Zhou, Z. R.; Ogden, S.; Leary, J. A. Linkage position determination in oligosaccharides: MS/MS study of lithium-cationized carbohydrates. *J. Org. Chem.* **1990**, *55*, 5444-5446.

57. Penn, S. G.; Cancilla, M. T.; Lebrilla, C. B. Fragmentation behavior of multiple-metal-coordinated acidic oligosaccharides studied by matrix-assisted laser desorption ionization Fourier transform mass spectrometry. *Int. J. Mass Spectrom.* **2000**, *195*, 259-269.

58. Huang, Y.; Dodds, E. D. Discrimination of isomeric carbohydrates as the electron transfer products of group II cation adducts by ion mobility spectrometry and tandem mass spectrometry. *Anal. Chem.* **2015**, *87*, 5664-5668.

59. Kornacki, J. R.; Adamson, J. T.; Håkansson, K. Electron detachment dissociation of underivatized chloride-adducted oligosaccharides. *J. Am. Soc. Mass Spectrom.* **2012**, *23*, 2031-2042.

60. Schaller-Duke, R. M.; Bogala, M. R.; Cassady, C. J. Collision-induced dissociation and electron transfer dissociation of metal-adducted oligosaccharides. *J. Am. Soc. Mass Spectrom.* **2018**, *29*.

61. Ciucanu, I.; Kerek, F. A simple and rapid method for the permethylation of carbohydrates. *Carbohydr. Res.* **1984**, *131*, 209-217.

62. Domon, B.; Costello, C. E. A systematic nomenclature for carbohydrate fragmentations in FAB-MS/MS spectra of glycoconjugates. *Glycoconj. J.* **1988**, *5*, 397-409.

CHAPTER 5: TRIVALENT LANTHANIDE METALS AS CHARGE CARRIERS FOR ELECTRON TRANSFER DISSOCIATION AND COLLISION-INDUCED DISSOCIATION OF OLIGOSACCHARIDES

5.1 Overview

The trivalent lanthanide metal series was investigated as metal adducts for structural analysis of glycans by electron transfer dissociation (ETD) and collision-induced dissociation (CID). Electrospray ionization (ESI) on mixtures of the trivalent metal nitrate salts and the tetrasaccharides produced $[M + Met - H]^{2+}$, $[M + Met + NO_3]^{2+}$, and $[M + Met - 2H]^{+}$, where M is the oligosaccharide and Met is the metal cation (except for radioactive promethium). With ESI of the larger heptasaccharide, both $[M + Met - H]^{2+}$ and $[M + Met]^{3+}$ were produced. The charge density of the lanthanide metals is less than that of the trivalent transition and group 13/boron group metal cations and allows for the formation of multiply charged precursor ions, which are necessary for ETD. Dissociation of $[M + Met - H]^{2+}$ by both ETD and CID for the tetrasaccharides yields extensive sequence information consisting of glycosidic bond cleavage, cross-ring cleavage, and internal cleavage ions, whereas dissociation of $[M + Met + NO_3]^{2+}$ only produced glycosidic bond fragmentation. ETD and CID of the tetrasaccharides leads to cleavage between and across every monosaccharide unit on the glycans. The fragmentation observed did not vary by metal identity regardless of the dissociation method. All metallated product ions contain at least two monosaccharide units, suggesting that the metal cation interacts with oxygens on multiple rings. The heptasaccharide maltoheptaose was included in the study to investigate size effects of the glycans; however, the dissociation observed with both CID and

ETD for both $[M + Met - H]^{2+}$ and $[M + Met]^{3+}$was limited. The results of this study indicated that all trivalent lanthanide cations show promise for sequencing glycans.

5.2 Introduction

The four basic categories of molecules involved in creating life are lipids, nucleic acids, proteins, and carbohydrates. Carbohydrates are the most abundant biological class of molecules and participate in a variety of processes including cell motility, protein folding, energy generation, and modification of the structures and functions of lipids and proteins.[1-3] Glycan expression plays a role in many disease states including the progression and migration of cancer cells. The relationship between structure and function of oligosaccharides is well known; thus, the importance of glycomics has been emphasized by researchers in recent decades.[3] The progress of glycomics is hindered by the lack of techniques for full characterization of the molecules.[4,5]

Carbohydrates have extreme structural complexity arising from isomeric monosaccharide building blocks that may vary in only one stereocenter.[6] Monosaccharides can exist as six membered pyranose rings or five membered furanose rings. The larger polysaccharide structures become even more complex with varying linkage position and anomeric configuration between each monosaccharide, as well as branching at multiple positions on each monosaccharide ring. A glycan can undergo sulfation, acetylation, phosphorylation, or attachment by glycosylation to a protein, further complicating analysis. Characterization of oligosaccharide structure involves the stereochemistry of the anomeric carbons, the position of the glycosidic bonds, the sequence of the monosaccharides, and identification of any branching or covalent modifications.[6]

Fast, accurate, highly sensitive methods for determining oligosaccharide structures are necessary. Recent advancements in mass spectrometry (MS) instrumentation and dissociation

methods have allowed the structural analysis of glycans.[7-10] The separation and characterization of oligosaccharides using MS requires the use of tandem mass spectrometry (MS/MS) to dissociate glycans into smaller fragments to reveal structural characteristics.[11-13] Dissociation of glycans occurs either across the glycosidic bond to produce sequence and monosaccharide characteristics, or across the monosaccharide rings, which provides structural information related to bond position and linkage. Many MS/MS techniques have been utilized to maximize the glycan structural information acquired. The most common technique used is collision-induced dissociation (CID),[14-23] but studies have also used infrared multiphoton dissociation (IRMPD),[24-30] ultraviolet photodissociation (UVPD),[31-36] and electron-based dissociation techniques (ExD).[16,24-28,37-49] The two most common electron-based techniques are electron capture dissociation (ECD) and electron transfer dissociation (ETD), which produce similar spectra and are believed to induce dissociation by the same mechanism.

Oligosaccharides can range from being neutral to highly acidic and, thus, can be difficult to protonate by electrospray ionization (ESI) or matrix-assisted laser desorption/ionization (MALDI) without derivatization or conjugation. In order to provide a charge for positive mode analysis, glycans are often analyzed with one more metal adducts.[13-15,18,19,22-24,29,41-43,49-60] Oligosaccharides contain many electron-rich oxygen and nitrogen atoms that are able to coordinate to the metal cations.[61] Multivalent metal cations can increase the charge state of the quasi-molecular ions formed by ESI. This allows for utilization of electron-based dissociation techniques that require a multiply charged precursor ion. Studies have also shown that fragmentation by MS/MS increases as the charge state on the precursor ion increases for both peptides and glycans.[24,44,49] Peptide studies have demonstrated the ability of trivalent metal cations to produce multiply charged quasi-molecular ions via ESI.[62-65]

In the work of Chapter 3, the trivalent metal ions Fe^{3+}, Al^{3+}, Y^{3+}, Sc^{3+}, and Cr^{3+} were explored as charge carriers for glycans but did not consistently produce multiply charged ions.[49] In the current study, the trivalent lanthanide metal series will be investigated as metal adducts for ETD and CID of glycans.

5.3 Experimental

All experiments were performed using a Bruker (Bruker Daltonics, Billerica, MA, USA) HCTultra PTM Discovery System high capacity quadrupole ion trap (QIT) mass spectrometer, which was discussed in Chapter 2. In the ESI source, the needle was held at ground and a high voltage of -3.5 kV was placed on the capillary, with an end plate offset of -500 V and a capillary exit voltage of 120 V. Nitrogen drying gas was heated to 250°C and flowed at a rate of 10 L/min. Nitrogen was also used as the nebulizer gas at a pressure between 5-10 psi. The amplitude of the activating voltage for CID experiments was 0.8 to 1.2 V and the collision gas was helium with a 30% to 200% collision energy sweep. All spectra shown are the result of signal averaging of 200 scans. Mixtures of metal nitrate salt and oligosaccharides in at 10:1 metal salt:oligosaccharide molar ratio were infused into the ESI source with a flow rate of 180 µL/hour. A KD Scientific (Holliston, MA, USA) syringe pump was used to infuse sample solutions that had a final concentration of 10 µM in methanol:water at a 50:50 volume ratio.

The reagent ion for ETD experiments was fluoranthene, which was generated in a negative chemical ionization (nCI) source with methane serving as the nCI reagent gas. The accumulation time for the reagent anion was 20 ms. The ion charge control (ICC) target was 300,000 to 400,000 to maximize electron transfer. The lower end *m/z* was set at 120 *m/z* and anion/cation reaction times were optimized at 400 ms. The “smart decomposition” function was enabled to facilitate dissociation of any charge reduced (ETnoD) product ions. Smart

decomposition uses resonant excitation to overcome attractive forces that may hold oligosaccharide fragments together following ETD.

The oligosaccharides were purchased from various vendors as listed in Section 2.5. Lanthanide series metal nitrate salts were purchased from Alfa Aesar (Ward Hill, MA, USA). Ultrapure Milli-Q 18 MΩ water was produced with a Barnstead (Dubuque, IA, USA) E-pure system.

5.4 Results and Discussion

The Domon and Costello nomenclature of labeling MS/MS product ions is used for all spectra, and is described in Section 2.7.[66] Colors and notation used to identify the product ions in the spectra are described in Section 3.4.2, and isobaric mass assignments can be found in Table 3.3. The symbolic structure of the oligosaccharides studied can be seen in Figure 2.14 and the expanded structures are in Figure 2.15.

5.4.1 Ion Formation by ESI

Electrospray ionization on mixtures of the tetrasaccharides and the lanthanide metal nitrate salts produced $[M + Met - H]^{2+}$, $[M + Met + NO_3]^{2+}$, and $[M + Met - 2H]^{+}$, where M is the oligosaccharide and Met is the metal cation. For the larger heptasaccharide, both $[M + Met - H]^{2+}$ and $[M + Met]^{3+}$ were produced. The addition of up to 5% acetic acid (by volume) did not change the ions formed, although it decreased the ion intensity in the spectra, probably due to degradation of the glycans. The intensity of the ions formed via ESI were not dependent on the lanthanide used. Previous work with the trivalent metal cations Al^{3+}, Cr^{3+}, and Fe^{3+} is discussed in Chapter 3 and did not consistently produce adducts or multiply charged ions. The charge densities for the lanthanide metals used in the study are shown in Table 5.1 and range from 1864 Q/R^3 for La^{3+} to 2991 Q/R^3 for Lu^{3+}, where Q is the charge on the metal cation in

1.6 x 10^{-19} Coulombs and R is the ionic radius of the metal in nm. This is significantly less than the 9750 Q/R^3, 6970 Q/R^3, and 6200 Q/R^3 for Al^{3+}, Cr^{3+}, and Fe^{3+}, respectively, and closer to Co^{2+} (2890 Q/R^3) and Zn^{2+} (2940 Q/R^3). The lack of trivalent metal adducts with the transition metals and group 13/boron group metal in Chapter 3 was attributed to the high charge density of the trivalent metal cations, promoting coordination to an oxyanion as opposed to a hydroxyl group, producing loss of protons during ESI.[49] The lower charge densities of the lanthanide metals may allow them to coordinate to neutral hydroxyl groups more favorably than the trivalent metal cations with higher charge densities, and may explain why lanthanides are able to form multiply charged ions with the oligosaccharides in the study, when other trivalent metals could not. Another defining characteristic of metal cations that may affect their coordination to glycans is their Lewis acidity and classification as hard acids, soft acids, or borderline. Hard metals interact with a base in a similar way as a proton would, by binding to a lone pair of electrons; therefore, hard metals will coordinate more strongly than a soft metal to a sugar.[67] The alkali metals, alkaline earth metals, lanthanides and aluminum, are all classified as hard metals. In contrast, the transition metals are borderline. All of the hard metals in the study formed adducts with the oligosaccharides, as did the divalent transition metals. The trivalent transition metals fall into the same borderline category as the divalent transition metals; however, the ionic radius of the trivalent metals is smaller than that of the divalent metals, which may also affect coordination to the glycan.

Table 5.1 Comparison of physical properties of trivalent lanthanide metal ions included in study.

Metal	Charge (Q)[a]	Ionic Radius (R)[b]	Charge Density (Q/R^3)[c]	First Ionization Energy (kJ/Mol)	Second Ionization Energy (kJ/Mol)	Third Ionization Energy (kJ/Mol)	Electron Configuration
La	3	0.1172	1864	538.1	1079.2	1850	$[Xe]4f^0$
Ce	3	0.115	1973	543.4	1057.1	1949	$[Xe]4f^1$
Pr	3	0.113	2079	527.8	1025.7	2086	$[Xe]4f^2$
Nd	3	0.1123	2118	533.1	1040.4	2130	$[Xe]4f^3$
Sm	3	0.1098	2266	544.5	1068.9	2270	$[Xe]4f^5$
Eu	3	0.1087	2336	547.1	1084.5	2400	$[Xe]4f^6$
Gd	3	0.1078	2395	593.4	1165.2	1980	$[Xe]4f^7$
Tb	3	0.1063	2498	565.8	1110.8	2110	$[Xe]4f^8$
Dy	3	0.1052	2577	573.0	1123.8	2210	$[Xe]4f^9$
Ho	3	0.1041	2660	580.9	1136.7	2200	$[Xe]4f^{10}$
Er	3	0.103	2745	589.3	1149.7	2190	$[Xe]4f^{11}$
Tm	3	0.102	2827	596.7	1164.1	2280	$[Xe]4f^{12}$
Yb	3	0.1008	2929	603.4	1175.1	2417	$[Xe]4f^{13}$
Lu	3	0.1001	2991	523.5	1363	2022	$[Xe]4f^{14}$

[a] Q in 1.6×10^{-19} C.

[b] R in nm.

[c] Q/R^3 in 1.6×10^{-19} C/nm^3.

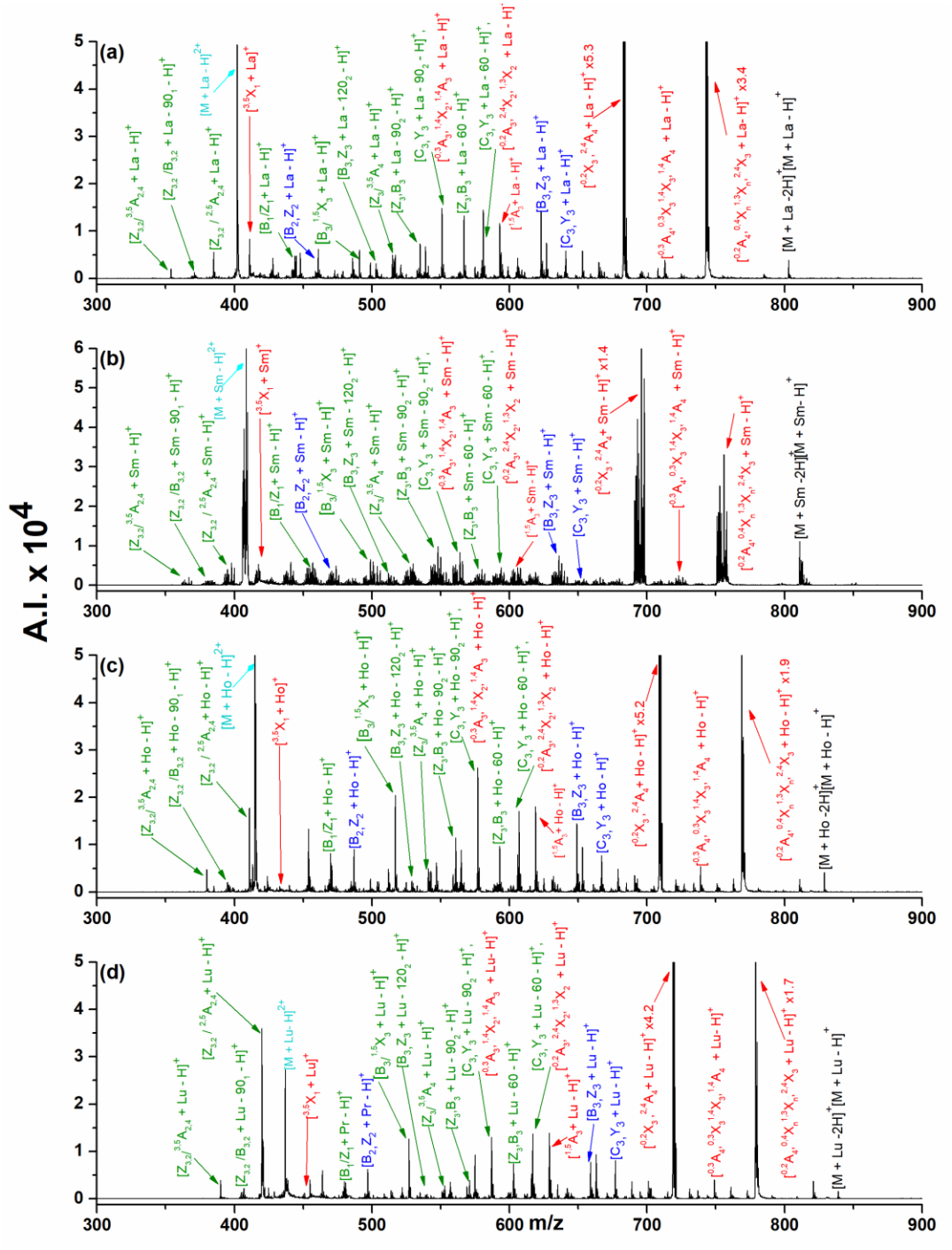

Figure 5.1 ETD mass spectra of maltotetraose for (a) $[M + La - H]^{2+}$, (b) $[M + Sm - H]^{2+}$, (c) $[M + Ho - H]^{2+}$, and (d) $[M + Lu - H]^{2+}$. Colors used to illustrate the product ions are red for cross-ring cleavages, blue for glycosidic bond cleavages, and green for internal cleavages. Refer to Table 3.3 for identities of internal cleavages indicated by mass lost. Undissociated precursor ion is labeled in light blue with a large light blue diamond arrow head. Product ions involving solely neutral losses are labeled in black.

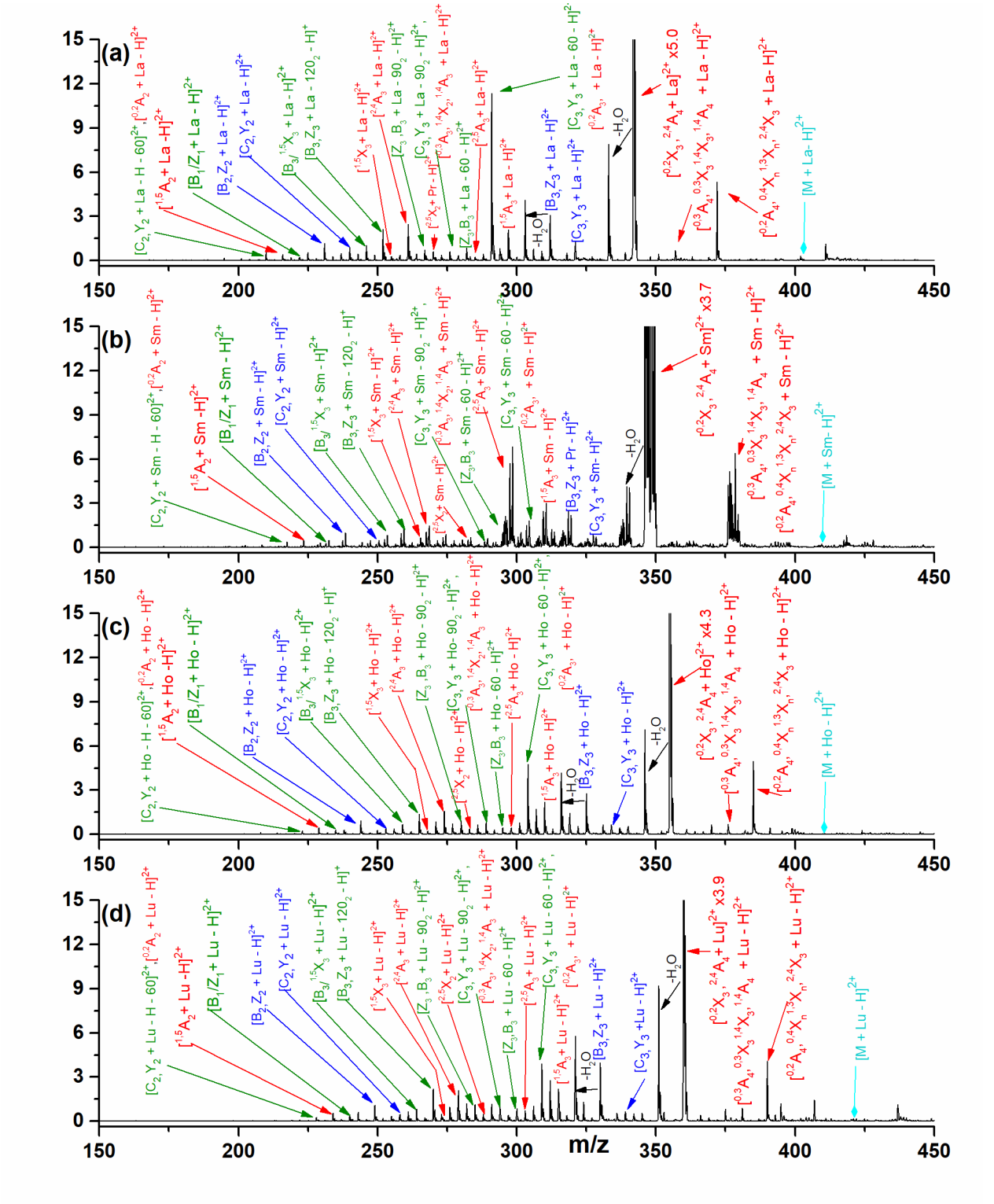

Figure 5.2 CID mass spectra of maltotetraose for (a) $[M + La - H]^{2+}$, (b) $[M + Sm - H]^{2+}$, (c) $[M + Ho - H]^{2+}$, and (d) $[M + Lu - H]^{2+}$. Refer to the Figure 5.1 caption for an explanation of the color codes.

5.4.2 Tandem Mass Spectrometry

Figure 5.1 shows ETD spectra obtained from maltotetraose $[M + Met - H]^{2+}$ cationized by La^{3+}, Sm^{3+}, Ho^{3+}, and Lu^{3+}, while Figure 5.2 shows CID spectra of maltotetraose $[M + Met - H]^{2+}$ with the same metal cations. As can be seen in these two figures, all fragmentation produced by the lanthanide metals is similar as one moves across the row of the Periodic Table for both dissociation types. The product ions seemingly vary only in intensity. This holds for all glycans in the study. Thus, throughout this discussion, La^{3+} will be used as representative for all the lanthanide metals in the study because it has one major isotope, which simplifies the spectra, and consistently yielded high quality spectra. Figures 5.3, 5.4, and 5.5, show ETD and CID spectra of $[M + La - H]^{2+}$ from galactotetraose, stachyose, and nystose, respectively. Figure 5.6 shows ETD and CID spectra from $[M + La]^{3+}$ and $[M + La - H]^{2+}$ from maltoheptaose. Dissociation of the tetrasaccharides with both ETD and CID caused glycosidic bond fragmentation between and across every monosaccharide unit with all product ions containing at minimum two monosaccharide units. This does not vary from studies in Chapter 3 of ETD with Co^{2+} adducts. The number and variety of product ions formed via ETD and CID with the trivalent lanthanides was greater than that seen in Chapter 3 with Co^{2+} for all the tetrasaccharides except ETD of [M + La – H] from nystose in Figure 5.5(a). For maltoheptaose, CID of both $[M + La]^{3+}$ and $[M + La - H]^{2+}$ produces glycosidic bond cleavage across the whole molecule, but ETD of these two ions does not dissociate the bonds on either side of the central glucose unit. Additionally, neither ETD nor CID produce any cross-ring fragmentation across the center glucose of maltoheptaose. This varies from the data in Chapter 3, where both dissociation techniques caused fragmentation between and across every glucose unit on maltoheptaose.

The tetrasaccharide in the study with the least variation in structure among its composite units is maltotetraose, which is made up of four glucose units all bonded with identical α 1→4 glycosidic bonds. ETD and CID of $[M + La - H]^{2+}$ from maltotetraose produced glycosidic bond cleavages, cross-ring cleavages, and internal cleavages, as seen in Figures 5.1 and 5.2, respectively. The ETD spectrum showed an increase in internal fragment ions in comparison to the work of Chapter 3 with Co^{2+}, including loss of 120 Da and 90 Da from $[B_3, Z_3 + La - H]^+$ and also the internal cleavage ions below 400 *m/z*. The internal fragment ions that are exact mass ions with loss of 60 and 90 Da from $[B_2, Z_2 + La - H]^+$ (which is cleavage of the glycosidic bond in the center of the molecule) are not present in the spectrum and neither is the corresponding glycosidic bond fragment containing the glycosidic oxygen. The cross-ring product ion $^{1,5}A_3$ appears in both the Co^{2+} and La^{3+} spectra, but the latter does not have the corresponding $^{1,5}A_2$ from the neighboring glucose or $^{2,5}X_1$, both of which form with Co^{2+}. The cross-ring fragment ion $^{3,5}X_1$ is unique to maltotetraose, and not found in any of the ETD or CID spectra for the other glycans. The variation in cross-ring ions with ETD between the Co^{2+} spectra and the La^{3+} spectra is interesting since the types of cross-ring fragments observed are more indicative of structural information. The amount of fragmentation in the CID spectrum is greater than that seen in Chapter 3, and the product ions are all doubly charged. All of the ions in the CID spectrum of maltotetraose in Figure 3.2 with Co^{2+} are observed with La^{3+} except for one internal ion $Z_3/^{2,4}A_4$ and the protonated glucose product ions with loss of water. There were multiple A and X ions and internal cleavage ions with La^{3+} that did not form with Co^{2+}. Dissociation with La^{3+} adducts produces a higher number and variety of fragment ions than Co^{2+} for the tetrasaccharides with both dissociation methods, but also contains many product ions that were not identified and therefore not useful. With the possibility of loss of water or other neutral

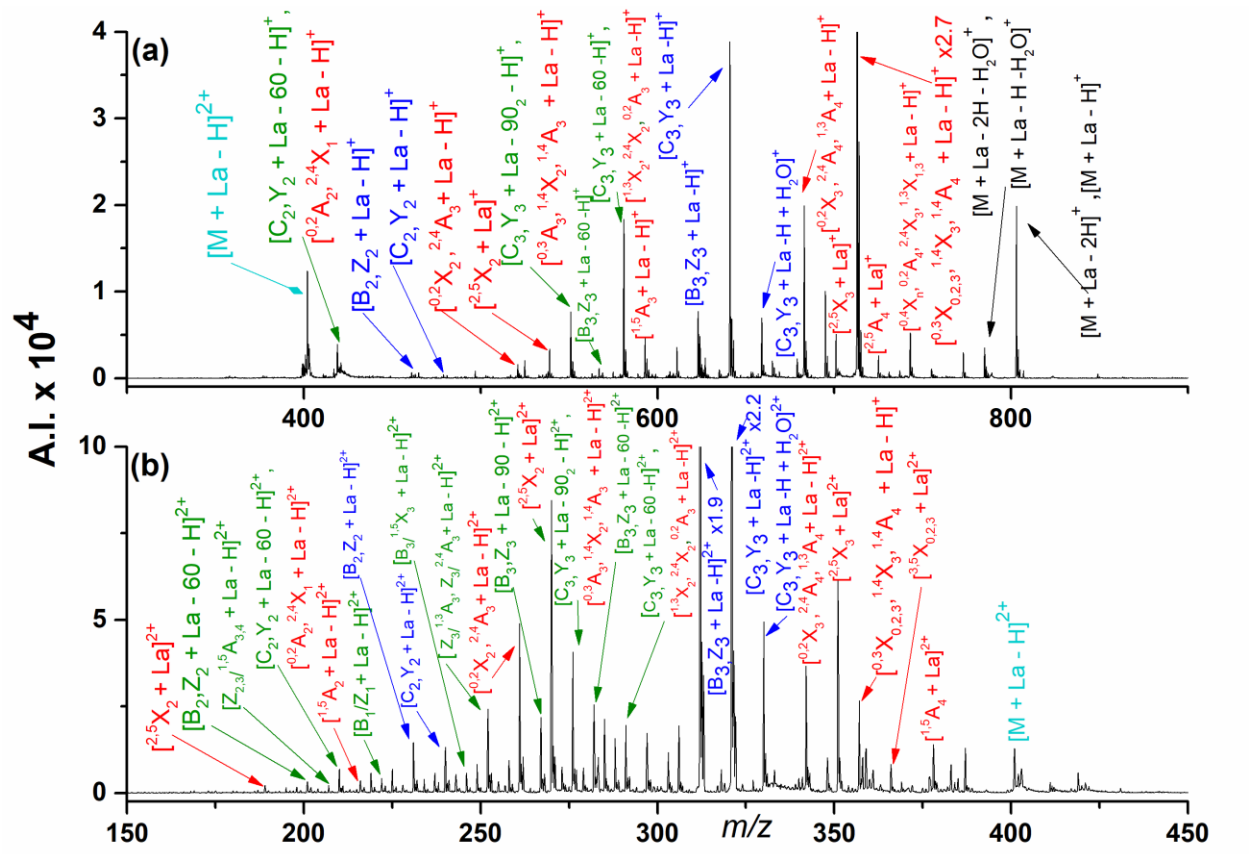

Figure 5.3 Mass spectra from (a) ETD and (b) CID of $[M + La - H]^{2+}$ from galactotetraose. Refer to the Figure 5.1 caption for an explanation of the color codes.

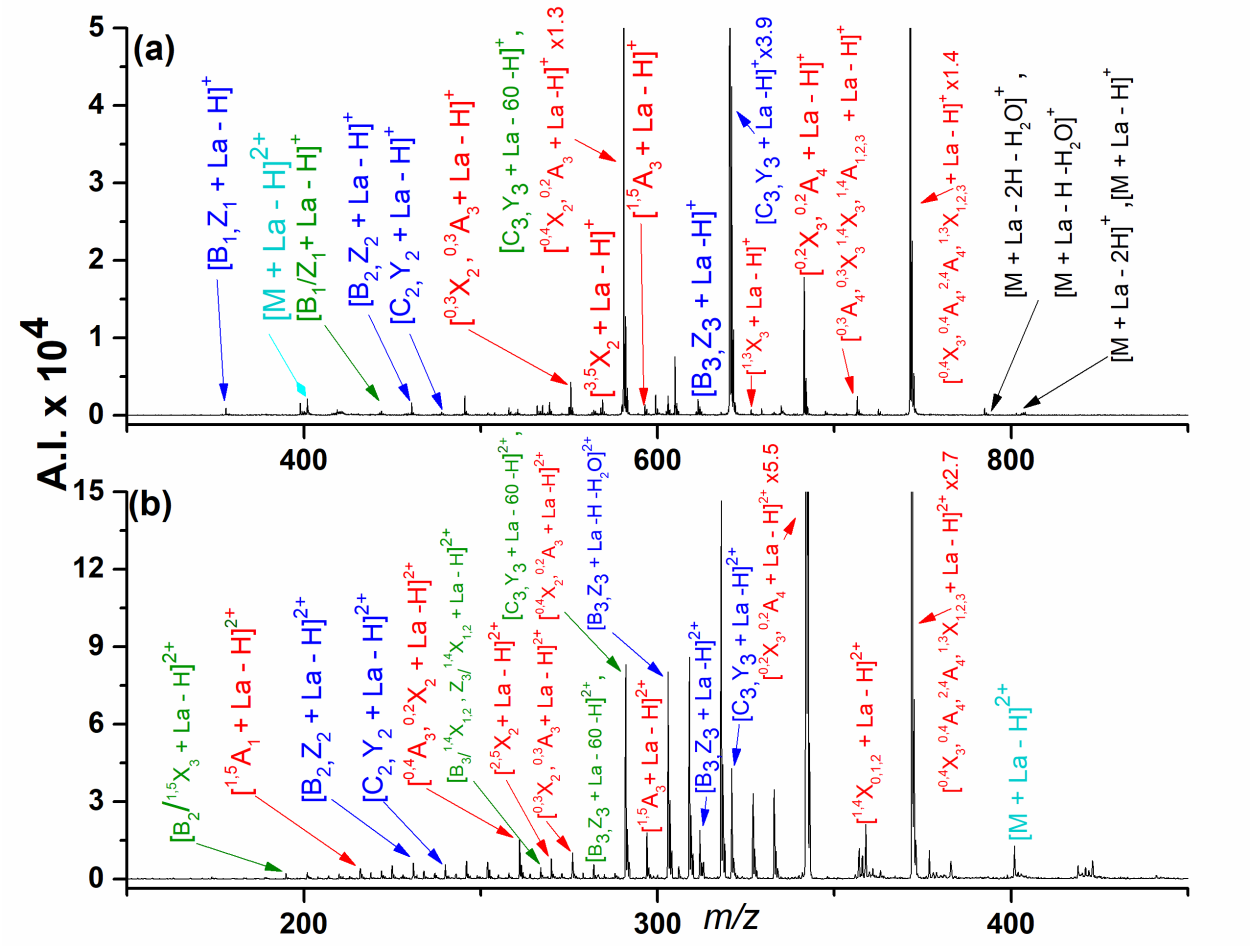

Figure 5.4 Mass spectra from (a) ETD and (b) CID of $[M + La - H]^{2+}$ from stachyose. Refer to the Figure 5.1 caption for an explanation of the color codes.

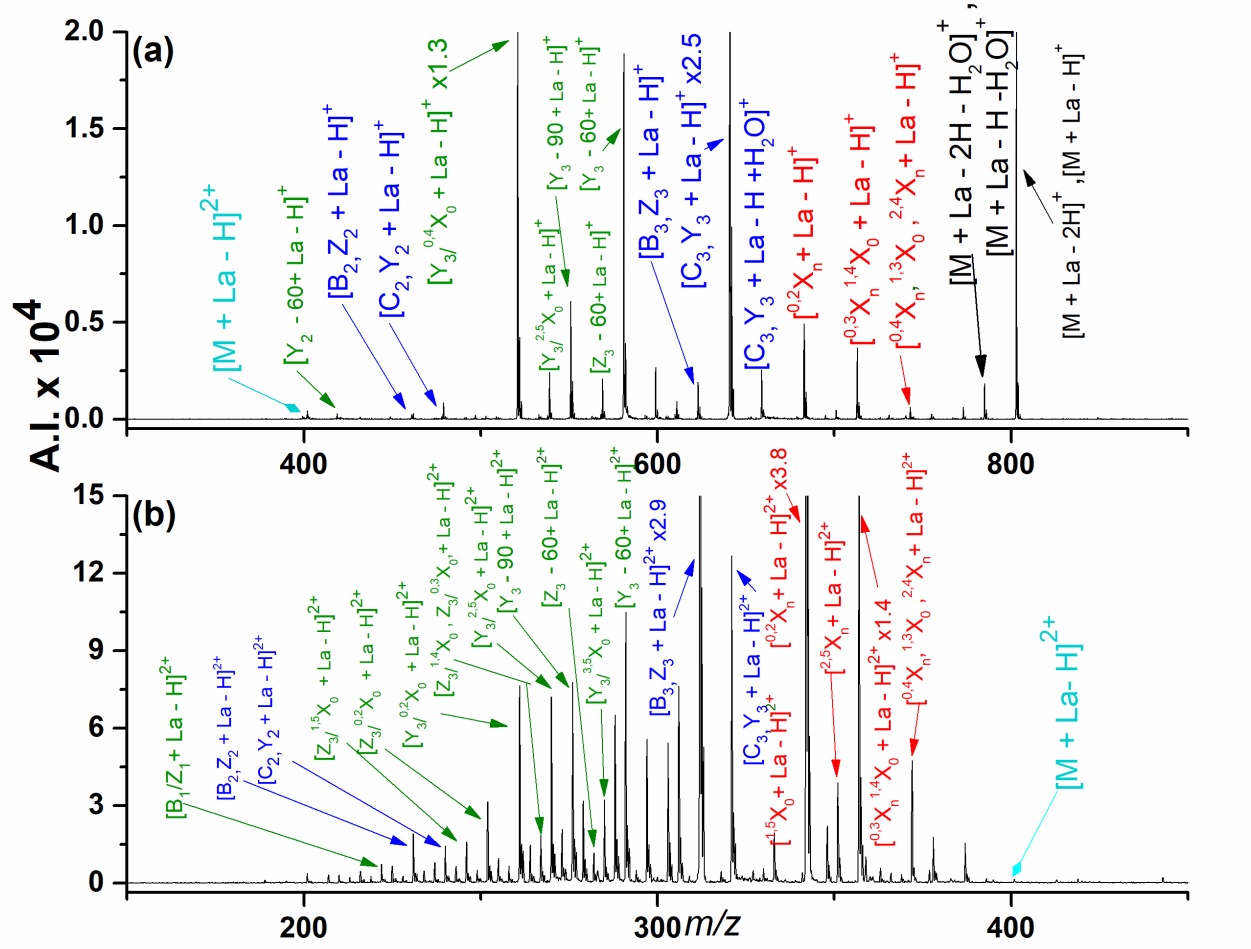

Figure 5.5 Mass spectra from (a) ETD and (b) CID of $[M + La - H]^{2+}$ from nystose. Refer to the Figure 5.1 caption for an explanation of the color codes.

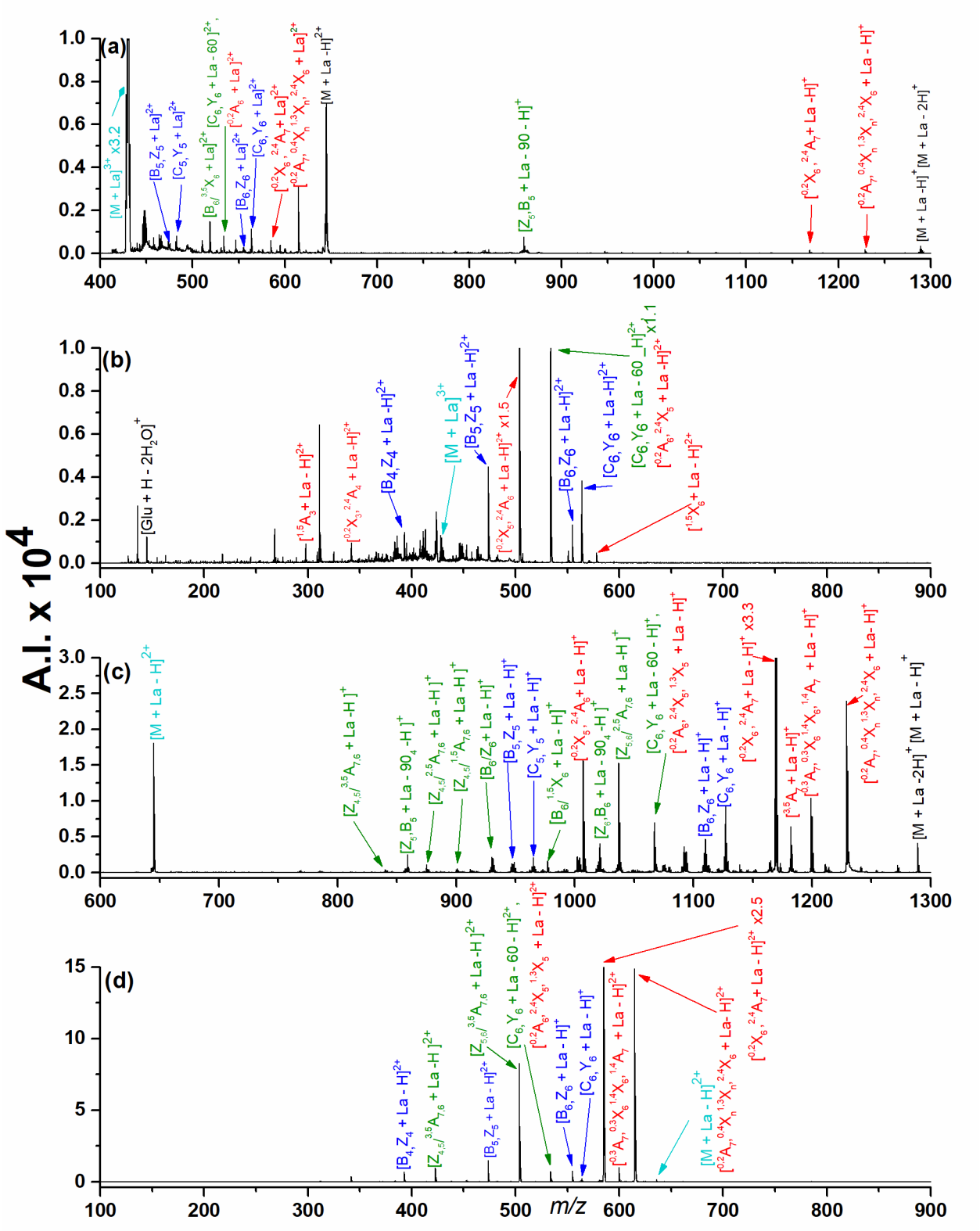

Figure 5.6 Mass spectra from (a) ETD and (b) CID of $[M + La]^{3+}$, as well as (c) ETD and (d) CID of $[M + La - H]^{2+}$from maltoheptaose. Refer to the Figure 5.1 caption for an explanation of the color codes.

losses on top of more fragmentation, the spectra with the lanthanide metals are more complicated and difficult to interpret. This, along with numerous internal fragment ions, could hinder the identification of spectra from unknown glycans. (Internal ions are generated from two cleavages, which remove both termini of the glycan from the product ion.)

Spectra for ETD and CID of maltotetraose with adducts of Ce^{3+}, Pr^{3+}, Nd^{3+}, Eu^{3+}, Gd^{3+}, Tb^{3+}, Dy^{3+}, Er^{3+}, Tm^{3+}, and Yb^{3+} can be seen in Figures 5.7 through 5.16, respectively. All of the metal cations produce the same fragmentation for each glycan in the study. The product ions will change *m/z* based on the mass and stable isotopes of the metal adduct and the isotopes, but the ions generated with any of the lanthanides are identical to the ions produced with La^{3+} The lanthanides metals with odd atomic numbers have only one or two stable isotopes and those with even atomic numbers have from four to seven stable isotopes. The intensity of the product ions may vary with the different metal adducts, but the base peak does not change. In some of the spectra where the metal cation has multiple isotopes (e.g., Figures 5.9 and 5.11), the product ion peaks overlapped, which made their identification difficult.

The tetrasaccharide 3α,4β,3α-galactotetraose, like maltotetraose, is only made up of one type of monosaccharide unit. The molecule consists of four galactose units bonded by both α 1→3 and β 1→4 glycosidic bonds. Figure 5.3 provides ETD and CID spectra of $[M + La - H]^{2+}$ from galactotetraose. The ETD spectrum shows an increase in internal fragment ions when compared to the data in Figure 3.14 with Co^{2+}, including loss of 60 Da from $[B_3, Z_3 + La - H]^+$, $[C_3, Y_3 + La - H]^+$, and $[C_2, Y_2 + La - H]^+$. ETD cross-ring product ions $^{2,5}X_2$, $^{2,5}X_3$, and $^{2,5}A_4$ are unique to galactotetraose and formed with both Co^{2+} in Figure 3.14 and with La^{3+} in the current study. There are no product ions produced by ETD on $[M + Co]^{2+}$ that do not appear in the lanthanide ETD spectra. The product ion $^{2,4}A_4$, which formed by cleavage across the

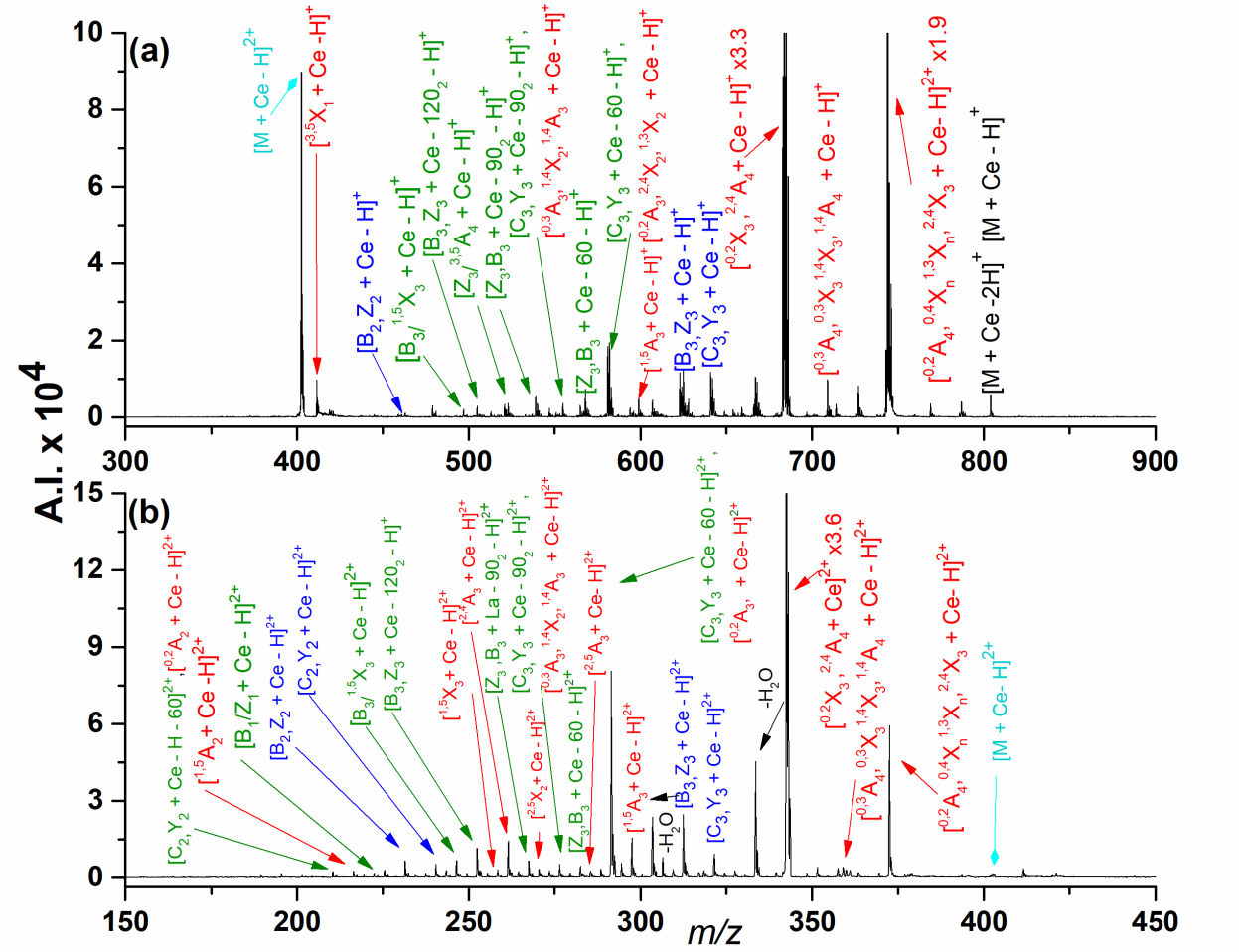

Figure 5.7 Mass spectra from (a) ETD and (b) CID of $[M + Ce - H]^{2+}$ from maltotetraose. Refer to the Figure 5.1 caption for an explanation of the color codes.

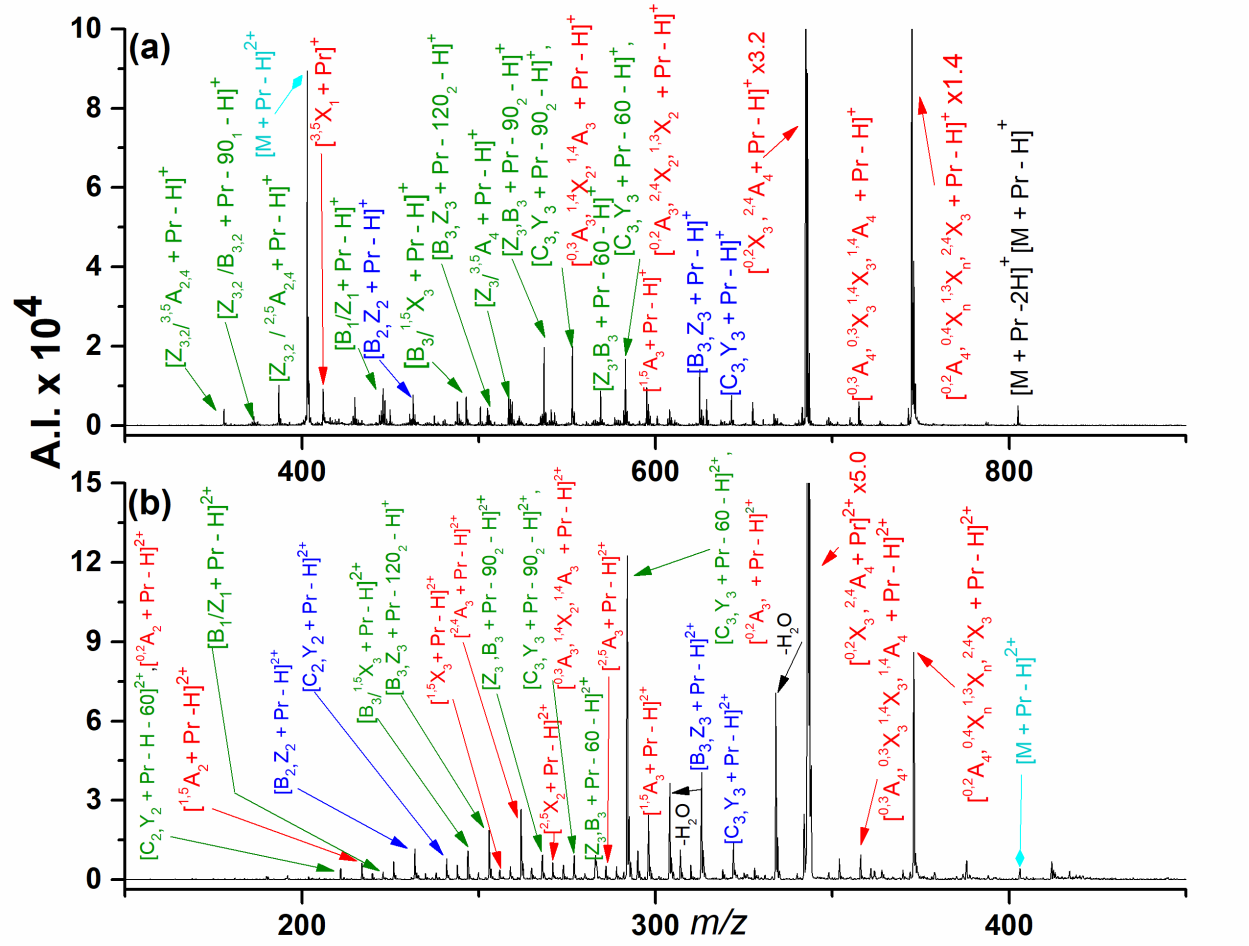

Figure 5.8 Mass spectra from (a) ETD and (b) CID of $[M + Pr - H]^{2+}$ from maltotetraose. Refer to the Figure 5.1 caption for an explanation of the color codes.

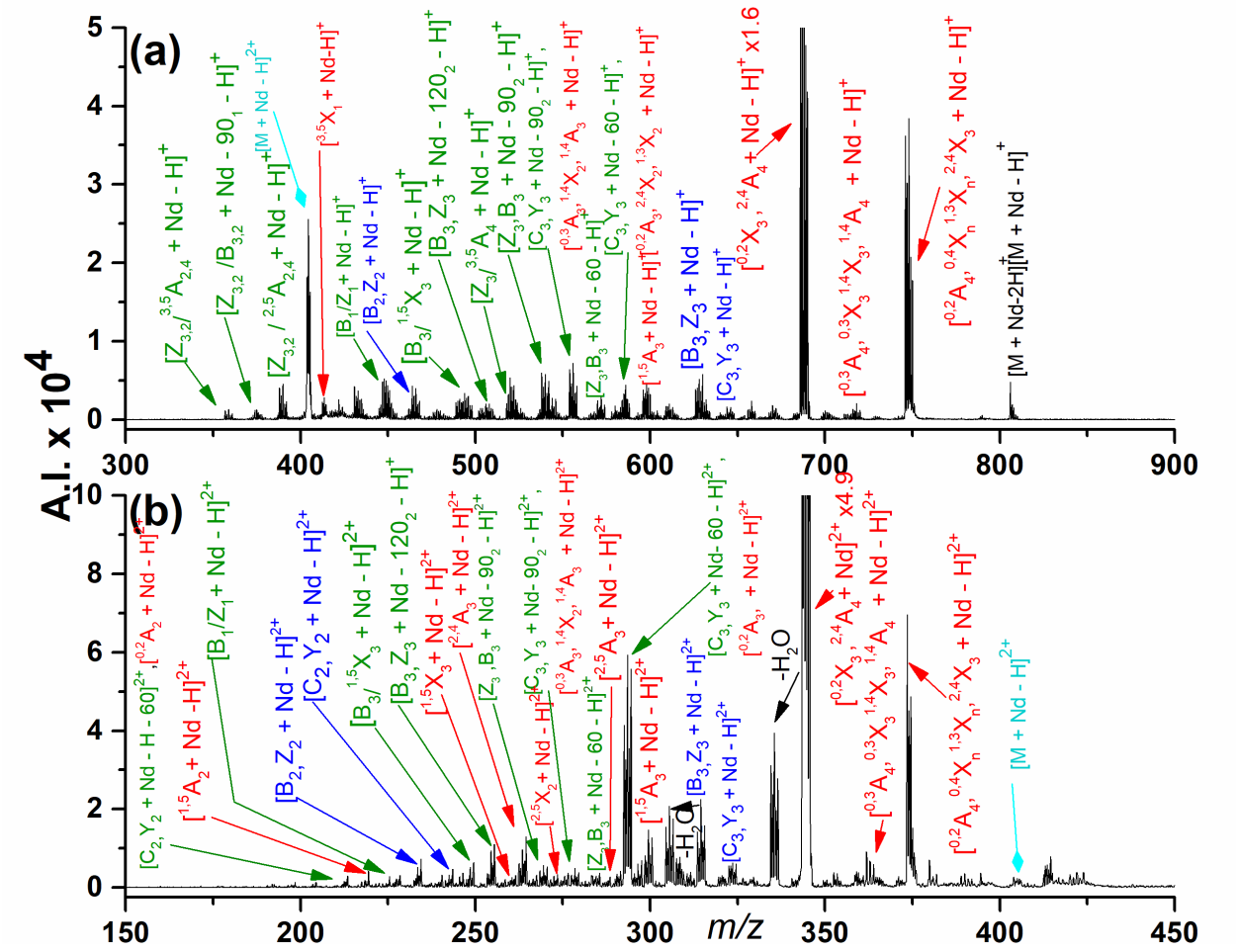

Figure 5.9 Mass spectra from (a) ETD and (b) CID of $[M + Nd - H]^{2+}$ from maltotetraose. Refer to the Figure 5.1 caption for an explanation of the color codes.

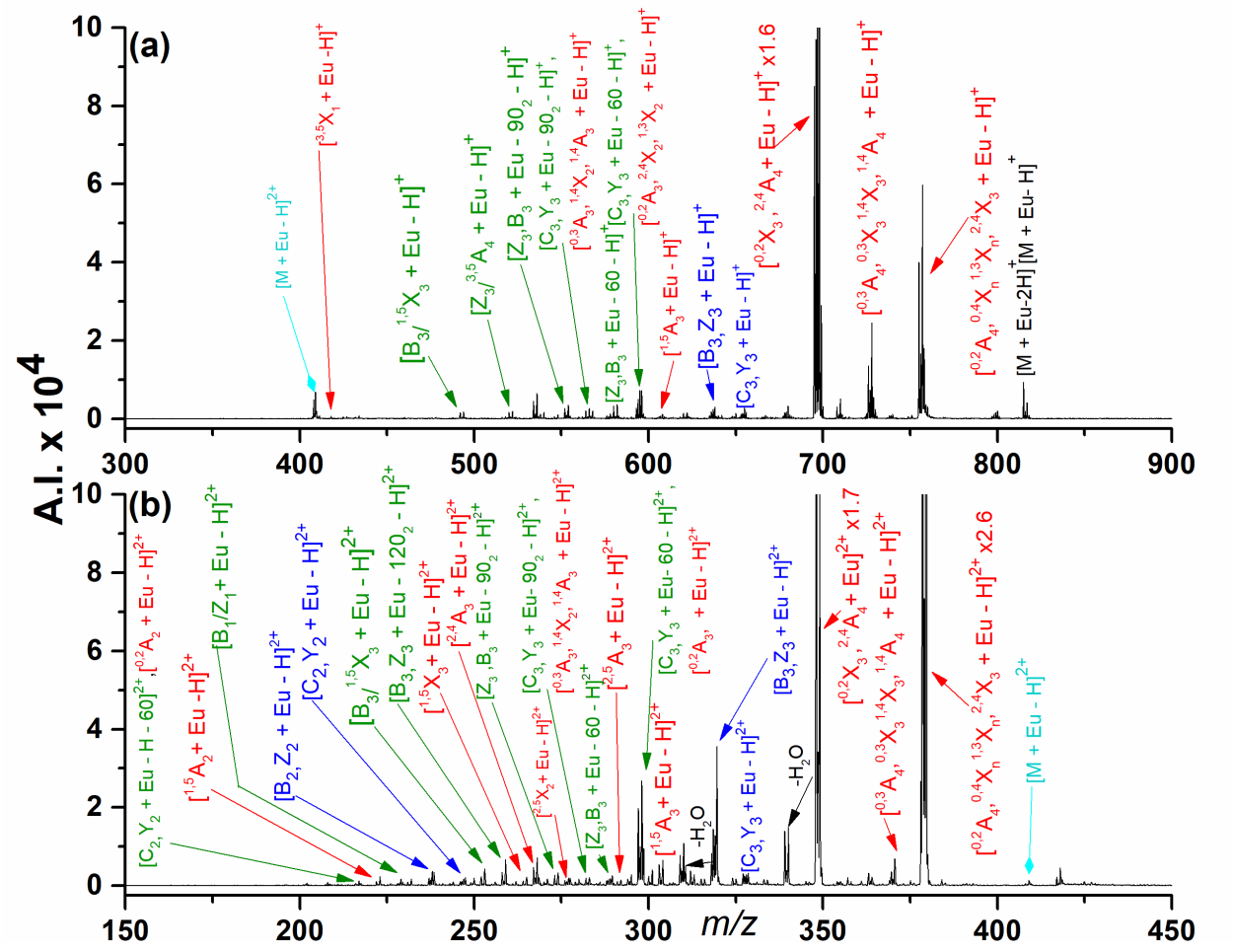

Figure 5.10 Mass spectra from (a) ETD and (b) CID of $[M + Eu - H]^{2+}$ from maltotetraose. Refer to the Figure 5.1 caption for an explanation of the color codes.

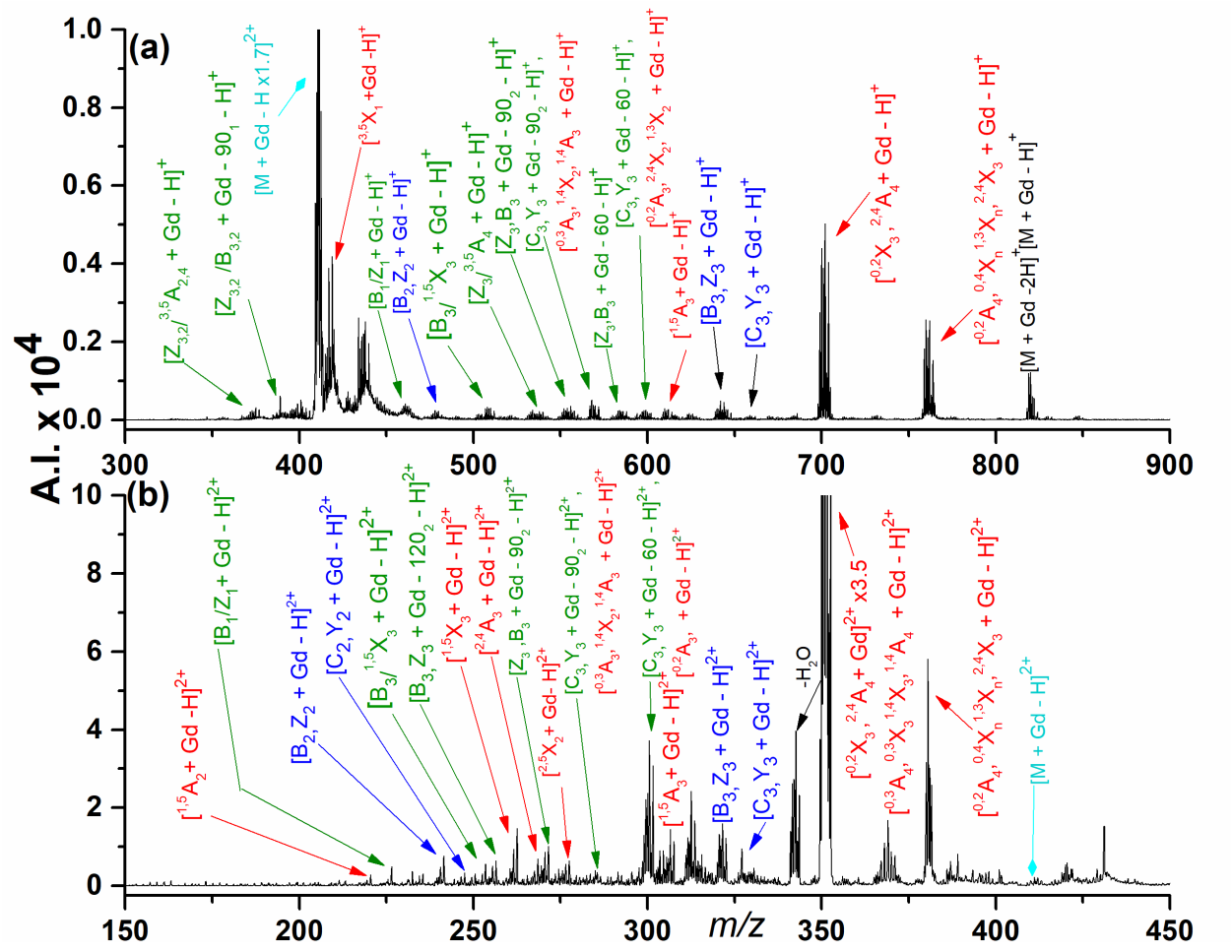

Figure 5.11 Mass spectra from (a) ETD and (b) CID of $[M + Gd - H]^{2+}$ from maltotetraose. Refer to the Figure 5.1 caption for an explanation of the color codes.

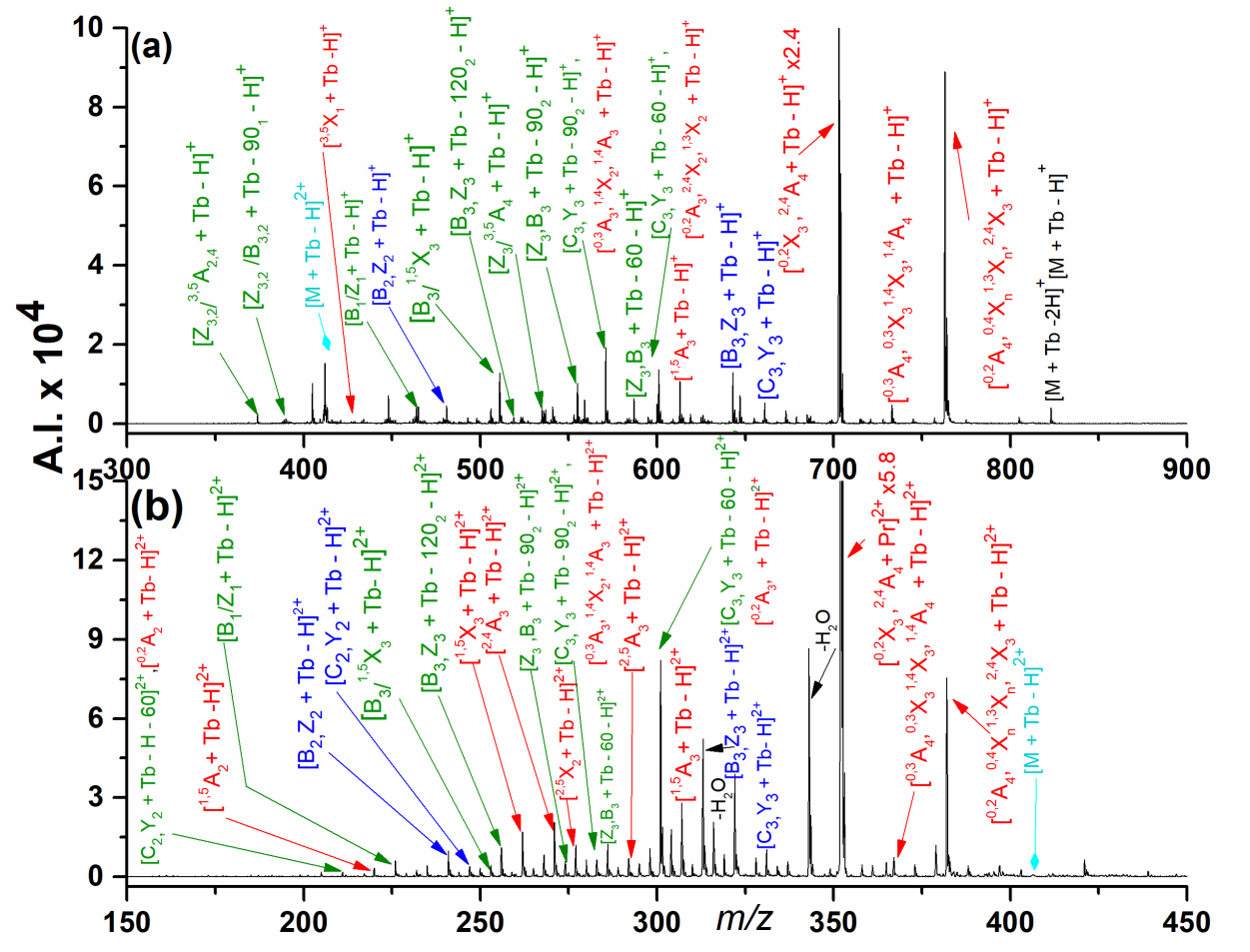

Figure 5.12 Mass spectra from (a) ETD and (b) CID of $[M + Tb - H]^{2+}$ from maltotetraose. Refer to the Figure 5.1 caption for an explanation of the color codes.

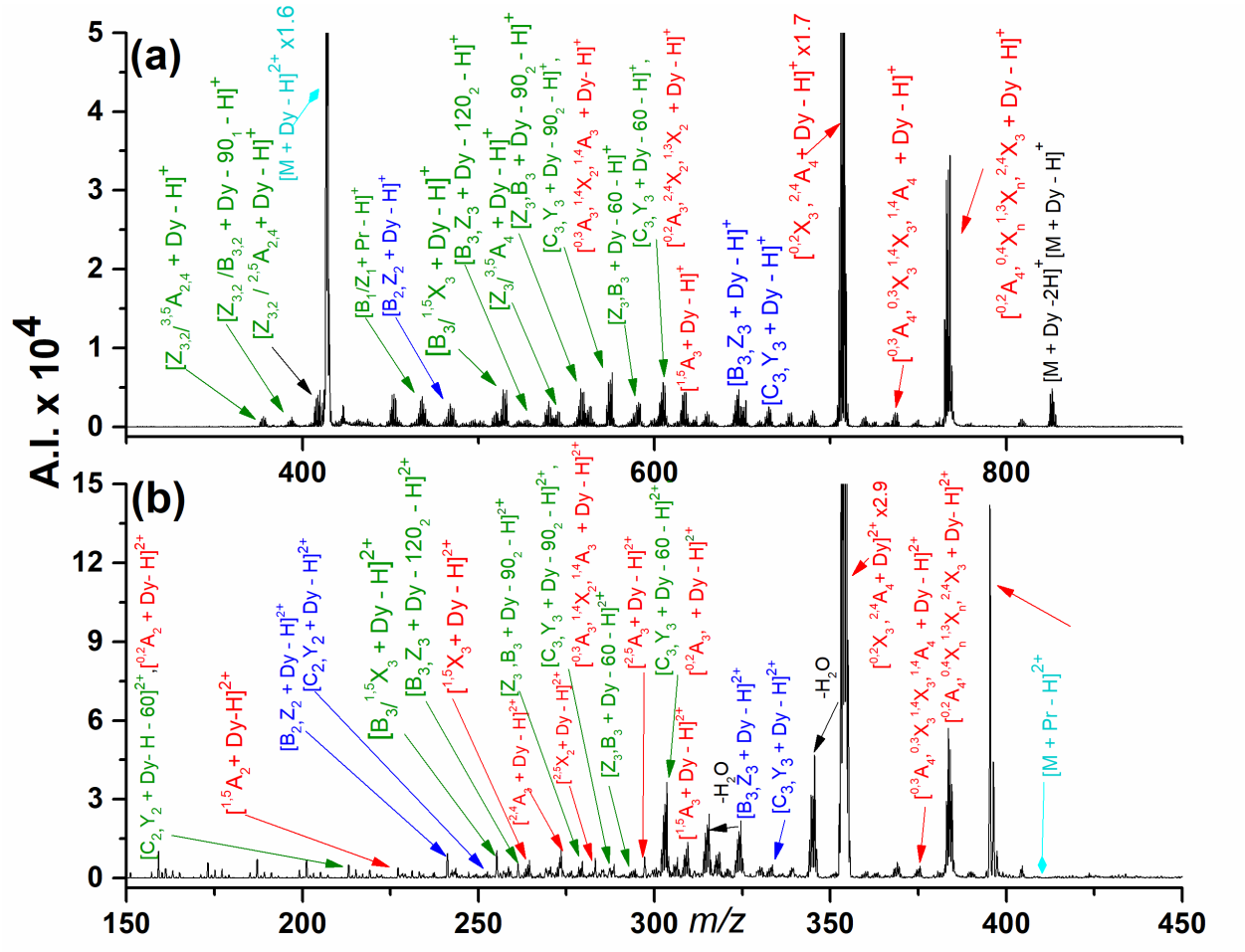

Figure 5.13 Mass spectra from (a) ETD and (b) CID of $[M + Dy - H]^{2+}$ from maltotetraose. Refer to the Figure 5.1 caption for an explanation of the color codes.

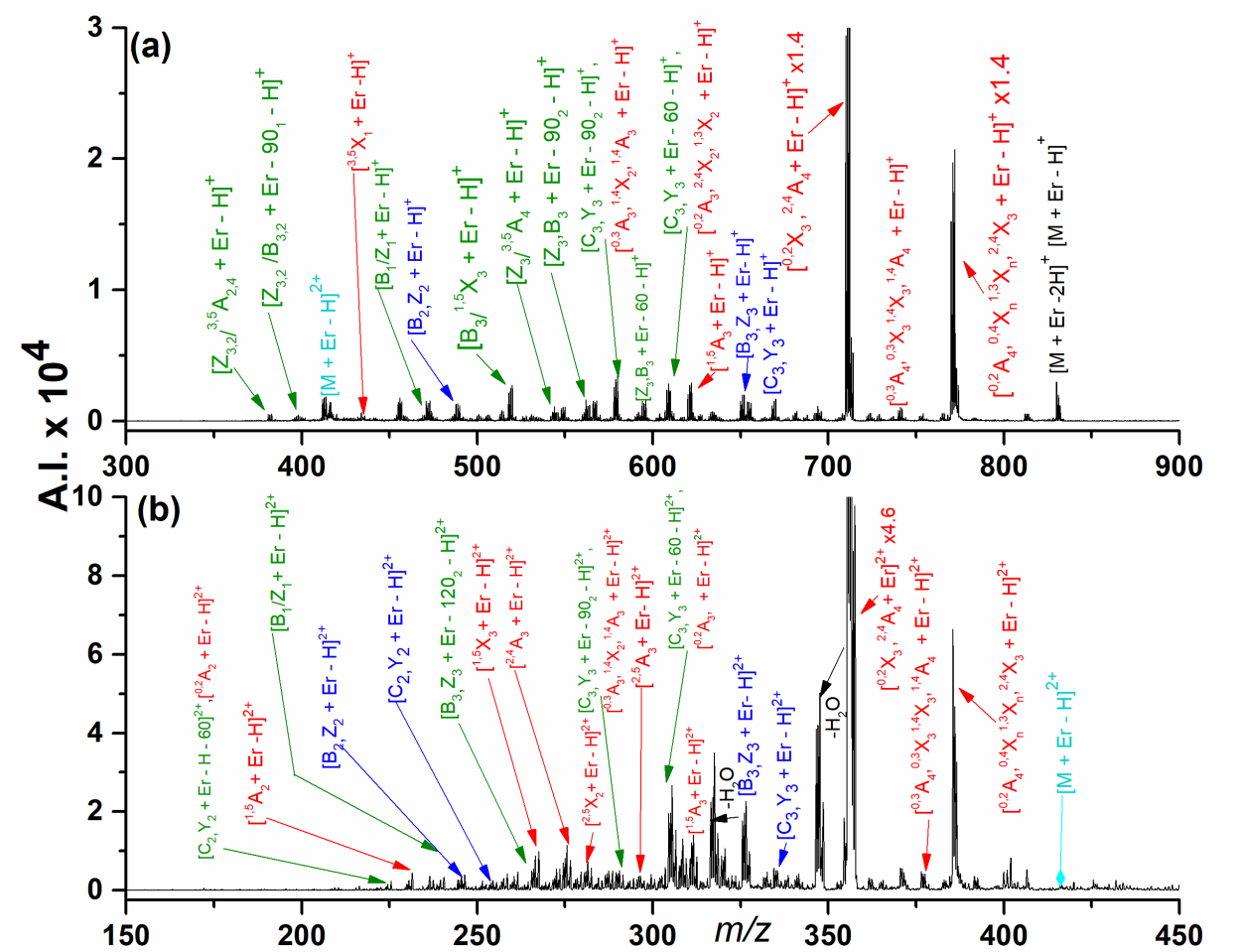

Figure 5.14 Mass spectra from (a) ETD and (b) CID of $[M + Er - H]^{2+}$ from maltotetraose. Refer to the Figure 5.1 caption for an explanation of the color codes.

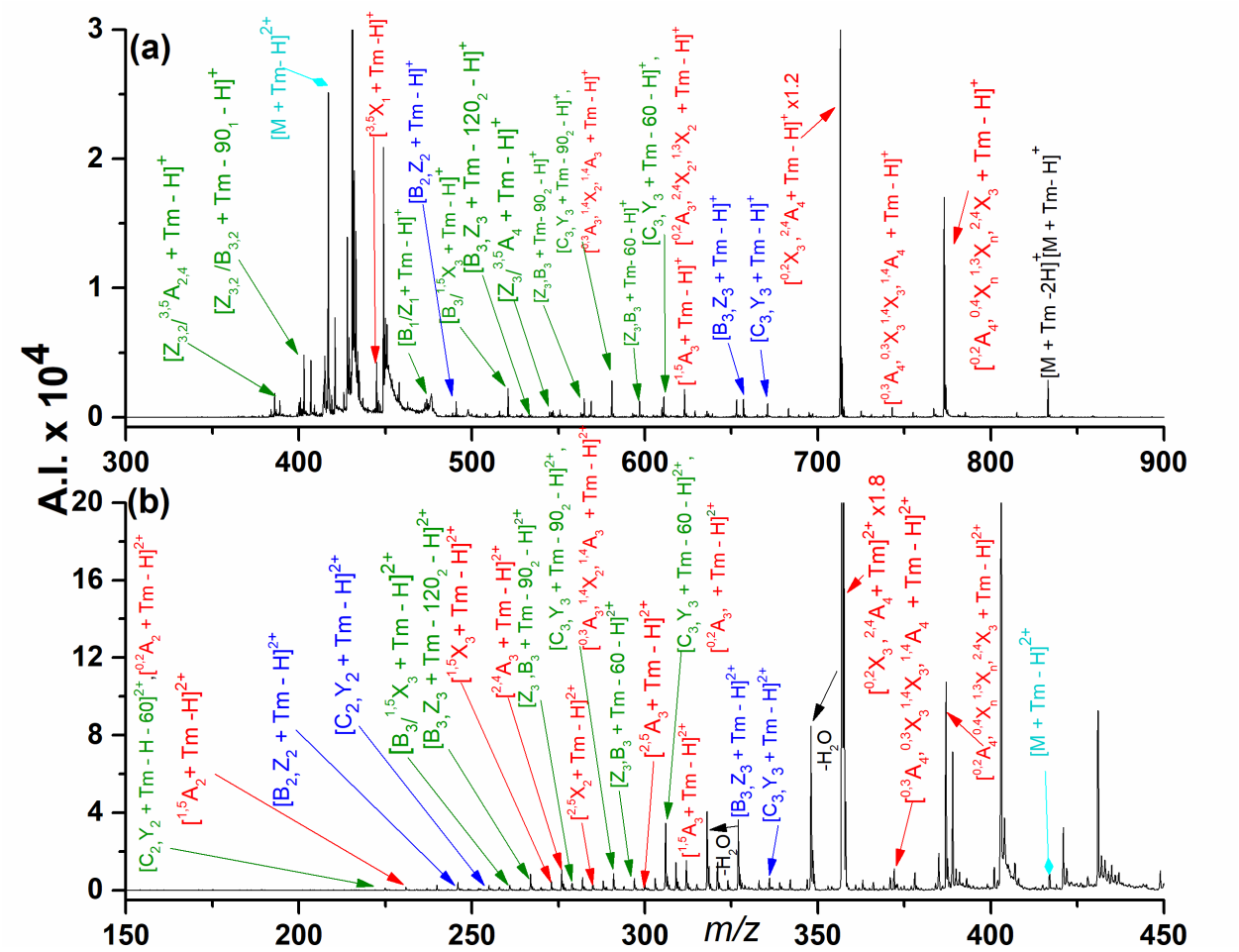

Figure 5.15 Mass spectra from (a) ETD and (b) CID of $[M + Tm - H]^{2+}$ from maltotetraose. Refer to the Figure 5.1 caption for an explanation of the color codes.

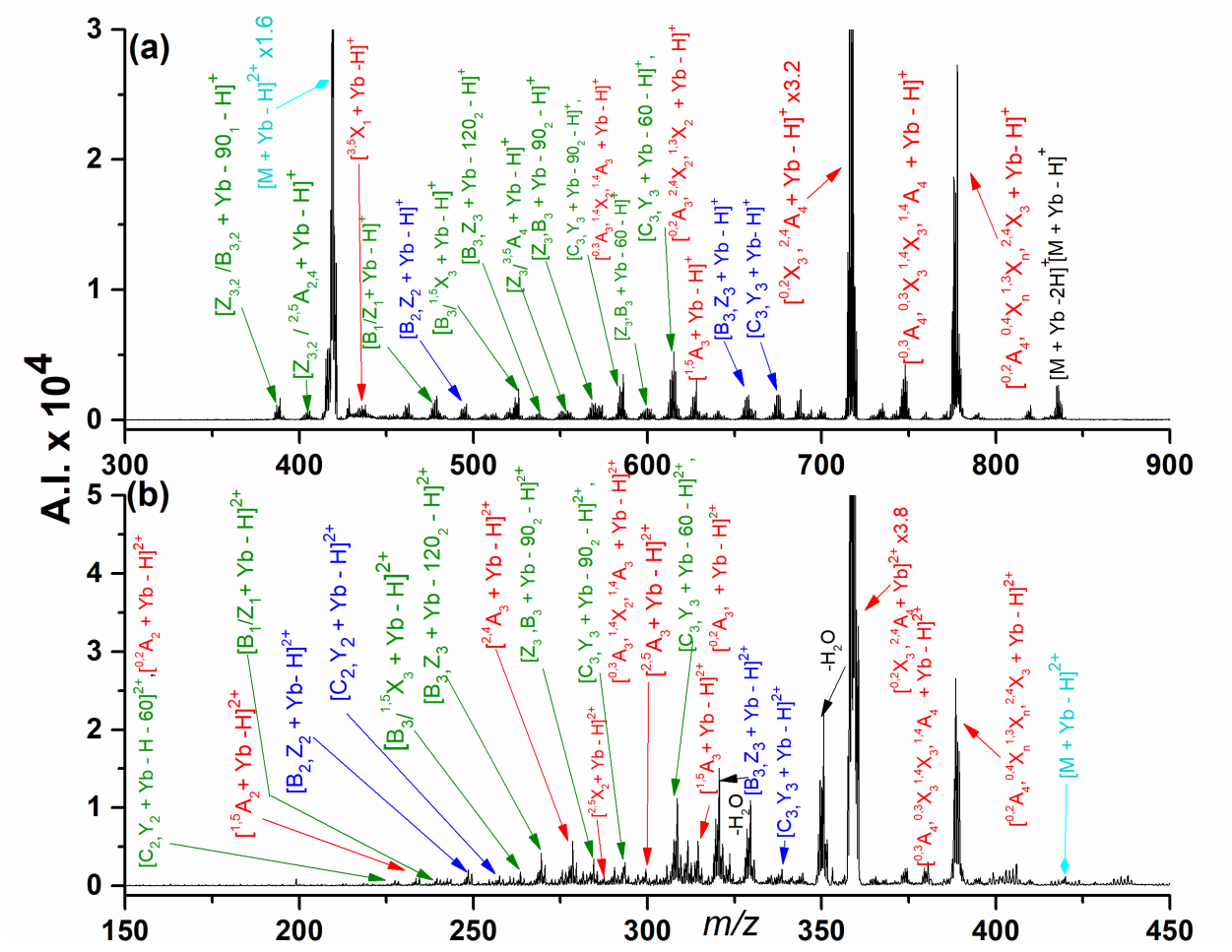
(a)
(b)
A.I. x 10^4
m/z
[M + Yb - H]2+ x1.6
[Z3,2 /B3,2 + Yb - 90_1 - H]+
[Z3,2 / 2,5A2,4 + Yb - H]+
[3,5X1 + Yb -H]+
[B1/Z1 + Yb - H]+
[B2, Z2 + Yb - H]+
[B3/ 1,5X3 + Yb - H]+
[B3, Z3 + Yb - 120_2 - H]+
[Z3/ 3,5A4 + Yb - H]+
[Z3,B3 + Yb - 90_2 - H]+
[C3, Y3 + Yb - 90_2 - H]+,
[0,3A3, 1,4X2, 1,4A3 + Yb - H]+
[Z3,B3 + Yb - 60 - H]+
[C3, Y3 + Yb - 60 - H]+,
[0,2A3, 2,4X2, 1,3X2 + Yb - H]+
[1,5A3 + Yb - H]+
[B3,Z3 + Yb - H]+
[C3, Y3 + Yb- H]+
[0,2X3, 2,4A4 + Yb - H]+ x3.2
[0,3A4, 0,3X3 1,4X3, 1,4A4 + Yb - H]+
[0,2A4, 0,4Xn 1,3Xn, 2,4X3 + Yb- H]+
[M + Yb -2H]+[M + Yb - H]+
[C2, Y2 + Yb - H - 60]2+, [0,2A2 + Yb - H]2+
[1,5A2 + Yb -H]2+
[B1/Z1 + Yb - H]2+
[B2, Z2 + Yb- H]2+
[C2, Y2 + Yb - H]2+
[B3/ 1,5X3 + Yb - H]2+
[B3, Z3 + Yb - 120_2 - H]2+
[2,4A3 + Yb - H]2+
[Z3,B3 + Yb - 90_2 - H]2+
[C3, Y3 + Yb - 90_2 - H]2+,
[2,5X2 + Yb - H]2+
[0,3A3, 1,4X2, 1,4A3 + Yb - H]2+
[2,5A3 + Yb - H]2+
[C3, Y3 + Yb - 60 - H]2+,
[1,5A3 + Yb - H]2+
[0,2A3, + Yb - H]2+
-H2O
-H2O
[B3, Z3 + Yb - H]2+
[C3, Y3 + Yb - H]2+
[0,2X3, 2,4A4 + Yb]2+ x3.8
[0,3A4, 0,3X3 1,4X3, 1,4A4 + Yb - H]2+
[0,2A4, 0,4Xn 1,3Xn, 2,4X3 + Yb - H]2+
[M + Yb - H]2+

reducing end monosaccharide, was present in the ETD spectra from both galactotetraose and maltotetraose and may be indicative of the oligosaccharide being a reducing sugar. The CID spectra for galactotetraose with La^{3+} shows an increase in fragmentation compared to Co^{2+}, similar to the increase in fragmentation with La^{3+} and maltotetraose. Every ion found in Figure 3.14(b) with Co^{2+} is also observed with La^{3+} in Figure 5.3 except for the protonated glucose product ions that include loss of water. The base peak in the CID spectra is $[C_3, Y_3 + La - H]^{2+}$, whereas the other oligosaccharides studied have cross-ring cleavages corresponding to loss of 120 Da from the precursor ion mass as the base peak; $^{0,2}X_n$ for nystose, $^{0,2}X_3$, $^{2,4}A_4$ for maltotetraose, $^{0,2}X_3$, $^{0,2}A_4$ for stachyose and $^{0,2}X_6$, $^{2,4}A_7$ for maltoheptaose. There were multiple cross-ring A and X ions and internal cleavage ions observed with La^{3+} that did not form with Co^{2+} including $^{1,5}A_2$, $B_3/^{1,5}X_3$, and $^{3,5}X_n$, which was unique to galactotetraose.

Stachyose is a non-reducing oligosaccharide made up of two galactose units and one glucose unit linked by α 1→6 glycosidic bonds, and one fructose unit with a β 1→2 glycosidic bond to the glucose. The fructose in the molecule prevents the glycan from having a reducing end. The β 1→2 glycosidic bond between the fructose and the glucose permits the monosaccharides to have more free rotation around the glycosidic oxygen, thus allowing the two rings to stack on top of one another. ETD and CID spectra of $[M + La - H]^{2+}$ can be seen in Figure 5.4 and show less fragmentation than maltotetraose and galactotetraose with both dissociation methods. The limited dissociation could be attributed to the non-reducing or stacking properties of the glycan. The ETD spectrum shows less internal cleavage ions than the other tetrasaccharides with only $[C_3, Y_3 + La - 60 - H]^2$ and $[B_1/Z_1 + La - H]^{2+}$ forming, neither of which are unique ions to stachyose. The Co^{2+} and La^{3+} adducts undergo ETD to produce different product ions; $^{1,3}X_2$, B_1/Z_1, and, $^{0,2}X_3$, $^{0,2}A_4$ are only present with the lanthanides, while

$^{0,1}A_2$, $^{3,5}A_3$, and $^{1,5}X_3$ are just a few of the product ions unique to the Co^{2+} spectrum in Figure 3.16. $[B_1, Z_1 + La - H]^{2+}$ was only observed with stachyose, and not present in any other ETD spectra in this study or in the work of Chapter 3. The increase in overall fragmentation via CID for stachyose with the lanthanides versus Co^{2+}, is smaller than for the reducing sugars in the study. The product ions in Figure 3.16(b) with Co^{2+} are also found with La^{3+} except for two cross-ring fragment ions, $^{2,5}X_3$, $^{4,5}X_3$ and the protonated glucose product ions with loss of water. There are multiple internal fragment ions and cross-ring product ions with La^{3+} that do not form with Co^{2+} including $^{1,5}A_2$, seen in the galactotetraose spectrum and $B_2/^{1,5}X_3$, and, $^{3,5}X_n$, which are unique to stachyose.

Nystose is a non-reducing sugar consisting of three flexible furanose fructose rings, and one glucose ring with both α and β 1→2 glycosidic bonds. Figure 5.6 shows ETD and CID on $[M + La - H]^{2+}$ from nystose. The ETD spectrum is dominated by internal fragment ions and has the highest intensity of electron transfer no dissociation (ETnoD) product of the glycans studied, similarly to the results seen in Figure 3.17 in Chapter 3. Occasionally an electron is transferred to a precursor ion during ETD and no dissociation occurs. This process is known as electron transfer no dissociation (ETnoD). In the Bruker HCTultra, "smart decomposition" is a process in which ETD occurs followed by resonant excitation at very low energy; this minimizes ETnoD and enhances ETD product ion formation by breaking hydrogen bonds that may hold the fragment ions together. ETD of $[M + Co]^{2+}$ produced cross-ring fragments $^{1,2}X_2$ and $^{3,5}X_n$, neither of which are observed with the trivalent lanthanide metal adducts. However, with the lanthanide metals, the cross-ring fragment ions with the same exact masses corresponding to eliminations of 60, 90, and 120 Da from the precursor ion were formed, none of which are sequence informative. Dissociation of nystose by CID produced more sequence informative

fragmentation than ETD, including cross-ring cleavage between every carbon on the monosaccharide unit, although the exact identity of the monosaccharide cannot be determined. This is indicative of the monosaccharides being linked together via only one carbon on the monosaccharide ring. The base peak in the spectrum is $[C_3, Y_3 + La - H]^{2+}$, which is unique to nystose. The number of internal fragments observed increases compared to the Figure 3.17, and there are more internal ions than with the other glycans. The internal ions can provide additional sequence information for glycans, but with nystose, it is impossible to determine which ring the cross-ring cleavage occurs on.

To investigate the effects of chain length and size on fragmentation with the trivalent lanthanide metals, maltoheptaose was studied and compared to maltotetraose. Maltoheptaose is made up of seven glucose units all linked by α 1→4 glycosidic bonds. ETD and CID of both $[M + La - H]^{2+}$ and $[M + La]^{3+}$ is used to compare the effects of precursor ion charge on dissociation. ETD of $[M + La]^{3+}$ on maltoheptaose produced both doubly and singly charged product ions; the fragmentation efficiency was lower than for any of the other ETD spectra. There is only one product ion in the ETD spectrum of $[M + La]^{3+}$ that does not appear in the ETD spectrum of $[M + La - H]^{2+}$, an internal ion, $B_6/^{3,5}X_6$. There is no glycosidic bond cleavage around the center glucose unit, as well as no cross-ring cleavage of the three middle glucose units. This is not the case in the work of Chapter 3, where fragmentation with Co^{2+} is across the entire molecule, as shown in Figures 3.18 and 3.19. The lack of fragmentation across the entire molecule is also observed with $[M + La - H]^{2+}$ as the precursor ion for ETD. However in the ETD spectrum of the doubly charged ion, there are multiple internal cleavage ions with the same exact mass that could correspond to multiple places where dissociation occurs along the molecule, such as $Z_4/^{3,5}A_7$ and $Z_5/^{3,5}A_6$. The glycosidic bond cleavage for $Z_4/^{3,5}A_7$ is around the

center glucose; however, it is impossible to differentiate between these two structural possibilities. There are more cross-ring fragment ions and internal fragment ions produced from $[M + La - H]^{2+}$ than $[M + La]^{3+}$. When the dissociation of maltoheptaose and maltotetraose via ETD are compared in Chapter 3 for Co^{2+} adducts, the types of product ions formed and efficiency of dissociation does not vary. However, with the lanthanides, there is significantly less fragmentation observed with maltoheptaose. The larger size of the glycan may allow maltoheptaose to wrap around the metal ion in a different fashion than the smaller tetrasaccharides, restricting fragmentation. The types of cross-ring cleavages and internal cleavages in the maltoheptaose spectrum can all be found in the maltotetraose spectrum except for $^{3,5}A_7$, and $Z_{4,5}/^{1,5}A_{7,6}$ from $[M + La - H]^{2+}$, but these ions do not involve fragmentation between and across all glucose units. There are also many internal and cross-ring cleavage types in the maltotetraose spectrum that do not occur with ETD of maltoheptaose.

For both $[M + La - H]^{2+}$ and $[M + La]^{3+}$, CID of is limited. Regardless of the charge on the precursor ion (2+ or 3+), the glycosidic bond fragmentation is the same. There is dissociation between every glucose unit on the glycan; however, only the loss of one glucose from either side of the molecule occurs on both sides of the oxygen in the glycosidic bond. Fragmentation of the glycosidic bonds between the other glucose units only forms B and/or Z ions, which do not contain the glycosidic oxygen. Besides the glycosidic bond fragmentation, the only other fragment ions appearing in both CID spectra are $[C_6, Y_6 + La - 60]^{2+}$ and/or $[^{0,2}A_6, {}^{1,3}X_5, {}^{2,4}X_5 + La]^{2+}$, which are exact mass ions and indistinguishable. The CID spectrum from $[M + La]^{3+}$contains two cross-ring ions across the center glucose, which does not occur with $[M + La - H]^{2+}$. The spectrum of $[M + La - H]^{2+}$ contains two sets of unique internal fragment ions with the same mass, $Z_4/^{3,5}A_7$ and $Z_5/^{3,5}A_6$, as well as $Z_5/^{3,5}A_7$ and $Z_5/^{3,5}A_6$. In addition, the

spectrum contains cross-ring product ions that correspond to loss of 60, 90, and 120 Da from the precursor ion. The types of product ions in the maltoheptaose spectrum also are seen in the CID spectrum of maltotetraose but they do not occur along all of the glucose units. The only ions from maltoheptaose that are not in the maltotetraose spectrum are produced with dissociation of $[M + La - H]^{2+}$, and are the internal ions $Z_{4,5}/^{3,5}A_{7,6}$ and $Z_{5,6}/^{3,5}A_{7,6}$. There are also many internal and cross-ring cleavages in the maltotetraose spectrum that do not occur with CID of maltoheptaose.

5.4.3 Impact of Metal Cation Properties

The lanthanide metals with even atomic numbers generally have a larger number of stable isotopes than the metals with odd atomic numbers. Consequently, the product ions in the spectra with the adducts of even atomic numbers are more difficult to identify and label due to overlapping of isotopic patterns. However, the lanthanide metals that have multiple isotopes could be useful for dissociation if the glycoconjugate being studied produces both metallated and non-metallated product ions. Ionic peaks with large isotopic composition would correspond to the metallated products, thus allowing differentiation of these two product ion types. Such isotopic analysis revealed that the product ions in this study are all metallated. In addition, the ETD product ions are all singly charged after transfer of the electron to a doubly charged precursor ion, and the CID product ions are all doubly charged. In the work of Chapter 3 and Chapter 4, CID with divalent metal cations produced both singly and doubly charged product ions.[49]

In Chapter 3, it was discussed that there are many metal properties that may influence metal ion coordination to and dissociation of the oligosaccharide.[49] The size of the metal is important for coordination to the glycan and can affect both types of dissociation.[22,23,49,68] The

ionic radii of the lanthanide metals can be seen in Table 5.1, and range from 0.1172 nm to 0.1001 nm for La^{3+} and Lu^{3+}, respectively. These values are larger than for most of the divalent metals studied in Chapter 3 except for Ca^{2+} at 0.114 nm, Na^{+} at 0.116 nm, and K^{+} at 0.152 nm. In Chapter 3, these larger metal cations did not produce the best fragmentation; however; additional factors must be considered since ionic radius does not appear to limit the dissociation with the lanthanide metal cations. With electron-based dissociation, the electron configuration of the metal and related properties such as recombination energy of the metal may affect dissociation. Recombination energy is the inverse of ionization energy (IE), which is the property found in the literature. These proposals were first made based on peptide studies, where it was observed that if capture of an electron is able to half or fully fill a d-orbital, then there is less fragmentation by electron capture dissociation (ECD).[69,70] Liu and Håkansson proposed that in electron-based dissociation of peptides with metal cations, the electron is first captured by the metal ion, and then transferred to the peptide backbone to induce fragmentation.[71] Commodore and Cassady[65] observed decreased fragmentation with Eu^{3+} in an ETD study of peptides, as did Williams and co-workers[62] with ECD of peptides. The trivalent lanthanides have an electron configuration of $[Xe]4f^{n}6s^{0}$, where n increases from 0 to 14 when moving across the series from La^{3+} to Lu^{3+}. Trivalent Eu^{3+}, therefore, has an electron configuration of $[Xe]4f^{6}$, which after the addition of one electron becomes $[Xe]4f^{7}$. This half-filled f orbital is very stable and causes a high third ionization energy (IE3) of 2400 kJ/mol. Theoretically, this high IE3 value would prevent the metal from transferring the electron to the peptide backbone, thus limiting dissociation. However, this phenomenon with Eu^{3+} is not observed with any of the oligosaccharides included in this study. As can be seen in Figure 5.10, the dissociation of maltotetraose with Eu^{3+} is essentially identical to that with the other lanthanide metals. This agrees with observations made

in Chapter 3, where metal cations with lower second IE (IE2) produced less fragmentation via ETD than metal cations with higher second IE. This supports the ECD mechanism proposed by Costello and co-workers, where dissociation is initiated by electron capture at the metal cation, which then abstracts a nearby hydroxyl group to form a carbon radical that can undergo sequential hydrogen migration and/or α-cleavages to form product ions. The pertinent portion of this mechanism can be seen in Figure 5.17.[43] In this process, an electron does not need to be transferred to the glycan and, thus, neither electron configuration nor IE will affect dissociation. This contrasts with the dissociation mechanism in ECD and ETD for peptides, where Liu and Håkansson[71] proposed that the electron is first captured at the metal ion and then transferred to the peptide backbone to induce fragmentation.

Dissociation via ETD on $[M + Met - H]^{2+}$ for the oligosaccharides investigated is extremely efficient, often with complete precursor loss to generate product ions. Dissociation with lanthanide metal adducts is much more efficient than with the metals studied in Chapter 3. The "smart decomposition" feature of the HCTultra quadrupole ion trap (QIT) was used during ETD experiments to further dissociate any charged reduced or ETnoD products. Smart decomposition uses resonant excitation to overcome attractive forces (e.g., hydrogen bonding) that may hold glycan fragments together following ETD. The effects of the smart decomposition feature can be seen in Figures 5.18 and 5.19, where ETD of $[M + Pr - H]^{2+}$ with and without smart decomposition is shown for nystose and maltoheptaose, respectively. The two spectra in each figure are on the same scale, and it can be seen that smart decomposition decreases the intensity of the precursor ion and the ETnoD charge reduced product ion, while increasing the intensity of all fragment ions. Smart decomposition decreases the intensity of the ETnoD product by a factor of 6.7 in Figure 5.18, and in Figure 5.19, by a factor of 140. In both figures,

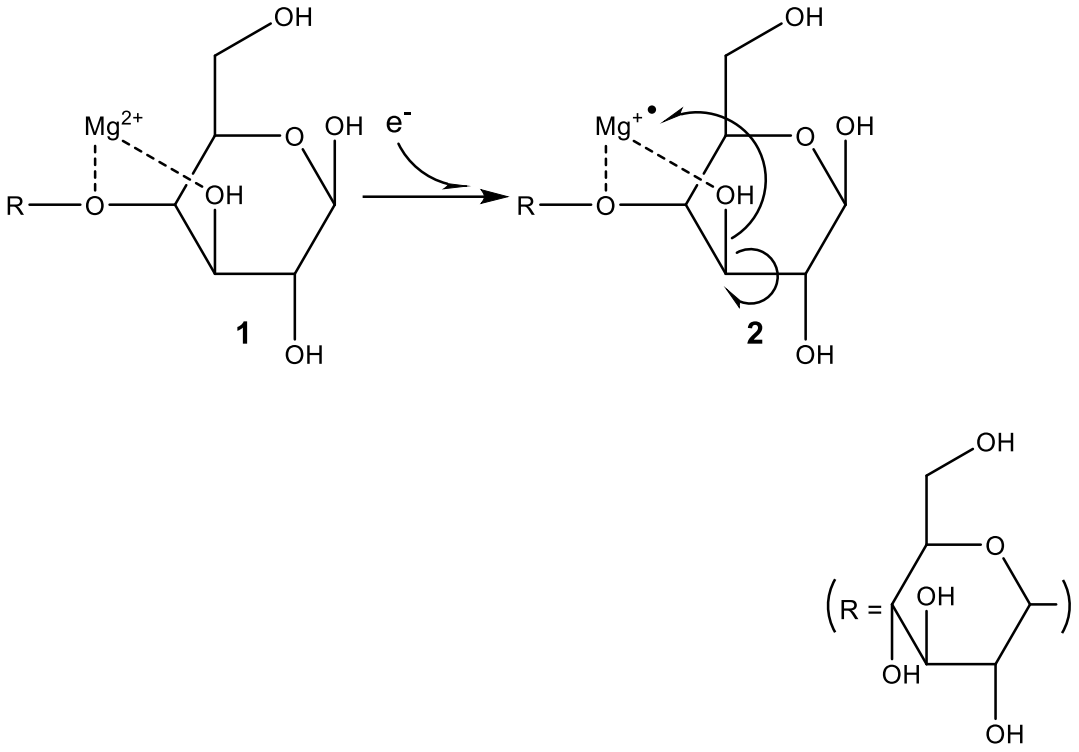

Figure 5.16 Mechanism for hydroxyl abstraction by the adducted metal cation during ECD/ETD of glycans. Adapted from reference 43.

there is an increase in ion intensity for all product ion times, most notably for the glycosidic bond fragment $[C_3, Y_3 + Pr - H]^{2+}$ from nystose, which is a factor of 23 higher. should not produce n new fragmentation, as the energy introduced is not high enough do break covalent bonds. Smart decomposition should not produce new fragmentation should not produce new fragmentation, as the energy introduced is not high enough do break covalent bonds.

5.5 Conclusions

Trivalent lanthanide metal cations readily adduct to underivatized tetrasaccharides to form $[M + Met - H]^{2+}$, $[M + Met + NO_3]^{2+}$, and $[M + Met - 2H]^{+}$ via ESI. Additionally, $[M + Met]^{3+}$ is formed for maltoheptaose. The charge density on the metal cation is postulated to affect the precursor ion formed. This is the first study to demonstrate that multiply charged ions can be formed via ESI with glycans and trivalent metal cations. The spectra produced upon dissociation by both ETD and CID on these complexes did not vary based on the lanthanide metal used. Unlike the work discussed in Chapter 3 involving univalent alkali, divalent alkaline earth, divalent and trivalent transition metal ions, and a group 13/boron group trivalent metal ion, for lanthanum adducts, the increase in chain length of the oligosaccharide affects fragmentation. Also, the dissociation of doubly or triply charged precursor ions of maltoheptaose with ETD or CID was minimal. This contrasted previous peptide studies (including one by Commodore and Cassady[65]) showing that europium, Eu^{3+}, was not useful for electron-based due to its tendency to retain the electron. This phenomenon does not occur for ETD of the oligosaccharides adducted with Eu^{3+}. This supports the ECD mechanism proposed by Costello and co-workers, where after electron capture, the metal cation abstracts a hydroxyl group, initiating fragmentation.[43] In this process, an electron does not need to be transferred to the glycan, and thus neither electron configuration or IE will affect dissociation. A significant overall conclusion from this research is

that the IE of the metal is important to the ability of the metal ion to adduct to glycans but is unimportant to the glycan fragmentation induced by ETD.

The ETD and CID spectra were complementary and together can provide the most sequence information for glycans. Dissociation with trivalent lanthanide metal adducts produces a higher number and variety of fragment ions than Co^{2+} for the tetrasaccharides with both dissociation methods, but also increases the difficulty of spectral interpretation. Further investigation of the lanthanide metal cations with larger glycans may allow a better understanding of the reasons for the poor fragmentation with maltoheptaose. Cationization of the tetrasaccharides in this study with trivalent lanthanide metals produces structurally informative dissociation and appears to be a promising tool for glycan analysis, at least for relatively short chain length glycans.

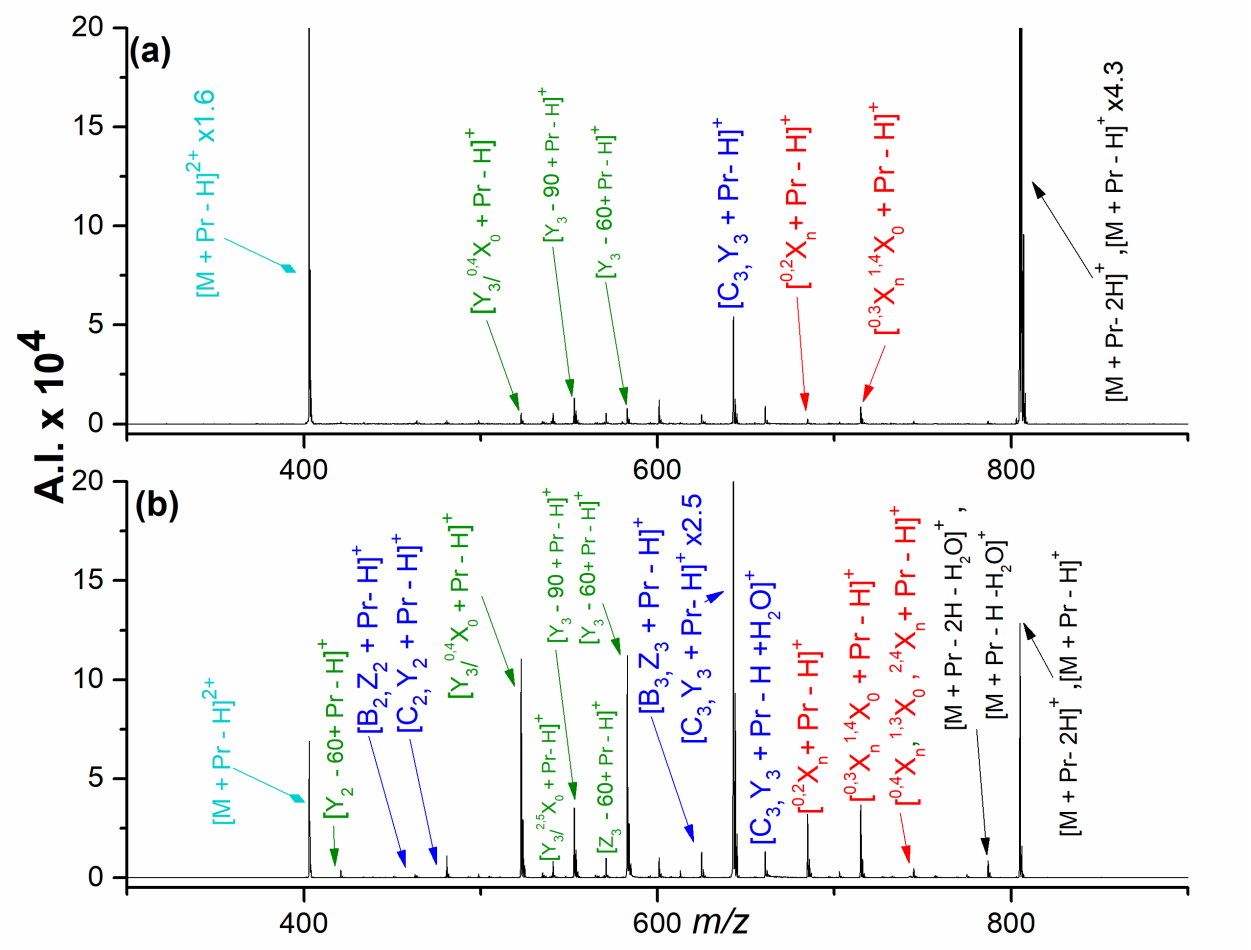

Figure 5.17 Mass Spectra from ETD of $[M + Pr - H]^{2+}$ from nystose (a) without and (b) with smart decomposition. Refer to the Figure 5.1 caption for an explanation of the color codes.

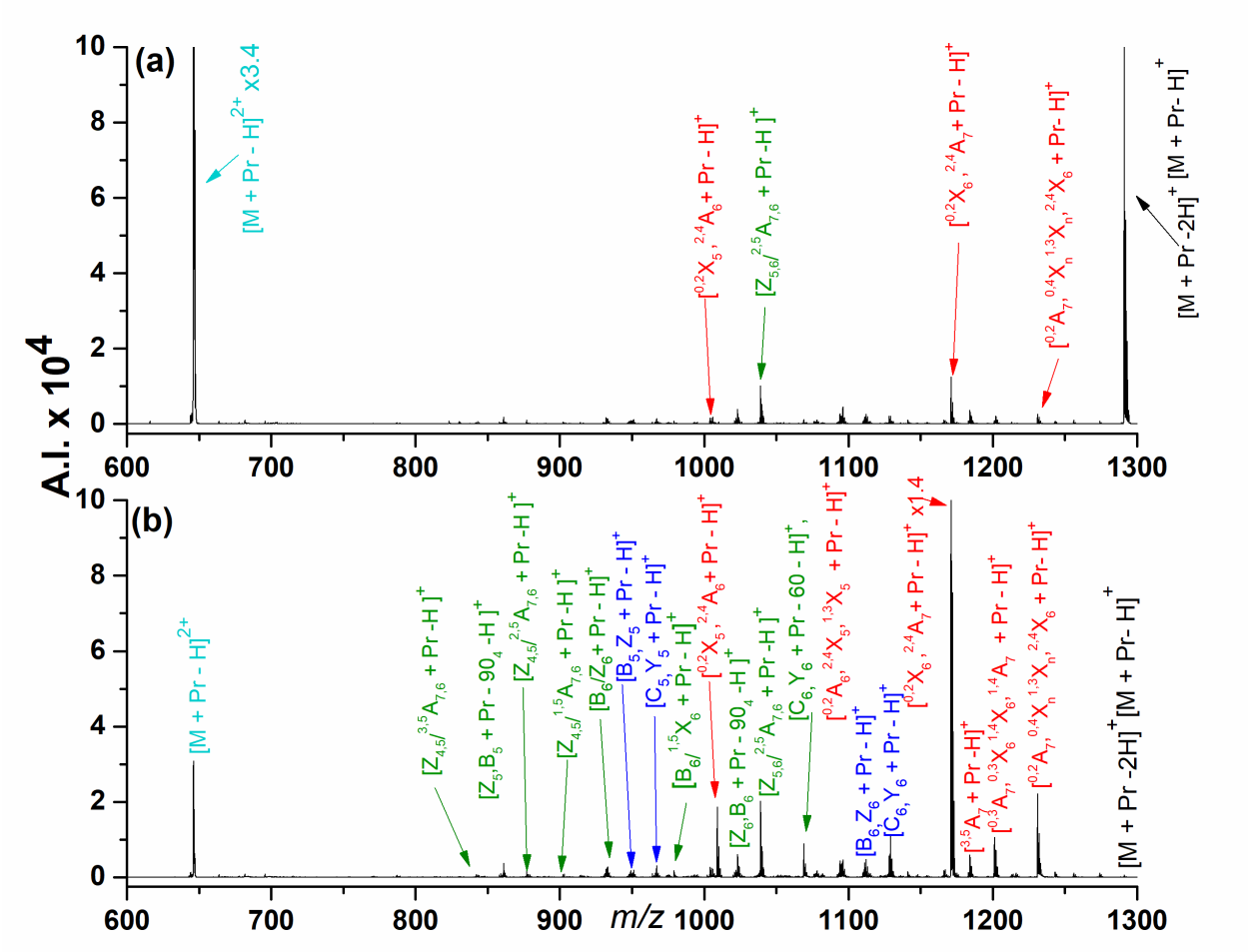

Figure 5.18 Mass Spectra from ETD of $[M + Pr - H]^{2+}$ from maltoheptaose (a) without and (b) with smart decomposition. Refer to the Figure 5.1 caption for an explanation of the color codes.

REFERENCES

1. Varki, A. Biological roles of glycans. *Glycobiology* **2017**, *27*, 3-49.

2. Varki, A.; Cummings, R. D.; Esko, J. D.; Aebi, M.; Darvill, A.; Hart, G. W.; Stanley, P. *Essentials of Glycobiology;* Cold Spring Harbor Laboratory Press: New York, 2015.

3. Cummings, R.D.; Pierce, J.M. The challenge and promise of glycomics. *Chemistry & Biology* **2014**, *21*, 1-15.

4. National Research Council (US) Committee on Assessing the Importance and Impact of Glycomics and Glycosciences *Transforming Glycoscience: A Roadmap for the Future;* National Academy of Sciences: Washington (DC), 2012.

5. Gray, C. J.; Migas, L. G.; Barran, P. E.; Pagel, K.; Seeberger, P. H.; Eyers, C. E.; Boons, G.; Pohl, N. L. B.; Compagnon, I.; Widmalm, G.; Flitsch, S. L. Advancing solutions to the carbohydrate sequencing challenge. *J. Am. Chem. Soc.* **2019**, *141*, 14463-14479.

6. Laine, R. A. A calculation of all possible oligosaccharide isomers both branched and linear yields 1.05 x 10(12) structures for a reducing hexasaccharide - the isomer-barrier to development of single-method saccharide sequencing or synthesis systems. *Glycobiology* **1994**, *4*, 759-767.

7. Fenn, J. B.; Mann, M.; Meng, C. K.; Wong, S. F.; Whitehouse, C. M. Electrospray ionization for mass spectrometry of large biomolecules. *Science* **1989**, *246*, 64-71.

8. Fenn, J. B.; Mann, M.; Meng, C. K.; Wong, S. F. Electrospray ionization--principles and practice. *Mass Spectrom. Rev.* **1990**, *9*, 37-70.

9. Hop, C E C A; Bakhtiar, R. An introduction to electrospray ionization and matrix-assisted laser desorption/ionization mass spectrometry: Essential tools in a modern biotechnology environment. *Biospectroscopy* **1997**, *3530*, 259-280.

10. Zaia, J. Mass spectrometry and glycomics. *OMICS* **2010**, *14*, 401-418.

11. Zaia, J. Mass spectrometry of oligosaccharides. *Mass Spectrom. Rev.* **2004**, *23*, 161-227.

12. York, W. S.; Agravat, S.; Aoki-Kinoshita, K. F.; McBride, R.; Campbell, M. P.; Costello, C. E.; Dell, A.; Feizi, T.; Haslam, S. M.; Karlsson, N.; Khoo, K.; Kolarich, D.; Liu, Y.; Novotny, M.; Packer, N. H.; Paulson, J. C.; Rapp, E.; Ranzinger, R.; Rudd, P. M.; Smith, D. F.; Struwe, W. B.; Tiemeyer, M.; Wells, L.; Zaia, J.; Kettner, C. MIRAGE: The minimum information required for a glycomics experiment. *Glycobiology* **2014**, *24*, 402-406.

13. Kailemia, M. J.; Ruhaak, L. R.; Lebrilla, C. B.; Amster, I. J. Oligosaccharide analysis by mass spectrometry: A review of recent developments. *Anal. Chem.* **2014**, *86*, 196-212.

14. Rabus, J. M.; Abutokaikah, M. T.; Ross, R. T.; Bythell, B. J. Sodium-cationized carbohydrate gas-phase fragmentation chemistry: Influence of glycosidic linkage position. *Phys. Chem. Chem. Phys.* **2017**, *19*, 25643-25652.

15. Campbell, M. T.; Chen, D.; Glish, G. L. Distinguishing linkage position and anomeric configuration of Glucose–Glucose disaccharides by water adduction to lithiated molecules. *Anal. Chem.* **2018**, *90*, 2048-2054.

16. Zhao, C.; Xie, B.; Chan, S.; Costello, C. E.; O'Connor, P. B. Collisionally activated dissociation and electron capture dissociation provide complementary structural information for branched permethylated oligosaccharides. *J. Am. Soc. Mass Spectrom.* **2008**, *19*, 138-150.

17. Harvey, D. J. Collision-induced fragmentation of underivatized N-linked carbohydrates ionized by electrospray. *J. Mass Spectrom.* **2000**, *35*, 1178-1190.

18. Lemoine, J.; Fournet, B.; Despeyroux, D.; Jennings, K. R.; Rosenberg, R.; De Hoffman, E. Collision-induced dissociation of alkali metal cationized and permethylated oligosaccharides: Influence of the collision energy and of the collision gas for the assignment of linkage position. *J. Am. Soc. Mass Spectrom.* **1993**, *4*, 197-203.

19. Lemoine, J.; Strecker, G.; Leroy, Y.; Fournet, B.; Ricart, G. Collisional-activation tandem mass spectrometry of sodium adduct ions of methylated oligosaccharides: Sequence analysis and discrimination between α-NeuAc-(2→3) and α-NeuAc-(2→6) linkages. *Carbohydr. Res.* **1991**, *221*, 209-217.

20. Zaia, J.; Miller, M. J. C.; Seymour, J. L.; Costello, C. E. The role of mobile protons in negative ion CID of oligosaccharides. *J. Am. Soc. Mass Spectrom.* **2007**, *18*, 952-960.

21. Dallinga, J. W.; Heerma, W. Positive ion fast atom bombardment mass spectrometry of some small oligosaccharides. *Biol. Mass Spectrom.* **1991**, *20*, 99-108.

22. Bythell, B. J.; Abutokaikah, M. T.; Wagoner, A. R.; Guan, S.; Rabus, J. M. Cationized carbohydrate gas-phase fragmentation chemistry. *J. Am. Soc. Mass Spectrom.* **2017**, *28*, 688-703.

23. Fura, A.; Leary, J. A. Differentiation of Ca^{2+}-coordinated and Mg^{2+}-coordinated branched trisaccharide isomers: An electrospray ionization and tandem mass spectrometry study. *Anal. Chem.* **1993**, *65*, 2805-2811.

24. Adamson, J. T.; Håkansson, K. Electron capture dissociation of oligosaccharides ionized with alkali, alkaline earth, and transition metals. *Anal. Chem.* **2007**, *79*, 2901-2910.

25. Adamson, J. T.; Håkansson, K. Electron detachment dissociation of neutral and sialylated oligosaccharides. *J. Am. Soc. Mass Spectrom.* **2007**, *18*, 2162-2172.

26. Adamson, J. T.; Håkansson, K. Infrared multiphoton dissociation and electron capture dissociation of high-mannose type glycopeptides. *J. Proteome Res.* **2006**, *5*, 493-501.

27. Wolff, J. J.; Laremore, T. N.; Leach, F. E.,III; Linhardt, R. J.; Amster, I. J. Electron capture dissociation, electron detachment dissociation and infrared multiphoton dissociation of sucrose octasulfate. *Eur. J. Mass Spectrom.* **2009**, *15*, 275-281.

28. Leach, F. E.,III; Xiao, Z.; Laremore, T. N.; Linhardt, R. J.; Amster, I. J. Electron detachment dissociation and infrared multiphoton dissociation of heparin tetrasaccharides. *Int. J. Mass Spectrom.* **2011**, *308*, 253-259.

29. Xie, Y. M.; Lebrilla, C. B. Infrared multiphoton dissociation of alkali metal-coordinated oligosaccharides. *Anal. Chem.* **2003**, *75*, 1590-1598.

30. Zhang, J. H.; Schubothe, K.; Li, B. S.; Russell, S.; Lebrilla, C. B. Infrared multiphoton dissociation of O-linked mucin-type oligosaccharides. *Anal. Chem.* **2005**, *77*, 208-214.

31. Morrison, K. A.; Clowers, B. H. Differential fragmentation of mobility-selected glycans via ultraviolet photodissociation and ion mobility-mass spectrometry. *J. Am. Soc. Mass Spectrom.* **2017**, *28*, 1236-1241.

32. Ko, B. J.; Brodbelt, J. S. 193 nm ultraviolet photodissociation of deprotonated sialylated oligosaccharides. *Anal. Chem.* **2011**, *83*, 8192-8200.

33. Klein, D. R.; Holden, D. D.; Brodbelt, J. S. Shotgun analysis of rough-type lipopolysaccharides using ultraviolet photodissociation mass spectrometry. *Anal. Chem.* **2016**, *88*, 1044-1051.

34. O'Brien, J. P.; Brodbelt, J. S. Structural characterization of gangliosides and glycolipids via ultraviolet photodissociation mass spectrometry. *Anal. Chem.* **2013**, *85*, 10399-10407.

35. Ko, B. J.; Brodbelt, J. S. Ultraviolet photodissociation of chromophore-labeled oligosaccharides via reductive amination and hydrazide conjugation. *J. Mass Spectrom.* **2011**, *46*, 359-366.

36. Brodbelt, J. S. Photodissociation mass spectrometry: New tools for characterization of biological molecules. *Chem. Soc. Rev.* **2014**, *43*, 2757-2783.

37. Wolff, J. J.; Chi, L.; Linhardt, R. J.; Amster, I. J. Distinguishing glucuronic from iduronic acid in glycosaminoglycan tetrasaccharides by using electron detachment dissociation. *Anal. Chem.* **2007**, *79*, 2015-2022.

38. Wolff, J. J.; Laremore, T. N.; Busch, A. M.; Linhardt, R. J.; Amster, I. J. Electron detachment dissociation of dermatan sulfate oligosaccharides. *J. Am. Soc. Mass Spectrom.* **2008**, *19*, 294-304.

39. Wolff, J. J.; Amster, I. J.; Chi, L.; Linhardt, R. J. Electron detachment dissociation of glycosaminoglycan tetrasaccharides. *J. Am. Soc. Mass Spectrom.* **2007**, *18*, 234-244.

40. Wolff, J. J.; Laremore, T. N.; Aslam, H.; Linhardt, R. J.; Amster, I. J. Electron-induced dissociation of glycosaminoglycan tetrasaccharides. *J. Am. Soc. Mass Spectrom.* **2008**, *19*, 1449-1458.

41. Kornacki, J. R.; Adamson, J. T.; Håkansson, K. Electron detachment dissociation of underivatized chloride-adducted oligosaccharides. *J. Am. Soc. Mass Spectrom.* **2012**, *23*, 2031-2042.

42. Yu, X.; Huang, Y.; Lin, C.; Costello, C. E. Energy-dependent electron activated dissociation of metal-adducted permethylated oligosaccharides. *Anal. Chem.* **2012**, *84*, 7487-7494.

43. Huang, Y.; Pu, Y.; Yu, X.; Costello, C. E.; Lin, C. Mechanistic study on electron capture dissociation of the oligosaccharide-Mg^{2+} complex. *J. Am. Soc. Mass Spectrom.* **2014**, *25*, 1451-1460.

44. Han, L.; Costello, C. E. Electron transfer dissociation of milk oligosaccharides. *J. Am. Soc. Mass Spectrom.* **2011**, *22*, 997-1013.

45. Darula, Z.; Medzihradszky, K. F. Glycan side reaction may compromise ETD-based glycopeptide identification. *J. Am. Soc. Mass Spectrom.* **2014**, *25*, 977-987.

46. Yang, J.; Mo, J. J.; Adamson, J. T.; Håkansson, K. Characterization of oligodeoxynucleotides by electron detachment dissociation Fourier transform ion cyclotron resonance mass spectrometry. *Anal. Chem.* **2005**, *77*, 1876-1882.

47. Budnik, B. A.; Haselmann, K. F.; Elkin, Y. N.; Gorbach, V. I.; Zubarev, R. A. Applications of electron-ion dissociation reactions for analysis of polycationic chitooligosaccharides in Fourier transform mass spectrometry. *Anal. Chem.* **2003**, *75*, 5994-6001.

48. Hersberger, K. E.; Håkansson, K. Characterization of *O*-sulfopeptides by negative ion mode tandem mass spectrometry: Superior performance of negative ion electron capture dissociation. *Anal. Chem.* **2012**, *84*, 6370-6377.

49. Schaller-Duke, R. M.; Bogala, M. R.; Cassady, C. J. Collision-induced dissociation and electron transfer dissociation of metal-adducted oligosaccharides. *J. Am. Soc. Mass Spectrom.* **2018**, *29*.

50. Cancilla, M. T.; Penn, S. G.; Carroll, J. A.; Lebrilla, C. B. Coordination of alkali metals to oligosaccharides dictates fragmentation behavior in matrix assisted laser desorption ionization/Fourier transform mass spectrometry. *J. Am. Chem. Soc.* **1996**, *118*, 6736-6745.

51. Penn, S. G.; Cancilla, M. T.; Lebrilla, C. B. Fragmentation behavior of multiple-metal-coordinated acidic oligosaccharides studied by matrix-assisted laser desorption ionization Fourier transform mass spectrometry. *Int. J. Mass Spectrom.* **2000**, *195*, 259-269.

52. Håkansson, K.; Cooper, H. J.; Emmett, M. R.; Costello, C. E.; Marshall, A. G.; Nilsson, C. L. Electron capture dissociation and infrared multiphoton dissociation MS/MS of an N-glycosylated tryptic peptide to yield complementary sequence information. *Anal. Chem.* **2001**, *73*, 4530-4536.

53. Orlando, R.; Bush, C. A.; Fenselau, C. Structural-analysis of oligosaccharides by tandem mass-spectrometry - collisional activation of sodium adduct ions. *Biomed Environ Mass Spectrometry* **1990**, *19*, 747-754.

54. Harvey, D. J. Ionization and collision-induced fragmentation of N-linked and related carbohydrates using divalent cations. *J. Am. Soc. Mass Spectrom.* **2001**, *12*, 926-937.

55. Asam, M. R.; Glish, G. L. Tandem mass spectrometry of alkali cationized polysaccharides in a quadrupole ion trap. *J. Am. Soc. Mass Spectrom.* **1997**, *8*, 987-995.

56. Konig, S.; Leary, J. A. Evidence for linkage position determination in cobalt coordinated pentasaccharides using ion trap mass spectrometry. *J. Am. Soc. Mass Spectrom.* **1998**, *9*, 1125-1134.

57. Zhou, Z. R.; Ogden, S.; Leary, J. A. Linkage position determination in oligosaccharides: MS/MS study of lithium-cationized carbohydrates. *J. Org. Chem.* **1990**, *55*, 5444-5446.

58. Huang, Y.; Dodds, E. D. Discrimination of isomeric carbohydrates as the electron transfer products of group II cation adducts by ion mobility spectrometry and tandem mass spectrometry. *Anal. Chem.* **2015**, *87*, 5664-5668.

59. Huang, Y.; Dodds, E. D. Ion-neutral collisional cross sections of carbohydrate isomers as divalent cation adducts and their electron transfer products. *Analyst* **2015**, *14*, 6912-6921.

60. Morrison, K. A.; Bendiak, B. K.; Clowers, B. H. Assessment of dimeric metal-glycan adducts via isotopic labeling and ion mobility-mass spectrometry. *J. Am. Soc. Mass Spectrom.* **2018**, *29*, 1638-1649.

61. Gyurcsik, B.; Nagy, L. Carbohydrates as ligands: Coordination equilibria and structure of the metal complexes. *Coord.Chem. Rev.s* **2000**, *203*, 81-149.

62. Flick, T. G.; Donald, W. A.; Williams, E. R. Electron capture dissociation of trivalent metal ion-peptide complexes. *J. Am. Soc. Mass Spectrom.* **2013**, *24*, 193-201.

63. Shvartsburg, A. A.; Jones, R. C. Attachment of metal trications to peptides. *J. Am. Soc. Mass Spectrom.* **2004**, *15*, 406-408.

64. Commodore, J. J.; Cassady, C. J. Effects of acidic peptide size and sequence on trivalent praseodymium adduction and electron transfer dissociation mass spectrometry. *J. Mass Spectrom.* **2017**, *52*, 218-229.

65. Commodore, J. J.; Cassady, C. J. The effects of trivalent lanthanide cationization on the electron transfer dissociation of acidic fibrinopeptide B and its analogs. *J. Am. Soc. Mass Spectrom.* **2016**, *27*, 1499-1509.

66. Domon, B.; Costello, C. E. A systematic nomenclature for carbohydrate fragmentations in fab-ms ms spectra of glycoconjugates. *Glycoconj. J.* **1988**, *5*, 397-409.

67. Nieboer, E.; Richardson, D. H. S. The replacement of the nondescript term 'heavy metals' by a biologically and chemically significant classification of metal ions. *Environ Pollut B* **1980**, *1*, 3-26.

68. Harvey, D. J.; Naven, T. J. P.; Küster, B.; Bateman, R. H.; Green, M. R.; Critchley, G. Comparison of fragmentation modes for the structural determination of complex oligosaccharides ionized by matrix-assisted laser desorption/ionization mass spectrometry. *Rapid Commun. Mass Spectrom.* **1995**, *9*, 1556-1561.

69. Kleinnijenhuis, A. J.; Mihalca, R.; Heeren, R. M. A.; Heck, A. J. R. Atypical behavior in the electron capture induced dissociation of biologically relevant transition metal ion complexes of the peptide hormone oxytocin. *Int. J. Mass Spectrom.* **2006**, *253*, 217-224.

70. Chen, X.; Fung, Y. M. E.; Chan, W. Y. K.; Wong, P. S.; Yeung, H. S.; Chan, T. W. D. Transition metal ions: Charge carriers that mediate the electron capture dissociation pathways of peptides. *J. Am. Soc. Mass Spectrom.* **2011**, *22*, 2232-2245.

71. Liu, H.; Håkansson, K. Divalent metal ion-peptide interactions probed by electron capture dissociation of trications. *J. Am. Soc. Mass Spectrom.* **2006**, *17*, 1731-1741.

CHAPTER 6: CONCLUDING REMARKS

The field of glycomics has been expanding at a rapid pace due to an increased understanding of the connections between glycoconjugates and disease states. However, the analysis of glycans and glycoconjugates has been particularly challenging due to the high structural complexity of these biological molecules. Fundamental studies into the dissociation of glycans and the development of methods to improve oligosaccharide sequencing are essential.

As described in the previous chapters, this dissertation explores the potential of electron transfer dissociation (ETD) and collision-induced dissociation (CID) as techniques for the characterization of glycans. The work herein has prompted many questions while also making ample contributions to the field of glycomics.

In Chapter 3, the ionization and cationization of the glycans with univalent alkali, divalent alkaline earth, divalent and trivalent transition metal ions, and a group13/boron group trivalent metal ion was found to produce $[M + Met]^+$, $[M + 2Met]^{2+}$, $[M + Met]^{2+}$, $[M + Met - H]^+$, and $[M + Met - 2H]^+$ most intensely along with low intensity nitrate adducts depending on the metal and sugar ionized. Surprisingly the trivalent metal cations did not produce multiply charged ions sufficient for ETD. The identity of the metal ion affected fragmentation by both techniques due to ionic radius, ionization energy (IE), and electron configuration of the metal used for adduction. Product ion type and intensities also varied based on the structure of the glycan. The ETD and CID spectra were complementary and can be used together to gain the most sequence information. For both dissociation techniques and all glycans studied, $[M + Co]^{2+}$ produced the most uniform structurally informative dissociation.

Chapter 4 expanded this research to the comparison of glycans with and without permethylation, a common derivatization technique. To date, this is the only work that directly compares the effects of derivatization to non-derivatization using tandem mass spectrometry (MS/MS). Again, for both dissociation techniques and all glycans studied, $[M + Co]^{2+}$ produced the most uniform structurally informative dissociation with and without derivatization. Permethylation reduced the production of fragment ions with both ETD and CID and reduced the structural information obtained by the dissociation. However, some of the exact mass ions in the non-derivatized spectra were able to be differentiated upon permethylation. The cross-ring cleavage product ion types found in the spectra of the permethylated and non-permethylated spectra varied in type and location with both dissociation methods. This implies that permethylation may affect the binding of the metal cation to the glycan or the mechanism of dissociation. As a future project, this effect could be probed by study of a series of smaller glycans (such as trisaccharides), varying them by only one glycosidic bond linkage location or monosaccharide type.

In Chapter 5 the experiments in Chapters 3 and 4 were expanded to use the trivalent lanthanide metal series. All lanthanide metals from lanthanum (La^{3+}) to lutetium (Lu^{3+}) excluding radioactive promethium (Pm^{3+}) were included in the study. Unlike the trivalent metals in Chapter 3, which were unable to produce multiply charged adduct ions, ESI on mixtures of the tetrasaccharides and the lanthanide metal cations generated $[M + Met - H]^{2+}$, $[M + Met + NO_3]^{2+}$, and $[M + Met - 2H]^{+}$, where M is the oligosaccharide and Met is the metal cation. For the larger heptasaccharide, both $[M + Met - H]^{2+}$ and $[M + Met]^{3+}$ were formed. The dissociation of these complexes by both techniques did not vary based on the lanthanide metal used, and the fragment ions produced were identical for each metal along the lanthanide series,

with occasional variations in ion intensities. Unlike previous peptide studies, including one by Commodore and Cassady[1] showing that europium (Eu^{3+}) was not useful for electron-based studies due to its tendency to retain the electron, this was not a problem for ETD of the oligosaccharides adducted with Eu^{3+}. ETD and CID of the lanthanide metal complexes produced significant fragmentation useful for sequence analysis. The lanthanide metal adducts induce more cross-ring and internal fragment ions than are observed in the work of Chapter 3.

Metallated glycan spectra are much more complex than protonated spectra. Additional work such as a systematic study of di- and trisaccharides consisting of only one type of monosaccharide with varying glycosidic bond linkage, along with theoretical modeling is needed to develop bioinformatics tools for spectral interpretation. These tools will allow for a better understanding of metallated ETD and CID behaviors and mechanisms with and without derivatization. It would also be important to expand the studies to metallated glycopeptides, glycosaminoglycans, and amide derivatized monosaccharides. The studies in this dissertation on "native" oligosaccharides is important for understanding the fundamentals of how the metal cations affect the dissociation of these biological molecules, but most of the glycans in the human body are glycoconjugates. The ability to apply these techniques to glycopeptides and sulfonated, sialylated, and phosphorylated glycoconjugates along with libraries of spectra or software that assist in interpreting the data, will be key in applying these methods to biological samples.

Investigation of the dissociation techniques and metallation of these glycoconjugates in the negative ion mode could possibly give another method to provide diagnostic fragmentation and structural analysis of glycans. Negative ion mode is less thoroughly studied with electron-based techniques[2-4] and more current software and automated techniques are based on

positive ion mode MS/MS. However, glycans are made up of many hydroxyl groups, which can easily form oxyanions in the negative ion mode, and can have acidic modifications such as phosphorylation, sialylation, and sulfonation. These molecules lend themselves well to being studied in the negative ion mode. A previous study by Jiang and Cole[5] showed that chloride, fluoride, and acetate adducts on glycans can produce structurally informative fragmentation with CID, and these adducts could be utilized to expand negative ion mode electron-based studies.

Coupling any of the techniques discussed in this dissertation with ion mobility spectrometry (IMS) may give another route for differentiating the exact mass/isobaric ions both before and after dissociation by observing changes in ion shape. IMS is a technique that can probe the structural conformations of gas-phase ions, and has been used to separate isomeric protonated and sodiated N-linked and O-linked glycans formed by ESI.[6,7] Metal adducts have been utilized in some IMS studies to explore the effects of metal ion radius and electron transfer on the collisional cross sections (CCS) in investigations of glycans.[8,9] Using metal adduction on glycans and glycoconjugates, IMS can be utilized as a separation technique for mixtures of isomeric samples. In future experiments, use of IMS after dissociation by CID and/or ETD, could allow the exact mass/isobaric fragment ions to be distinguished based on their gas-phase conformations. Stereoisomeric glycans have been found to form diastereomeric coordination complexes in the presence of metal cations.[10-12] This means that stereochemical differences in the glycans are translated into differences in the complexes that are formed with metal adduction. These metal complexes may then differ in physical properties, and would have different CCS values, allowing for differentiation of the isomers. Combining IMS studies of the same samples before and after dissociation may give information on the fragmentation pathways that produce certain types of ions, and may allow differentiation of isomeric precursor ions.

REFERENCES

1. Commodore, J. J.; Cassady, C. J. The effects of trivalent lanthanide cationization on the electron transfer dissociation of acidic fibrinopeptide B and its analogs. *J. Am. Soc. Mass Spectrom.* **2016**, *27*, 1499-1509.

2. McFarland, M. A.; Marshall, A. G.; Hendrickson, C. L.; Nilsson, C. L.; Fredman, P.; Månsson, J. Structural characterization of the GM1 ganglioside by infrared multiphoton dissociation, electron capture dissociation, and electron detachment dissociation electrospray ionization FT-ICR MS/MS. *J. Am. Soc. Mass Spectrom.* **2005**, *16*, 752-762.

3. Wolff, J. J.; Amster, I. J.; Chi, L.; Linhardt, R. J. Electron detachment dissociation of glycosaminoglycan tetrasaccharides. *J. Am. Soc. Mass Spectrom.* **2007**, *18*, 234-244.

4. Wolff, J. J.; Chi, L.; Linhardt, R. J.; Amster, I. J. Distinguishing glucuronic from iduronic acid in glycosaminoglycan tetrasaccharides by using electron detachment dissociation. *Anal. Chem.* **2007**, *79*, 2015-2022.

5. Jiang, Y.; Cole, R. B. Oligosaccharide analysis using anion attachment in negative mode electrospray mass spectrometry. *J. Am. Soc. Mass Spectrom.* **2005**, *16*, 60-70.

6. Williams, J. P.; Grabenauer, M.; Holland, R. J.; Carpenter, C. J.; Wormald, M. R.; Giles, K.; Harvey, D. J.; Bateman, R. H.; Scrivens, J. H.; Bowers, M. T. Characterization of simple isomeric oligosaccharides and the rapid separation of glycan mixtures by ion mobility mass spectrometry. *Int. J. Mass Spectrom.* **2010**, *298*, 119-127.

7. Jin, C.; Harvey, D. J.; Struwe, W. B.; Karlsson, N. G. Separation of isomeric O-glycans by ion mobility and liquid chromatography–mass spectrometry. *Anal. Chem.* **2019**, *91*, 10604-10613.

8. Huang, Y.; Dodds, E. D. Discrimination of isomeric carbohydrates as the electron transfer products of group II cation adducts by ion mobility spectrometry and tandem mass spectrometry. *Anal. Chem.* **2015**, *87*, 5664-5668.

9. Huang, Y.; Dodds, E. D. Ion-neutral collisional cross sections of carbohydrate isomers as divalent cation adducts and their electron transfer products. *Analyst* **2015**, *14*, 6912-6921.

10. Allscher, T.; Klüfers, P.; Mayer, P. Carbohydrate–metal complexes : Structural Chemistry of Stable Solution Species. In *Glycoscience: Chemistry and Chemical Biology*; Fraser-Reid, B. O., Tatsuta, K. and Thiem, J., Eds.; Springer Berlin Heidelberg: Berlin, Heidelberg, 2008; 1077-1139.

11. Zheng, Y. J.; Ornstein, R. L.; Leary, J. A. A density functional theory investigation of metal ion binding sites in monosaccharides. *J. Mol. Struct. Theochem* **1997**, *389*, 233-240.

12. Whitfield, D. M.; Stojkovski, S.; Sarkar, B. Metal coordination to carbohydrates. structures and function. *Coord. Chem. Rev.* **1993**, *122*, 171-225.